Natural Resources Canada | Ressources naturelles Canada

GEOLOGICAL SURVEY OF CANADA
OPEN FILE 9238

Mineralization and alteration at the Doyon deposit, Doyon-Bousquet-LaRonde mining camp, Quebec: example of an Archean sub-seafloor Au(-Cu) vein system

A.G. Galley and P. Mercier-Langevin

2025

Canada

GEOLOGICAL SURVEY OF CANADA
OPEN FILE 9238

Mineralization and alteration at the Doyon deposit, Doyon-Bousquet-LaRonde mining camp, Quebec: example of an Archean sub-seafloor Au(-Cu) vein system

A.G. Galley[1,2] and P. Mercier-Langevin[3,4]

[1]Natural Resources Canada, Geological Survey of Canada, 601 Booth Street, Ottawa, Ontario K1A 0E8
[2]Current address: Malleus Consulting Inc., 1450 Randall Avenue, Ottawa, Ontario K1H 7R7
[3]Natural Resources Canada, Geological Survey of Canada, 490, rue de la Couronne, Québec, Quebec G1K 9A9
[4]Current address: Agnico Eagles Mines limited, 145 King Street East, Toronto, Ontario M5C 2Y7

2025

Recommended citation
Galley, A.G. and Mercier-Langevin, P., 2025. Mineralization and alteration at the Doyon deposit, Doyon-Bousquet-LaRonde mining camp, Quebec: example of an Archean sub-seafloor Au(-Cu) vein system; Geological Survey of Canada, Open File 9238, 141 p. https://doi.org/10.4095/pc9ed7rddb

Publications in this series have not been edited; they are released as submitted by the author.

ISSN 2816-7155
ISBN978-0-660-75691-2
Catalogue No. M183-2/9238E-PDF
https://doi.org/10.4095/pc9ed7rddb

Mineralization and alteration at the Doyon deposit, Doyon-Bousquet-LaRonde mining camp, Quebec, Canada: Example of an Archean subsea-floor Au(-Cu) vein system

Alan G. Galley[1,2*] and Patrick Mercier-Langevin[3,4]

[1]Geological Survey of Canada, 601 Booth Street, Ottawa, Ontario K1A 0E8
[2]Current address: Malleus Consulting Inc., 1450 Randall Avenue, Ottawa, Ontario K1H 7R7
[3]Geological Survey of Canada, 490, rue de la Couronne, Québec, Québec G1K 9A9
[4]Current address: Agnico Eagles Mines limited, 145 King Street East, Toronto, Ontario M5C 2Y7

Corresponding author email: aggalley@gmail.com

ABSTRACT

The Doyon Au(-Cu) vein deposit is part of a district-wide Au-rich, intrusion-associated and VMS mineralizing event that comprises the Doyon-Bousquet-LaRonde camp. The Doyon Au(-Cu) deposit consists of a corridor of overlapping vein stockworks that is rooted within the late stage trondhjemite-tonalite sill component of the 2698 Ma low Al-K and high Na Mooshla Intrusive Complex (MIC) and extends into an overlying, coeval, volcanic-hosted dacite sill complex. The earlier, low-grade Au stockwork consists of quartz-pyrite-rutile-chalcopyrite-Au veins and veinlets and an overprinting higher grade quartz-carbonate-pyrite-chalcopyrite-Au vein stockwork. The latter comprises the Grand Duc, West Zone and zones 1 and 2 Doyon orebodies. These vein stockworks are hosted within zones of moderate to strong sericite and sericite-aluminosilicate dominant alteration zones, the latter containing areas of residual quartz. Within the MIC these alteration zones overprint extensive chlorite-albite-epidote alteration, which in turn overprints zones of biotite-potassic feldspar and quartz-tourmaline dominant alteration. The unusual association of an Au(-Cu) porphyry-epithermal system with a low-Al, low-K tholeiitic-calc-alkaline TTD magmatic suite is due to the unusual moderately high oxidation state of the MIC and its anomalously high F content which allowed concentration and transport of Au and Cu to a subvolcanic, subsea-floor hypabyssal environment.

The characteristics of the vein mineralization and attendant host alteration are somewhat like that described for Phanerozoic Au-Cu porphyry-epithermal systems and unlike that ascribed to

orogenic Au deposits. The overprinting deformation and regional metamorphism and structural control of the auriferous ore shoots are evidence for a strong overprinting and control that took place during regional deformation.

INTRODUCTION

The Doyon Au(-Cu) vein system is part of the Doyon-Bousquet-LaRonde (DBL) mining camp, located in the Archean southern Abitibi greenstone belt between the towns of Rouyn-Noranda and Val-d'Or, Québec (Figs. 1 and 2). It represents one of Canada's largest volcanogenic massive sulphide (VMS) districts Au districts (Galley et al., 2007; Mercier-Langevin et al., 2007a, 2020). The Au-rich VMS deposits, the disseminated and vein-style gold deposits, and the intrusion-associated gold deposits of the DBL mining camp yielded a cumulative production of 107.5 Mt of ore at an average grade of 4.85 g/t Au by the end of 2019. The total past production, current reserves, and estimated resources for the camp amount to approximately 894 t Au (Mercier-Langevin et al., 2021; Figs. 3 and 4) in addition to significant Cu, Zn and Ag.

The Bousquet Formation and DBL camp area have undergone several increments of deformation, and the high degree of strain exhibited by the deposits volcanic host rocks and by parts of the altered and mineralized zones has resulted in various interpretations with respect to the timing and origin of mineralization. These range from deformed synvolcanic deposits to those related to syn- to late-regional deformation (Mercier-Langevin et al., 2017). This includes the Doyon Au(-Cu) vein system, one of the largest deposits of the DBL camp. The Doyon deposit has been interpreted to be either a subsea-floor hybrid epithermal-VMS style or magmatic-hydrothermal system (Filion et al., 1977; Valliant and Hutchinson, 1982; Langshur, 1990; Gosselin, 1998; Galley and Lafrance, 2014; Yergeau et al., 2022a, b) or an orogenic gold system (Guha et al., 1982; Hoy et al., 1990; Marquis et al., 1990; Trudel et al., 1992; Savoie et al., 1990; Tourigny and Chartrand, 1994; Belkabir, 1995).

The purpose of this paper is to integrate published and unpublished observations and data on the Doyon Au(-Cu) deposit to characterize this important mineral system in the context of its host geology and define its importance in relation to understanding the unique precious metal content

of the world class DBL mining camp.

Figure 1*. Location of the Abitibi greenstone belt within the Archean Superior province of Canada (from Monecke et al., 2017).*

EXPLORATION HISTORY

Prospecting in the DBL camp area during the 1920s and 1930s resulted in the discovery of the Mic Mac and Mooshla shear-hosted Au(-Cu) deposits that were mined between 1942 and 1947 (Figs. 3 and 4). Despite intermittent exploration in the district between the 1930s and 1970s, the first major discoveries were made in the late 1970s and early 1980s, leading to the development of the Doyon, Bousquet 1 (now part of LaRonde Zone 5 mine), and Dumagami (later renamed Donald J. LaRonde, or LaRonde 1) base and precious metal deposits (Lulin, 1990; Mercier-Langevin et al., 2021). During the 1990s underground exploration from the Donald J. LaRonde mine workings led to the discovery of the world-class LaRonde Penna gold-rich massive sulphide deposit. Further exploration in the early 2000s from the Doyon underground workings led to the

discovery of the Westwood deposit. Both the LaRonde Penna and Westwood mines are presently in production.

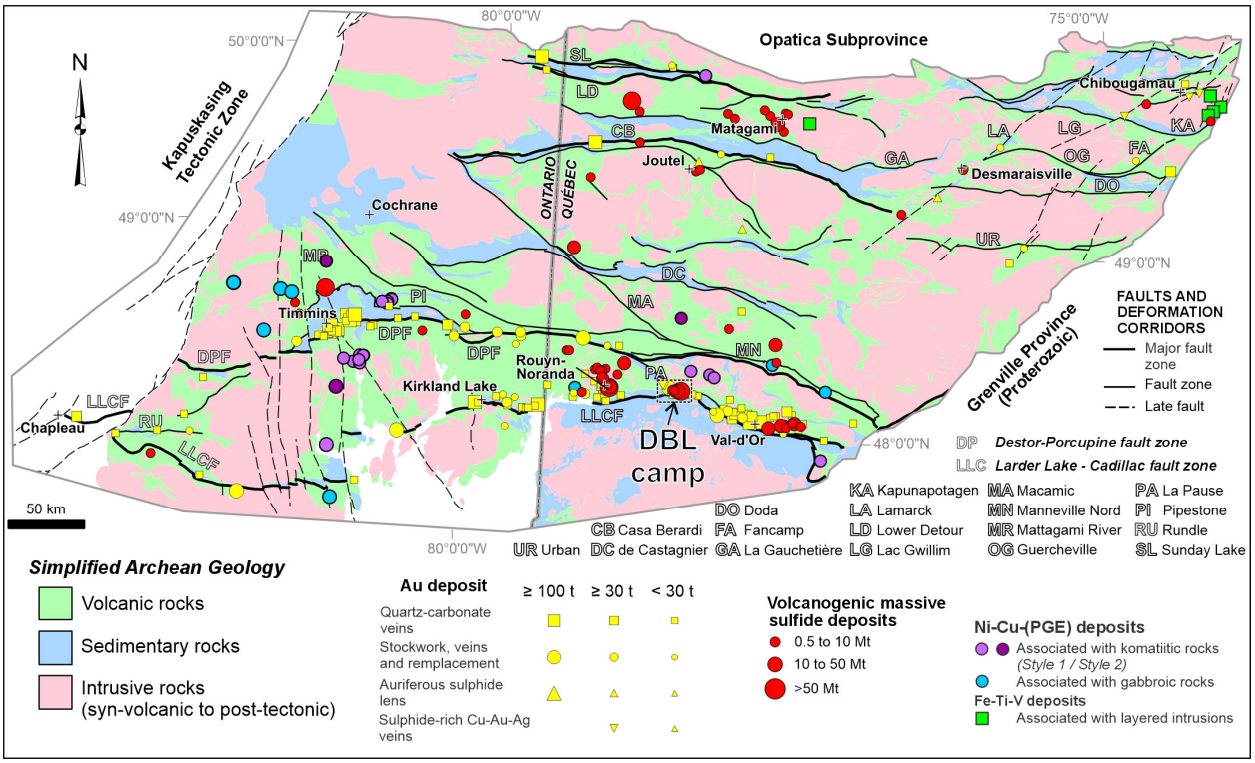

Figure 2. *Geologic map of the Abitibi greenstone belt showing the distribution of supracrustal rocks and intervening domes of intrusive rocks (modified from Mercier-Langevin et al., 2024 and Dubé and Mercier-Langevin, 2020). The map also shows the boundary between the southern and northern parts of the Abitibi greenstone belt.*

Intermittent exploration took place on what is now the Doyon mine property between 1910 and the early 1930s (Savoie et al., 1990). Between 1933 and 1940 trenching and shallow drilling by Mooshla Gold Mines Ltd. and O'Leary Malartic Mines Ltd. resulted in the discovery of the Mooshla A and Mooshla B showings within the Mooshla intrusive complex (Fig. 3), and of the Warrenmac sulphide corridor near the Bousquet River by Warrenmac Mines in 1938 (Mercier-Langevin et al., 2021). Further exploration to the east to verify the extension of these auriferous quartz-pyrite-chalcopyrite

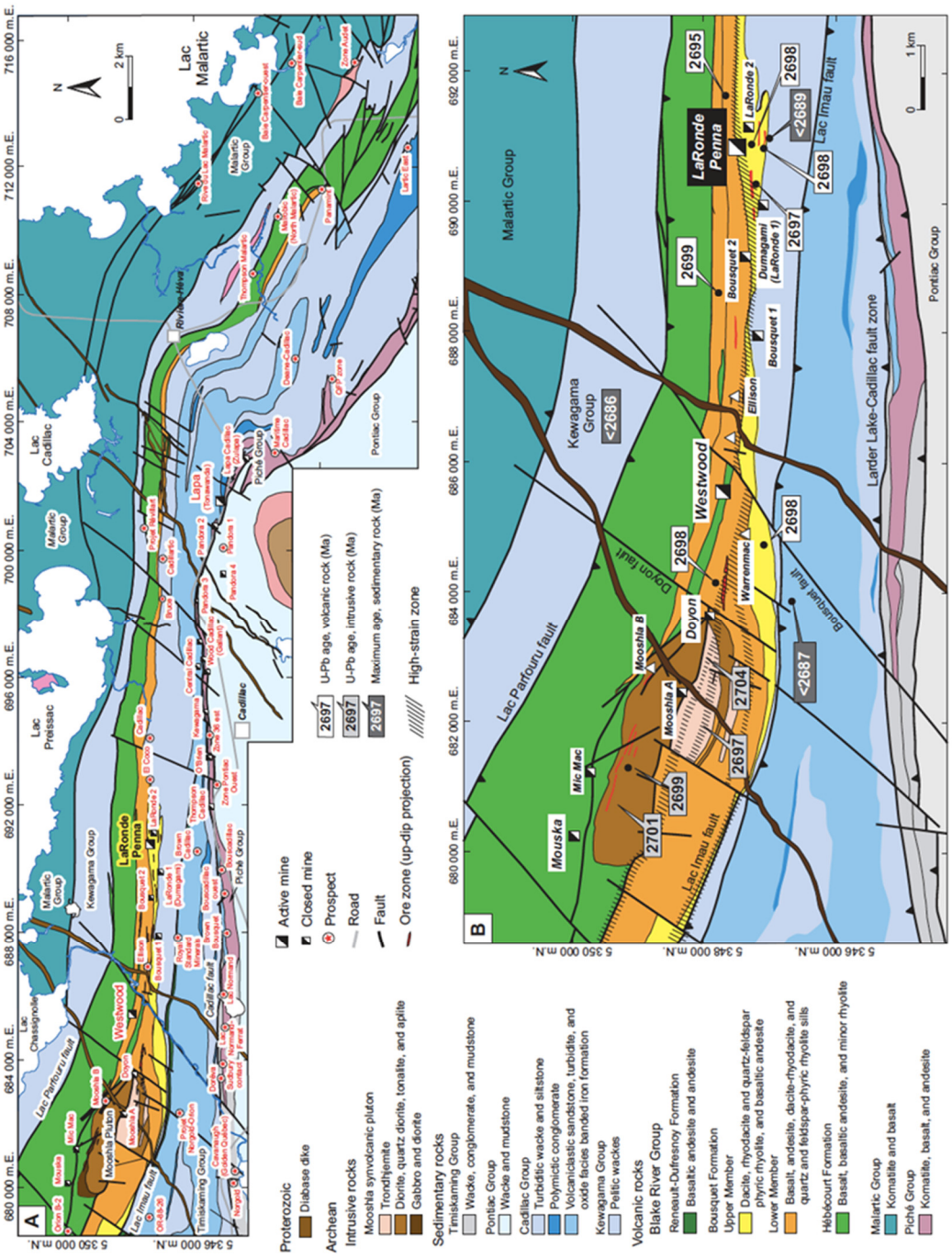

Figure 3. *Geology and mineral deposits of the Doyon-Bousquet-LaRonde and Cadillac mining camps (from Mercier-Langevin et al., 2017).*

vein systems led to the discovery of the Westwood-Cadillac showing. Extraction from Mooshla A and Westwood-Cadillac in these early years is estimated to have been 4,444 tonnes at an average grade of 27 g/t Au. This included 2.88 t grading 197 g/t Au at Westwood-Cadillac. The Mic Mac

deposit was discovered in 1936 (Cassel Duval Mines Ltd.) and Mic Mac Mines Limited developed and operated the mine from 1942 to 1947 producing a total of 3.34 t Au (Mercier-Langevin et al., 2021). There were several geophysical and drilling programs between 1941 and 1971 to expand these reserves, but with little success.

In 1972 a joint exploration program between the Société Québécoise d'Exploration Minière (SOQUEM) and Silverstack Mines Ltd. included induced polarization surveys and follow-up drilling which led to the discovery of Doyon Zone 1. Extension of drilling to the S and W to better understand the geological setting of this vein system led to the discovery of Zone 2, which had no apparent geophysical signature. After Silverstack Mines Ltd. was purchased by Long Lac Minerals Ltd. in 1977, development began of an open pit mine covering both Zones 1 and 2. A 1993 drill program to follow the western extension of Zone 2 led to the discovery of the West Zone. In 1986 Cambior Inc. acquired a 50% interest in the Doyon Gold Mines, and by 1998 became the sole owner and operator. In 2006, Iamgold Corporation merged with Cambior Inc. and acquired the Doyon mine property, which included the then operating Mouska mine and the part of the property on which the eventual Westwood discovery was made. By the time the Doyon mine closed in 2009 the deposit totaled 31.62 Mt grading 5.31 g/t Au for a total of 167.95 tonnes Au (Mercier-Langevin et al., 2017). Low grade material from the early years were added to the Westwood mine production in the last few years, for a global production of 32 Mt at 5.26 g/t Au (168.2 t Au) from the Doyon deposit (Mercier-Langevin et al., 2021).

METHODOLOGY

This open file report is a summary and integration of previously published government reports, maps and journal papers, and unpublished observations and data from unpublished theses (see references) as well as personal communications with the Doyon and Westwood mine geologists. These summaries were further integrated with unpublished research from data collected between 2000 and 2022 by the Geological Survey of Canada.

This new work has resulted in significant modifications to the Galley and Lafrance (2007) and Galley and LaFrance (2014) geology maps of the Mooshla intrusive complex and its host strata.

These modifications were mainly the result of a detailed review of key diamond drill logs and associated geochemical data, inclusion of a recent unpublished cross section and associated geochemical data through Doyon Zones 1 and 2, as well as the detailed mapping of the Westwood deposit host stratigraphy by Yergeau (2015) and Yergeau et al. (2015, 2022a, b).

GEOLOGICAL SETTING OF THE DOYON DEPOSIT

The DBL camp is hosted by rocks within the 2704 to 2695 Ma Blake River Group of the Archean southern Abitibi greenstone belt (McNicoll et al., 2014; Fig. 2). In the study area (eastern part of the Blake River Group), the steeply south dipping rocks of the Blake River Group consist of two formations: the Hébécourt Formation overlain by the lower and upper members of the Bousquet Formation (Lafrance et al., 2003; Mercier-Langevin, 2005; Mercier-Langevin et al., 2007b, c). The Hébécourt Formation is in fault contact to the north with the younger Archean meta-sedimentary strata of the Kewagama Group (≤2686 ± 2 Ma: Davis, 2002) (Fig. 3) which are also cut by 2680.7 +/- 1 Ma tonalite dykes (Mueller et al., 2012). The upper, southern contact of the Bousquet Formation to the south is disconformable (and highly strained) with the siliciclastic strata and minor iron formation of the Cadillac Group (≤2687.4 ± 1.2 Ma in the Doyon mine area: Lafrance et al., 2005).

Blake River Group

In the immediate Doyon mine area, the Hébécourt Formation (Lafrance et al., 2003) forms the fault-bounded base to the Blake River Group and is divided into three units (Figs. 3 and 5). Most of the strata are tholeiitic aphyric basalt flows (unit 1.1) and associated gabbroic sills. Near its upper contact are occurrences of plagioclase glomerporphyritic and magnetite-rich basaltic andesite flows (unit 1.2) along with several discrete tholeiitic rhyolite flow complexes which host the Mic Mac deposit and parts of the Mouska Au-Cu deposit (unit 1.3; Figs. 3 and 5).

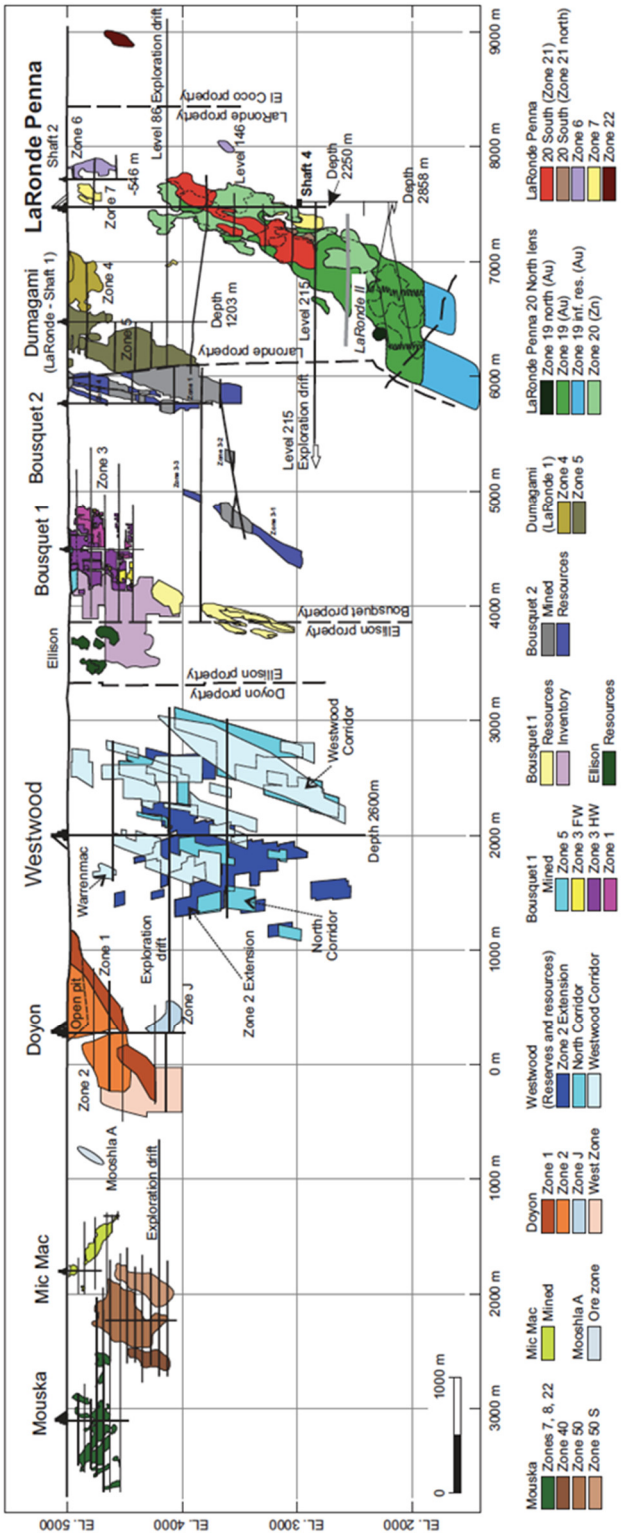

Figure 4. *Composite longitudinal view (looking north) of the Doyon-Bousquet-LaRonde mining camp. The outlines of zones and lenses include production, reserves, and resources, including some historical, non-NI 43-101 compliant reserves and resources (Mercier-Langevin et al., 2017).*

The upper pillowed flows of the Hébécourt Formation are intruded by a laterally extensive blue quartz and feldspar porphyritic synvolcanic tholeiitic rhyolite sills (unit 2.1: Bousquet felsic sill complex). It is dated at 2698.6 ± 1.5 Ma (Lafrance et al., 2003) and is coeval with the overlying lower Bousquet tholeiitic to transitional calc-alkalic units.

Bousquet Formation lower member

Conformably overlying the Hébécourt Formation is the 600 m-thick tholeiitic to transitional lower member of the Bousquet Formation (Figs. 3 and 5) which is divisible into distinctive units. It consists of unit 3.0 (Bousquet scoriaceous tuff units (Mercier-Langevin et al., 2008) basaltic to andesitic amydaloidal pillowed flows on the western flank of the Mooshla intrusive complex changing to coarse, locally scoriaceous volcanic breccia and minor hornblende-plagioclase porphyritic dacite along its eastern flank. On the western flank of the Mooshla intrusive complex unit 3.0 is overlain by a thick succession of dacite to rhyodacite lobe-hyaloclastite flows and associated volcaniclastic deposits (unit 4.1). This unit is intruded by numerous sills and dykes of the Doyon stage of the MIC that represent the unit's eastern contact. These strata are interlayered with and overlain by unit 4.4 (Bousquet heterogeneous unit) massive to pillowed basaltic andesite of tholeiitic to transitional magmatic affinity (Lafrance et al., 2003; Yergeau et al., 2022a) that define the top of the Bousquet Formation lower member. Two suites of hypabyssal intrusive rocks are present along the contact between units 3.0 and 4.4. Unit 4.2 (Doyon glomerophenocrystic unit: 2698.3 ± 0.9 Ma; Lafrance et al., 2005; Yergeau et al., 2022a) consists of dacitic sills, dykes and subsurface flow lobes. Unit 4.3 (Doyon felsic sills) consists of a series of calc-alkalic rhyodacitic sills intruded along the same contact. These massive to strongly foliated sills can have a composite thickness of over 200 m and are in part spatially related with Au mineralization at both the Doyon mine Zones 1 and 2 and with the Zone 2 Extension at the nearby Westwood auriferous polymetallic deposit (Savoie et al., 1991; Wright-Holfeld et al., 2010, 2011; Yergeau et al., 2015, 2022a, b) (Figs. 5 and 6). Both intrusive units have a transitional to calc-alkalic affinity (Lafrance et al., 2005), with the dacite sills compositionally like the felsic rocks of the overlying Bousquet Formation upper member, and late phases of the Mooshla intrusive complex (Yergeau et al., 2022a).

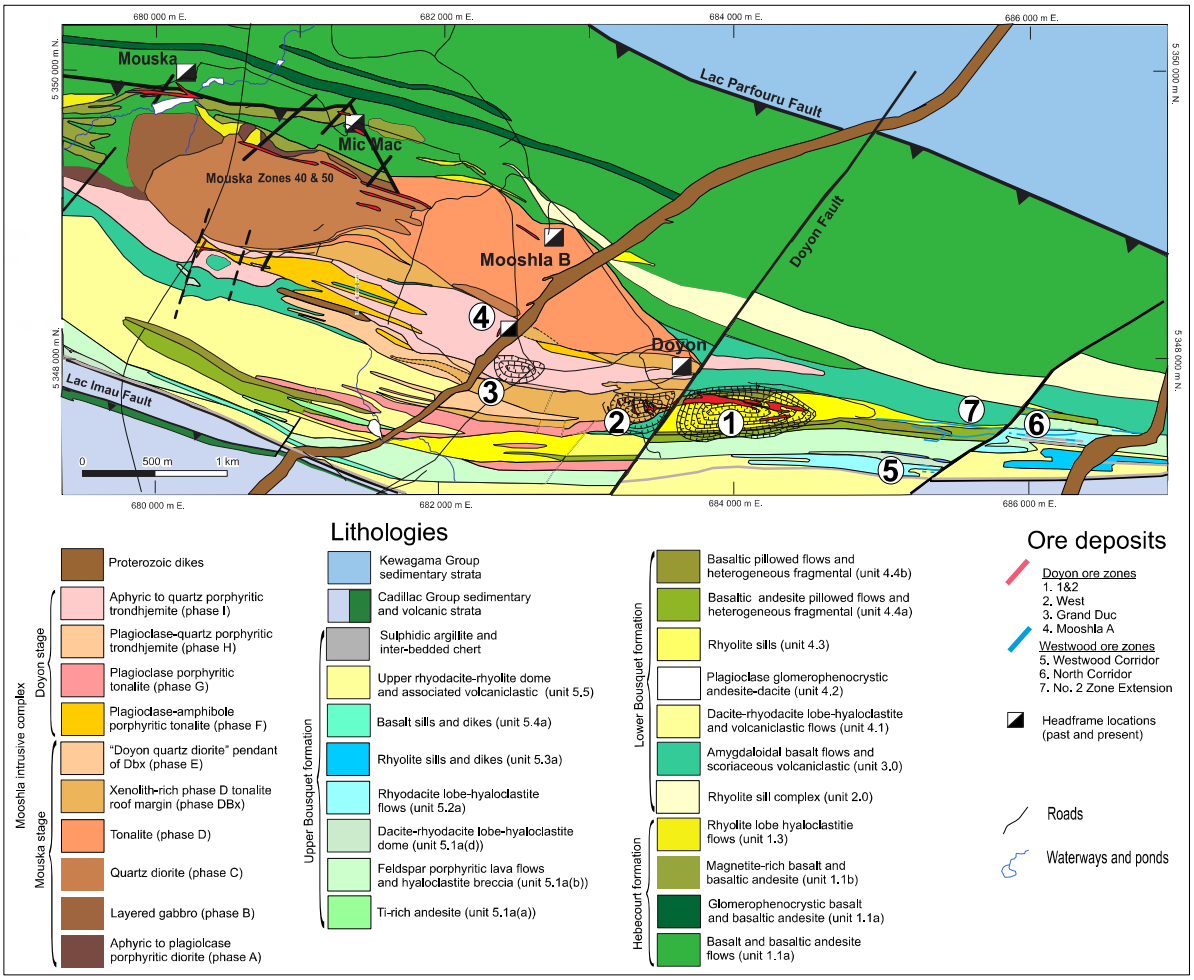

***Figure 5**. Geology of the Mooshla intrusive complex and host stratigraphy, including significant mineral deposits and occurrences (modified from Galley and Lafrance, 2014).*

Bousquet Formation upper member

The upper member of the Bousquet Formation is dominated by transitional to felsic volcanic and shallow intrusive rocks of transitional to calc-alkalic magmatic affinity (Lafrance et al., 2003; Mercier-Langevin et al., 2007b, c, 2009; Yergeau et al., 2022a), forming flows, lobes, flow-breccia deposits, and sill complexes. The lowermost unit 5.1 has been subdivided into four subunits based on contrasting composition and style. The four subunits are complexly intercalated, with subunits 5.1a-(b) (Doyon andesite-dacite) and 5.1a-(d) (Doyon dacite-rhyodacite) being the most continuous and volumetrically important. Unit 5.1 is overlain by a sequence of feldspar phyric felsic volcaniclastic and effusive flows (domes and lobes) that are geochemically like

subunit 5.1s-(d) but generally more felsic (unit 5.2a: Doyon rhyodacite: 2698. 0 ± 1.0 Ma: Lafrance et al., 2005; unit 5.2b: 2698.3 ± 0.8 Ma; Mercier-Langevin et al., 2007b). A feldspar- and quartz-phyric rhyolite (unit 5.3) was emplaced on top of the rhyodacite-rhyolite unit 5.2. Unit 5.3 has been subdivided in two subunits in Yergeau et al. (2022a, b): subunit 5.3a (Westwood blue quartz-phyric rhyolitic sills, and subunit 5.3a-(b) (Westwood feldspar-phyric rhyolitic dome). The blue quartz-phyric facies has been dated at 2697.8 ± 1 Ma (Mercier-Langevin et al., 2007b).

A basaltic andesite unit (unit 5.4a: Westwood upper mafic sills and dykes) forms an important part of the Bousquet Formation upper member sequence. It is mainly exposed underground and only in a few outcrops on the surface. The geochemistry of the unit is distinct from the other units of the upper member of the Bousquet Formation (57% SiO_2, 1.1% TiO_2, and 50 ppm Zr; Mercier-Langevin et al., 2007c, 2009; Yergeau et al., 2022a). The unit comprises a massive sill-dyke complex and a few narrow sills. The sill and dyke complex is characterized by a major feldspar-phyric facies and a local, fine-grained amygdaloidal facies.

Unit 5.5 is the stratigraphically uppermost unit of the Bousquet formation in the Doyon and Westwood deposits area, with a U-Pb zircon date of 2697.5 ± 1.1 Ma (McNicoll et al., 2014). These consist of feldspar-phyric, calc-alkalic rhyodacite volcaniclastic strata and locally massive lobes and localized cryptodomes.

Mooshla Intrusive Complex

The Doyon segment of the DBL camp, or its western part, hosts the Mooshla intrusive complex (MIC), the largest exposed synvolcanic intrusive complex present in the eastern part of the Blake River Group (Figs. 3, 5 and 6). The lower part of this synvolcanic intrusive body is host to parts of the Mouska Au(-Cu) vein deposit, whereas the upper half hosts the West and Grand Duc zones of the Doyon Au(-Cu) vein system, as well as the past producing Mooshla A prospect (Mercier-Langevin et al., 2007d; Fig. 5).

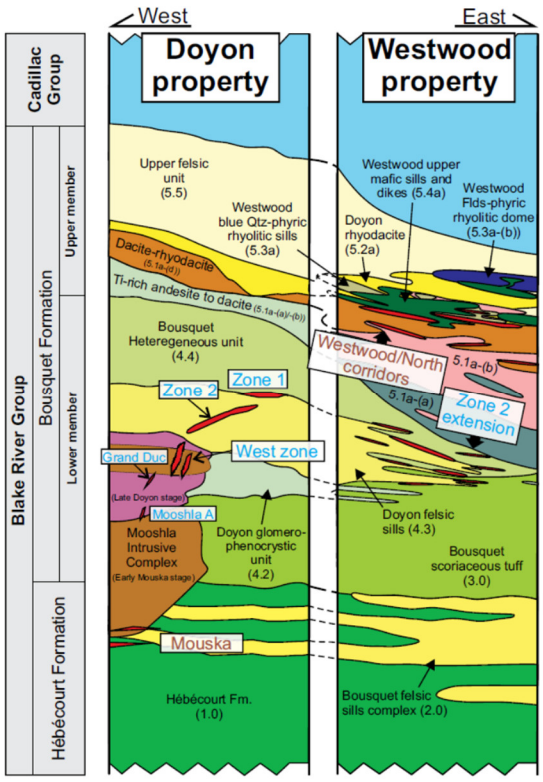

Figure 6. *Correlation of the reconstructed (schematic) stratigraphy hosting the Doyon and Westwood Au systems showing that the unit 4.3 felsic sill complex hosts the Doyon Zones 1 and 2 and the Westwood Zone 2 Extension. From Yergeau et al. (2022b). Readers are referred to Mercier-Langevin et al. (2009), Yergeau (2015), and Yergeau et al. (2015, 2022a, b) for type sections.*

The MIC is a composite intrusion consisting of a series of eight broadly coeval intrusive phases that were emplaced along the contact between the Hébécourt and Bousquet formations (Figs. 5, 6 and 7) (Galley and Lafrance, 2014). The intrusive complex is approximately 5 km in strike length and up to 1.2 km in width with the contained phases divided into two stages of emplacement (Figs. 5 and 7). The older, tholeiitic to transitional calc alkalic Mouska stage (phases A to E) was initiated by injection of several aphyric to plagioclase porphyritic diorite sills (phase A). These were intruded and partially assimilated by a well-layered and differentiated gabbroic laccolith (Phase B), which was subsequently overlapped to the east by a crudely layered quartz diorite stock (phase C). The quartz diorite body was then intruded along its eastern margin, and partially along it's hanging wall contact by several sparsely xenolithic, massive tonalite stocks (phase D). The top of both the quartz diorite and the tonalite phases have xenolithic hanging-wall contacts containing

abundant mixed angular to sub-angular fragments of the phase A diorite and basalt of the Hébécourt Formation (DBx phase; Figs. 5 and 7).

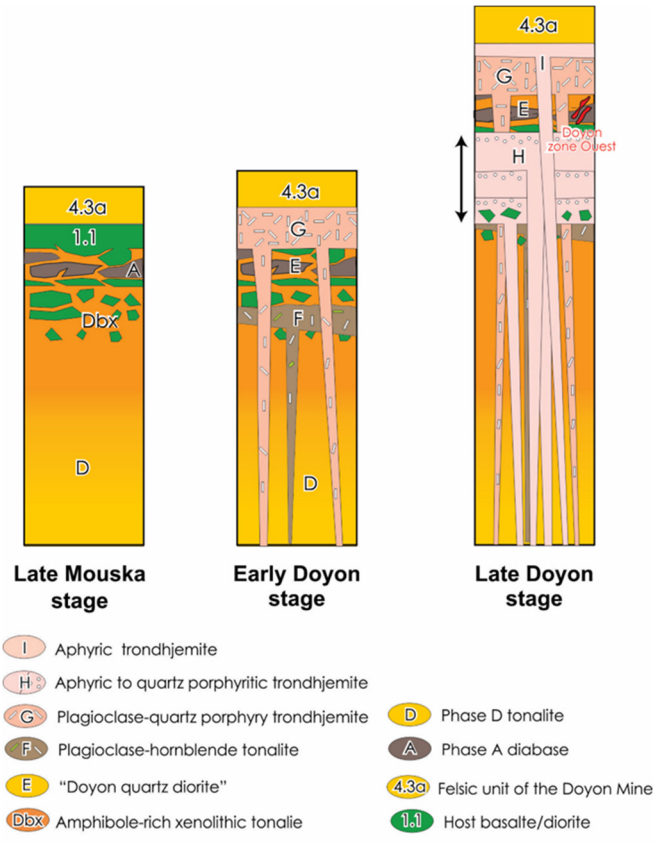

***Figure** 7. Cartoon illustrating the paragenesis of the various phases of the Mooshla intrusive complex. Note that the Doyon West Zone is partially within a pendant of the early magmatic stage (from Galley and Lafrance, 2014).*

The tholeiitic to transitional low K calc-alkalic Mouska stage phases are intruded and overlain by a series of Doyon stage low K calc-alkalic porphyritic tonalite and trondhjemite composite sills and dykes (phases F, G, H and I; Figs. 5 and 7). Sills of feldspar-hornblende porphyry and feldspar porphyry tonalite intruded the tops of the early-stage quartz diorite and tonalite. In places the feldspar porphyry tonalite infills spaces between angular xenoliths of quartz diorite and early tonalite (Fig. 8A).

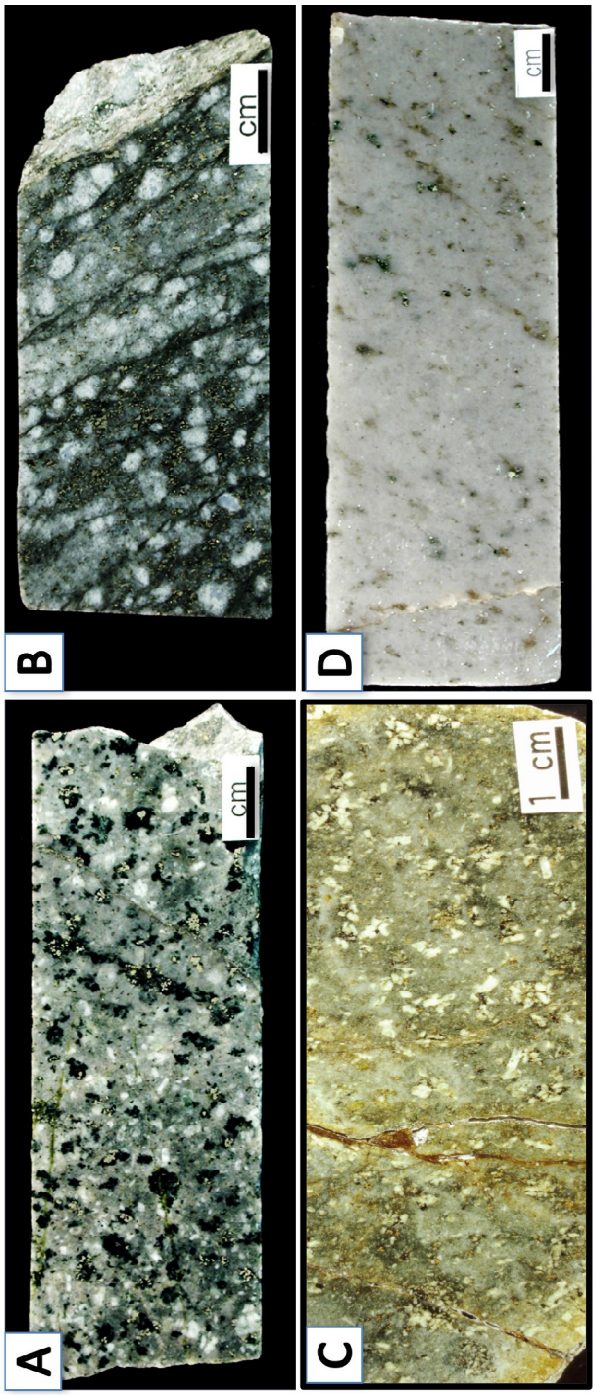

Figure 8. *Examples of late-stage MIC phases that host part of the Doyon mineralization.* ***A***. *Phase F plagioclase-hornblende porphyritic tonalite, ddh NG94-02, 864 m. Photograph by A. Galley, NRCan photo 2023-626.* ***B***. *Phase G chlorite-altered plagioclase porphyritic tonalite, ddh 1106-96, 140 m. Photograph by A. Galley, NRCan photo 2023-627.* ***C***. *Phase H plagioclase porphyritic trondhjemite, UTM NAD 83 Zone 17 680428 E, 5348650 N. Photograph by A. Galley, NRCan photo 2023-628.* ***D***. *Phase I quartz porphyritic to aphyric trondhjemite, ddh 775-87, 1223 m. Photograph by A. Galley, NRCan photo 2023-629.*

The more voluminous quartz and quartz-feldspar porphyritic trondhjemite phase consists of up to a dozen individual sills up to 300 m thick with aphyric bases and more phenocryst-rich tops (Figs. 5, 8B and D). Some sills are characterized by intervals with up to 60% angular xenoliths of feldspar porphyritic diorite, tonalite, quartz diorite and fine grained felsic volcanic. The xenoliths, especially those with more mafic compositions, appear to be partially assimilated in places, and have interacted, possibly through dehydration (Russell et al., 1995) (Fig. 9B and C), with the intruding feldspar porphyry and trondhjemite magmas. The xenolith dehydration resulted in abundant miarolitic cavity formation in the xenolith-rich zones (Figs. 9A-D). These cavities can form up to 30% of the volume of the host trondhjemite and have a variety of shapes including that of pipe vesicles (Fig. 9A). They are up to several centimetres in diameter and infilled with a variety of mineral assemblages. These mineral assemblages will be described in the alteration section of the paper.

Above and below the composite sill complex, thinner sills and dykes of trondhjemite intrude the lower early stage of the MIC and the overlying feldspar porphyritic tonalite and massive to brecciated pendants of early-stage quartz diorite and tonalite. This pendant is known locally as the Doyon quartz diorite (Phase E). This massive to xenolithic pendant appears to play a significant role in the localization of the Doyon West and Grand Duc zones of the Doyon Au(-Cu) quartz-sulphide vein stockwork and dissemination-style deposit (Stone, 1988; Savoie et al., 1990; Gosselin, 1998). Trondhjemite sills also extend into the units above and to the east of the main MIC mass.

A lower hemisphere stereogram plot of several Doyon late stage porphyritic tonalite and trondhjemite dykes, which do not appear to be folded, indicates that in their present orientation they show rough groupings in ENE and NW directions (Fig. 10). Assuming they were emplaced prior to deformation (based on age relationships) and an average 70^{o} southerly dip of the MIC phase contacts (based on the general dip of the volcanic stratigraphy and main fabrics in the study area), the average original late-stage dyke orientations then become both shallowly and steeply west dipping forming a series of thin sills and dykes.

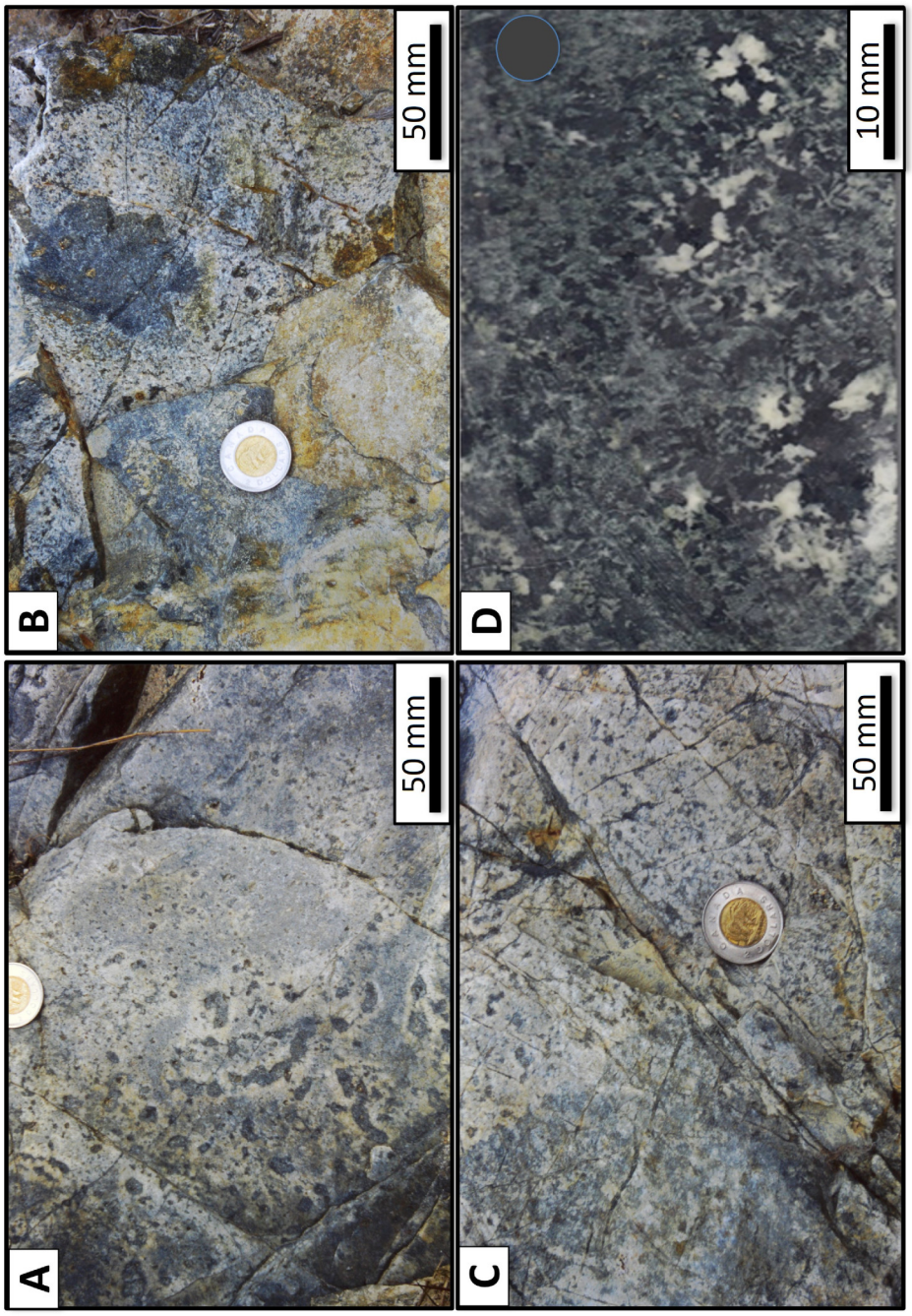

Figure 9. *Examples of the xenolithic contact between trondhjemite and the Doyon quartz diorite. Station location UTM NAD83 Zone 17 682186 E, 5347973 N.* ***A****. Miarolitic cavities, some shaped like pipe vesicles in trondhjemite. Note the characteristic fine-grained granophyric rims. Photograph by A. Galley, NRCan photo 2023-630.* ***B****. Ameboid-shaped diorite xenolith enveloped by granophyric trondhjemite with a dense concentration of miarolitic cavities. Photograph by A. Galley, NRCan photo 2023-631.* ***C****. Partially digested xenolith in granophyric and miarolitic trondhjemite. Photograph by A. Galley, NRCan photo 2023-632.* ***D****. Diorite xenolith with secondary coarse growths of amphibole, biotite and plagioclase typical of partially dehydrated and assimilated bodies. Photograph by A. Galley, NRCan photo 2023-633.*

The MIC feeder dykes to the late stage porphyritic tonalite and trondhjemite sills are clustered along the eastern and western margins of the MIC along with a series of post Doyon stage late dykes. These post-MIC dykes include aplite, rhyolite and aphyric to plagioclase porphyritic diorite dykes. The rhyolite and diorite dykes are compositionally compatible with some of the volcanic units in the upper member of the Bousquet formation (Galley and Lafrance, 2014) whereas the aplite dykes have highly fractionated calc-alkalic compositions. Several of the aphyric diorite dykes cross the Doyon West Zone Au(-Cu) vein stockwork, but unfortunately could not be dated (Lafrance et al., 2005). The entire volcano-plutonic succession is transected by a large Proterozoic diabase dyke that postdates all types of mineralization in the area (Fig. 3).

Timing and depth of the MIC origin and emplacement

Several characteristics of the MIC indicate that it was emplaced at a relatively shallow depth (<1 kbar or approximately 3 km) within a volcanically active subsea-floor environment (Galley and Lafrance 2014; Neyedley et al, 2021b). Early geochronology work indicated that the early tonalite magmas of the MIC were emplaced at 2701 ± 1 Ma (Zhang et al., 1993) but more recent work has provided better constraints on the timing of emplacement for the MIC. A U-Pb zircon age of 2698.4 ± 0.4 Ma was obtained on a sample from the quartz-diorite of phase C (McNicoll et al., 2014) and a single U-Pb zircon age obtained from the MIC trondhjemitic phase of 2696.9 ± 1.0 Ma (Lafrance et al., 2005) indicate that the intrusion is of similar age to the upper Bousquet member (Galley and Lafrance, 2014; McNicoll et al., 2014). The geochemistry of the late-stage intermediate to felsic phases of the MIC is comparable to that of units 5.2 and 5.5 of the upper member of the Bousquet Formation (Galley and Lafrance, 2014) whereas the geochemistry of the early-stage phases is like that of the units of the lower member of the Bousquet Formation.

The results of detailed petrography, high-precision U-Pb geochronology, accessory mineral thermobarometry, and zircon trace element chemistry studies by Neyedley et al. (2021b) indicates that the Mooshla intrusive complex is not only compositionally diverse but has a complex P-T time evolution during which the different magma types originated from different crustal sources. It is proposed that a complex history of partial melting, and fractional crystallization from multiple magma chambers took place at temperatures between 700-800^{o}C at pressures that ranged

from 0.5 to 1.1 GPa at 18.5 to 40 km crustal depth. This includes several phases of both quartz diorite and tonalite presently grouped as phases C and D that explains their complex internal contact relationships (Galley and Lafrance, 2014). This magmatic history is considered normal for the generation of Archean TTG suites. High precision CA-ID-TIMS U-Pb zircon dating suggests an interval of slightly less than 1.5 Ma years between the emplacement of the tholeiitic dominant Mouska stage and the calc-alkalic dominant later Doyon stage MIC intrusive phases (Neyedley et al., 2021b). This suggests the existence of a protracted thermal corridor that originated deep in the lithosphere and controlled magmatic and hydrothermal activity during the formation of the Bousquet Formation.

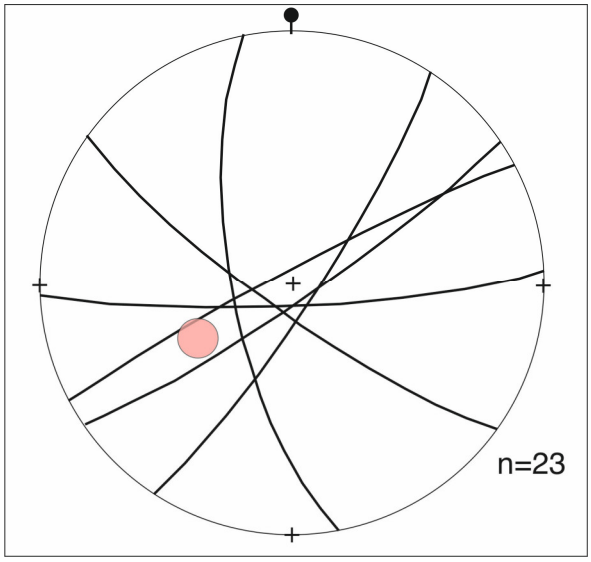

Figure 10. *Lower hemisphere stereogram illustrating the present orientations of several Doyon late stage porphyritic tonalite and trondhjemite dykes cutting the Doyon early-stage intrusive phases and host volcanic strata. The red dot represents the average plunge of the Doyon ore bodies. Note that the plunge of the Doyon system lies along the plane of the dominant trondhjemite dyke set suggesting a possible primary structural control and focus for the Doyon mineral system.*

MIC association with seafloor hydrothermal activity

The MIC is spatially associated with VMS-style hydrothermal systems that include pre-MIC sulphide mineralized zones (Gunning, 1941; Langshur, 1990; Belkabir and Hubert, 1995). Where the Mouska stage quartz diorite and tonalite phases are in hanging-wall contact with the upper part of the Hébécourt Formation and the lower member of the Bousquet Formation volcanic strata the latter are affected by varying degrees of silicification and Fe-Mg metasomatism like

other known examples of subsea-floor hydrothermal activity related to the generation of VMS mineralization (Galley, 1993; Franklin et al., 2005; Galley et al., 2007). The xenolithic hanging wall margin (DBx phase: Fig. 3) contains abundant evidence of the *in-situ* dehydration of mafic xenoliths (Fig. 9D), including miarolitic haloes and pegmatitic xenolith margins. This suggests that the host basaltic andesite and perhaps the Phase A diorite, were hydrated before assimilation into the tonalite magma, most likely from convecting seawater (Russell et al. 1995; McLeod and Sparks, 1998; Galley and Lafrance, 2007 and references therein).

Several VMS occurrences are recognized above these alteration zones including a thin Zn-enriched exhalite at the base of unit 4.4, probably at the contact with the underlying unit 3 along which unit 4.3 was intruded. The Warrenmac massive sulphide zone to the Westwood deposit lies at the top of unit 5.1 (Fig. 3). If the MIC was the heat source for convective subsea floor hydrothermal activity it was most likely emplaced at depths of 2000 m or less (Galley, 1993; Franklin et al., 2005).

Lastly, most of the MIC phases contain abundant disequilibrium textures that includes granophyric groundmass, irregular shaped miarolitic cavities and hydrothermal brecciation (Fig. 9A-C). From the presence of remnant primary igneous hornblende, Neyedley et al. (2021b) calculated an approximately 4% magma water content for the early stage tonalite, which would have allowed rapid disequilibrium crystallization and miarolitic cavity growth at relatively shallow (<1 kbar) emplacement into a subsea-floor environment.

Deformation and metamorphism

The Archean rocks in the Doyon segment of the DBL camp have undergone several phases of folding, shearing and faulting, an understanding of which is critical to modeling the style and timing of the Doyon Au(-Cu) vein system. The high degree of strain exhibited by the deposit's volcanic host rocks and by parts of the altered and mineralized MIC has resulted in various interpretations with respect to the timing and origin of the Doyon vein system.

Three phases of deformation are recognized: the oldest penetrative foliation is poorly developed and formed during formation of D_1 NW trending isoclinal folds. The more prominent D_2 event

(regional D_3 event of Dubé and Mercier-Langevin, 2020) is characterized by E-W to ESE striking and steeply SSW dipping penetrative regional foliation and a steep- to moderate SW plunging lineation (Fig. 4, 11). They are accompanied by the development of several discrete shear zones, some of which define a series of major northward directed thrust faults (e.g., Lac Imau Fault; Fig. 2) that, in places, define major formational contacts. In other instances, these shear zones represent intraformational high angle oblique reverse faults, along which varying degrees of late-stage strike slip movement has taken place as defined by stretching lineations and slickensides (Gosselin, 1998; Tourigny and Chartrand, 1998) (Fig. 11). The hanging wall contact of the MIC is bordered and overprinted by a number of these high strain zones with the highest degrees of strain within domains of sericite-rich alteration (Figs. 5 and 12). One lineament of this fault set is mapped along the northern margin

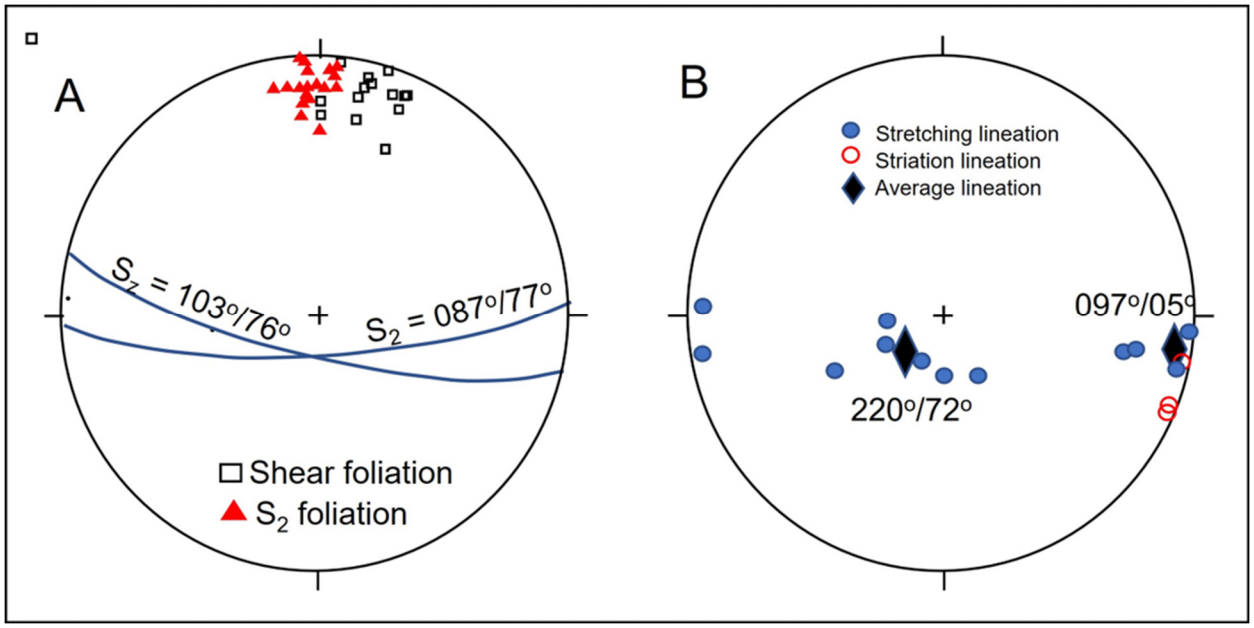

Figure 11. *Lower hemisphere stereograms from Gosselin (1998) of various lineations associated with the regional S_2 schistosity and emplacement of the North and South shear zones that overprint, rotate and dismember sections of the Doyon Au vein system.*

of the intrusive complex, and another along its southern boundary. The southern high strain zone encapsulates the Doyon Zones 1 and 2, with parallel high strain zones crossing the Doyon stage intrusive phases of the MIC and associated West, Grand Duc and Mooshla Au zones (Marquis et al., 1990; Savoie et al., 1991; Gosselin, 1998) (Fig. 12). The late strike slip movement is apparently restricted to the highly strained MIC contact with the volcanic rocks, referred to by Gosselin (1998)

as the South Shear. There appears to have been very little, large-scale movement along these Blake River Group-hosted D_2 high strain zones, as there is little apparent displacement of unit contacts.

The D_3 phase of deformation is marked by the development of a series of NE striking faults that offset all earlier structural features. Faulting is accompanied in places by the development of a crenulation cleavage. Examples include the Doyon fault (Fig. 5). Formation of the Doyon Fault resulted in a small degree of apparent sinistral offset of the Doyon deposit (Fig. 5). The presence of the East Orion Fault in past publications (e.g., Lafrance et al., 2005) is somewhat problematic, as it does not appear to offset the Mouska Stage of the MIC, nor does it terminate the western extent of the Doyon stage sills and dykes (Fig. 5) and it was therefore taken out of the revised map of the study area (Fig. 5) as the geology could be confidently mapped on both sides of that previously inferred structure.

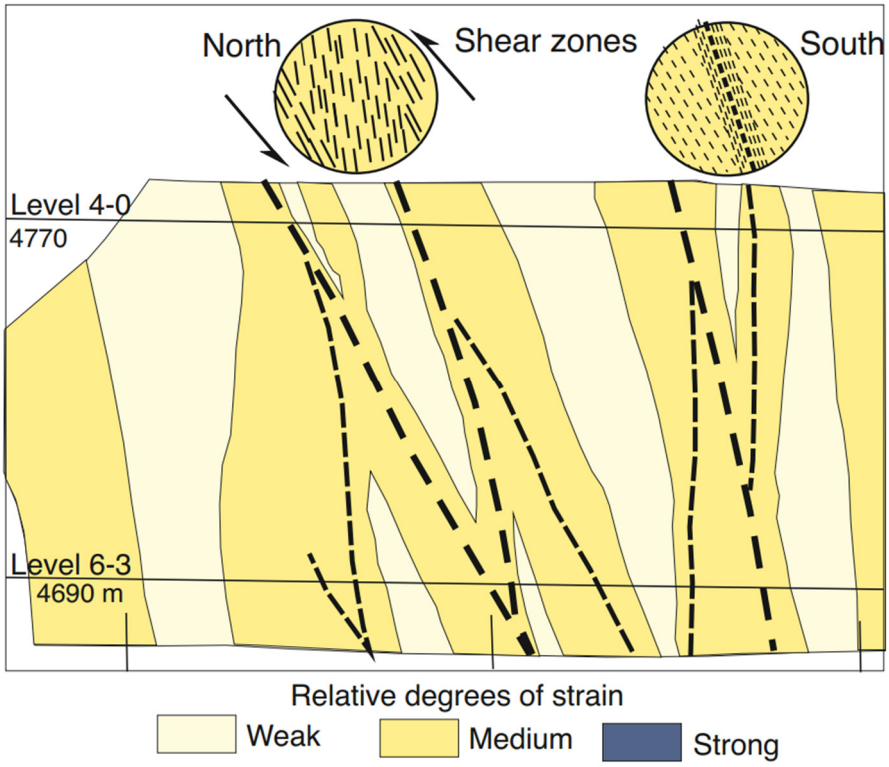

***Figure 12**. Looking east along a cross section of high strain zones affecting the zones 1 and 2 vein arrays along the south margin of the MIC (Gosselin, 1998).*

Regional upper greenschist metamorphism is approximately coeval with the D_2 deformation in the Doyon deposit environment. Non-oriented biotite and actinolite porphyroblasts in the MIC phases indicates that peak of thermal metamorphism took place late in the development of the S_2 foliation, whereas the S_2 schistosity is largely defined by the orientation of deformed and re-oriented volcanic clasts, quartz-sulphide veins, pyrite grains and aluminosilicate porphyroblasts, and retrograde chlorite and sericite (Marquis et al., 1990; Belkabir and Hubert, 1995; Dubé et al., 2004; Mercier-Langevin, 2005). Near the Doyon deposit much of the peak metamorphic assemblage has been retrograded to a lower greenschist assemblage, with prograde actinolite and biotite replaced with chlorite, and kyanite and andalusite replaced by quartz, kaolinite, diaspore and pyrophyllite (see section below on alteration). The possible equilibrium growth of chlorite and biotite, and the presence of co-existing aluminosilicates may be influenced by the anomalous concentrations of F in and around the MIC. The resulting Fe avoidance in affected phyllosilicates may account for the abundance of Mg-chlorite, Mg-biotite and phlogopite due to anomalous PT conditions during metamorphism (Zaleski 1989; Mason, 1992; Gaillard et al., 2018 and references therein) as further discussed below.

Geology of the Doyon Au(-Cu) system

The Doyon Au(-Cu) system consists of a series of auriferous quartz-sulphide vein arrays that have a collective strike length of over 1200 m, a width of up to 300 m, and plunges 55 to 70° to the WSW for over 1000 m (Figs. 5 and 13). The various components of the Doyon vein system are hosted within a zone of alteration and variable strain that extends ~4200 m eastward across the late-stage MIC intrusive phases and unit 4.3 to include the Westwood deposit Zone 2 Extension (Fig. 5) (Yergeau et al., 2022a). The presence of an encompassing >20 ppb Au anomaly (Fig. 14) and continuation of a quartz-sericite-pyrite-rutile alteration envelope between the two deposits caused Iamgold's personnel, Mercier-Langevin et al. (2009), and Wright-Holfeld et al. (2010, 2011) to hypothesize that the along strike Westwood Zone 2 Extension is in fact similar in geologic setting and alteration type as the Doyon Zone 2 orebody. This was later confirmed by Yergeau et al. (2015, 2022a, b).

The Doyon vein system is widest within the late phases of the MIC (West, Grand Duc and Mooshla A zones) where it consists of over 10 south striking distinct vein stockworks, with the Grand Duc

and Mooshla A representing the more diffuse and lower grade zones. In the stratigraphic hanging wall to the MIC the vein system narrows down to two major vein arrays (Zone 2) accompanied by thinner, disconnected vein stockworks along its north margin. Zone 1 overlaps the eastern end of Zone 2 and is the stratigraphically highest component of the Doyon vein system and consists of two parallel vein stockworks (Savoie et al., 1986, 1990).

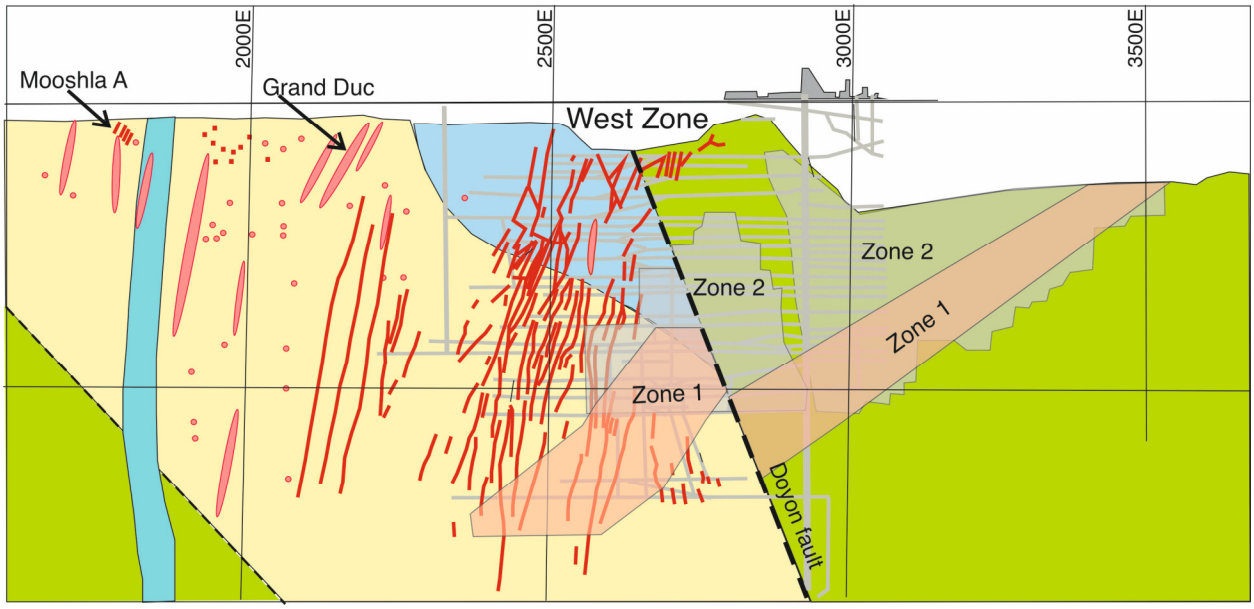

***Figure 13**. 6670m longitudinal section (looking N) through the Doyon vein system with gold zones and Doyon Fault plane brought into the section over an ~100 m width. Light grey framework represents Doyon mine underground workings under the mineshaft buildings. Dark pink dots and lozenges represent higher-grade Au drill hole intersections. Modified from IAMGOLD Corp. compilation.*

Mining of Doyon zones 1 and 2 started as an open pit operation in 1980 and gradually switched to an underground operation. These two zones are located principally east of the NE striking D_3 Doyon Fault, but the oblique sinistrally offset extensions of both ore bodies have been traced over 100 m west of this structure, where they are included as part of the Doyon West Zone (Fig. 15). A near surface West Zone vein stockwork begins west of the Doyon Fault and was exploited through a second open pit and continued exploitation underground (Fig. 13). Exploration to the W and N of the West Zone revealed low grade (<1 g/t Au) auriferous quartz-pyrite-chalcopyrite vein stockworks up to the western margin of the late-stage MIC and up to the basal contact of the Phase I trondhjemite (Fig. 15). They include the Mooshla A and Grand Duc easterly vein trends, both transected and dextrally offset by a NE trending Proterozoic diabase dyke. The Mooshla A vein

trend hosts the Mooshla A deposit as a tight, small stockwork of quartz-pyrite-chalcopyrite veins and veinlets (Fig. 5) (Filion et al., 1977; Savoie et al., 1990). Up until recently these two vein trends were considered too low grade until 2019 when IAMGOLD Corp. developed these low-grade vein stockworks as the Grand Duc orebody in an open pit operation to compensate for temporarily reduced production at the Westwood mine (Mercier-Langevin et al., 2021).

The following description of the principal ore zones includes earlier descriptions and observations by Filion et al. (1977), Guha et al. (1982), Chénard (1990), Savoie et al. (1990), Marquis et al. (1990), Gosselin (1998) and Mercier Langevin et al. (2007d, 2017). It also integrates observations made by the Geological Survey of Canada in field campaigns and mine visits between 2000 and 2021.

Doyon Zone 1

Zone 1 produced 3.0 Mt at a grade of 5.4 g/t Au with a cutoff of 2.7 g/t Au between 1980 and 1989 (Savoie et al., 1990). It was discovered approximately 200 below surface where it is hosted within highly altered and schistose felsic sills of unit 4.3 and enclosed pendants of chloritic schist representing unit 4.4 mafic volcanic strata of the Bousquet Formation lower member (Figs. 6, 13 and 15). There are two separate, strongly deformed and elongated vein arrays defined as subzones 1.1 and 1.2. The two stockworks are within a broader halo of disseminated pyrite. Subzone 1.1 is hosted within a sericite rich and highly schistose and altered felsic sill, or at the contact between two felsic sills. The subzone strikes 090^{o} parallel to the D_2 schistosity, plunging 55^{o} WSW parallel to the principal L_2 lineation. The zone is 180 m long, up to 15 m wide, and extended for 130 m down plunge to where it is offset by approximately 40 m of oblique sinistral movement along the Doyon Fault (Figs. 5 and 13). Subzone 1.2 is hosted within a sliver of strongly chlorite-sericite altered mafic volcaniclastic rock between two strongly quartz-sericite-pyrite-aluminosilicate-allanite-rutile altered sills. To the west of the Doyon Fault, Zone 1 is traced for over 100 m westward where it is situated in the structural hanging wall of the Doyon West Zone. At its eastern termination Zone 1 does not end abruptly, but rather is transposed and dismembered where it is cut by the strong east-west S_2 foliation. Filion et al. (1977) suggest that the former may well be the dismembered continuation of Zone 2.

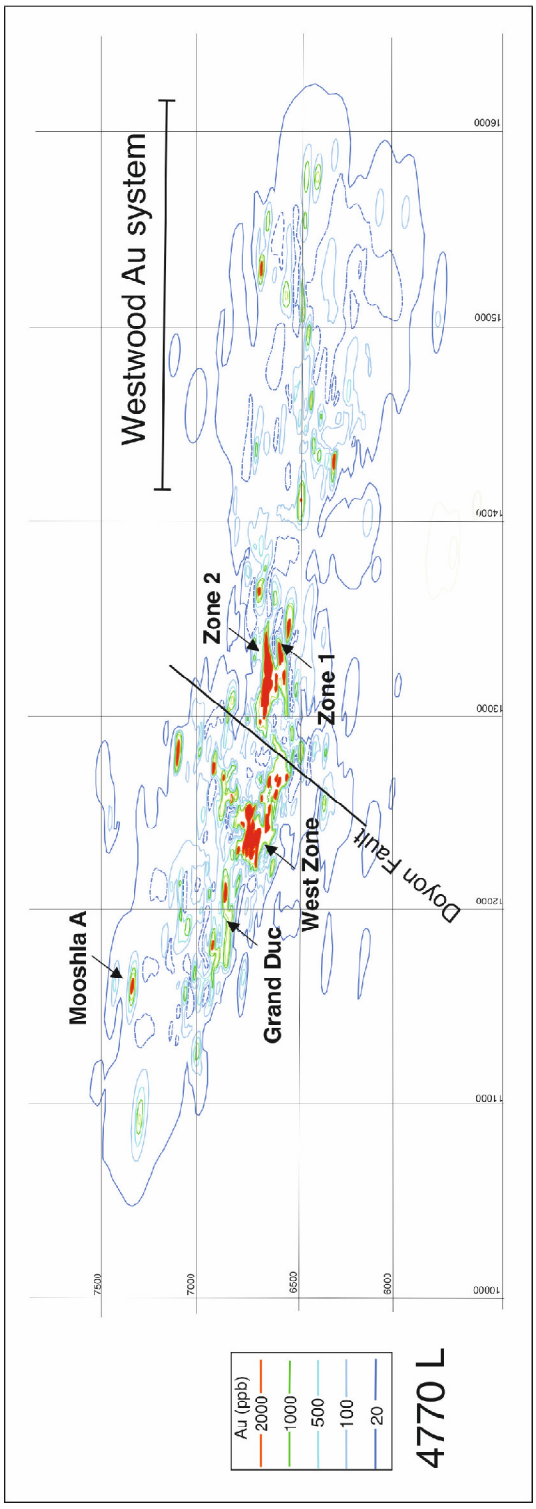

Figure 14. *East-west-biased contour plot of Au values >20 ppb (with background concentrations defined as <5 ppb) that envelopes both the Doyon and Westwood vein systems as part of the evidence that the two deposits are temporally and genetically linked. Grid is north-south (1000 m spacing)/east-west (500 m spacing). Iamgold Inc. assay data taken from surface sampling and near-surface drill data.*

The principal concentrations of gold mineralization in Zone 1 were characterized by numerous strongly deformed centimetre scale, interlaminated pyrite-quartz veins and veinlets with up to 70% pyrite (Savoie et al., 1990) (Fig. 16A). These vein concentrations had haloes of 5 to 20% disseminated pyrite grains 1 to 3 mm in size. Veins extending outside the disseminated pyrite envelope did not carry much gold (Y. Lei, personal communication, 2008). Gold is present as very fine grains either interstitial to the pyrite grains in the veins or wall rocks, and at the border of silicate grains within the wall rocks. The subzone 1.2 vein set is generally less quartz rich (<30%).

Doyon Zone 2

Zone 2 produced 14.8 Mt grading 5.1 g/t Au, with a cut-off of 2.7 g/t Au between 1980 and 1989 (Savoie et al., 1990). More production came from Zone 2 after 1989 but precise numbers could not be obtained. Zone 2 is hosted principally within schistose and altered rocks of unit 4.3 Doyon felsic sill complex, which intrudes along the contact between the Bousquet scoriaceous tuff units and the mafic lavas of the overlying Bousquet heterogeneous unit 4.4 (Figs. 5 and 15). The Doyon felsic sill complex is intruded by dykes and thin sills of the MIC late stage trondhjemite and feldspar porphyritic tonalite, which also predate the Zone 2 vein system. The western end of Zone 2 transects the underlying unit 3.0 polymictic volcanic breccia (Figs. 15 and 16). There are also small pockets of veins and associated alteration present within the footwall of the unit 3.0 coarse-grained volcaniclastic strata.

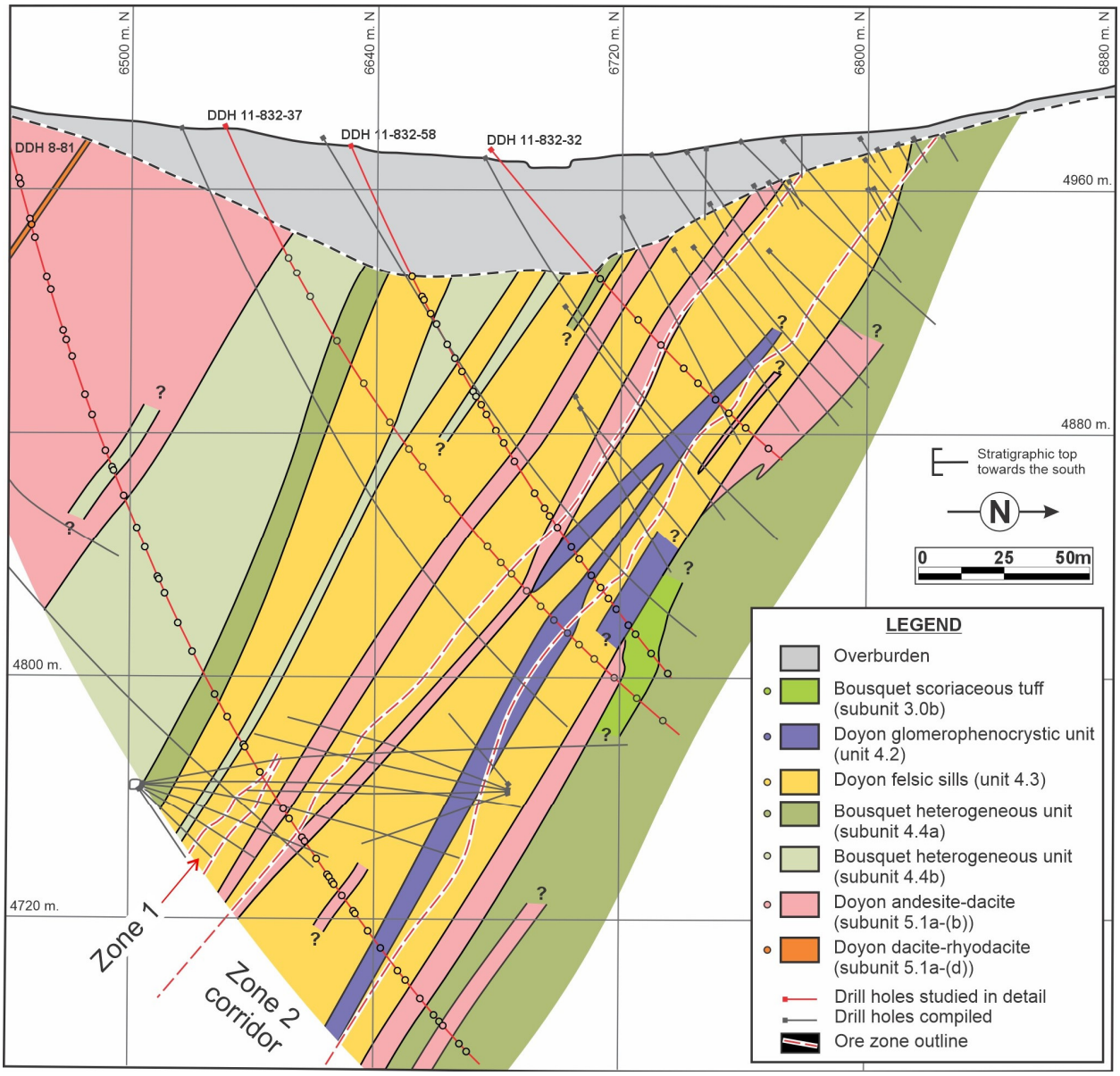

Figure 15. *North-South section through zones 1 and 2 defined through reevaluation of drill core. See Appendix 1 for details about units discrimination.*

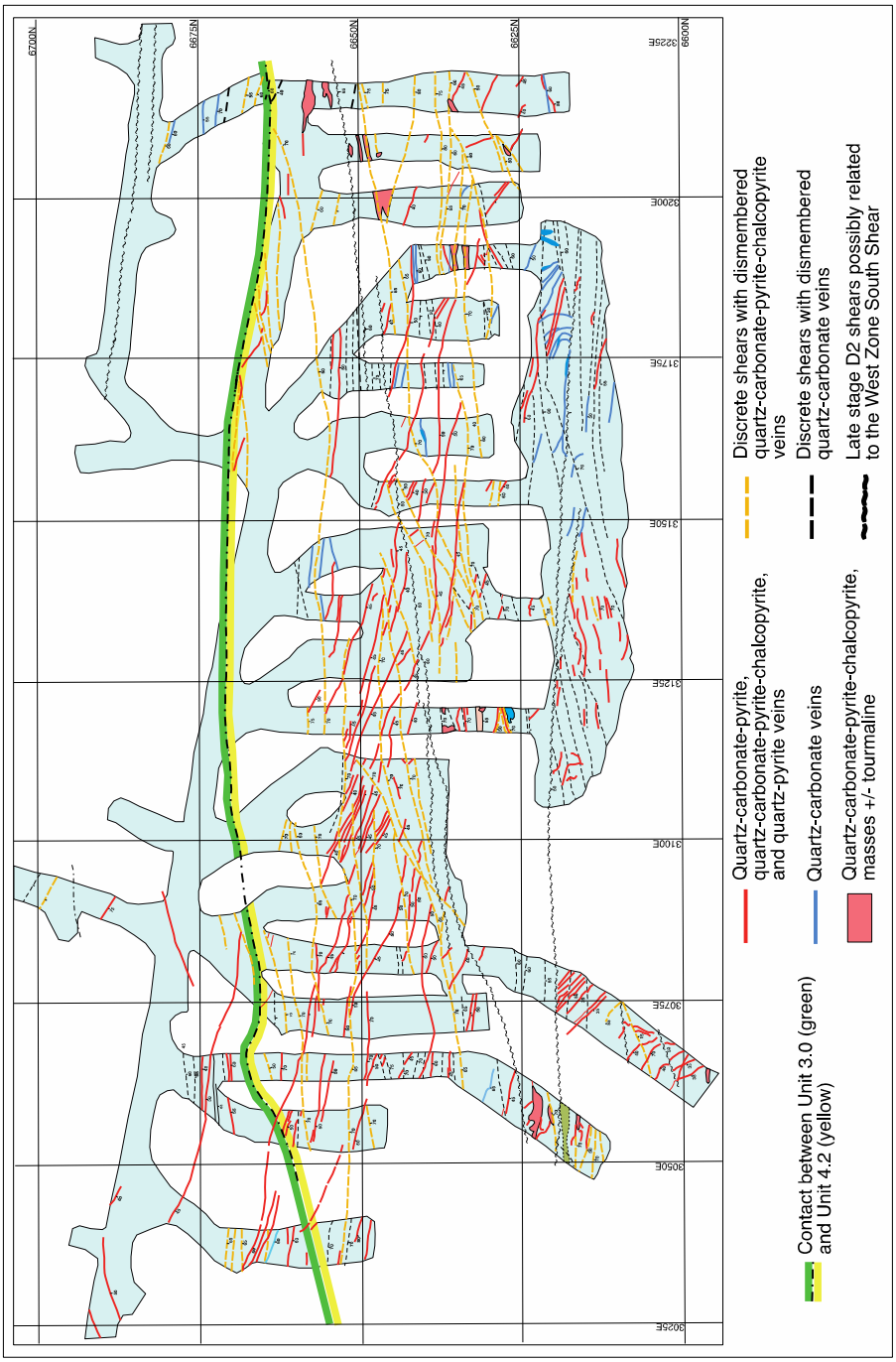

Figure 16. *Reproduction from Iamgold Corp. Level 5-2 maps of the detailed Zone 2 vein architecture in relation to units 3.0 and 4.3 contact and D_2 shears.*

The mineralized zone is up to 900 m in strike length, varies in width from 15 to 60 m, and has been traced for at least 600 m down dip along its plunge of 55° along a WSW trend. It consists of two principal stockwork zones, along with a more diffuse and discontinuous footwall subzone along the contact between units 3.0 and 4.3. Most of Zone 2 is hosted within the unit 4.3 felsic sill complex and within slivers of mafic volcaniclastic strata between sills. Within 100 m of the Doyon Fault the vein stockworks cross into the footwall unit 3.0 mafic breccia unit as it strikes southward across the dominant S_2 schistosity. There is an oblique sinistral displacement of approximately 40 m of Zone 2 along the D_3 Doyon Fault. To the west of the Doyon Fault the Zone 2 vein system strikes E-W parallel to the strong S_2 shear foliation for 100 m before it transitions into the eastern end of the West Zone vein stockwork (Figs. 13 and 17). The E-W Zone 2 vein set west of the Doyon. The Zone 2 vein stockworks include two principal sets of auriferous quartz-carbonate-sulphide veins (Figs. 14 and 17). The main set strikes on average ESE with dips ranging from 40 to 60°. The dominant east striking S_2 foliation crosses this vein set at a 15° angle and in places the associated deformation has caused the veins to buckle, be offset, and become brecciated. The second auriferous vein orientation is hosted within a series of discrete D_2 shears that form an anastomosed easterly striking pattern at angle with the S_2 schistosity, and the ESE vein sets. These shears appear to have formed in highly sericitized wall rock to this second quartz-carbonate-sulphide vein set, in which veins are elongated, granulated, and segmented. Some shear segments also contain deformed quartz-carbonate veins with no visible sulphide. The ESE vein set is offset on a metres scale by the D_2 shears, most commonly in an apparent sinistral fashion, but locally with an apparent dextral offset. A second set of well-defined late D_2, moderate to steeply S-dipping discrete shears whose branches in places encapsulate sets of sigmoidal quartz-carbonate veins and associated pods of quartz-carbonate-pyrite-chalcopyrite± tourmaline.

The principal Zone 2 gold mineralization is hosted in centimeter to decimetre scale quartz-dolomite-calcite-pyrite-chalcopyrite veins, with 10-75% sulphide. Also present are smaller, secondary veins of pyrite-quartz and pyrite. Gold grade is related to the abundance of chalcopyrite (up to 10% in veins) and the presence of tellurides, including calaverite ($AuTe_2$), tetradymite ($Bi_2Te_2S_2$), and tellurobismuthite ($BiTe_2$) present as remobilized veinlets in both the vein sulphides and quartz gangue (Savoie et al., 1990).

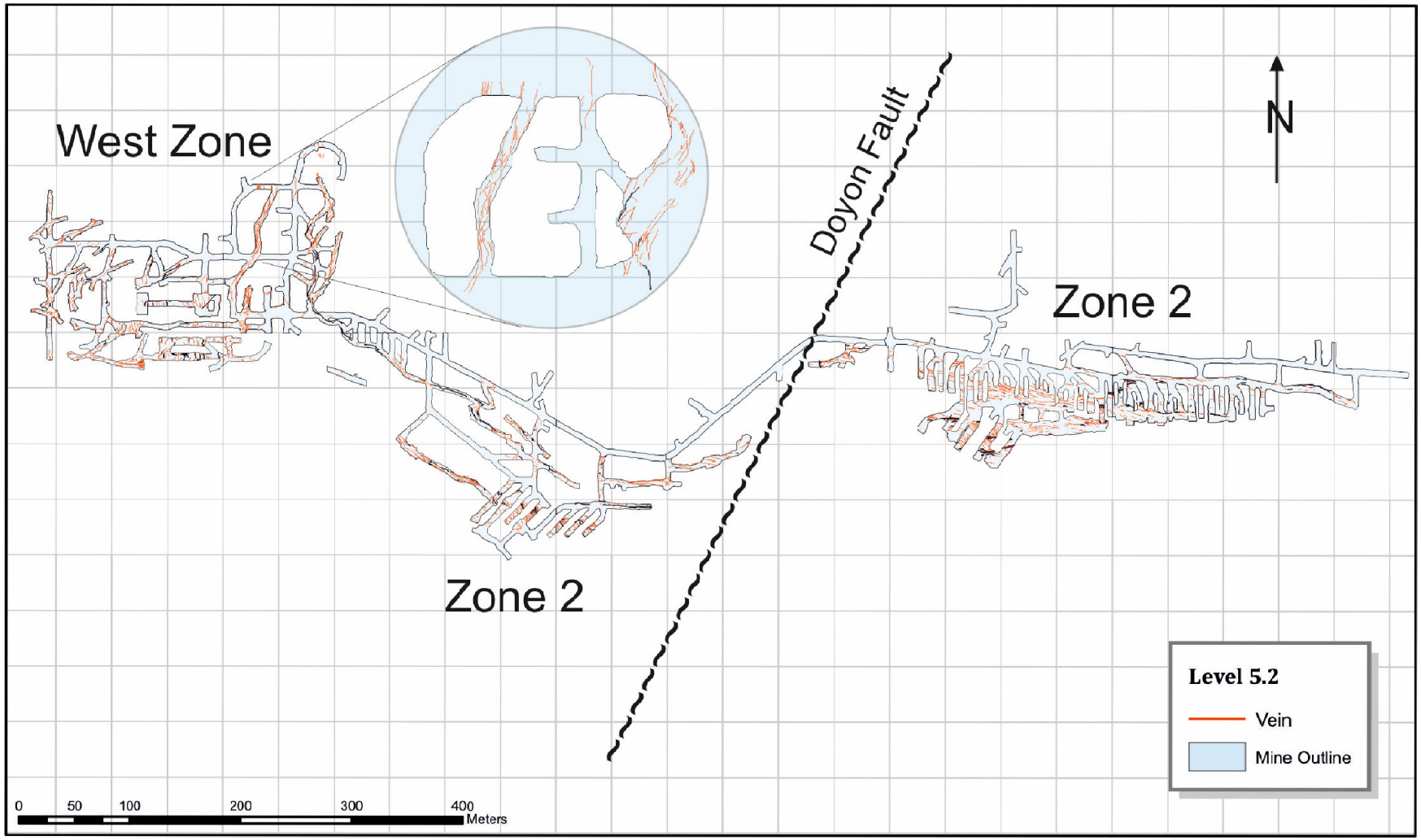
West Zone
Doyon Fault
N
Zone 2
Zone 2
Level 5.2
Vein
Mine Outline
0
50
100
200
300
400
Meters

Figure 17. *Vein distribution on Doyon mine Level 5 which connects Zone 2 with the West Zone. From the eastern, or right-hand side Zone 2 consists of an ESE striking vein array. It is offset sinistrally by the Doyon Fault, after which it curves to the NW to where the dominantly northerly trending West Zone vein array is located. Magnified inset shows the nature of the vein stockworks. Redrafted from the files of IAMGOLD Corp.*

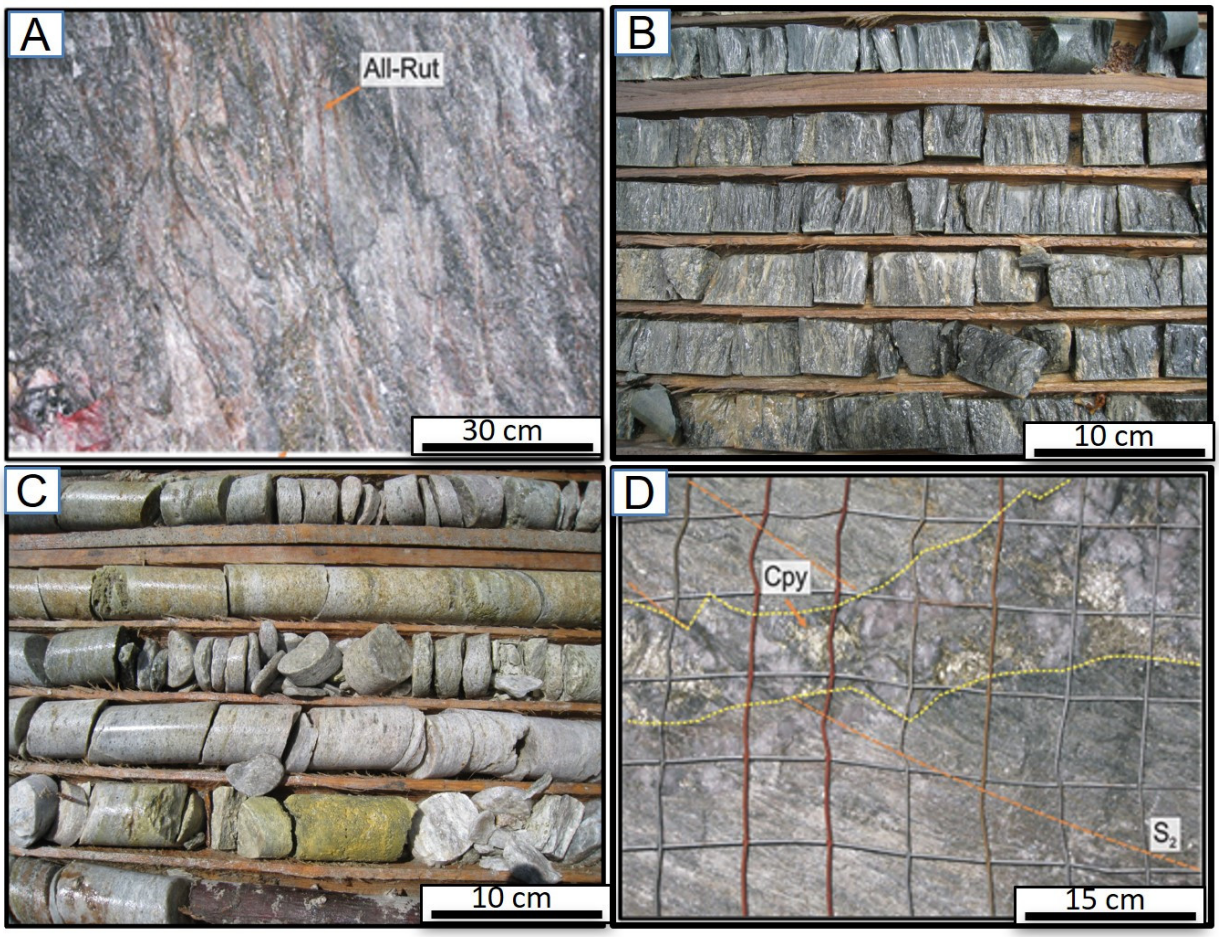

Figure 18. A*. Looking eastward at Zone 1 stope wall with characteristic dismembered auriferous quartz pyrite veins parallel to the D_2 shear foliation. Wall rock consists of quartz-sericite-pyrite-rutile-allanite schist with anastomosing quartz-rutile veinlets. Photograph by P. Mercier-Langevin, NRCan photo 2023-634.* ***B****. Chlorite-schist with 5% granoblastic pyrite, bleached intervals. Doyon Zone 2 footwall, ddh 11-832-58, 590'to 625'interval. Photograph by P. Mercier-Langevin, NRCan photo 2023-635.* ***C.*** *Sericite-quartz-pyrite-rutile schist with trace aluminosilicate porphyroblasts and/or grey quartz micro-phenocrysts, Doyon Zone 2 proximal hanging wall, ddh. 11-832-58, 375-400' interval. Photograph by P. Mercier-Langevin, NRCan photo 2023-636.* ***D****. Zone 2 auriferous quartz-pyrite-chalcopyrite brecciated during development of the the S_2 schistosity and offset by more discrete D_2 shears. Photograph by P. Mercier-Langevin, NRCan photo 2023-637.*

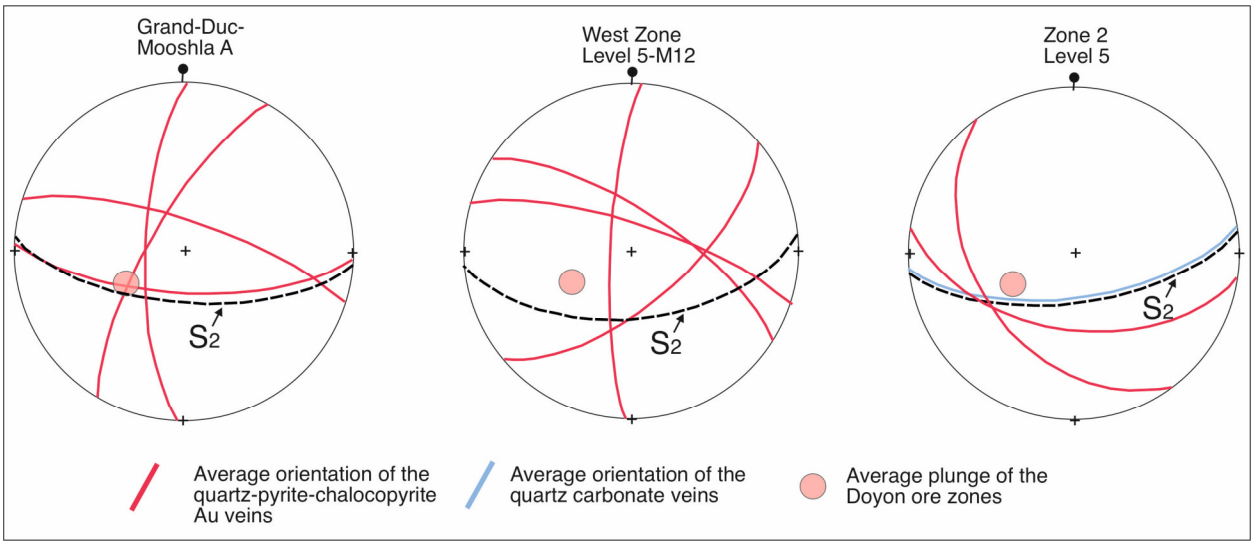

Figure 19. *Lower hemisphere stereograms (right to left) of vein orientations from Doyon Zone 2, West Zone, and the Grand Duc-Mooshla A zones. Although the average plunge of the Doyon vein systems lies close to plane for the S_2 foliation, it also lies along the plane of the dominant trondhjemite dyke set as shown in Figure 10.*

Doyon West Zone

The Doyon West Zone complex stockwork vein system has an E-W strike length of approximately 500 m and extends NNE away from the upper MIC contact for about 250 m. It has been traced down plunge 60-70º WSW to WNW for at least 1000 m.

The segment of Zone 2 west of the Doyon Fault was included in the mining plan for the West Zone and in fact merges with the West Zone *sensu stricto* arbitrarily at the upper MIC contact (Fig. 17). This east striking segment of Zone 2 is hosted within strongly sheared and altered unit 3.0 coarse mafic breccia and within unit 4.3 felsic sill complex (Figs. 20A and 21). Approaching the strongly altered MIC upper margin the vein array begins to curve eastwards to strike SE dipping 60º within the feldspar porphyry tonalite MIC border phase (Figs. 21 and 22). The S-striking, steeply W-dipping veins are hosted near surface mainly within the Doyon quartz diorite and porphyritic tonalite phases (Figs. 22 and 23). As the vein system crosses the contact with the trondhjemite both to the north and at about 150 m depth the vein population expands and intensifies to over 250 m wide, and the principal veins strike SSW to SW dipping on average 70º (Figs. 19 and 23). At about 200 m below the quartz diorite-trondhjemite contact the West Zone vein stockwork separates into a several arbitrarily defined higher grade (>3 g/t Au) N-S striking vein arrays (Figs. 21 and

23). On its western margin the West Zone stockwork system slowly dissipates over several hundreds of metres through a series of lower grade (<1 g/t Au) quartz-sulphide vein clusters that include the Grand Duc and Mooshla A zones (Figs. 13 and 14).

Although the principal West Zone vein arrays define a systematic variation in strike direction within the MIC from west to SW the more detailed vein architecture is more complex due to both differing primary vein orientations and overprinting deformation. Within the more uniform textured and homogeneous trondhjemite phase the primary architecture of the vein system is most apparent (Figs. 19 and 24). An overall reticular pattern dominates, with dominant, steeply dipping ENE-WSW and NNW-SSE trends, with trend dominance changing from the former to the latter with the change to the more felsic trondhjemite from more mafic quartz diorite and tonalite. In places the ENE-WSW dominant set has dextral jogs along the NNW-SSE trend, and in other instances these metre-scale dextral jogs take place across a series of NNW-SSE trending ladder veins (Fig. 26A). Both dominant vein sets show examples of bifurcation and branching that predate overprinting shear-related deformation.

Where the vein sets transect the Doyon quartz diorite and feldspar porphyritic tonalite the NNW-SSE vein set trends to a more southerly steeply dipping orientation. In exposures of the M vein system on Level 8-0 (Fig. 24) the NNW-SSE vein trend bends into this more southerly direction suggesting the change may be due at least in part to overprinting deformation. In places this vein set is strongly compressed and folded (Figs. 25 and 26B). Close to the volcanic-intrusive south contact the Iamgold Corp. mining geologists postulate that the vein arrays have undergone larger scale folding (Fig. 21) due to shortening during D_1 and D_2 events (Gosselin, 1998).

At the scale of individual veins there is abundant evidence for vein displacement and remobilization along S_2 foliation planes (Gosselin, 1998) (Fig. 25). This includes centimetre scale vein offsets and remobilization of principally chalcopyrite into piercement structures developed along S_2 foliation planes (Fig. 20B and C). The S_2 schistosity is observed to transect many of the veins, forming a sigmoidal pattern within the more altered vein margins, and brecciation and annealing of vein quartz (Fig. 25). The presence of planar and buckled quartz-sulphide veins with

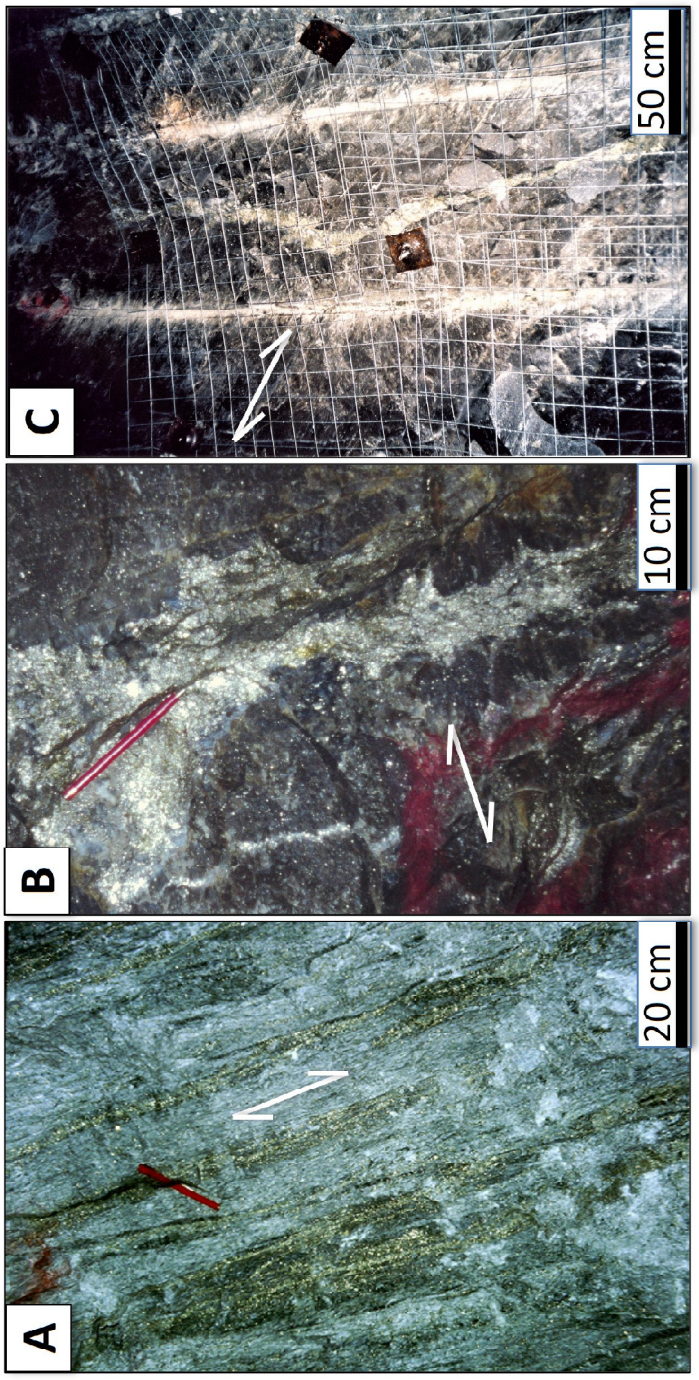

Figure 20. A. *Looking eastward at exposure of strongly deformed quartz-pyrite-chalcopyrite veins in a quartz-sericite-rutile-pyrite-(aluminosilicate) schist. Extension of Zone 2 west of the Doyon Fault. Level 9-1, Stope I-33 (4470 m, 655 m below surface). Photograph by A. Galley, NRCan photo 2024-0053.* ***B.*** *Deformed and brecciated quartz-pyrite-chalcopyrite vein with piercement structures formed by sulphides remobilized along the S_2 foliation planes. Level 8-0, Stope M12.). Photograph by A. Galley, NRCan photo 2024-0046.* ***C.*** *Series of West Zone quartz-pyrite-chalcopyrite veins with the veins and altered margins preferentially re-oriented along the S_2 schistosity planes. Photograph by G. Gosselin, NRCan photo 2024-0863.*

parallel strike directions (Figs. 20C and 26B) indicates that there may well be different stages of vein generation in relation to the deformation history of the deposit.

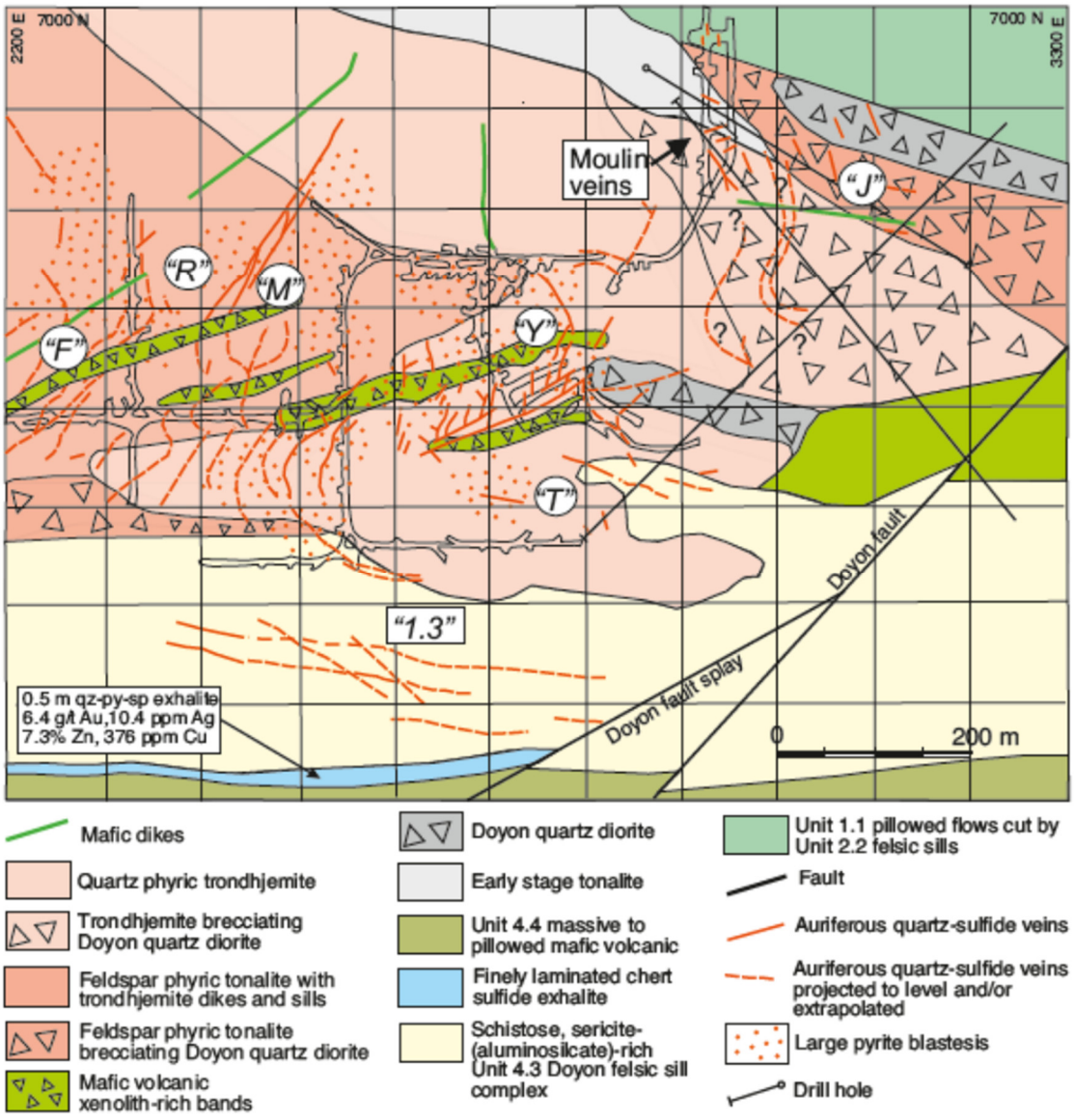

Figure 21. *Level 12-0 through the Doyon West Zone and extension of Zone 2 (marked "I.3") west of the Doyon Fault. The host MIC stratigraphy involves complex overprinting in time and space and the determined phase boundaries approximate to coincide where an intrusive phase becomes dominant. Much of the trondhjemite and feldspar porphyritic tonalite phases are quartz-sericite-pyrite-rutile altered to varying degrees. The red dots represent concentrations of pyrite-chlorite-epidote aggregates to 10 mm in size. Letters in quotation marks denote separate vein arrays as defined by the Iamgold Inc. mine geologists. Diagram modified from an Iamgold Corp. level plan. Elevation 4343 m at 657 m below surface.*

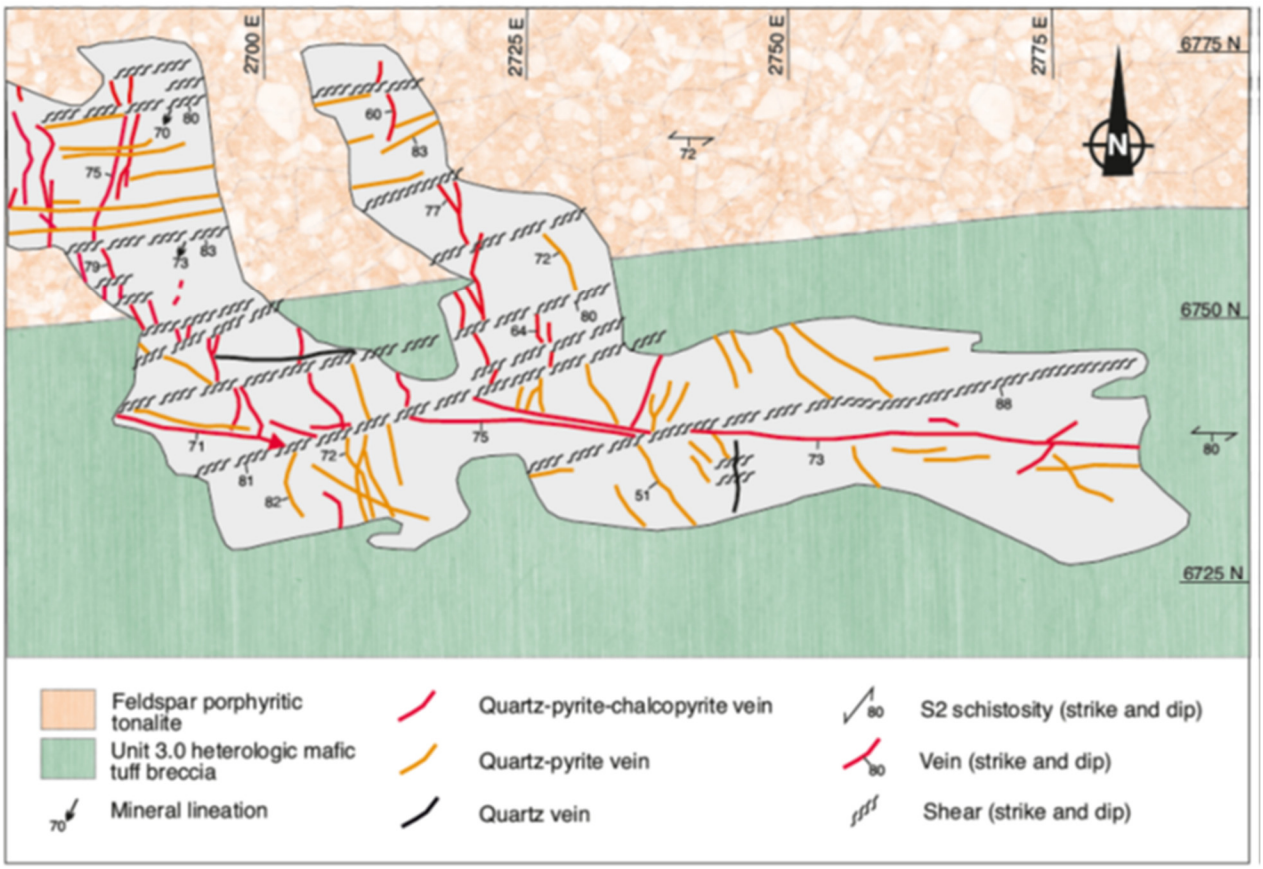

Figure 22. *Detailed map of the continuation of the E-W trending Zone 2 vein system intersecting the NNW trending West Zone vein stockwork as exposed in early stages of the West Zone open pit excavation. Note the acute angle between the Zone 2 veins and S_2 discrete shears that cross and offset the former (from Savoie et al., 1990).*

The vein system is further affected by a series of discrete, anastomosing shear zones present in the MIC and hanging-wall volcanic and intrusive units defined as the South and North shear zones (Marquis et al., 1990; Savoie et al., 1990; Gosselin, 1998) (Figs. 12 and 26C). These discrete shears are characterized by intense chlorite alteration (Doyon quartz diorite and porphyritic tonalite hosts) or sericite-quartz-rutile alteration trondhjemite and host highly deformed and dislocated segments of the Doyon quartz-sulphide and later quartz tourmaline and quartz carbonate veins. They vary in width from discrete slip planes to decimetre-wide shear zones (Figs. 25 and 26C).

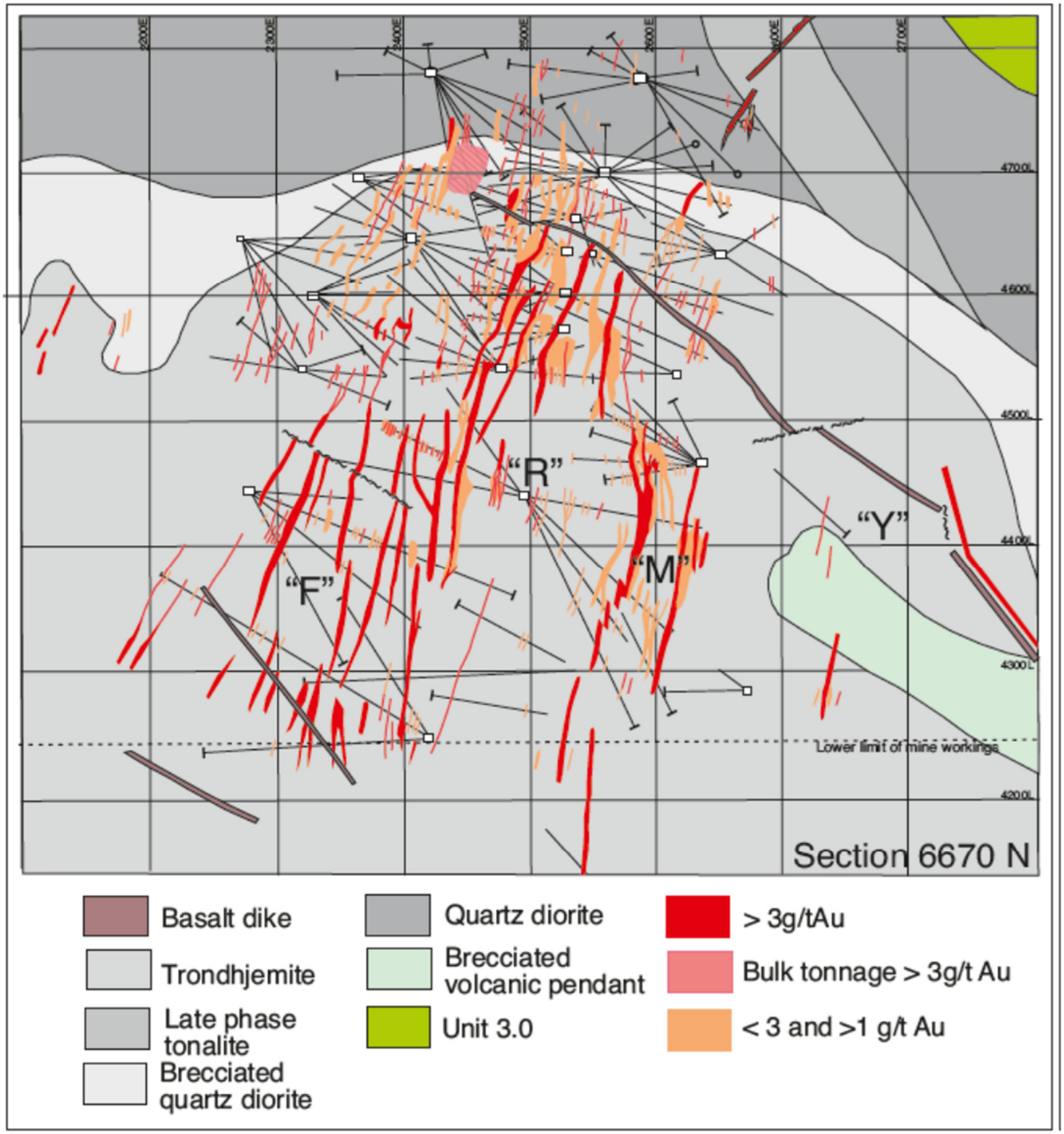

Figure 23. *Cross section section 6670 N looking north of the West Zone vein array (modified from Iamgold Corp. Doyon underground mine sections).*

The anastomosing North shear corridor crosses most of the West Zone striking east and dipping approximately 70º to the south. The dominant intersection lineation averages 146/61º. Vein dislocations and associated slickensides indicate dextral and sinistral reverse movement (Fig. 19).

This does not coincide with the moderate to steep SW plunge of the West Zone vein stockworks. The two foliations present (097° and 081° strike) are non-coaxial to the dominant stretching lineation and the 081° foliation is therefore considered to be refraction of the regional S_2 schistosity (Figs. 19 and 25).

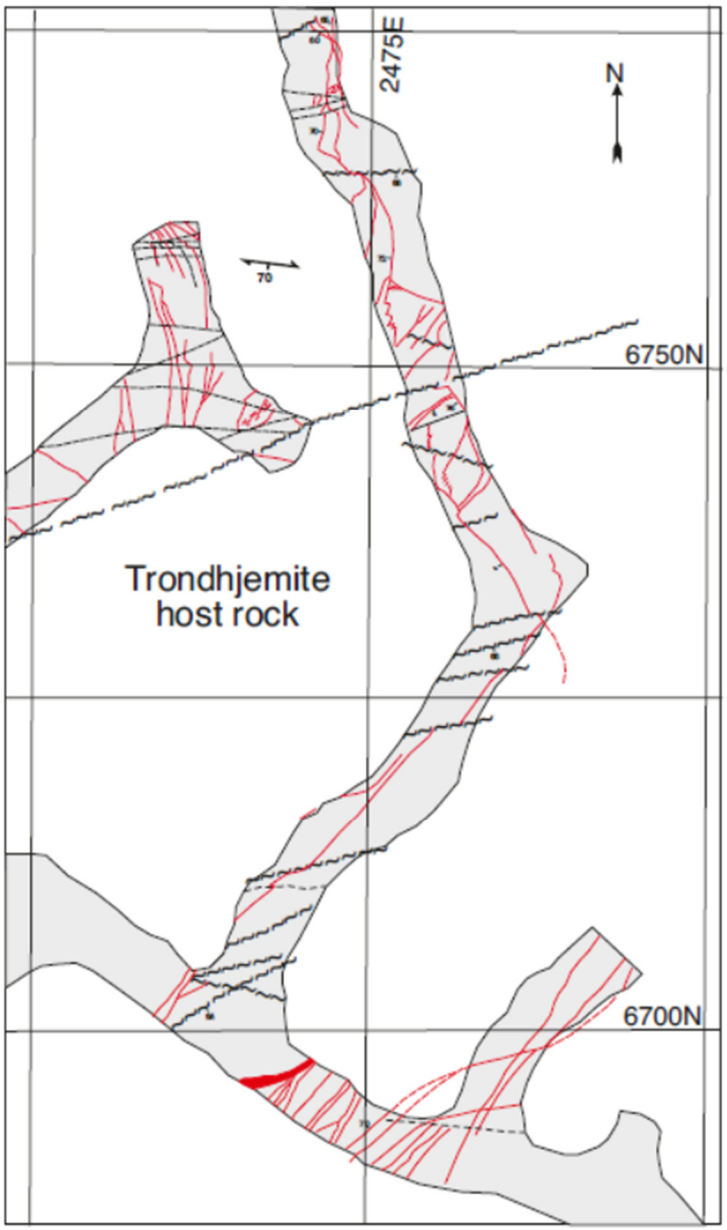

Figure 24. *Level 8 exposure of the West Zone M-12 vein system hosted within the MIC trondhjemite with a more rectilinear configuration than the veins strongly deformed and re-oriented along the south margin of the Au zone. Note that in places the quartz-sulphide veins are interconnected with longer veins commonly curvilinear. Some buckling and offset by both the S_2 regional schistosity and the more discrete D2 shears. Reproduced from Iamgold Corp. level plans.*

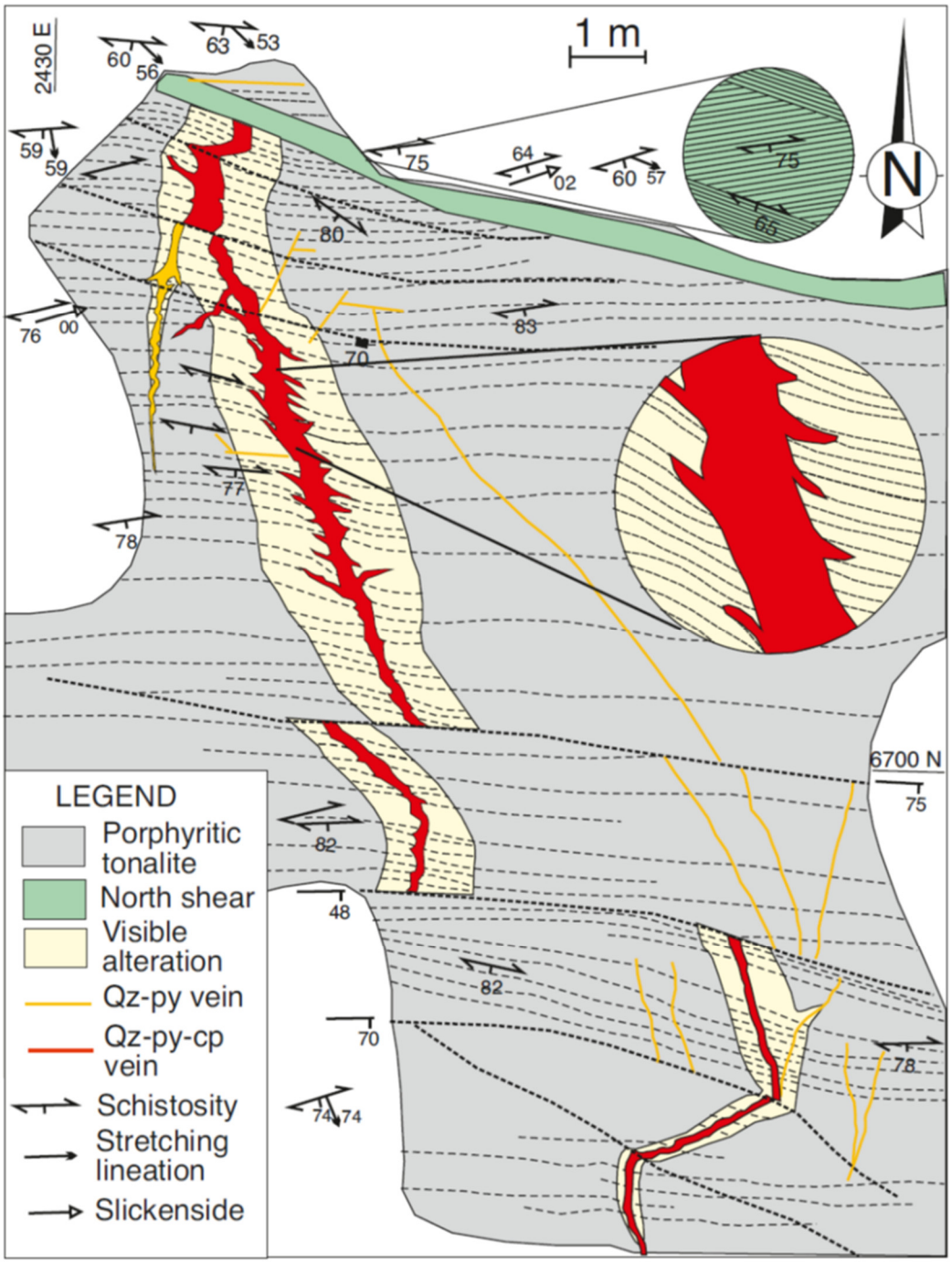

Figure 25. *Segment of a north-south vein illustrating the overprinting effects of the D2 deformation and subsequent offsets by later D_2 discrete shear planes. Vein E-20, Level 4 (4770 m elevation, 230 m below surface) (from Gosselin, 1998).*

The South shear corridor borders the southern extent of the West Zone but overprints the Zone 2 extension west of the Doyon Fault. It is oriented 103/76° and contains a steeply dipping stretching lineation (220/72°) overprinted by sub-horizontal striations plunging 097/05° (Fig. 19). This suggests that early oblique reverse movement along the south shear corridor evolved to dominantly strike slip. Within the MIC intrusive host phases, the primary auriferous vein system consists of quartz (5–95%), pyrite (5–60%), chalcopyrite (trace to 80%), and trace sphalerite, pyrrhotite, galena and bornite (Gosselin, 1998). Gold grades are empirically higher, with higher Cu grades even though the correlation coefficient between the two elements at deposit scale is <0.6. Gold is present as native Au and, in Au tellurides, including petzite (Ag_3AuTe_2), calaverite ($AuTe_2$), and hessite (Ag_2Te) (Neyedley et al., 2021a). Subsidiary gangue minerals include dolomite and calcite (Savoie et al., 1990). The principal vein sets range up to 25 cm thick, with the larger veins traced for up to 200 m. The vein stockwork changes composition with the West Zone vein stockworks more chalcopyrite-rich and contain more calcite (2–5%) than dolomite than the Zone 2 veins.

In at least some cases, the veins appear to be composite, with separate parallel to crosscutting zones of pyrite-chalcopyrite and quartz and quartz-carbonate veins and pods (Fig. 27A). Internal vein brecciation of the thicker quartz-carbonate-sulphide veins resulted in a *durchbewegung*, or pseudo-breccia character, with subrounded vein quartz domains in a remobilized sulphide matrix (Fig. 27b). Vein quartz is polygonized and elongate parallel to S_2. Gold and tellurides occupy small fractures that transect both sulphides and gangue minerals. Thin veinlets of pyrite and/or chalcopyrite in the host rocks to the larger quartz-sulphide veins indicate remobilization of the sulphides (and accompanying Au) to outside of the primary veins.

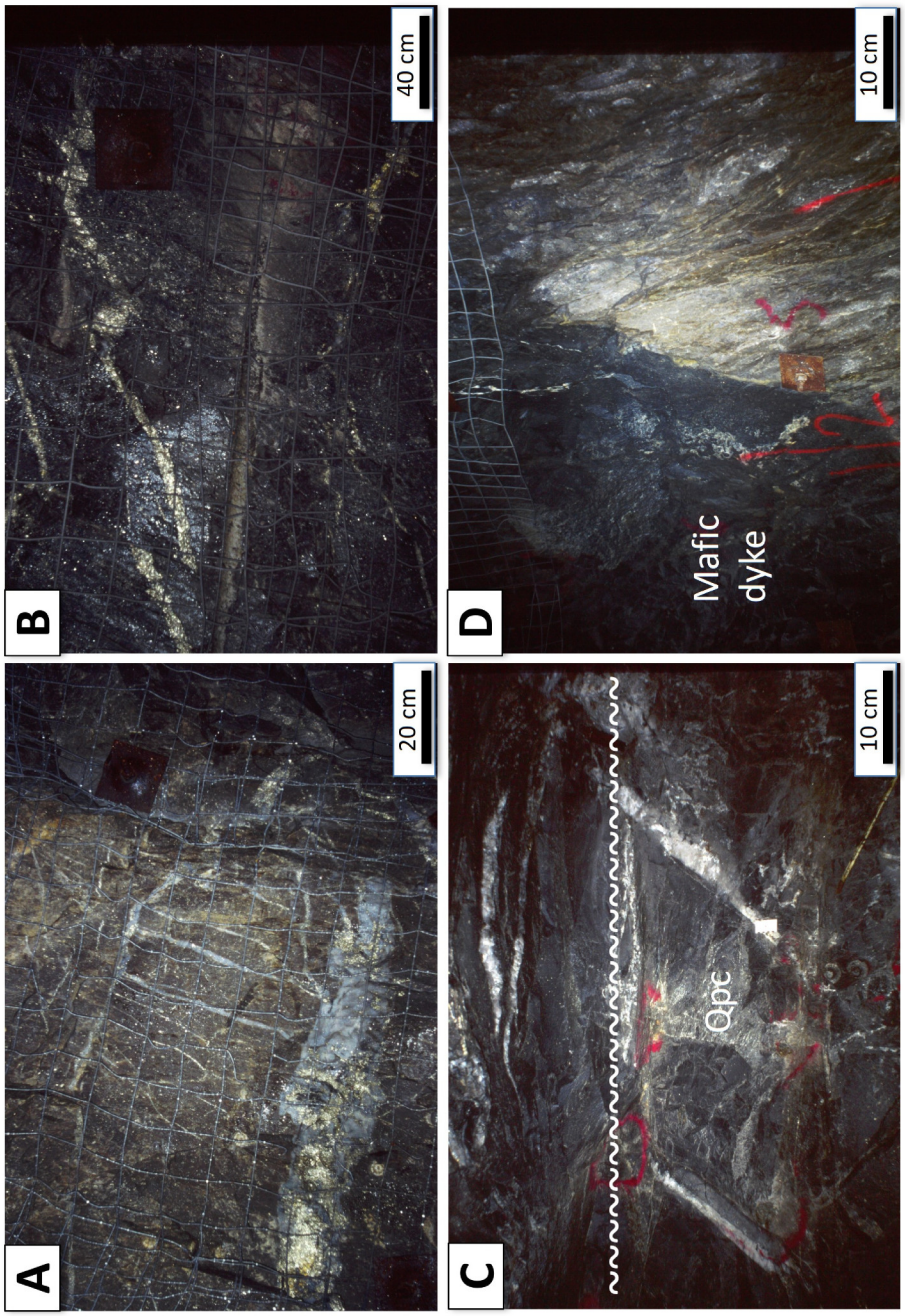

Figure 26. A. *Ladder veins attaching two quartz-pyrite-chalcopyrite veins with a dextral step out to the east. Looking at the back, with north to the right (Level 9-2, M12 main vein, 655 m below surface). Photograph by A. Galley, NRCan photo 2023-641.* ***B.*** *North-south pyrite vein buckled perpendicular to S_2 with later offset along a D_2 shear plane. Note late planar tourmaline vein with bleach margin crossing the pyrite vein Level 9-2, F48 vein set). Photograph by A. Galley, NRCan photo 2023-642.* ***C.*** *East-west D2 shear truncating previously deformed quartz-pyrite-chalcopyrite vein (Qpc) and more planar quartz-carbonate veins (Level 9-2, Stope T-15) Photograph by A. Galley, NRCan photo 2023-643.* ***D.*** *Chlorite altered mafic dyke sharply truncates previously highly deformed quartz-pyrite-chalcopyrite vein (Level 9-2, M12 main vein, Stope Y2-3). Photograph by A. Galley, NRCan photo 2023-644.*

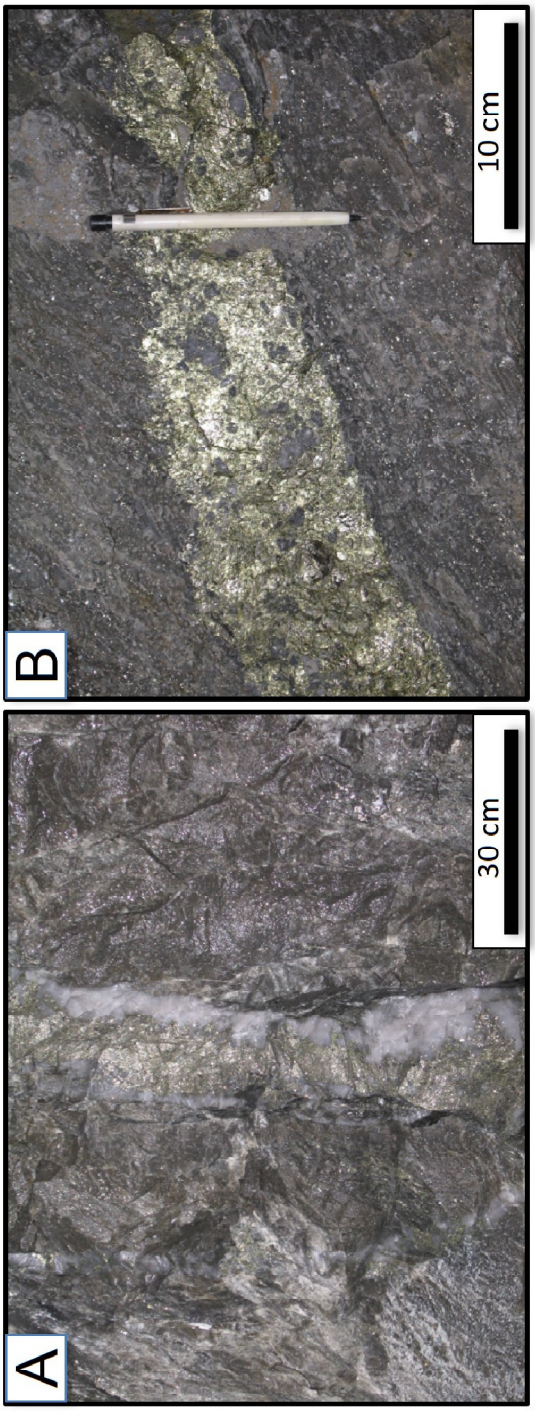

Figure 27. A. *Auriferous north-trending quartz-pyrite-chalcopyrite in trondhjemite with a separation of quartz and sulphide components. Level 8-0 Stope M12. Photograph by P. Mercier-Langevin, NRCan photo 2023-645.* ***B.*** *High grade (up to 60 g/t Au) chalcopyrite-rich vein with angular fragments of original quartz matrix. In some cases, brecciated auriferous vein contain strongly sericite-altered wall rock fragments. Level 8-0 Stope M12. Photograph by P. Mercier-Langevin, NRCan photo 2023-646.*

The Grand Duc and Mooshla A gold zones

Auriferous quartz-pyrite-rutile-(chalcopyrite) and quartz-carbonate-chlorite-pyrite-chalcopyrite vein stockworks and disseminations extend WNW from the Doyon West Zone at least as far as the eastern end of the MIC late Doyon phases and is collectively referred to here as the Grand Duc-Mooshla A (GDMA) vein array (Figs. 13 and 28). The veins form two east-west trending domains near the bottom and top of the trondhjemite composite sill complex that are spatially associated with two zones of increased sericite alteration accompanied by a series of anastomosing quartz-sericite-pyrite-rutile enriched shear zones (Figs. 29A-D). In the Grand Duc open pit, these two mineralized corridors are informally referred to herein as the CT zone (~5 m-thick, between 1 and 2 g/t on average), in the trondhjemite and xenolith-rich contact zone (Dbx phase of Galley and Lafrance, 2014), and the ”Diluted zone” (~5–10 m thick, 0.8 to 1 g/t Au on average), within the trondhjemite (Fig. 30A), both being part of the same broad E-W sericite-altered corridor. The planar sericite-rich zones are “stratiform” within the trondhjemite sill complex and may be controlled in part by primary grain size variation, zones of increased xenolith concentration, and miarolitic cavity density. The accompanying auriferous vein arrays are connected by a N-S striking vein array along the east and west margins of the NE trending Proterozoic diabase dyke (Fig. 28). Although the mineralized envelope is E-W with disseminated pyrite and pyrite-chalcopyrite-quartz-chlorite±carbonate veins and dm-thick masses (boudinaged veins: Fig. 30B, C and D), both the CT and “Diluted” zones contain discontinuous N-S veinlets that are difficult to model (capped at 35 g/t Au) because of drilling pattern, vein size and lack of continuity, but nonetheless contribute significant gold to the GDMA

The vast majority of the GDMA vein array is hosted within the trondhjemite phase. Anomalous Au values are also present in thinner trondhjemite sills and dykes hosted within the Doyon quartz diorite. There are isolated occurrences of auriferous quartz-sulphide veins within both the feldspar tonalite and hanging-wall quartz diorite. No extension of the GDMA auriferous quartz-sulphide vein array is recognized below the contact between the trondhjemite sill complex and the underlying early-stage MIC phases.

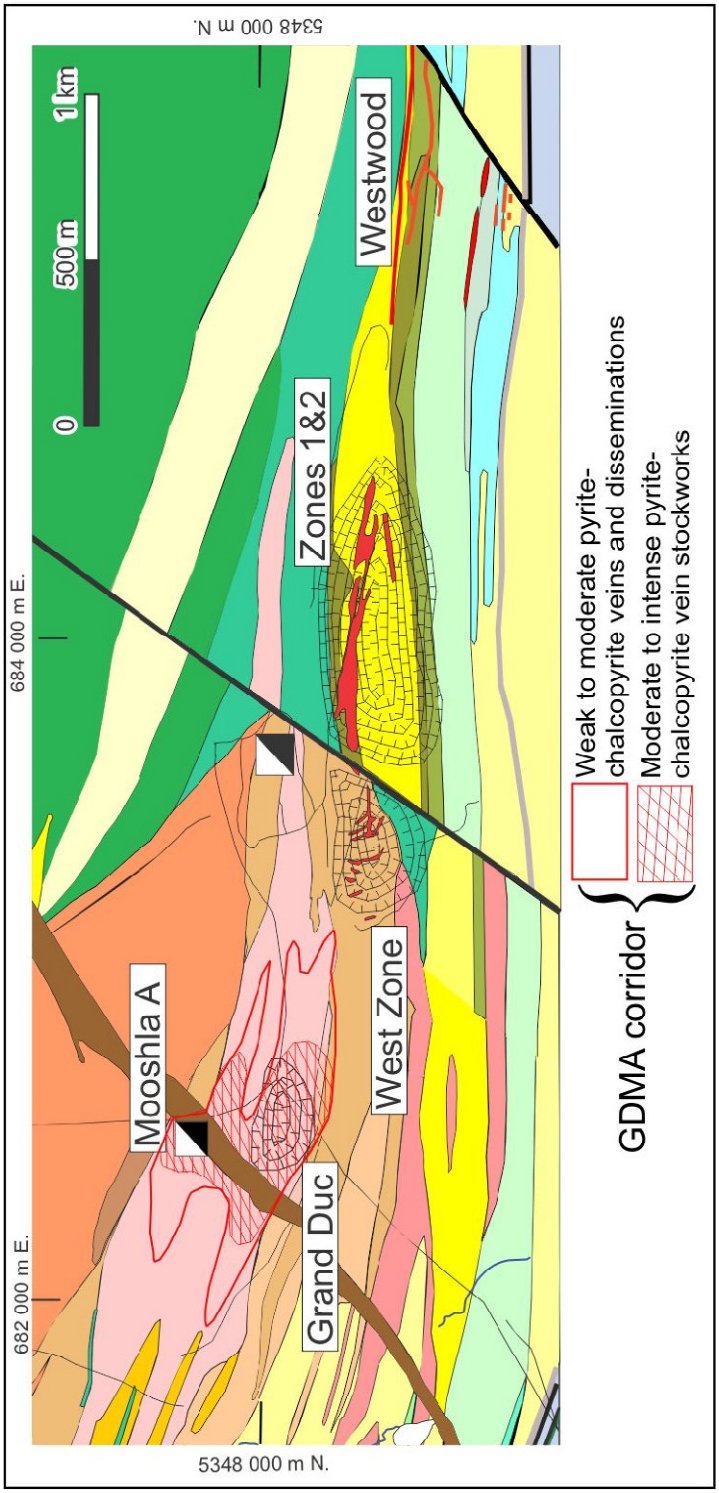

Figure 28. *Widespread envelope of auriferous pyrite-chalcopyrite veins stockworks and disseminations extend from the West Zone eastwards and is defined herein as the GDMA corridor. Black line represents the Doyon Fault. See Figure 5 for geology legend. Map modified from Iamgold Corp. company files.*

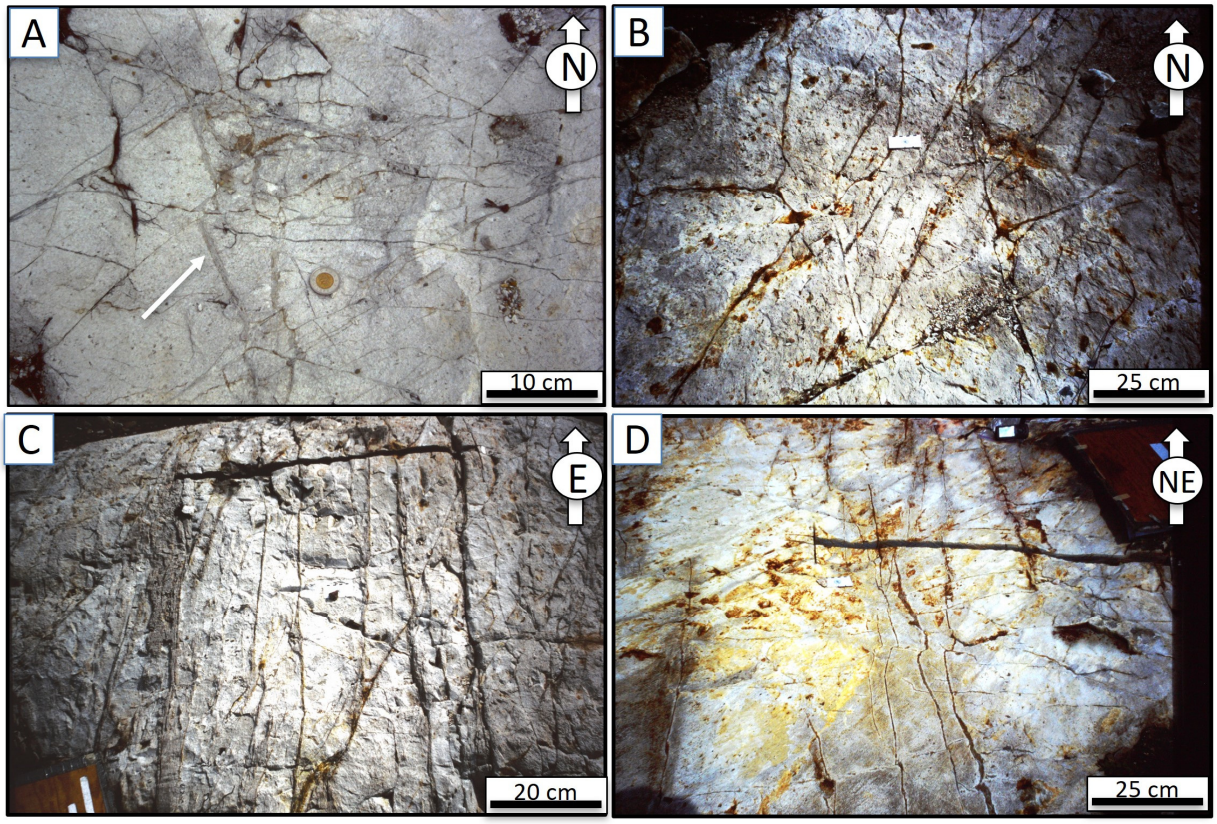

***Figure 29. A**. A spiderweb-like array of thin quartz-pyrite veins with dominant NE and WNW trends typical of the GDMA vein system away from the west striking anastomosing shear zones. Note that the vein array offsets an earlier set of quartz-sericite-rutile veins (white arrow). UTM NAD 83, Zone 17, 682190 E, 5348011 N. Photograph by A. Galley, NRCan photo 2023-651. **B.** A denser set of auriferous quartz-pyrite veins forming a stockwork. Darker patches of trondhjemite are more sericite rich. UTM NAD 83, Zone 17, 682219 E, 5348044 N. Photograph by A. Galley, NRCan photo 2023-652. **C.** Strong set of W-striking planar (sheeted) quartz-pyrite veins interconnected with NE and WNW striking veinlet. They cross the wider quartz-sericite-pyrite-rutile filled fracture on the left-hand side of the photo, which is the same as documented in Figure 28c with anastomosing shear zone immediately further west. UTM NAD 83, Zone 17, 682219 E, 5348044 N. Photograph by A. Galley, NRCan photo 2023-653. **D.** Strong NE striking quartz-pyrite-(chalcopyrite) vein set within the present Grand Duc mining envelope. Note the halo of sericite-rich alteration (grey colouration). UTM NAD 83, Zone 17, 682304 E, 5347962 N. Photograph by A. Galley, NRCan photo 2023-654.*

The GDMA auriferous quartz-sulphide vein array is densest east of the Proterozoic diabase dyke where it was formerly known as the Low-Grade Zone and is the focus for production at the newer Grand Duc open pit (Figs. 14 and 28). Individual veins are up to 10 cm in width and assay up to

ten to hundred g/t Au, but their sparse density and uneven distribution make for an overall lower grade (0.65 g/t Au or less for the entire area, with slightly richer corridors such as the CT zone) than the cut off grades for the Doyon mine past producing ore bodies (Fig. 31). At the northernmost limit of the Au trend is a series of several south and SW striking, larger quartz-sulphide veins up to 15 cm in width that comprise the Mooshla A gold zone (Filion et al., 1977) (Fig. 28).

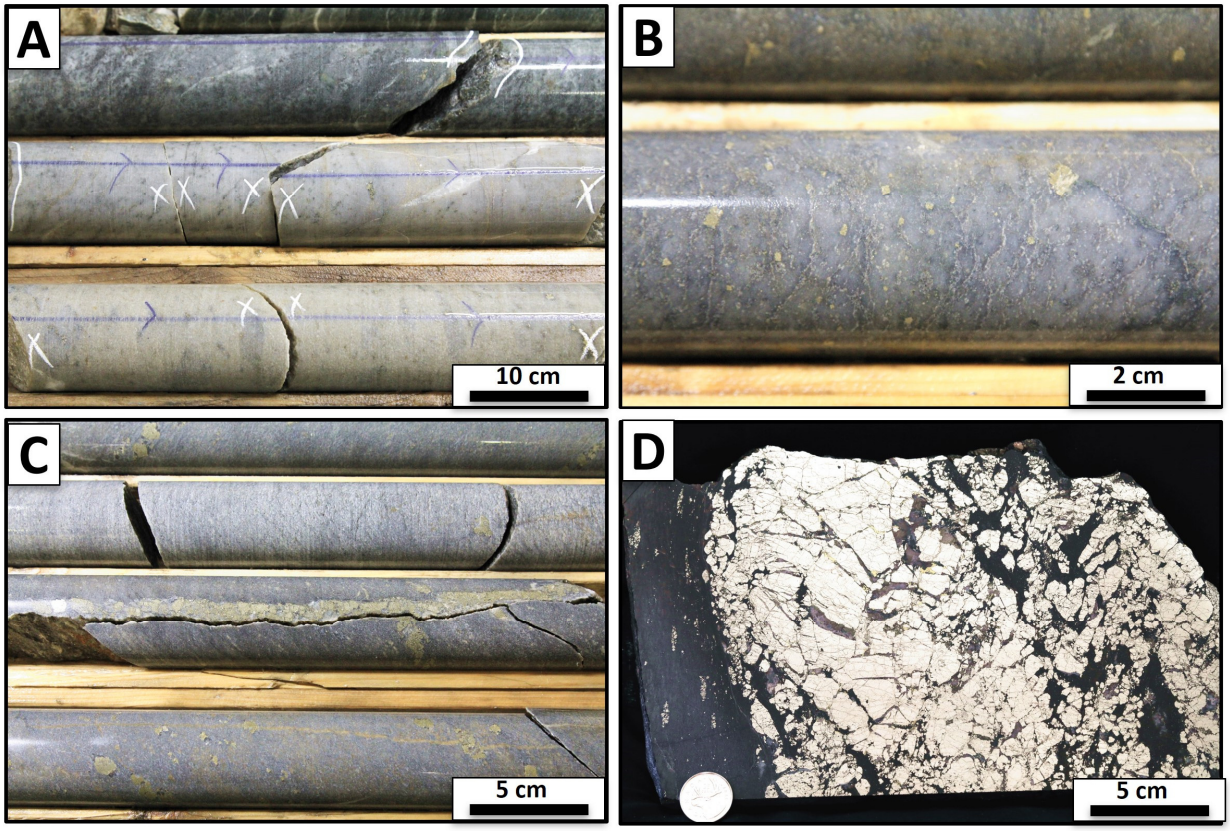

***Figure 30**. **A**. Contact between unmineralized phase E Doyon quartz diorite (top of photograph) and the sericite-altered trondhjemite host of the Grand Duc CT zone, ddh SGD-1999-21, 20-25m. Photograph by P. Mercier-Langevin, NRCan photo 2023-647. **B**. Disseminated granoblastic pyrite in sericite-altered trondhjemite, ddh SGD-1999-21, 85m. Photograph by P. Mercier-Langevin, NRCan photo 2023-648. **C**. Deformed N-S pyrite-carbonate-quartz vein in trondhjemite, Grand Duc zone, ddh SGD-199-21, 115m. Photograph by P. Mercier-Langevin, NRCan photo 2023-649. **D**. Large (~30 cm thick) mass of deformed granoblastic pyrite with traces of interstitial chalcopyrite, Grand Duc zone. Photograph by P. Mercier-Langevin, NRCan photo 2023-650.*

The vein architecture of the Grand Duc-Mooshla A vein system is much the same as the other described gold zones at the Doyon deposit (Figs. 19 and 32). The dominant vein strike is SSW and dipping steeply to the west. Several of the longer auriferous quartz-sulphide veins, including the

set defining the Mooshla A deposit, strike southerly, again with steep dips. The E-W s vein arrays are overprinted by the E-striking steeply S-dipping, sericite-quartz-pyrite-rutile-rich anastomosing shear zones, with dismembered and deformed veins present within the shears (Figs. 19 and 29C-D). The shear zones overprint, deflect, and crenulate the regional S_2 foliation to a strike of N130/75 with fold axes plunging N225/80.

Away from the discrete sericite-rich high strain zones the quartz-sulphide veins have a well-defined WSW-NNW rectilinear pattern with the veins forming an interconnected array (Figs. 19, 29 and 32).

The principal vein sulphides at Grand Duc are pyrite and chalcopyrite, with subsidiary sphalerite and pyrrhotite. Accessory ore minerals at Grand Duc are comprised of tellurobismuthite (Bi_2Te_3), volynskite ($AgBiTe_2$), native Te, tsumoite (BiTe) or tetradymite (Bi2Te2S), altaite (PbTe), petzite, calaverite, and hessite (Neyedley et al., 2021a). Gold grades tend to be higher in the presence of chalcopyrite, but as in the West Zone the Au-Cu correlation is not always consistent. Gold is also preferentially associated with zones of pyrite, either disseminated or in veins/boudinaged veins.

Spatially associated with the principal quartz-pyrite-chalcopyrite vein arrays are a number of other vein stockworks and micro-breccias. Thin millimetre-scale pyrite±chalcopyrite vein stockworks are common and can account for multi-gram Au assays in places. Also common are chalcedonic quartz infilled micro-breccias and coarser-grained quartz vein stockworks with minor sericite, chlorite and carbonate. The quartz-sericite-rutile ±carbonate alteration zones commonly contain thin sericite-rutile, sericite-epidote and sericite-quartz-rutile veins. Also common are veins and veinlets of quartz-chlorite-pyrite ±epidote/clinozoisite and carbonate. Gypsum is present in some veins. Tourmaline is also a common constituent of both quartz-sericite and quartz-chlorite veins. The only veins that cut across the principal auriferous quartz-sulphide vein array are extensional quartz-carbonate and quartz-tourmaline veins. The latter can contain remobilized pyrite and chalcopyrite from the principal quartz-sulphide veins and can themselves be auriferous.

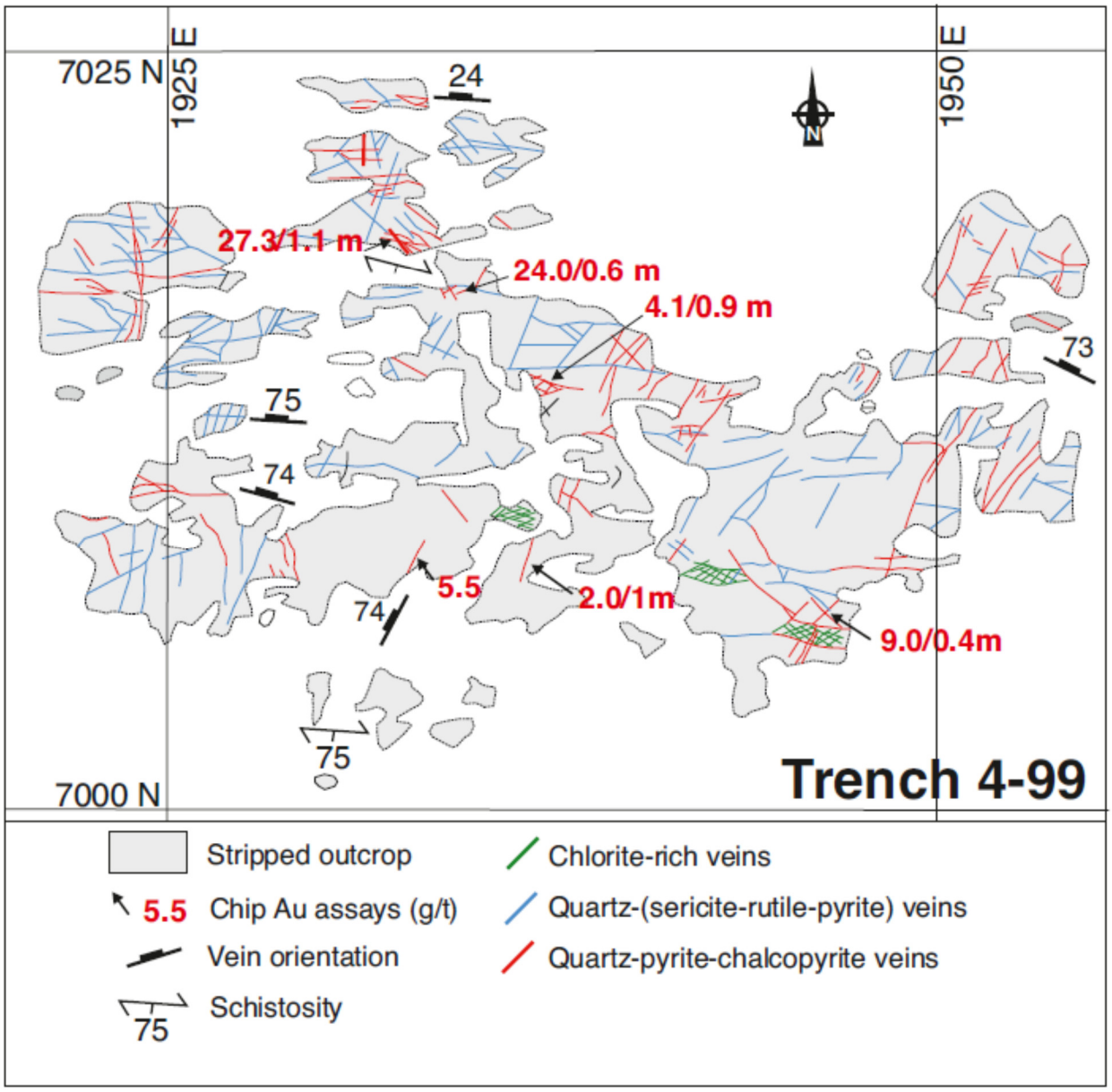

Figure 31. *Outcrop map of part of the trench system exposing the Grand Duc vein system hosted by trondhjemite at the centre of the present open pit mining operation. Channel sample assays indicate the range of Au values within the dominantly SE striking quartz-pyrite-chalcopyrite vein set. Blue coloured veins represent both quartz veins in which no Au was detected, and older quartz-sericite-rutile veins. Trench map copied from Iamgold Corp. files. Location denoted by Doyon mine grid.*

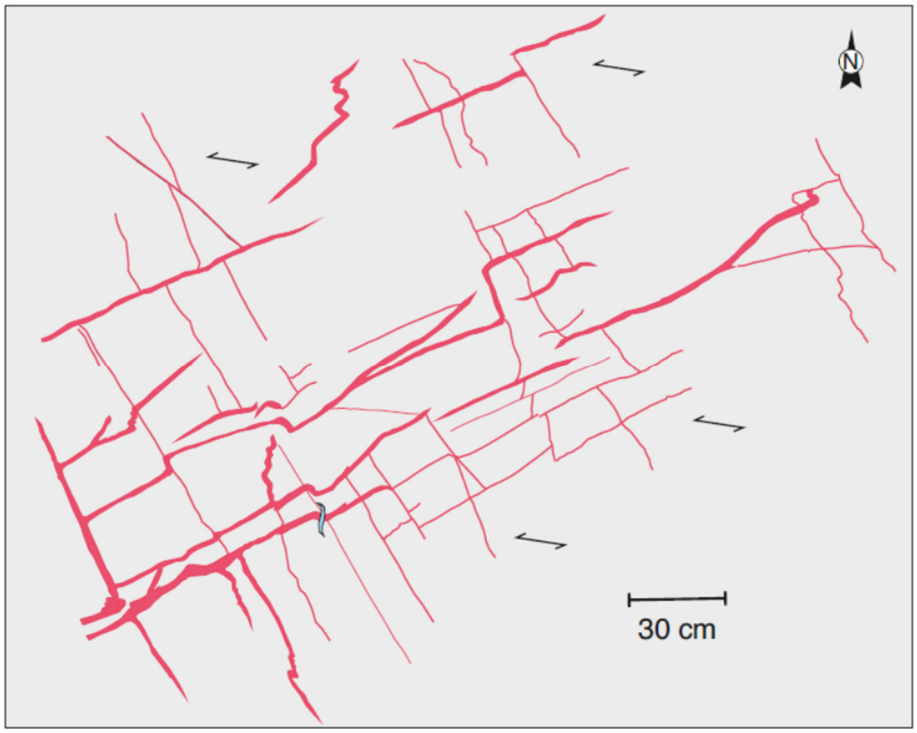

Figure 32. *Drawing from Figure 29D photo illustrating in greater detail the interconnected nature of the auriferous quartz-pyrite-chalcopyrite system and the dominant SW strike of the vein array. Note that the vein segment at high angle to foliation show evidence of buckling. UTM NAD 83, Zone 17 682304 E, 5347962 N.*

ALTERATION SPATIALLY ASSOCIATED WITH THE DOYON AU(-CU) MINERAL SYSTEM

Defining alteration facies spatially associated with the Doyon Au(-Cu) vein system is complicated by overprinting of pre- and syn-magmatic-hydrothermal and hydrothermal fluid events in the MIC and its host volcanic rocks, an inhomogeneous distribution in primary host rock composition, and the effects of multiple deformation events, and syn-main regional deformation prograde and retrograde regional metamorphism. Pre-auriferous quartz-sulphide alteration paragenesis and characteristics must be first described to better recognize the mineral and geochemical characteristic of the alteration associated with the overprinting Doyon Au(-Cu) event.

Volcanic-hosted hydrothermal alteration and mineralization

A volcanic-hosted hydrothermal alteration event was recognized by Belkabir and Hubert (1995) and Galley and Lafrance (2014) in the vicinity of the MIC and is temporally related to several cycles of DBL district-wide VMS seafloor hydrothermal activity (Dubé et al., 2007; Mercier-Langevin et al., 2020). These hydrothermal fluid cycles affect the volcanic stratigraphy hosting the MIC and can be traced from within the pillowed to massive flows of the upper part of the tholeiitic Hébécourt Formation up section to near the upper contact to the upper Bousquet Formation calc-alkalic volcaniclastic strata and flows (Yergeau et al., 2022a, b).

Hébécourt Formation alteration and mineralization

A ≥400 m-thick section of variably strained and altered unit 1.0 pillowed flows is present between unit 1b feldspar glomerporphyritic basaltic andesite north of the former Mic Mac mine site and the northern contact of the MIC phase D tonalite (Fig. 5). Within this upper section of the Hébécourt Formation the rocks are affected by several ductile to brittle ductile strain zones defined by moderate to strong shearing and cataclasis of various units of basalt, basaltic andesite, and rhyolite (Tourigny et al., 1988; Belkabir and Hubert, 1995; Belkabir et al., 1998; Lafrance et al., 2003). Kinematic indicators show that these steeply south-dipping features were generated in large part by high angle reverse motion directed to the north (Tourigny et al., 1988; Belkabir and Hubert, 1995). Lafrance et al. (2003) suggest that the high-angle reverse movement was originally formed

during thrusting with possible stratigraphic duplication within the upper Hébécourt Formation, although Belkabir and Hubert (1995) believe that the altered stratigraphy is generally homoclinal.

Massive flow facies have bleached thermal contraction features altered to quartz-epidote-albite and amygdales filled with actinolite, quartz, pyrite and pyrrhotite (Fig. 33A). These massive flow sections are cut by numerous veins and breccias infilled with epidote and quartz. The pillowed flow facies have moderately to strongly bleached margins altered to quartz-epidote-albite and amygdales filled with actinolite, pyrite, pyrrhotite and chalcopyrite (Fig. 33B). The variolitic pillow margins are cut by an extensive network of epidote veins and veinlets. Interpillow hyaloclastite is commonly gossanous and altered to actinolite, quartz and pyrrhotite ±magnetite. Outcrops exposing the footwall stratigraphy to the Mic Mac Au deposit consists of a succession of amygdaloidal pillowed and sheet flows, with subsidiary ameboid pillow breccia and interflow breccia. The pillowed breccia is sulphide-stained, silicified and epidote-altered along thermal expansion fractures and pillow margins. An outcrop directly south of the former Mic Mac Au mine site exposes a heterolithologic volcanic breccia containing a mixture of bleached and chlorite-altered mafic volcanic fragments as evidence that the bleaching event(s) due to hydrothermal alteration described above were almost certainly synvolcanic (Fig. 33C).

Both the Mic Mac and Mouska Au deposits are situated within this strongly deformed and altered succession of massive to pillowed andesitic basalt and basalt of the upper part of the Hébécourt Formation (Belkabir and Hubert, 1995; Asselin, 1999) (Fig. 5). The principal ore zones for both are hosted within a zone up to 20 m thick of chlorite-biotite schist bordered on both sides by chlorite schist that extends 1200 m between the two deposits. The chlorite biotite schist contains highly deformed massive to semi-massive auriferous pyrrhotite-chalcopyrite-pyrite-quartz vein stockworks (e.g., Zone 07 at the former Mouska mine). These highly deformed vein sets are overprinted by extensional quartz-pyrrhotite-chalcopyrite veins. At the Mouska deposit there was a further six ore zones comprised of deformed vein stockworks within parallel and discordant chlorite biotite schist zones between the Zone 07 and an overlying horizon containing a series of tholeiitic rhyolite domes that extends along the north margin of the MIC (Fig. 5. Near the margin of the intrusive complex the tonalite phase contains a metres-wide xenolith of rhyolite with a quartz-pyrrhotite-pyrite vein stockwork.

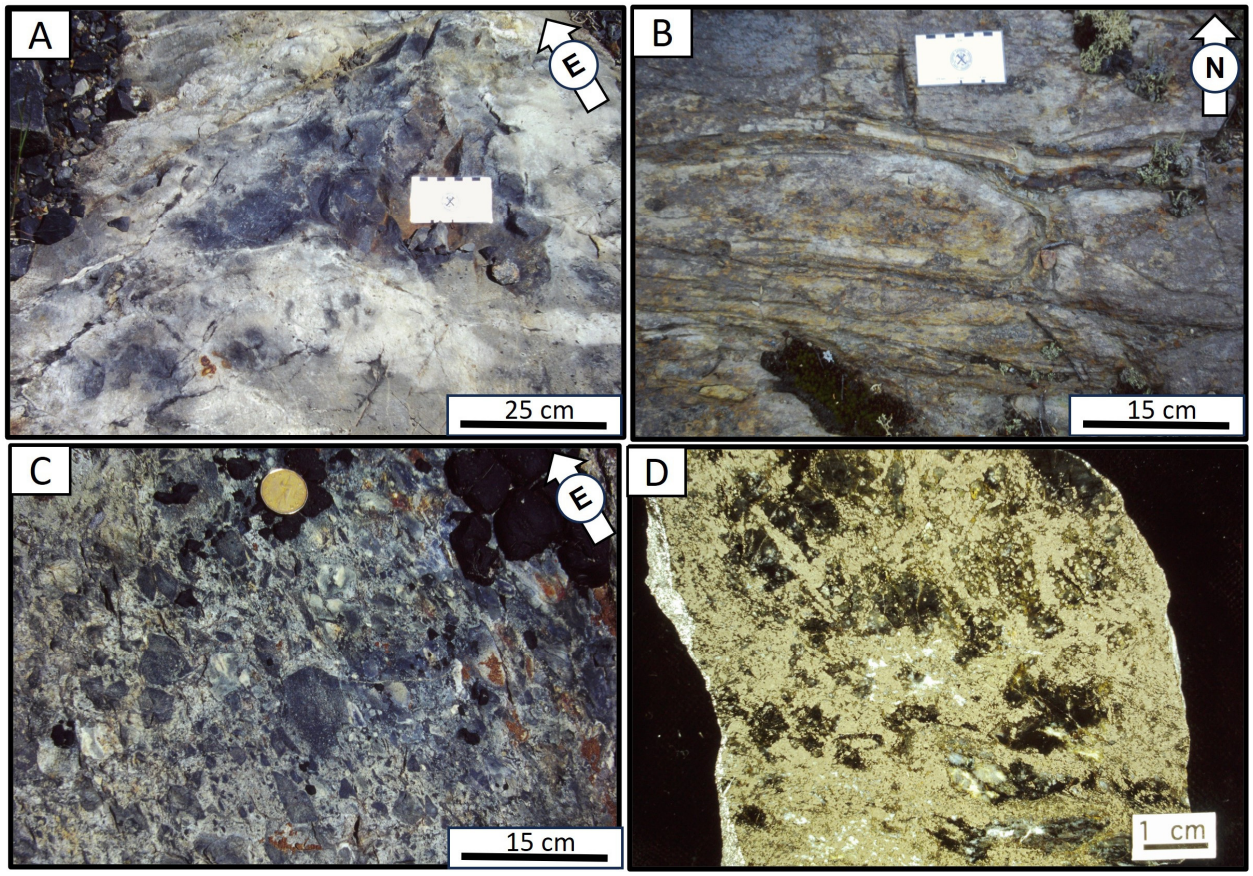

***Figure 33. A**. Unit 1.0 massive flow facies with heterogeneous bleaching caused by quartz-albite-epidote alteration commonly controlled by thermal cracks and amygdale concentrations. Cut by buckled epidote-quartz veins. UTM NAD 83, Zone 17, 682604 E, 5349308 N. Photograph by A. Galley, NRCan photo 2023-655. **B.** Unit 1.0 pillowed flow facies with strongly quartz-epidote-albite altered margins and amygdales infilled with actinolite. Interpillow hyaloclastite altered to quartz-actinolite and infilled with pyrrhotite, chalcopyrite and pyrite. Facing south. UTM NAD 83, Zone 17, 682604 E, 5349308 N. Photograph by A. Galley, NRCan photo 2023-656. **C.** Outcrop of unit 1.0 heterolithologic volcanic breccia immediately south of the Mic Mac former mine headframe. Note the infilling/replacement of inter-clast areas with quartz and sulphide. UTM NAD83, Zone 17, 681201 E, 5349699 N. Photograph by A. Galley, NRCan photo 2023-657. **D.** Polished grab sample from the Mic Mac mine dump of deformed pyrrhotite-chalcopyrite vein stockwork in strongly chlorite-altered rock. Photograph by A. Galley, NRCan photo 2023-658.*

There is no evidence elsewhere in the DBL of VMS-type mineralization within the upper section of the Hébécourt Formation. For the Mouska-Mic Mac system, it can be postulated that these chlorite-rich schist zones and accompanying auriferous sulphide vein stockworks define deformed VMS proximal alteration pipes (Belkabir and Hubert, 1995), but their origin is further complicated by an overprint at the Mouska mine of at least four (syn-D_2?) quartz-pyrite-pyrrhotite-chalcopyrite

vein stockwork zones within the early quartz diorite and tonalite phases of the adjacent MIC. They are hosted within up to 50 cm-wide zones of foliated, silica- and biotite-altered tonalite that parallel the easterly striking deformation zones containing the volcanic hosted vein systems (Asselin, 1999; Mercier-Langevin et al., 2007d).

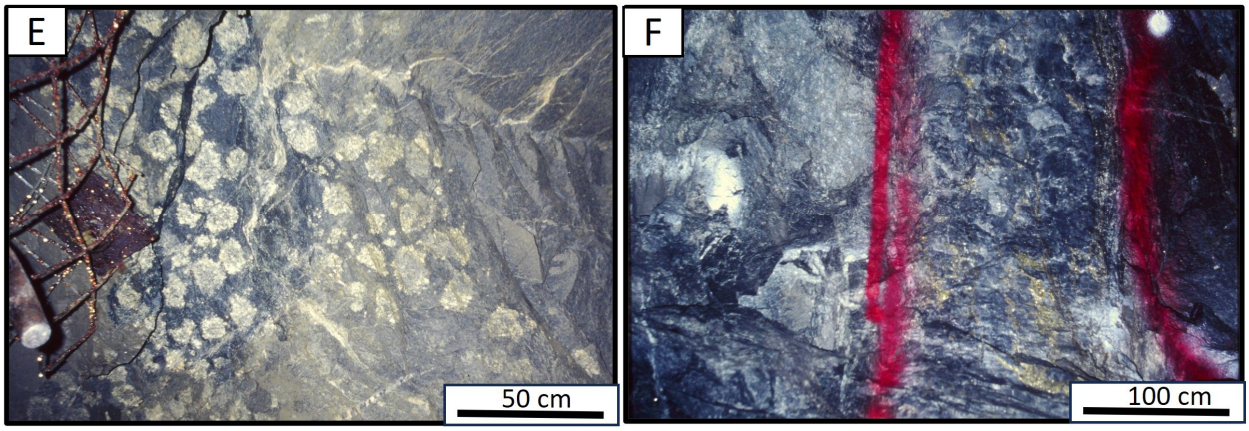

Figure 33. E. *Underground photo from the Mouska mine Zone 07 showing rhyolite fragments rimmed with euhedral feldspar crystals in a strongly chlorite-altered groundmass. Photograph by A. Galley, NRCan photo 2023-659.* ***F.*** *Underground photo from the Mouska Zone 07 showing a coarse rhyolite breccia with a strongly chlorite-altered groundmass containing pyrrhotite-chalcopyrite vein stockwork. Photograph by A. Galley, NRCan photo 2023-660.*

Bousquet Formation lower member alteration and mineralization

The overlying unit 3.0 of the Lower Bousquet Formation varies from dominantly amygdaloidal pillowed basalt (Fig. 34A) and associated hyaloclastite above the western hanging-wall contact of the MIC to mainly scoriaceous basalt breccia with thin interlayered ameboid basalt flows along the eastern flank of the intrusive complex (Fig. 5). Disseminated to semi-massive magnetite ±pyrite and chalcopyrite fills interpillow interstices and fills amygdales within the pillow tops. The scoriaceous breccias are partially to strongly bleached by albite-quartz-epidote ±pyrite alteration (Fig. 34B). This alteration is strongest along chilled clast margins. The altered pillowed basalts contain a weak vein stockwork of pyrite-pyrrhotite-chalcopyrite accompanied by quartz-chlorite-biotite-garnet alteration. Along the eastern margin of the MIC the bleached unit 3.0 flow units also contain significant amounts of intergranular anhydrite. Deformed carbonate-quartz veins are prominent throughout this unit. Thin mafic dykes present commonly have irregular to ameboid margins that are variably bleached, as are contained dyke contact flow-banding and contact parallel cooling fractures (Fig. 34C).

Bousquet Formation upper member alteration

The contact between unit 3.0 and the overlying unit 4.1 of the upper member of the Bousquet Formation is transitional, with interlayering of unit 3.0 bleached pillowed basalt with finely layered unit 4.1 dacite-rhyodacite tuff and lapilli tuff. This is readily observable on surface and in drill core stratigraphically above the western half of the MIC. From this contact up section to the 4.1-4.4a units contact, this dacite-rhyodacite unit is affected to varying degrees by discrete zones of primary feldspar destruction and accompanying Na depletion with chlorite-biotite and chlorite-sericite alteration. Nearer the overlying unit 4.4 contact there is an increase in the amount of carbonate present in the variably altered unit 4.1 strata.

These alteration zones are most intense near the base of unit 4.1 where it is interlayered with mafic rocks of unit 3.0. The alteration zones are associated with zones of sparse quartz-sulphide veining with anomalous Cu and Zn values. The alteration and associated Na depletion continues further west in unit 4.1 as zones of possible semi-conformable alteration affecting the hyaloclastite facies of the lobe-hyaloclastite flow complex. These zones of Na depletion can also be traced eastward in unit 4.1 up to the main bulk of the Doyon stage intrusive phases of the MIC. From both outcrop and drill core observation these altered strata are crossed by relatively unaltered dykes and thin sills of late-stage MIC feldspar porphyry tonalite.

The alteration of unit 4.4 basalt and basaltic andesite flows varies in degree and intensity. The western half of the unit is dominated by massive to pillowed flows. These flows are affected by weak to moderate chlorite-biotite-carbonate-pyrite alteration with subsidiary quartz and tourmaline. In places this includes sparse weak chlorite-biotite-pyrite vein stockworks. The eastern two thirds of this unit is dominated by coarse fragmental flows containing a spectrum of variably bleached and altered mafic clasts.

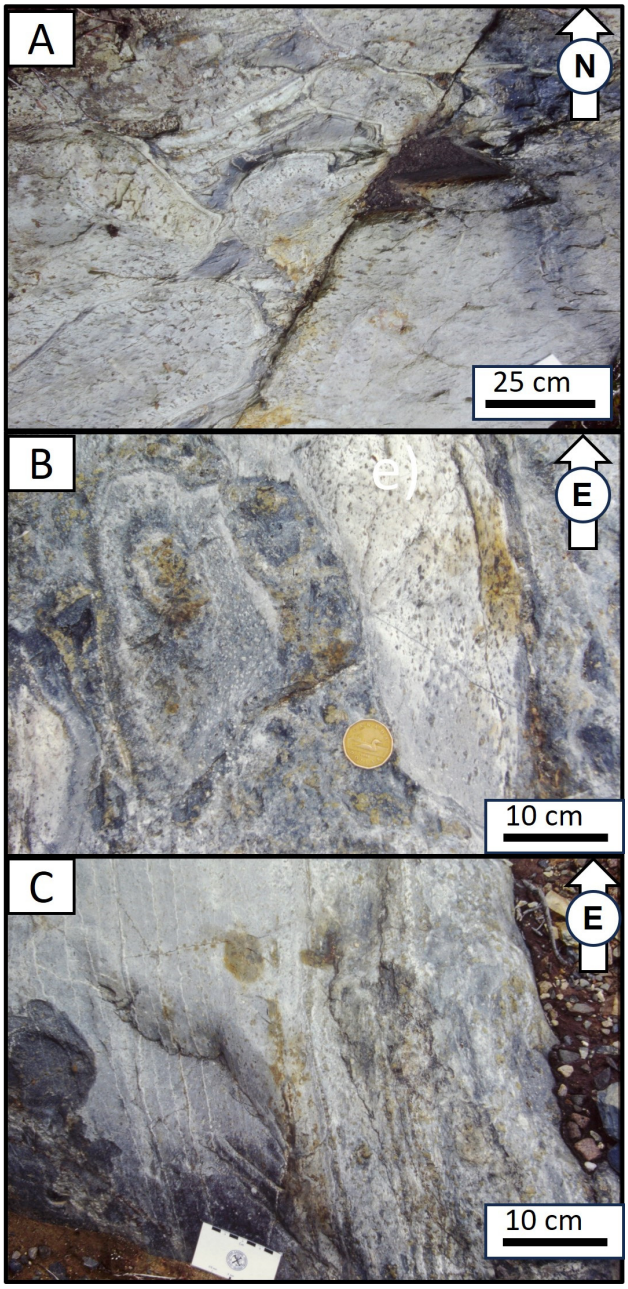

Figure 34. A. *Unit 3.0 highly amygdaloidal pillowed flow facies with strongly quartz-epidote-albite altered rims and interpillow hyaloclastite replaced by magnetite, quartz, chlorite, pyrite and epidote. Looking south. UTM ND83, Zone 17, 683859 E, 5347958 N. Photograph by A. Galley, NRCan photo 2023-661.* ***B.*** *Unit 3.0 scoriaceous coarse mafic pillow breccia along north edge of Zone 2 open pit containing variably quartz-epidote-albite-chlorite altered mafic clasts, some cored with epidote-rich domains. Partial bleached margins suggest alteration before flow fragmentation. UTM NAD83, Zone 17, 683859 E, 5347958 N Photograph by A. Galley, NRCan photo 2023-662.* ***C.*** *Flow banded mafic dyke (left) crossing unit 3.0 scoriaceous and strongly bleached coarse pillow breccias. Note bleaching of the flow banding and thermal extension cracks in the dyke. UTM NAD83, Zone 17, 683859 E, 5347958 N. Photograph by A. Galley, NRCan photo 2023-663.*

Much of the lower part of the overlying Bousquet Formation unit 4.4 is intruded by the unit 4.3 Doyon felsic dyke swarm and overprinted by varying degrees of quartz-sericite-pyrite-rutile-allanite ±aluminosilicate alteration spatially associated with the Doyon-Westwood auriferous quartz-sulphide vein event. Associated with the aluminosilicate-rich alteration type are zones of intense leaching characterized by vuggy, silica rich remnants of unit 4.3 felsic sills. These alteration types will be described in more detail under the following section on intrusion-hosted alteration.

At the upper contact to unit 4.4 there is sporadic recognition of a <1 m-thick “exhalite" horizon with interlaminated quartz, pyrite and sphalerite that can contain grades of up to several ppm Au (Iamgold Corp. maps and drill records). Further up section there is a series of auriferous massive sulphide lenses and associated veins that includes the Warrenmac occurrence (Savoie et al., 1991; Mercier-Langevin et al., 2009; Wright-Holfeld et al., 2010, 2011; Yergeau et al., 2022a, b) These lenses are hosted along the contact between calc-alkalic rhyodacite flow-dome complex (unit 5.1a-(d)) and overlying volcaniclastic strata, some of which contain clasts of auriferous pyrite-sphalerite (Fig. 5).

Significance of the volcanic-hosted alteration zones

The extensive zones of semi-conformable mafic volcanic-hosted hydrothermal alteration described in units 1.0 and 3.0 are well documented in various Precambrian VMS districts, including the well-documented Archean Noranda camp (Rusty Ridge andesite formation), Sturgeon Lake (Darkwater formation) and the Paleoproterozoic Snow Lake VMS district (Hidden Lake formation) (Galley, 1993; Skirrow and Franklin, 1994; Santaguida, 1999; Galley et al., 2000; Gibson and Galley, 2007; Bailes et al., 2016). Net mass gain calculations and oxygen isotope results from these VMS camps (Santaguida, 1999; Holk et al., 2008) indicate that the bleaching, silica dumping and moderate sulphide formation is the result of interaction of the glass-rich pillow margins and volcaniclastic strata with heated (<250^{o}C) circulating seawater (Skirrow and Franklin, 1994; Holk et al., 1998; Santaguida, 1999). The resultant seawater-rock interaction breaks down the unstable basalt glass into clays, zeolites and quartz, and dumps silica and sulphides into pillow interstices and amygdales (Skirrow and Franklin, 1994; Galley et al., 2007; Gibson and Galley,

2007). These near-seafloor (100–200 m) bleaching events result in proximal sulphide-silica-chlorite precipitation both in the interpillow interstices and as thin overlying chert-sulphide-tuff intervals known as exhalites (Sangster, 1978; Franklin et al., 1981; Kalogeropoulos and Scott, 1989). In the Noranda camp the most prominent of these exhalite units is called the C Contact Tuff, whereas in the Snow Lake VMS camp the Mudd Lake exhalite overlies the bleached Hidden Lake basalts. In the Doyon region there is no evidence of exhalite formation at either at the upper unit 1.0 nor the upper unit 3.0 contacts. The semi-massive concentrations of magnetite ±silica and sulphide in the pillow interstices near the upper contact of unit 3.0 above the western half of the MIC may be a surrogate for the formation of sulphide-oxide-rich exhalite at this contact, or evidence for the generation of a high temperature fluid reservoir zone at the base of the Bousquet Formation (cf. Galley, 1993; Franklin et al., 2005; Bailes et al., 2016;). The upper contact of unit 3 also marks a major discontinuity in the whole-rock oxygen isotope signature (Appendix 2). Rocks below the contact have low $\delta^{18}O$ signatures (<4‰), suggesting high-temperature subsea-floor alteration, whereas rocks above that contact (south) have heavier signatures (>6‰).

In the hotter (>350^{o}C), deeper (1-2 km) parts of subsea-floor hydrothermal systems the circulating seawater has evolved into a hot, low pH fluid that much more effectively destroys silicate minerals thereby liberating metals to form metal reservoirs to VMS-type sulphide mineralization at or near the seafloor (Galley, 1993; Franklin et al., 2005). Primary actinolite-albite-clinozoisite is a common alteration mineral assemblage in the former and Fe-rich clays, zeolites and chlorite in the latter. The overprinting by greenschist facies regional metamorphism in the DBL precludes the mineralogical distinction in the affected basalts hosting the MIC. The VMS-like characteristics of at least part of the Mouska and Mic Mac zones along the same interval as the bleached unit 1.0 basalt suggests that this alteration event was also the product of shallow seafloor interaction between rapidly cooling pillowed flows and seawater.

The MIC likely intruded into this preexisting seafloor hydrothermal system. There is no stable isotope evidence that the various intrusive phases interacted with a hot, reduced, active hydrothermal system as observed in some other VMS-related subvolcanic intrusive systems (Galley, 1993; Neyedley et al., 2021b) where the interaction of circulating hot hydrothermal fluids and seawater cause rapid cooling and fracturing of the crystallizing magma with resultant fracture-

controlled alteration and rapid crystallization textures and features. There is some evidence of rapid cooling through granophyre growth in the early stage tonalite, but this is probably related to magma interaction with wall rock xenoliths as described in the next section. There are abundant epidosite pods and fracture infillings in parts of the early quartz diorite and tonalite MIC phases indicating extensive breakdown of Ca plagioclase under temperature conditions suitable for the formation of albite, epidote and actinolite. The presence of pervasive Na addition (Galley and Lafrance, 2014) could be the result in part of late magmatic-hydrothermal alteration due to volatile release of a water rich magma system as evidenced in the MIC study by Neyedley et al. (2021b) and at the Westwood deposit east of the Doyon mine (Yergeau et al., 2022a, b).

MIC-hosted pre-Doyon Au(-Cu) vein system alteration

The pre-Doyon vein system alteration of the MIC includes veining and alteration affecting only the early Mouska stage intrusive phases. Succeeding veining and alteration affecting both the early Mouska and later Doyon stages are described in the following section. As described in Galley and Lafrance (2014) the gabbro, quartz diorite and tonalite phases are affected by varying degrees of Na-Ca alteration. Most of the primary plagioclase in these intrusive phases is first rimmed by albite, or less commonly perthitic alkali feldspar and the remnant cores replaced with sericite and epidote. Primary pyroxene and hornblende are replaced with actinolite, biotite, magnetite and titanite, overprinted with retrograde chlorite. The gabbro and quartz diorite phases are further characterized by epidote-rich lenses and fracture infillings. This extensive alteration was proposed by Galley and Lafrance (2014) to be the product of auto-metamorphism perhaps reinforced by the ingestion of circulating connate seawater from the hydrothermal altered volcanic host strata.

Accompanying these hydrothermal events are complex magmatic-hydrothermal and hydrothermal features and alteration that pre-date the Doyon Au(-Cu) vein system emplacement. As described in Galley and Lafrance (2014) the hanging-wall contacts to the Mouska early phase quartz diorite and tonalite is defined by a xenolith-rich margin developed by magma injection into layered gabbro, porphyritic diorite, quartz diorite and host mafic volcanic strata. The partial ingestion and dehydration of these xenoliths resulted in the development of an actinolite, epidote, clinozoisite, magnetite, titanite, and blue quartz (due to rutile inclusions) mineral assemblage within the granophyric host rock.

The magmatic-hydrothermal mineral assemblage is accompanied by the development of numerous aplitic narrow "vein-dykes" up to 20 cm wide with albite-rich haloes and diffuse bleached contacts. In places these aplite veins grade laterally into open spaced veins with rims of coarse-grained titanite, actinolite and quartz and cores of clinozoisite. The aplite veins have irregular bleached margins of sericite, carbonate, epidote and titanite. These magmatic-hydrothermal features and mineral assemblages are crossed by dykes of hornblende-plagioclase and plagioclase porphyritic tonalite, and quartz and quartz-feldspar porphyritic trondhjemite feeder dykes to the overlying Doyon stages of the MIC and basalt feeder dykes to the Bousquet Formation upper member mafic units (Galley and Lafrance, 2014).

The second stage brecciation of the Doyon quartz diorite/tonalite pendant was the result of injection of late stage porphyritic tonalite and trondhjemite along its margins and emplacement of associated dykes and thin sills within the pendant. In addition to xenoliths of the Doyon quartz diorite pendant along its upper contact, the trondhjemite sill complex contains xenolith rich layers containing angular to ameboid shaped fragments of early-stage MIC plus felsic and mafic volcanic clasts (Fig. 9B-C). Clasts of the previously magmatic-hydrothermally altered Doyon quartz diorite contain secondary plagioclase-amphibole knots and cavities typical of dehydrated mafic xenoliths; the former a product of partial melting and the latter of mass loss and resultant porosity generation (Russell et al., 1995; McLeod and Sparks, 1998) (Fig. 9D). The mafic xenoliths are further characterized by pervasive actinolite-epidote-pyrite-quartz alteration with cavities infilled with fibrous amphibole rims and quartz-pyrite-epidote cores. Some diorite xenoliths are altered to albite-sericite-biotite-epidote with clots of quartz-chalcopyrite-epidote and chlorite along with extensive epidote-chlorite-quartz sericite veining.

Alteration spatially associated with the Doyon Au(-Cu) system

Alteration and associated veining spatially associated with the Doyon mineral system is described from earliest to latest based on cross-cutting relationships with the MIC intrusive phases and other associated alteration mineral assemblages. The vein stockworks and associated alteration mineral assemblages described here overprint all the late-stage MIC dykes and sills along with the

Phase E xenolithic roof pendant and have a spatial association with the Doyon mineral system (Fig. 35; Tables 1-2).

Vein dykes

Centimetre-wide aplite vein-dykes are associated with the felsic to mafic dyke swarm exposed at the tonalite-hosted Mooshla B Au occurrence (Fig. 35). They are also associated with the felsic-mafic dyke swarm crossing the western margin of the MIC on the Authier property (Fig. 35). These vein dykes can either form apophyses off larger trondhjemite dykes or form individual bodies with planar to irregular margins. Their open space cores contain euhedral crystals of alkali feldspar, quartz, biotite, pyrite, epidote and chalcopyrite, with several ppm of Mo (Fig. 36A). These vein dykes are affected by sericite alteration and are crossed by both chlorite-magnetite-pyrite and quartz-pyrite-sericite-rutile vein stockworks and appear to represent a high temperature (~400-500ºC) magmatic-hydrothermal transition phase (Carten et al., 1988; Seedorf, 2005).

Silicification

Vein controlled silicification postdates emplacement of the late stage trondhjemite dykes and sills (Fig. 36B-C). It is associated with trondhjemite dykes crossing the early stage tonalite, where the silicification event is overprinted by chlorite-magnetite-pyrite and quartz-sericite-pyrite-rutile vein stockworks (Fig. 36D; Tables 1-2). The planar quartz-feldspar veins are <10 mm in width and in places contain angular fragments of wall rock. They have distinctive bleached, silicified margins extending from the veins by 10's of centimetres. The silicified margins are characterized by a zone, or "cloud" centimetres wide of 5–10% disseminated <5 mm long black tourmaline crystals (Fig. 36C). These tourmaline cloud veins are also present within the trondhjemite sill complex where they are again overprinted by both chlorite and sericite rich veins and attendant alteration.

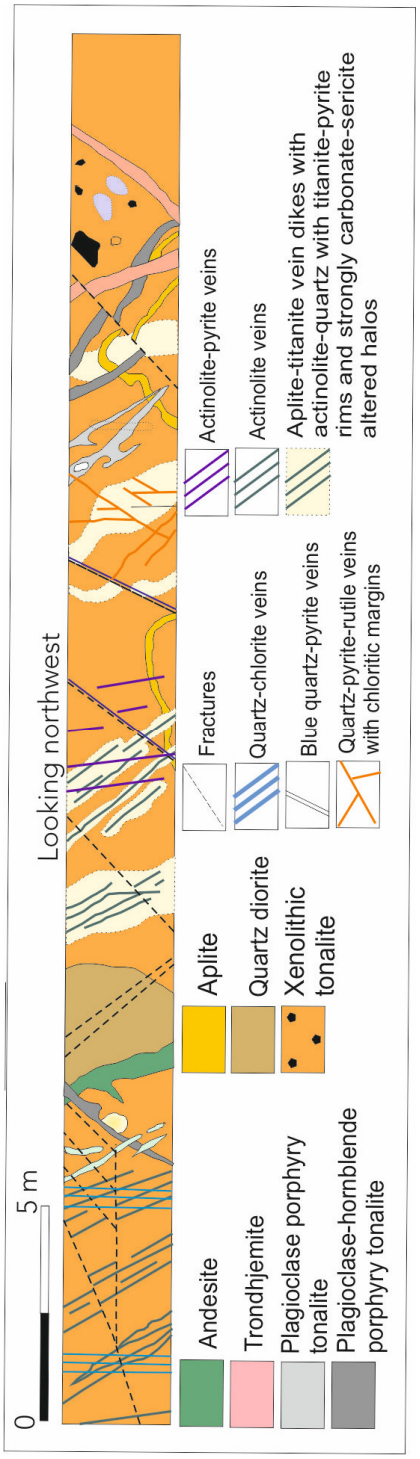

Figure 35. *Section of the NE-trending 666 exploration drift, Mouska Mine illustrating a traverse through the MIC late stage and Bousquet Formation upper member dyke swarm and associated alteration hosted within xenolithic Phase D early stage tonalite. The dyke swarm is located along the western margin of the late-stage MIC.*

Potassium feldspar-quartz veins

In rare instances quartz-potassium feldspar-biotite veinlets and fracture-fillings with potassium feldspar-rich margins cross granophyric to spherulitic phases of the Phase I trondhjemite (Fig. 37; Tables 1-2). A limited number of samples were stained to identify feldspar type where feldspar rims quartz and quartz-biotite veinlets. In places, the potassium feldspar altered vein margins have biotite-rich outer rims (Fig. 37C). These may be much more widespread within the trondhjemite sills but have not been identified to date. There is no apparent association of this alteration phase with the Au(-Cu) mineralization.

Table 1. *Mineral assemblages that are present in the host rocks to the Doyon mineral system.*

Mineral	Least altered		Silicic	Potassic	Chlorite		Biotite		Sericite		Al-silicate		Residual quartz
	Mafic	Felsic	Felsic	Felsic	Mafic	Felsic	Mafic	Felsic	Mafic	Felsic	Mafic	Felsic	Felsic
Pyrite													
Pyrrhotite													
Chalcopyrite													
Magnetite													
Ilmenite													
Titanite													
Rutile													
Allanite													
Chlorite													
Mg chlorite													
Muscovite													
Phengite													
Biotite													
Mg biotite													
Phlogopite													
Al-silicates													
Mn garnet													
Tourmaline													
Carbonate													
Anhydrite													
Gypsum													
Quartz													
Potassium feldspar													
Albite													
Plagioclase													
Epidote-clinozoisite													
Allanite													
Actinolite													
Hornblende													
Pyroxene													
Olivine													

Quartz- biotite- chlorite-pyrite alteration

Occupying the core of the Doyon Au(-Cu) system where it affects the trondhjemite, hybrid quartz diorite and porphyritic tonalite phases of the MIC is a fracture-controlled quartz-Mg biotite/phlogopite-chlorite-pyrite ±chalcopyrite alteration assemblage in association with crosscutting Fe-carbonate veinlets (Fig. 37; Tables 1 and 2). Along the east margin of the West Zone vein system

Table 2. *Vein-hosted mineral assemblages that define a progressive development of alteration facies spatially associated with the Doyon mineral system.*

Vein progression	Host lithology					
	Qtz diorite	**Tonalite**	**Doyon QD**	**Trondhjemite**	**Porphyritic tonalite**	**Unit 4.3 sills**
Aplite vein dykes (qtz-fsp-ep-py-cp)						
Qtz-tm-py (cloud)						
Muscovite bx						
Qtz-bi-py-cp-(cb-fl) bx						
Qtz-anyd-py-cp						
Chl-qtz-mgt-(ab-tit-fl)						
Qtz-py-mu-rut-(fl)						
Qtz-py-mu-ep-rut						
Qtz-cb-chl-mu-py-cp (Au)						
Qtz-kspar*			?		?	
Qtz-Fe-cb						
Qtz-tm-py (cloud)						
*unknown extent due to limited staining						
	Anomalous Au					
	Lode veins					
ab=albite, anyd=anhydrite, bi=biorite, bx=breccia, cb=carbonate, chl=chlorite, cp=chalcopyrite, ep=epidote, Fe-cb=iron carbonate, fl=fluorite, fsp=feldspar, kspar=potassium feldspar, mgt=magnetite, mu=muscovite, py=pyrite, qtz=quartz, rut=rutile, tit=titanite, tm=tourmaline.						

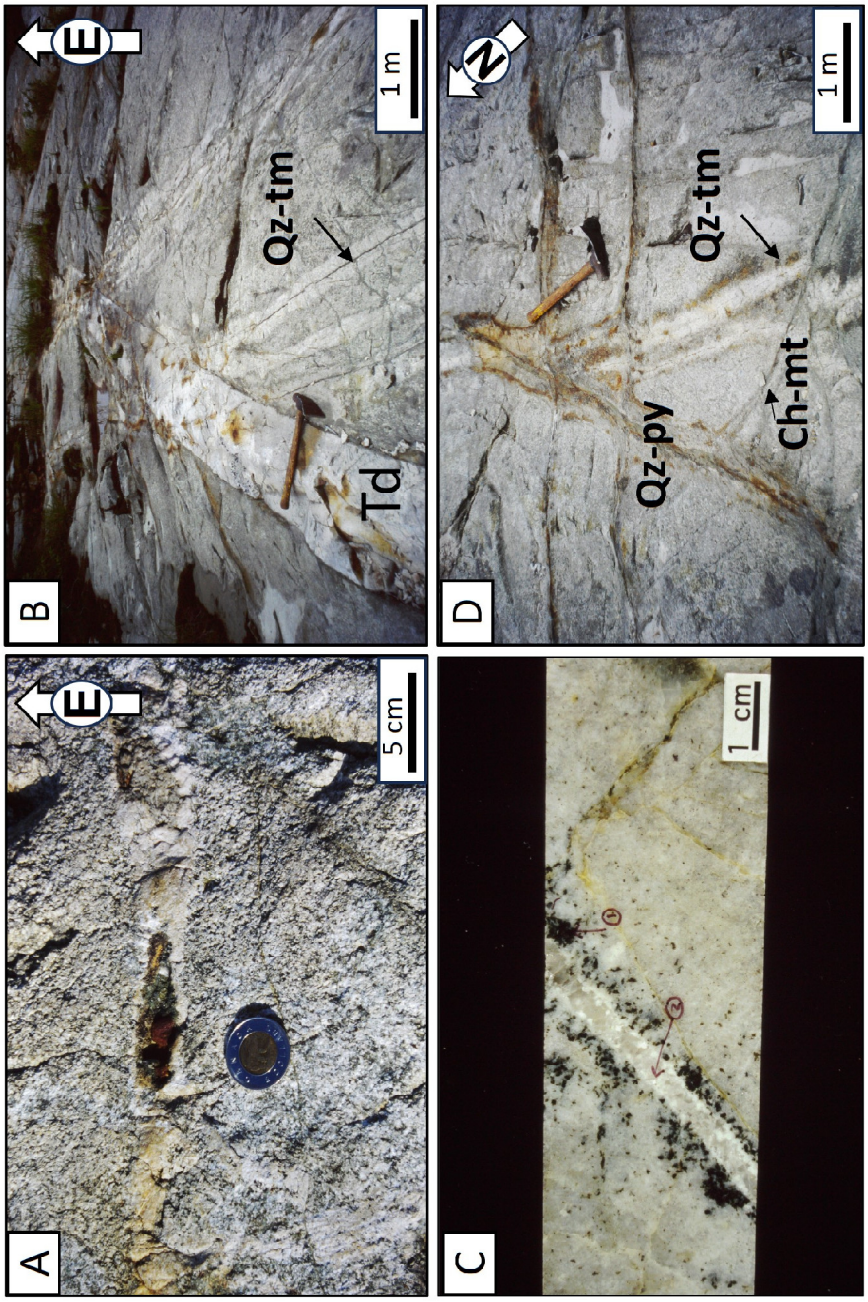

Figure 36. A. *Aplitic vein dyke associated with Phase I trondhjemite dykes at the Mooshla B showing (UTM NAD 83, Zone 17, 682765 E, 5348786 N). Photograph by A. Galley, NRCan photo 2023-664.* ***B****. Phase I trondhjemite dyke hosted within Phase D tonalite and crossed by early quartz-tourmaline veins with wide silicified margins and rims rich in disseminated tourmaline (cloud veins). Photograph by A. Galley, NRCan photo 2023-665.* **C***. Polished core section of a quartz-feldspar vein with a tourmaline-rich margin (cloud vein) crossing a trondhjemite sill. DDH 96-682 (477 m). Photograph by A. Galley, NRCan photo 2023-666.* ***D.*** *Quartz-tourmaline cloud veins crossed by a chlorite-magnetite-albite-(pyrite) vein stockwork which in turn I crossed by quartz-pyrite-epidote-titanite veins that are weakly Au enriched. Photograph by A. Galley, NRCan photo 2023-667.*

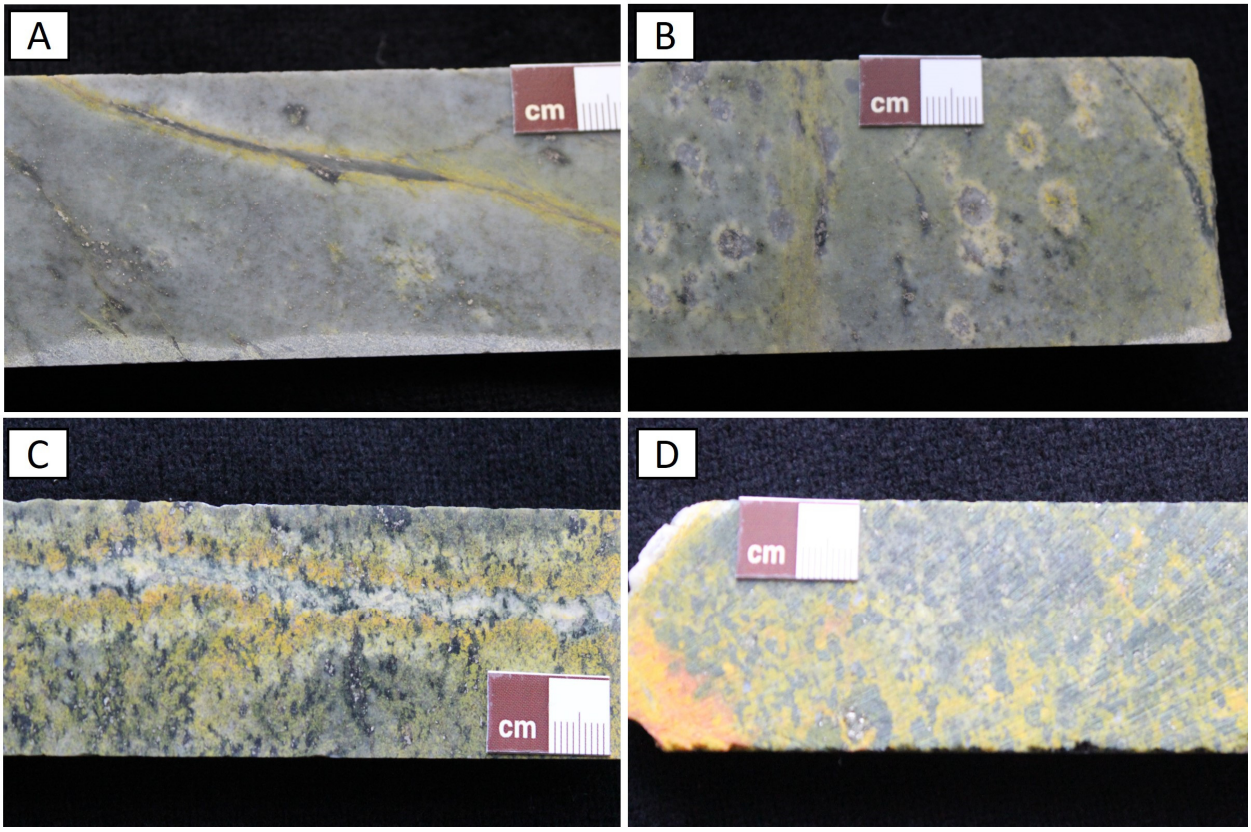

Figure 37. A. *Thin quartz vein with a potassium feldspar rich margin in moderately sericite-pyrite altered Phase I trondhjemite (ddh 1106-95-183 m). Photograph by A. Galley, NRCan photo 2023-668.* ***B.*** *Moderately sericite-pyrite altered Phase I trondhjemite with pyrite-clinozoisite ovoids rimmed with euhedral plagioclase all crossed by diffuse potassium feldspar altered zones associated with quartz veinlets (ddh 1106-95, 183.5 m). Photograph by A. Galley, NRCan photo 2023-669.* ***C.*** *Biotite-chlorite altered granophyric trondhjemite crossed by quartz veinlet with a cm-wide potassium feldspar rich margin (ddh NG94-01, 896 m). Photograph by A. Galley, NRCan photo 2023-670.* ***D.*** *Granophyric trondhjemite with pervasive potassium feldspar alteration next to a K-feldspar vein (NG94-01,931 m). Photograph by A. Galley, NRCan photo 2023-671.*

this alteration type predominates within the host trondhjemite and at depth is accompanied by patchy occurrences of spessartine garnet with secondary (metamorphic?) biotite. The presence of chalcopyrite in this vein system is erratic and is accompanied by anomalous Au values up in the g/t range. This alteration assemblage is not present within the rock units into which the MIC intrudes (i.e. units 3.0, 4.3 and 4.4) east of the Doyon Fault. For the most part this alteration event is characterized by *in situ* fracturing and infilling (Fig. 38A-B), but on rare locations there are zones in which breccia vein rock fragments are dislocated and rotated in a groundmass of quartz,

biotite and chlorite, pyrite and chalcopyrite (Fig. 38C-D). In places the groundmass includes infilling by a distinctive opaque blue quartz containing abundant needles of rutile. The fracture and micro-breccia margins are strongly bleached in places. There are also minor occurrences of anhydrite-carbonate-quartz and fluorite where this alteration facies affects the hybrid quartz diorite and porphyritic tonalite. An exposure of strongly biotite-pyrite-altered Doyon quartz diorite hosts a north-trending, 50 cm-wide West Zone quartz-pyrite vein just west of the Doyon Fault line. A sample of this vein assayed at 150 g/t Au (D. Yergeau; pers comm.). Weak to moderate biotite-chlorite-carbonate alteration overprints the actinolite-epidote-feldspar alteration previously described in the hybrid quartz diorite-tonalite in outcrops around which the Grand Duc open pit now exists (Figs. 5, 28).

This alteration zone is overprinted by a fine network of chlorite-biotite-Fe carbonate-pyrite-chalcopyrite veins that extend out into the bordering sericite-rich alteration facies. In places these veins appear to be an extension of the biotite-rich fracture system, but in other cases they cut across the fractures.

Chlorite-albite- carbonate-pyrite alteration facies

The most peripheral alteration zone for the Doyon ore system is dominated by chlorite and Fe-carbonate, with ancillary concentrations of albite, sericite, pyrite, anhydrite, fluorite and tourmaline (Table 1). This alteration assemblage overprints the MIC trondhjemite exterior to the sericite-quartz-pyrite-rutile alteration facies down to the contact with early-stage MIC tonalite and quartz diorite. In several drill intersections there appears to be a larger concentration of Fe-carbonate where this alteration type is peripheral to the Au(-Cu) vein stockworks. This alteration assemblage is accompanied by quartz-chlorite-carbonate-pyrite, anhydrite-quartz-carbonate-pyrite and quartz-carbonate-tourmaline veining. Of these, the first two are overprinted by the dominant S_2 schistosity, whereas the tourmaline-bearing veins appear to accompany, or postdate the penetrative fabric. Nevertheless, their presence is particular to the chlorite-Fe carbonate-pyrite alteration facies.

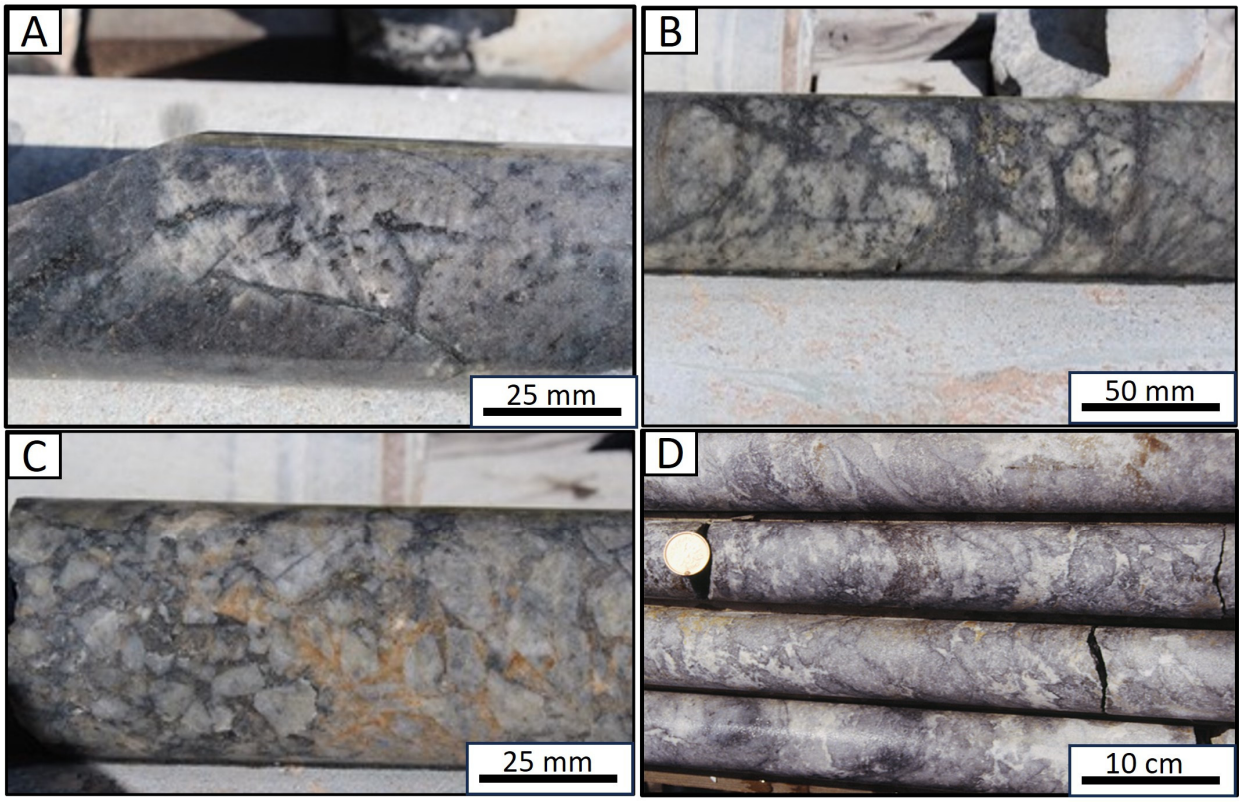

Figure 38. A. *A fine biotite fracture system in host spotted trondhjemite. Spots are also biotite-dominated along with chlorite and pyrite (ddh R2549, 99.3 m). Photograph by A. Galley, NRCan photo 2023-672.* ***B.*** *More intense biotite-chlorite-rich fracturing of trondhjemite with associated bleaching of the host rock (ddh R2549-145). Photograph by A. Galley, NRCan photo 2023-673.* ***C.*** *More intense biotite-chlorite-pyrite-carbonate brecciation and rotation of bleached trondhjemite clasts (ddh R2549, 145.5 m). Photograph by A. Galley, NRCan photo 2023-674.* ***D.*** *Strong brecciation of trondhjemite with biotite-rich rims on dislocated clasts and a quartz-pyrite breccia infilling (ddh R2549, 147.5 m). Photograph by A. Galley, NRCan photo 2023-675.*

Sericite-dominant alteration facies

Iamgold geologists mapped a broad halo of sericite-rich alteration approximately 3000 m long and up to 500 m wide in places (Fig. 39; Tables 1-2). It encompasses all known ore bodies in the Doyon system (Mooshla A, Grand Duc, West Zone, Zone 2 and Zone 1) and includes the Zone 2 Extension ore bodies of the Westwood mineral system east of Doyon (Yergeau et al., 2022a, b). Within this defined halo there are variations in both intensity and associated mineral assemblages.

The broader zone of weak to moderate sericite alteration in the trondhjemite and late phase tonalite primary plagioclase and biotite is partially to fully replaced by a sericite-chlorite-epidote-pyrite-

carbonate-titanite metamorphic mineral assemblage. In the xenolithic trondhjemite and Phase E hybrid quartz diorite-tonalite the actinolite-chlorite-albite mineral assemblages are replaced with biotite, chlorite, epidote and Ti oxides (titanite and rutile). Both the hybrid quartz diorite-tonalite and the cross-cutting sericite-altered trondhjemite and late stage tonalite phases are crossed by numerous deformed veinlets of quartz-epidote and quartz-epidote-chlorite-pyrite. In the miarolitic cavities previously described (Fig. 9), the primary amphibole-chlorite-albite dominated mineral assemblage is replaced with biotite, epidote, pyrite and Ti oxides. Along with this sericite-epidote-chlorite dominated alteration mineral assemblage is the presence of thin planar quartz-tourmaline-pyrite veins with cm-wide haloes of fine-grained disseminated tourmaline.

The more intense sericite altered zones within the trondhjemite are characterized by a "spotted" appearance. These coarser-grained knots are 2 to 7 mm in diameter and appear to have nucleated on plagioclase phenocrysts. These knots are similar in dimension to the miarolitic cavities but do not appear to have been formed by open space filling and are devoid of bleached aplitic or granophyric rims. The knots vary in composition from epidote-quartz-pyrite-chlorite-rutile to biotite-chlorite-magnetite ±spessartine at depth (>500 m) towards the eastern margin of the late-stage MIC.

Approaching the most intense zones of sericite alteration the knots, or overgrowths are dominated by pyrite clusters up to 7 mm in width. The pyrite has irregular, anhedral, porous cores with accessory chalcopyrite and rutile. The anhedral core has a rim of more solid crystalline pyrite, which in turn have rims of chlorite and epidote and sometimes biotite-epidote margins. These silicate rims tend to be aligned along the dominant S_2 foliation trend.

The most intense sericite alteration zones are readily apparent within the trondhjemite phases and are focused on NNE and ESE striking, steeply dipping fractures containing a sericite-quartz-pyrite-Ti oxide mineral assemblage (Fig. 40A-D). This fracture system also controls, at least in part, the distribution of auriferous quartz-pyrite-chalcopyrite veins (Fig. 40B). At the southern extremity of the West Zone the sericite-Ti oxide rich fracture system and associated quartz-pyrite-chalcopyrite vein stockwork is overprinted by the strong shear foliation that characterizes this alteration type where spatially associated with the unit 4.3 felsic sill complex which hosts Zones 1 and 2 (Figs. 5

and 39). Monazite becomes an accessory mineral within this part of the alteration system. The unit 4.3 sericite-pyrite-Ti oxide-monazite alteration also overprints the units 3.0 and 4.4 mafic volcanic rocks in proximity to the felsic dyke swarm.

Sericite-quartz-pyrite- aluminosilicate alteration

In the southern third of unit 4.3 the sericite-pyrite-Ti oxide-monazite fracture-controlled alteration merges with a zone of intense sericite-quartz-aluminosilicate alteration that has obliterated the original primary igneous textures of the host rock (Fig. 41). Pseudomorphs of andalusite are replaced by kyanite, which in turn is partially replaced with pyrophyllite and diaspore. The result is an almost total obliteration of any original rock texture so that immobile trace element geochemistry is the only evidence for identifying primary compositions. East of the Doyon Fault the aluminosilicate zone is host to Doyon Zone 1, which is characterized by an increase in disseminated pyrite with attendant and discontinuous quartz-pyrite-(chalcopyrite) veins and veinlets. The aluminosilicate zone continues for several hundred metres east of the Doyon Fault following the upper contact of unit 4.3 in the absence of any significant Au mineralization (Fig. 38). In places along this upper unit 4.3 contact the overlying unit 4.4 massive mafic volcanic strata are cut by <5 mm-wide veins rich in aluminosilicate.

Residual quartz zone

The aluminosilicate alteration facies is locally overprinted by a series of stratiform lenses, tens of decimetres thick and tens of metres long, of fine-grained, granoblastic to ribbon-textured quartz-sericite-rutile alteration characterized by a variably vuggy texture (Fig. 41A–C). Within this vuggy quartz zone, the primary rock textures have completely disappeared, and only irregular patches remain of the earlier formed sericite-rich alteration (Fig. 41B). The vuggy texture suggests that volume loss took place during a period of leaching that appears to have overprinted the previously formed sericite-rich alteration. The vugs are irregular in shape and are lined with euhedral quartz and minor pyrite and can take up over 50% of the rock volume in places. The local preservation of this assemblage and texture is probably due to the more competent rheology of silica-rich zones in much softer, sericite-dominated rocks. Moreover, deformation might have partly destroyed and obscured other areas of residual quartz (i.e. Fig. 41B).

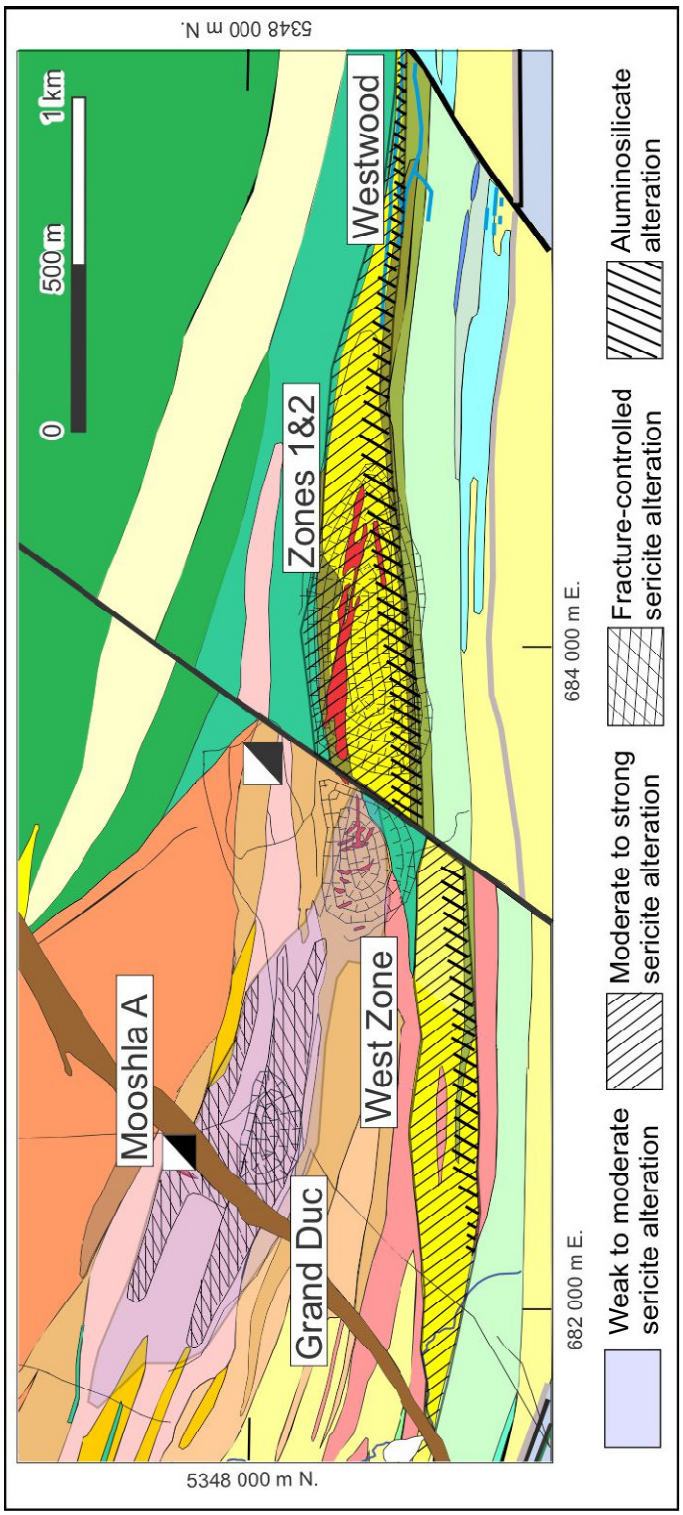

Figure 39. *Surface and near surface distribution of sericite-rich alteration zones centered around unit 4.3 felsic sill-dyke complex and the Doyon late-stage phases of the MIC. The sericite alteration halo envelopes the MIC-hosted Mooshla A, Grand Duc and West zones, plus zones 1 and 2 of the Doyon system and Zone 2 Extension of the Westwood system. For geological unit identification see the legend in Figure 5.*

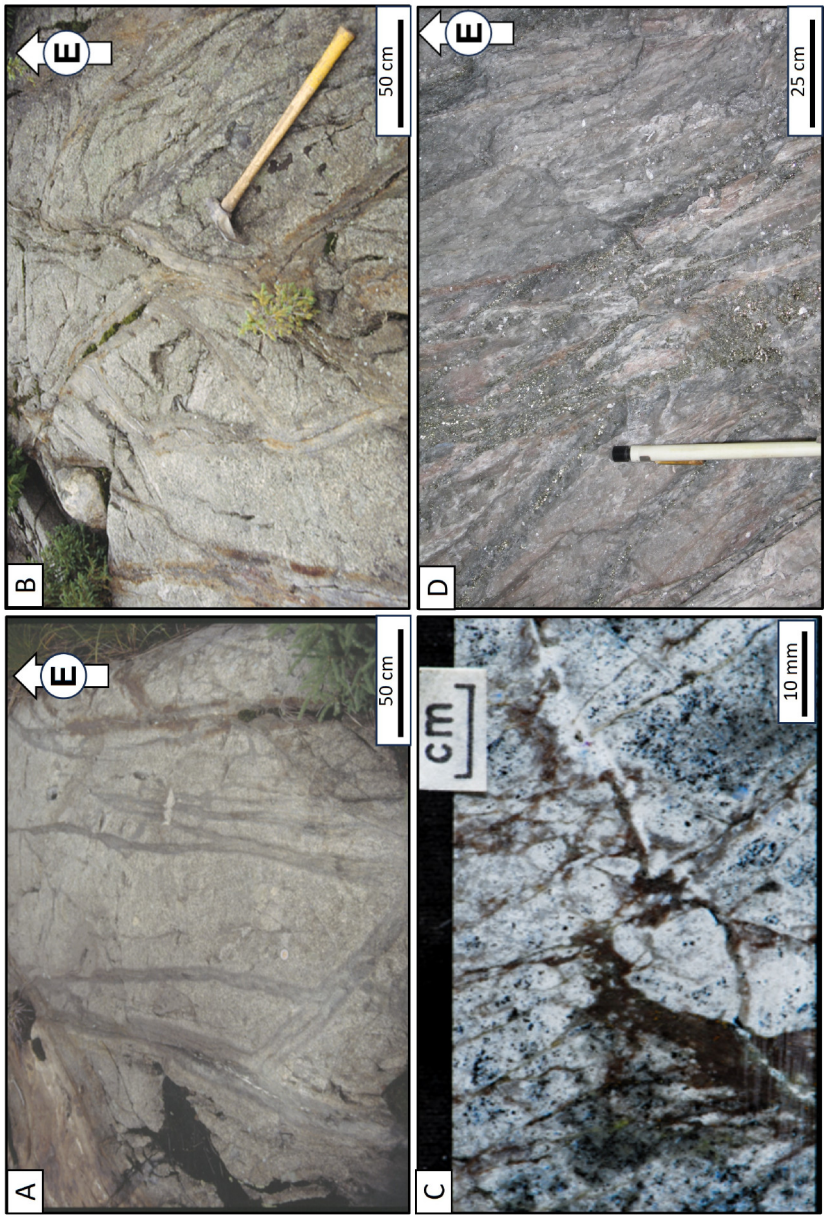

Figure 40. A. *Looking ESE along a typical zone of intense sericite-quartz-pyrite-Ti oxide. In some instances, the sericite-rich zones rim <5mm veins of quartz-rutile and in other instances veins of auriferous quartz-pyrite-rutile ±chalcopyrite as defined by the linear zones of Fe oxide. Photograph by A. Galley, NRCan photo 2023-676.* ***B.*** *Quartz-pyrite-rutile-chalcopyrite veins hosted by some of the NNE and ESE striking sericite-rich zones. Hammer pointing north. Photograph by A. Galley, NRCan photo 2023-677.* ***C.*** *An example of Ti-oxide rich quartz-sericite vein stockwork within the most intense zones of sericite alteration. Photograph by A. Galley, NRCan photo 2023-678.* ***D.*** *An example of strongly deformed intense sericite alteration with anastomosing stockworks of auriferous quartz-rutile and quartz-pyrite-chalcopyrite-rutile-allanite Photograph by P. Mercier-Langevin, NRCan photo 2023-679.*

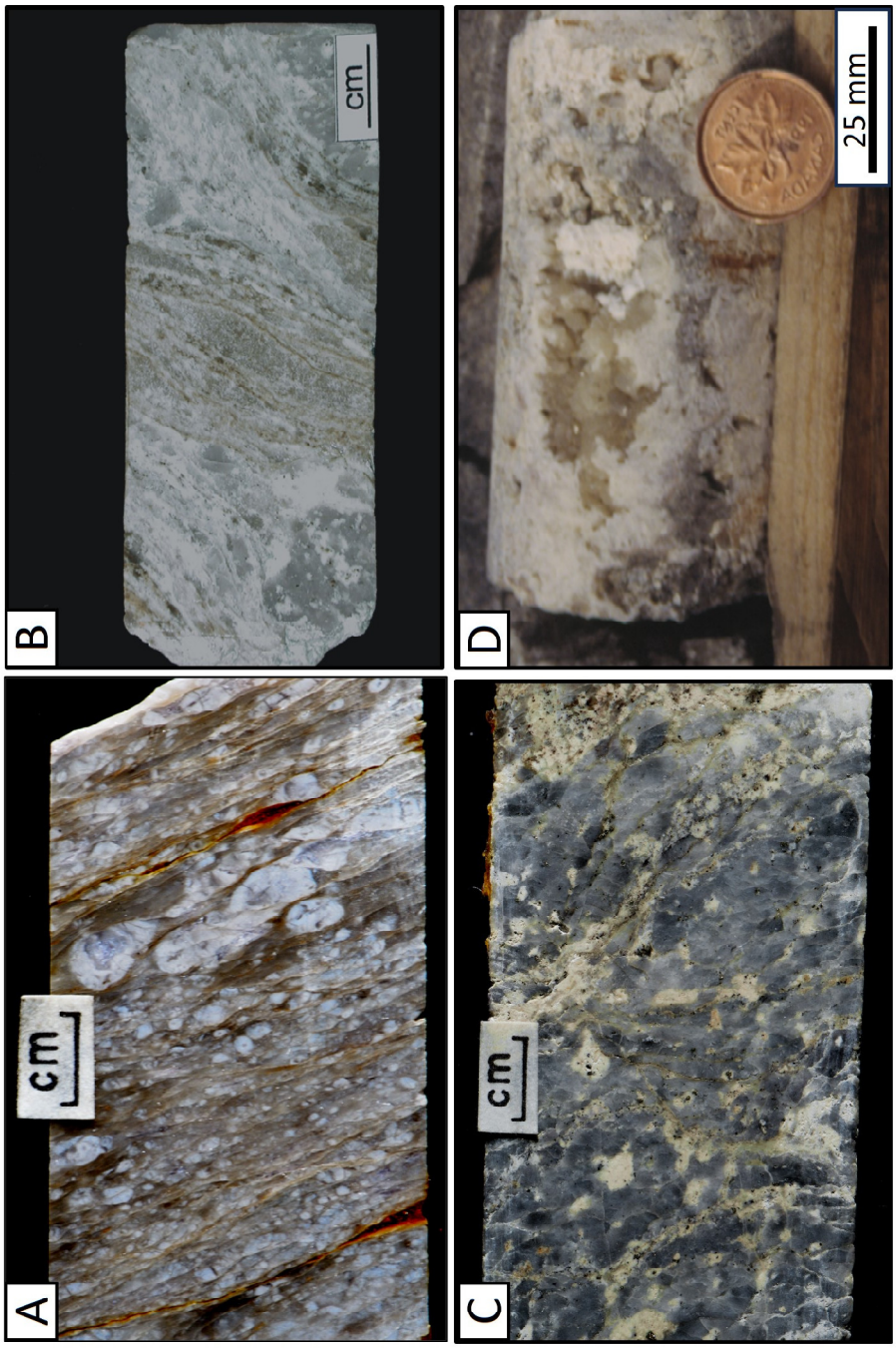

Figure 41. A. *Remnant aluminosilicate porphyroblasts in strongly foliated sericite-pyrite-Ti oxide alteration, with segmented thin sulphide veinlets. Photograph by A. Galley, NRCan photo 2023-680.* ***B.*** *Remnant sericite-rich patches with accessory diaspore along the margin of a residual quartz domain. Note the strong foliation. Photograph by A. Galley, NRCan photo 2023-681.* ***C.*** *Strongly silica-altered rock with disseminated small cavities. Photograph by A. Galley, NRCan photo 2023-682.* ***D.*** *The most intense form of quartz flooding with interconnected vugs partially infilled with euhedral quartz. Photograph by A. Galley, NRCan photo 2023-683.*

Syn- to post-deformation veins

The deformed and metamorphosed vein systems described above are crossed by several types of veins that are clearly syn- to post-main S_2 fabric. This includes planar veins and coarser-grained pods of quartz-sulphide-carbonate-tourmaline, quartz-carbonate-chlorite, anhydrite-chalcopyrite and quartz-potassium feldspar. The sulphide-bearing late veins are associated with areas of known auriferous quartz-sulphide vein mineralization, whereas the quartz-carbonate-chlorite veins are common within zones of strong shear foliation.

The anhydrite-carbonate-chalcopyrite veins hosted in the trondhjemite sill complex are rare and weakly to moderately deformed. These veins are somewhat of an enigma with regards to their origin. There is abundant evidence of anhydrite intergrown with quartz and chlorite in the trondhjemitic groundmass (Neyedley et al. 2021b). Interstitial anhydrite is also present within the groundmass of the altered unit 3.0 basalt along the eastern margin of the late-stage MIC (Savoie et al., 1991). Sulphur isotope analyses of one of the anhydrite-carbonate-sulphide veins were 0 to 5 per mil $\delta^{34}S$ for the chalcopyrite and 13 per mil $\delta^{34}S$ for the anhydrite. Taking into account that the analysis is limited to one sample, the difference in values between the chalcopyrite and anhydrite gives a calculated temperature of over 600ºC, which is above any reasonable regional metamorphic temperature for the mineral assemblages in the host rock.

Auriferous quartz vein-associated alteration

Due to the high degrees of strain undergone by the Zones 1 and 2 vein systems and their association with a large envelope of intense sericite-dominated alteration, it is difficult to discern alteration assemblages directly associated with the vein margins. The more cohesive nature of the intrusive host rocks to the West Zone and GDMA vein stockworks allow for more consistent vein-alteration relationships to be recognized.

Within the trondhjemite the Au-quartz vein intensely altered margins are commonly 3 times the width of the veins (Gosselin, 1998). The proximal alteration assemblage is dominated by sericite, quartz, pyrite, Ti oxides and calcite. Outside of this bleached margin plagioclase is altered to chlorite, quartz, epidote, pyrite and calcite, with minor biotite. Within the bleached margins of porphyritic tonalite-hosted Au-quartz veins, the mineral assemblage consists of quartz, sericite,

chlorite, biotite, calcite and epidote. Although the intrusion-hosted Doyon vein systems are commonly associated with the broader zones of sericite-rich alteration described above there is no consistent and direct relationship between the intensity of the vein margin alteration with that of the broader sericite-rich alteration zones.

Regional metamorphic effects

The mineral assemblages from surface to approximately 500 m depth are compatible with upper greenschist facies and subsequent retrograde lower greenschist metamorphism. At this depth there is a biotite-garnet isograd, with the underlying alteration mineral assemblages affected by lower amphibolite facies regional metamorphism. The presence of this sub-horizontal metamorphic isograd is also present at the nearby Westwood deposit (Yergeau et al., 2015). Also, there is Mg-biotite present above the biotite-garnet isograd (Mg-Fe biotite-spessartine) and Mg-chlorite stable below the isograd. In other parts of the Doyon-Bousquet-LaRonde camp Mn-rich garnet is present accompanying the upper greenschist facies regional metamorphic assemblages (Valliant and Barnett, 1982; Tourigny et al., 1989, 1993; Marquis et al., 1990; Dubé et al., 2007, 2014; Mercier-Langevin et al., 2007b; Yergeau et al., 2022a). The importance of this will be discussed in the section on alteration geochemistry, but it does add complications with regards to determining the timing of alteration and mineralization.

Alteration geochemistry

A study of the geochemical changes that took place in the formation of the Doyon Au(-Cu) system involves numerous rock types, which makes comparison of geochemical variation according to the type and degree of alteration a challenge. In a case such as the Doyon hybrid quartz diorite phase of the MIC there is a high degree of inhomogeneity due to the variability in the percentage of brecciated quartz diorite and the trondhjemitic and tonalitic groundmass. Within the host volcanic package where the unit 4.4 mafic volcanic rocks are intruded by numerous felsic sills and dykes it is also difficult to clearly define geochemical variations due solely to the introduction of hydrothermal fluid. It was decided therefore to restrict the study of secondary geochemical variation principally to the trondhjemite phases of the MIC as a detailed description of the alteration within the Bousquet Formation volcanic strata and associated unit 4.3 felsic sill complex is given in Yergeau (2015) and Yergeau et al. (2022b). The clustering of the trondhjemite

samples is dictated by their dominant mineral assemblages as defined in the previous section. The difficulty arises from the fact that successive alteration facies form from the overprinting of the previous zones, resulting in a geochemical overlap between alteration zones in most cases.

Geochemical histograms

Variations in element concentrations in relation to the Doyon gold zones are illustrated as element and element ratio histograms from drill hole geochemical data representative of sections through Zone 2, West Zone, Grand Duc and Mooshla A (Figs. 42–45). These are derived from published (e.g., Galley and Dubé, 2014; Mercier-Langevin et al., 2024b) and unpublished whole rock geochemical data from this study, and from the company geochemical database (readers are referred to Iamgold for access to historical whole-rock geochemical data), with the West Zone section being a composite from several drill holes. The elements included are those most affected by alteration and mineralization plus TiO_2 and Zr as a ratio to differentiate primary rock compositions. The ratio of MnO/MgO is used to define the presence of anomalous Mn and Ba/K_2O to map the abundance of sericite. Also included are Ishikawa et al. (1976) alteration index (AI), Large et al. (2001) chlorite-carbonate-pyrite alteration index (CCPI), and Williams and Davidson (2004) advanced argillic alteration index (AAAI).

The Zr/TiO_2 ratio can be directly correlated with the graphic logs to define the various rock types present. Values over 500 represent both unit 4.3 felsic dykes and phase I trondhjemite. The established Au zones are principally hosted by these two units, with smaller anomalous Au zones in the West Zone and Grand Duc sections representing the sparser Au vein networks crossing the Doyon quartz diorite and phase G porphyritic tonalite. In the Mooshla A section an additional zone labeled here as the *Conduit Zone* represents the southerly trending veins observed at surface connecting the Grand Duc and Mooshla A zones.

All four sections show a close association of Au and Cu for all the Au zones, with anomalous, but low levels of Ag and Zn. There is a strong depletion of Na of unit 4.2 throughout the Zone 2 section (Fig. 42). This is opposed to an overall higher Na_2O level in the host trondhjemite for the West and Grand Duc zones (Figs. 43 and 44). In the Mooshla section, the Na enrichment is restricted to the margins of the Proterozoic diabase dyke.

Except for the Grand Duc section, there is a general higher background in K_2O concentration that is not directly related to the position of the Au zones. This coincides with higher Ba/K_2O indicating the presence of variable sericite alteration throughout the sections, but mainly in the more felsic units. This is accompanied by low Ca values, although elevated CO_2 in Zone 2 suggests the presence of traceable (Fe-Mg) carbonate. A Mn anomaly is present along the hanging-wall contact to Zone 2. All three alteration indices are elevated throughout the section. In the Mooshla A section (Fig. 45) there is a coincident increase in concentrations of Na, MnO, MgO, BaO and LOI where the Conduit Zone is bisected by the late Proterozoic diabase dyke.

In summary, the alteration indices, including Ba/K_2O indicate the presence of overall pervasive alteration that reflects an early Na metasomatic event accompanied by weak to locally moderate carbonate alteration. This was followed by an influx of more K-rich fluid with a sporadic increase in Mn. The gold zones are defined by significant concentrations of Au and Cu accompanied by elevations in Ag and Zn content to < 1ppb and <100 ppm, respectively.

Bivariate alteration plots

A series of bivariate plots compares the AI alteration index to some key geochemical oxides and elements (Fig. 46). The five alteration mineral assemblages described earlier are further divided on these plots to include a chlorite facies subset with sericite-altered fractures and a sericite facies subset that includes significant epidote.

The concentration of Na_2O significantly lowers with increased alteration intensity, until it almost completely disappears in the most intensely altered sericite- and Al-silicate-rich, and in quartz flooded samples and in samples where there is a complete absence of feldspar. K_2O concentration steadily increases from the chlorite through biotite to the sericite alteration types and decreases through the Al-silicate and quartz flooded alteration types with lesser sericite and the increased presence of quartz.

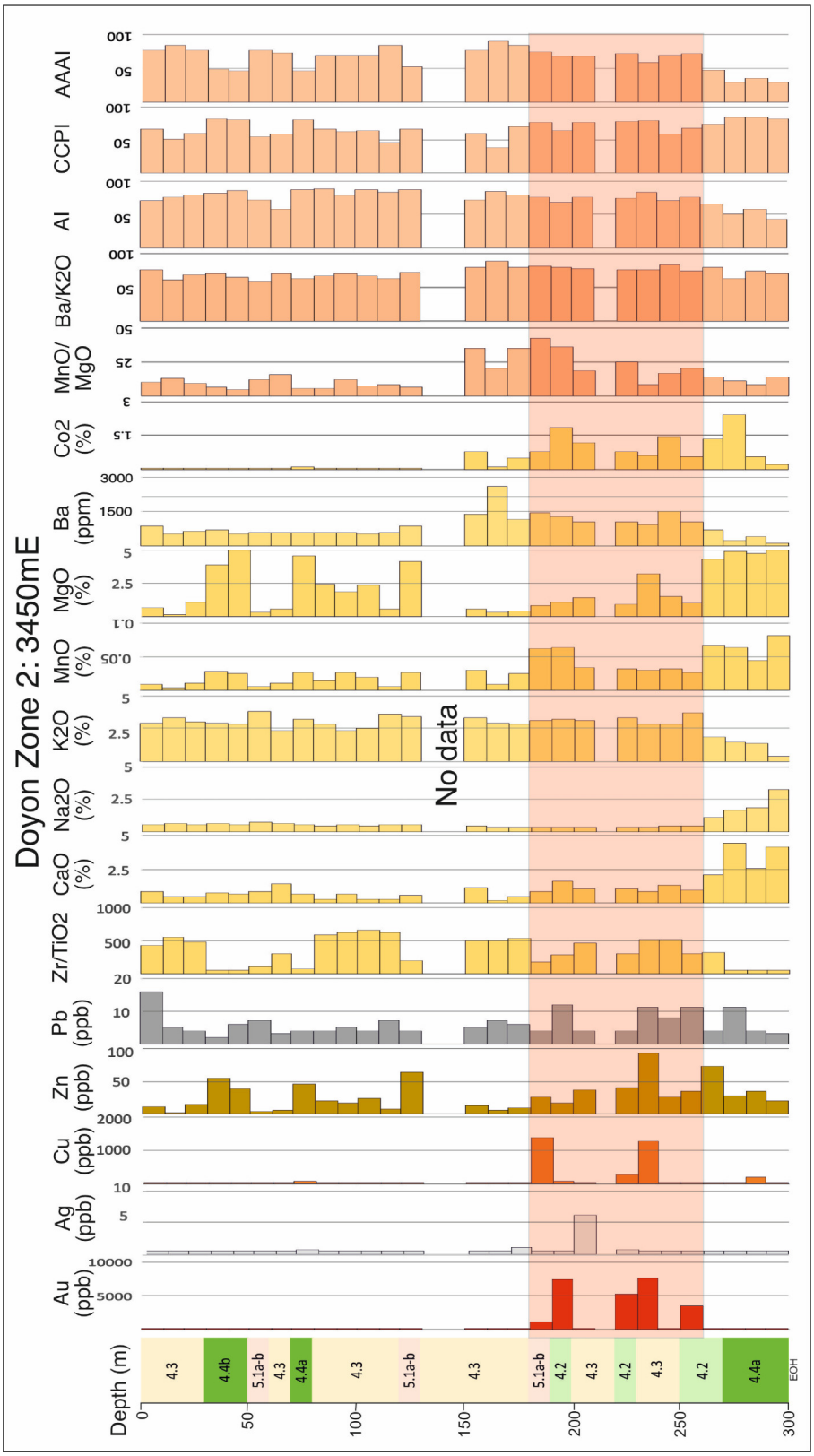

Figure 42. *Geochemical profile of ddh 8-81 through Zone 2 at 3450mE (mine coordinates). Unit descriptions appended to Figure 5. Red shading denotes the main ore zone intersection.*

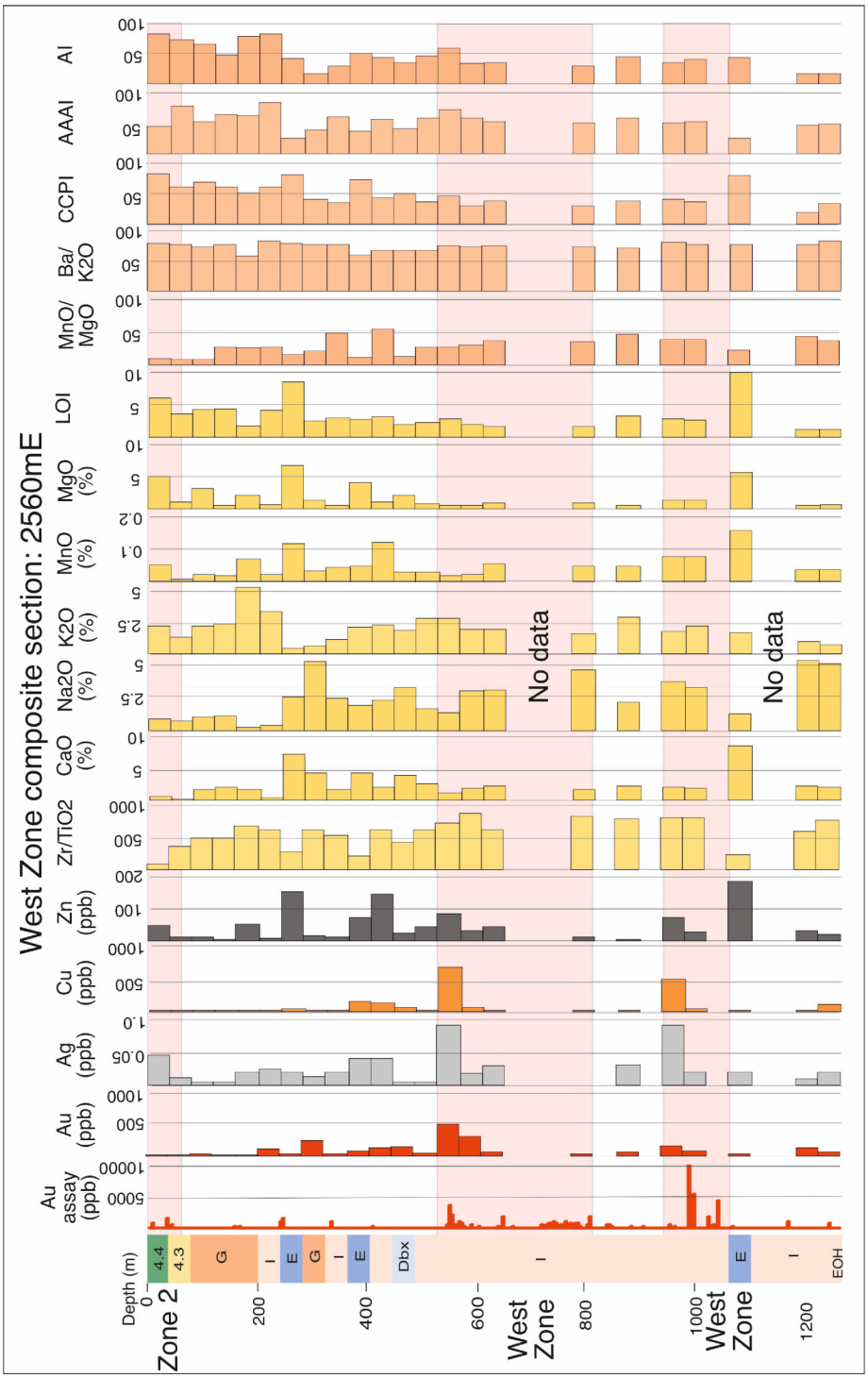

Figure 43. *Geochemical composite profile of from ddh 775-87 and ddh 88-863 on the 2560mE mine section through the western part of the West Zone ore body. Unit descriptions appended to Figure 5. Red shading denotes the main ore zone intersection. Zone 2 denotes extension of this orebody west of the Doyon Fault. The lower notation for the West Zone could be either the NNE striking M orebody or perhaps the easterly extension of the Grand Duc orebody.*

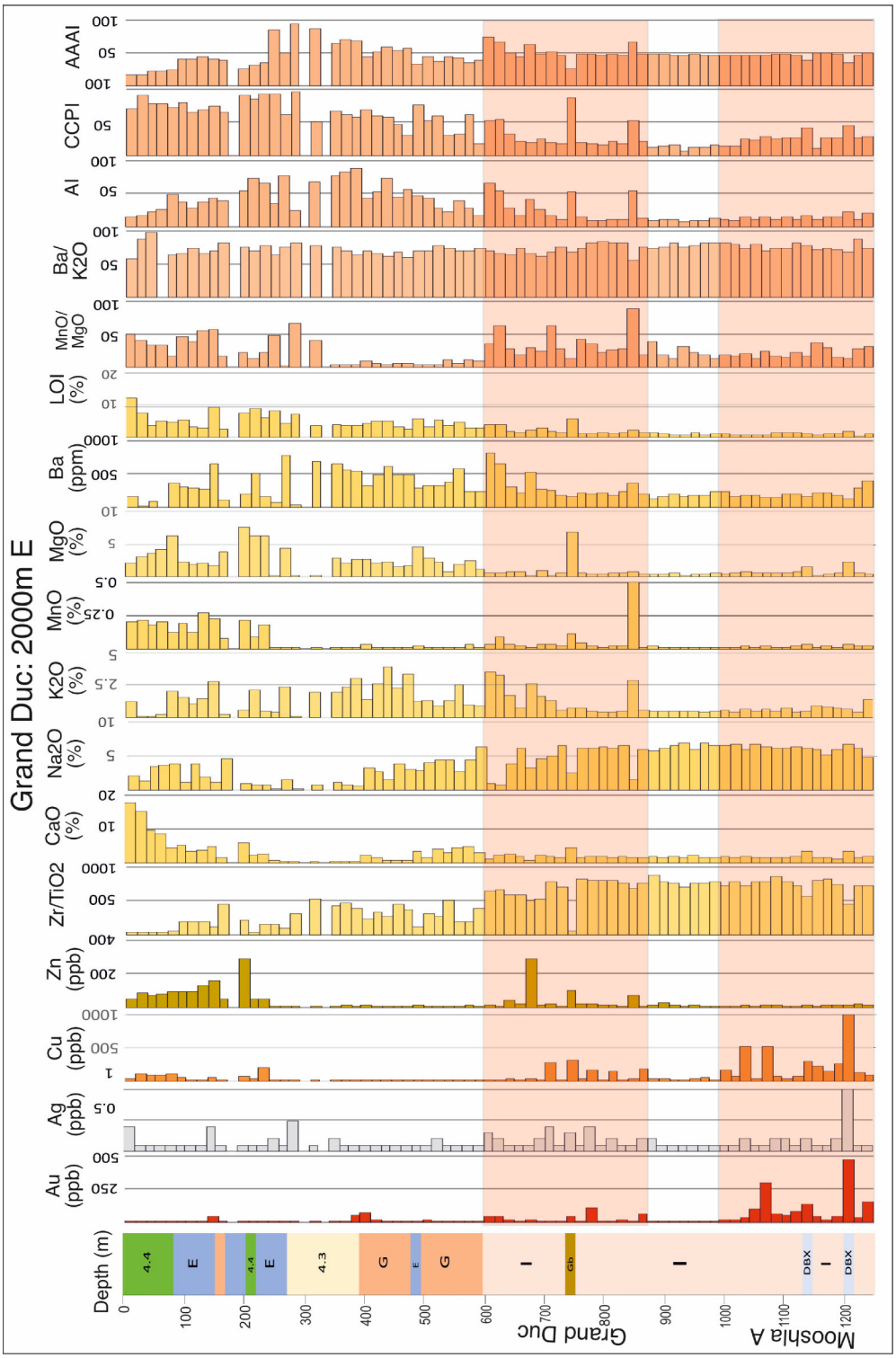

Figure 44. *Geochemical composite profile of ddh 95-1099 through the western part of the Grand Duc and Mooshla A zones. Unit descriptions appended to Figure 5. Red shading denotes the main ore zone intersection.*

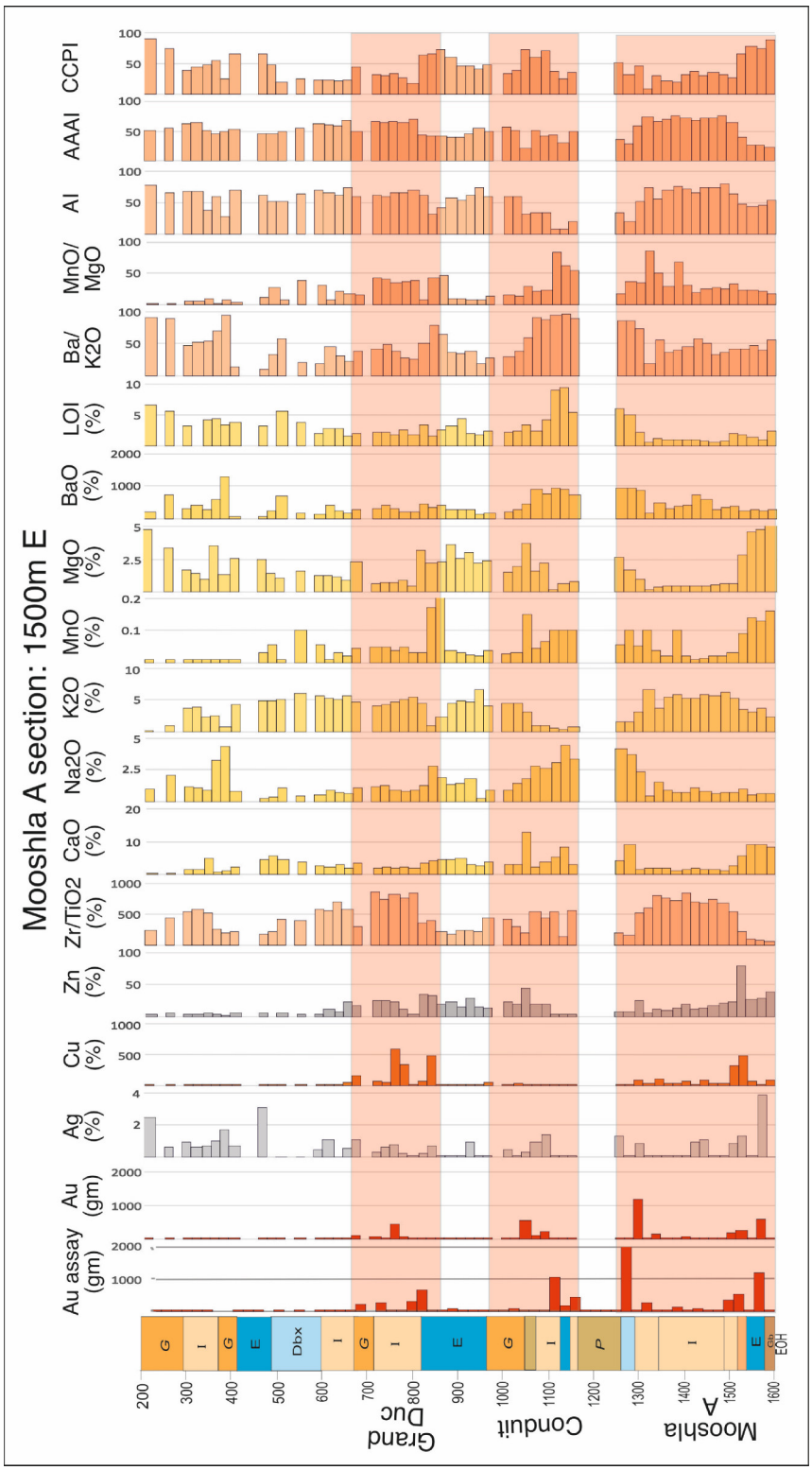

Figure 45. *Geochemical composite profile of ddh 95-1106 on section 1500mE mine section. This section captures the Grand Duc and Mooshla A vein systems, as well as the intervening and connecting auriferous vein array denoted in this paper as the Conduit Zone. Unit descriptions appended to Figure 5. Red shading denotes the main ore zone intersection.*

Variation in MgO follows two trends: the first is a progressive increase MgO with increased alteration intensity. Mineral analysis correlates this trend with increased amounts of Mg-rich biotite to phlogopite, and phengitic sericite. The lower trend shows no increase in MgO and starts with epidote-rich sericite facies and progresses with increased AI values to mainly the Al-silicate and quartz flooded facies. This is in part due to the absence of chlorite in much of the latter trend, but also suggests that the unit 4.3-related alteration does not include the addition of MgO.

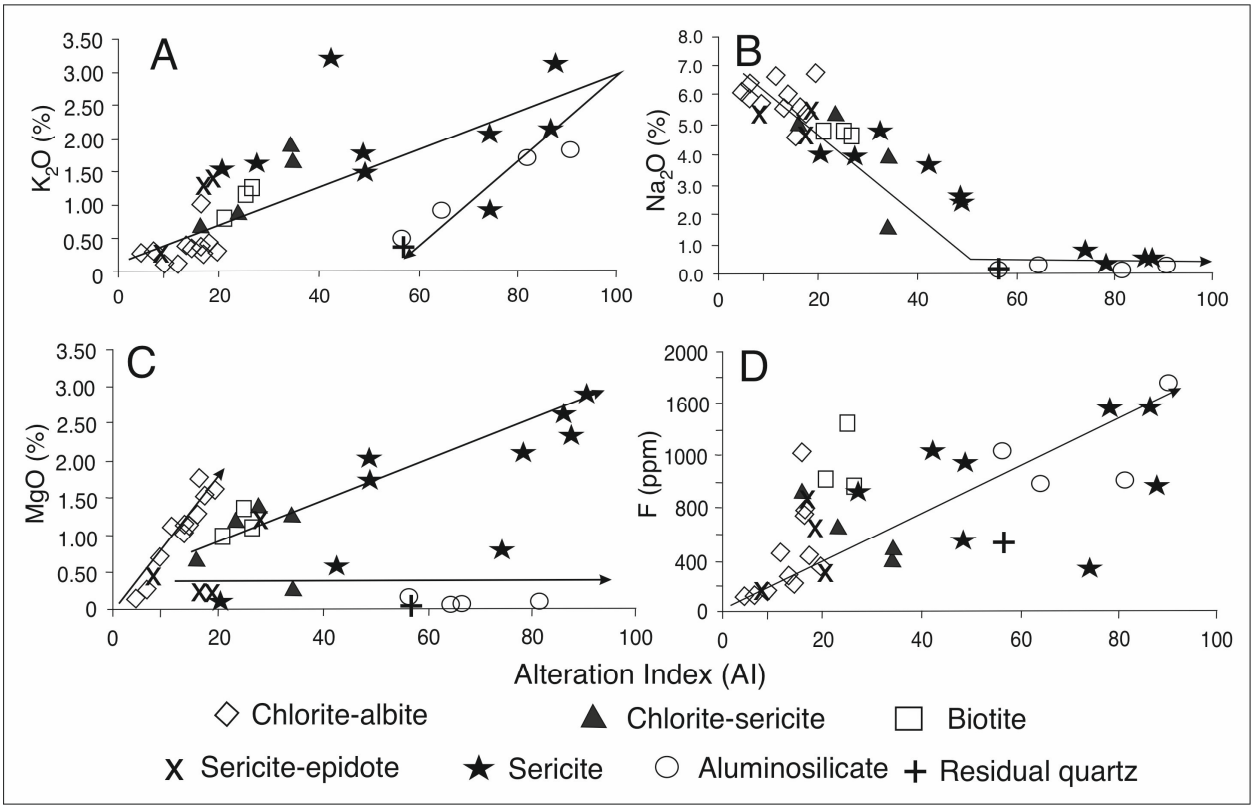

Figure 46. *Alteration index versus some key alteration indicator element within samples of trondhjemite.* ***A****. The diagram shows an increase in K with alteration intensity except within the aluminosilicate and residual quartz facies, where K2O decreases with lower concentrations of sericite.* ***B****. The diagram shows a decline in the Na from the chlorite-albite--rich faces through the biotite and sericite-rich alteration to near zero Na2O concentrations in the aluminosilicate-rich facies and the residual quartz zones.* ***C****. Mg contents within the chlorite-albite facies suggest the presence of both low and high Mg chlorite, perhaps representing metamorphic and hydrothermal types respectively. There also appears to be two other separate trends, one from Mg biotite and phlogopite to a Mg enriched sericite sub-facies, and another with both chlorite and biotite missing from the mineral assemblages.* ***D****. The F content in the trondhjemite generally increases with increased levels of alteration.*

Fluorine as an alteration indicator

A selected sample set from the MIC and host rocks were analysed for fluorine (Mercier-Langevin et al., 2024b). Fluorine analyses were completed due to the recorded presence within the alteration halo about the Doyon mineral system of fluorite in veinlets and the high fluorine content of Mg-rich biotite and phlogopite, and in small part within some muscovite and chlorite (Geological Survey of Canada, unpublished data). The definition of high fluorine contents for transitional tholeiitic to low-K calc alkalic compositions is difficult due to the limited number of studies done for this range of compositions, as many studies including fluorine focus on A-type granites that host epithermal fluorine deposits. Studies of the halogen content of an Icelandic tholeiitic series suggest that primary igneous values range to a maximum of 300 ppm (Stecher, 1998), whereas trondhjemite from various tholeiite to low-K calc alkaline suites suggest that fluorine contents for unaltered rocks range up to 800 ppm (Bailey, 1977). For this study any concentration, regardless of rock type, over 1000 ppm will be considered to be due to some alteration process (Fig. 46).

The linear relationship between fluorine and the AI alteration index (Fig. 46), and the fact that a range of fluorine concentrations from 150 to 2875 ppm are present across a range of lithologic compositions is a strong indication that anomalous concentrations of this element (>1000 ppm) was either introduced or concentrated during alteration processes affecting the MIC. It is worthwhile then to plot fluorine compositions on the MIC centered geology map to further determine the location, size and extent of the higher fluorine values present (Fig 46). High fluorine contents (>1000 ppm F) within the early-stage MIC are focused on late-stage dykes and a sheared and chlorite altered basaltic dyke at the Mooshla B gold occurrence and within a sheared quartz-pyrite-sericite vein hosted within a late stage trondhjemite dyke. Fluorine concentrations >500 ppm are concentrated within the early stage MIC about a late-stage porphyritic tonalite-trondhjemite sill-dyke swarm crossing with western MIC and the overlying volcanic strata.

The highest fluorine concentrations coincide with the alteration zones associated with the Doyon mineral system (Fig. 47). Analyses from both surface outcrop and diamond drill core samples indicate the presence of a carapace of high fluorine that overprints the upper two thirds of the late-stage MIC (including the pendant of early-stage quartz diorite). It extends into the overlying highly

altered unit 4.3 dacite sill complex where it extends eastward to include the Doyon zones 1 and 2 mineralization with fluorine concentrations between 500 and 1500 ppm F (Fig. 47). Published data from Yergeau et al. (2022a, b) and Mercier-Langevin et al. (2024b) indicates that there are few, if any fluorine values >500 ppm associated with the Zone 2 Extension or any of the other Westwood ore zones. Not plotted in Figure 47 are the results from an underground drill hole that intersected a deep part of the West Zone vein system where 10 sample analyses ranged from 950 to 2303 ppm fluorine. This suggests a continuous fluorine anomaly linking the results from the surface drill holes with those plotted for Zone 2.

Correlation coefficient calculations comparing fluorine concentrations to major elements and indicator trace elements, including Au and Cu, indicate very few associations. Positive correlations are moderate to non- existent.

The "strongest" are with Rb (0.5), K_2O (0.48), Ag (0.42) and Tl (0.41). The moderate F-Rb association is explained by the presence of fluorine with Mg rich biotite and phlogopite, and the F-K_2O association with an erratic presence in muscovite. The Ag-Tl moderate association will be discussed later as a possible epithermal association. These moderate fluorine associations indicate that much of its presence is as fluorite.

Alteration box plots

Alteration box plots devised by Large et al. (2001) are mostly used for discerning alteration trends within VMS- and epithermal deposit-hosting volcanic strata. The Hashimoto alteration index ($AI = 100 \times [MgO + K_2O]/[MgO + K_2O + CaO + Na_2O]$: Ishikawa et al., 1976) and advanced argillic alteration index ($AAAI = 100 \times SiO_2/[SiO_2 + (10 \times MgO) + (10 \times CaO) + (10 \times Na_2O)]$: Williams and Davidson, 2004) are compared with the chlorite-carbonate-pyrite index ($CCPI = 100 \times (MgO + Fe_2O_3^T)/(MgO + Fe_2O_3^T + Na_2O + K_2O)$: Large et al., 2001) as two separate plots. The validity of using this plot type for intrusion hosted alteration will be discussed in the appropriate section below. These plots are generated for six different sections through the volcanic and intrusive stratigraphy that best characterizes alteration-mineralization mineral and geochemical relationships (Figs. 48 and 49). Apart from the 95NG-02 plots the data is plotted separately for the volcanic and intrusive rocks.

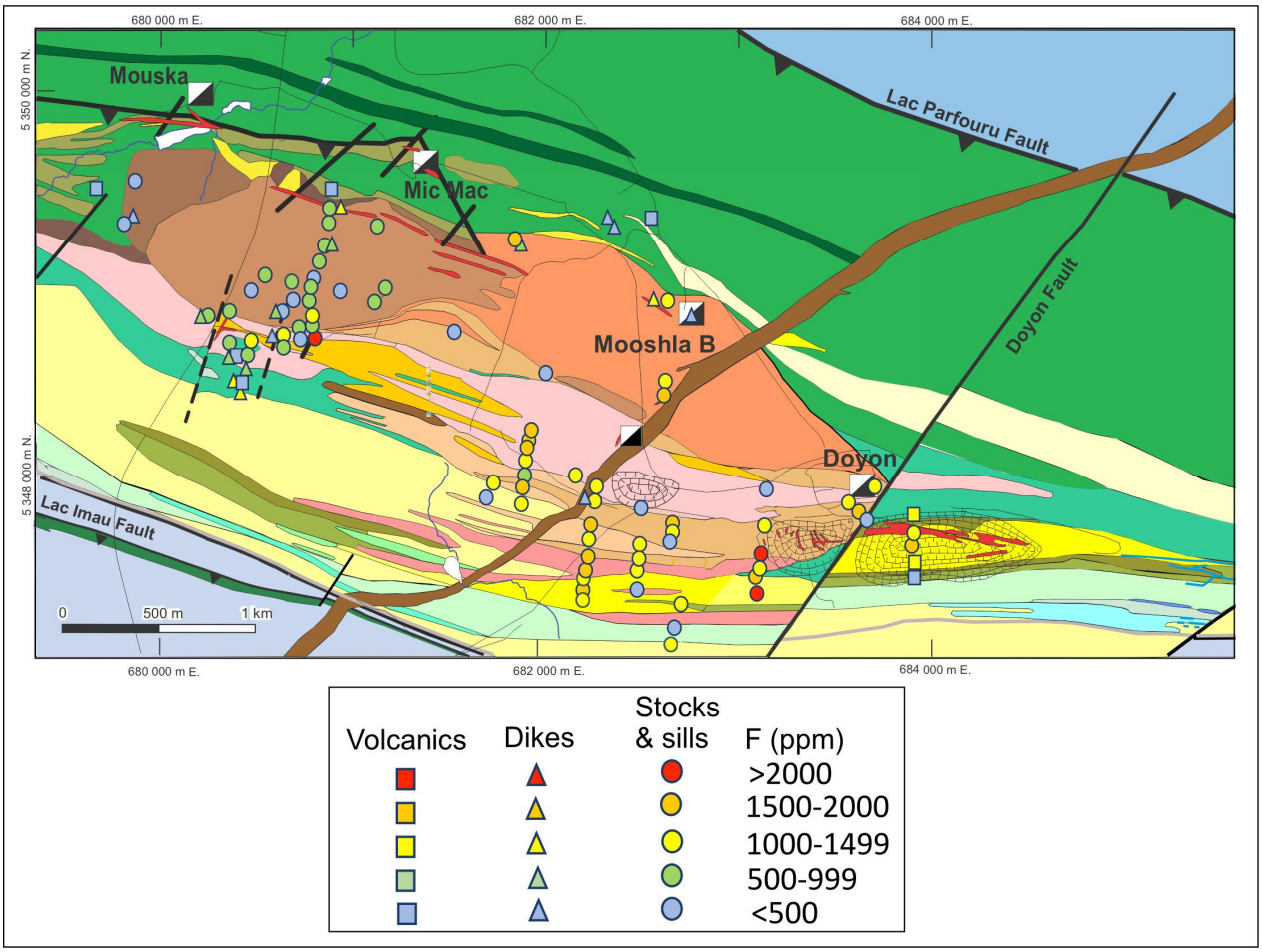

Figure 47. *Fluorine analyses of both surface and diamond drill hole samples. Drill hole values shown for Zone 2 are a composite from a sampled drill hole fence. See Figure 5 for the geology legend.*

The box plots for Zone 2 include alteration trends affecting lower and upper Bousquet volcanic units and the unit 4.3 felsic sill-dyke complex (Fig. 48A). On both plots the trends are towards increasing intensities of sericite, chlorite and chlorite sericite dominated alteration typical for this Au(-Cu) ore zone host rocks. In the West Zone alteration box (Fig. 48B) plots the unit 4.3 felsic sills and host unit 4.4 basaltic andesite continue to show sericite and chlorite alteration trends, whereas the porphyritic tonalite (phase G) and trondhjemite (phase I) of the Mooshla intrusive complex show a mix chlorite-sericite alteration and epidote-carbonate to epidote-carbonate-albite typical of the outer margins of the West Zone vein stockwork mineralization.

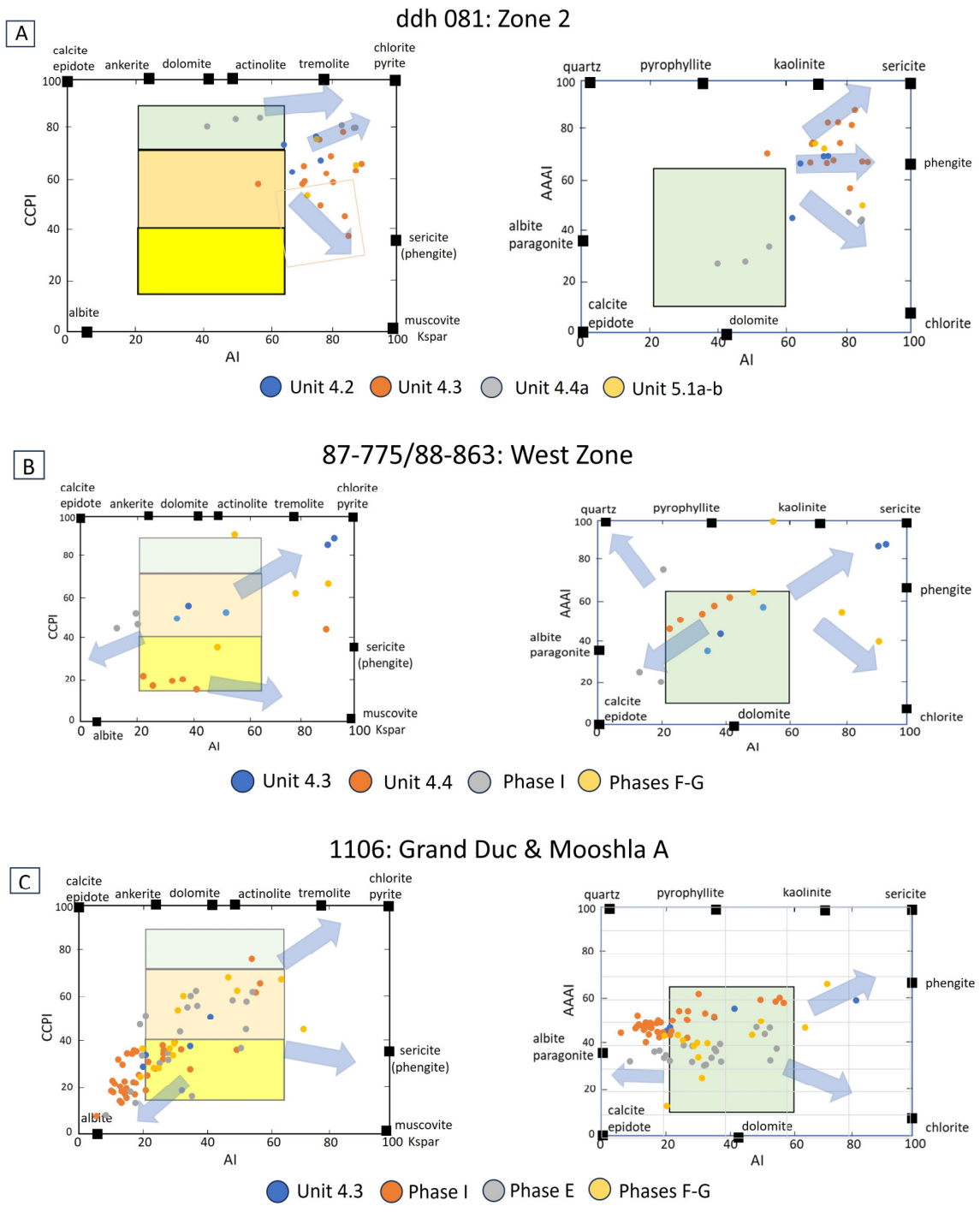

Figure 48. *Alteration box plots of:* ***A.*** *ddh 081 intersection through Zone 2.* ***B.*** *Composite drill hole intersection through the West Zone, and* ***C.*** *ddh 1106-95 drill hole intersection through the Grand Duc and Mooshla A zones. The boxes in the CCPI vs. AI box plot represent the fields for least altered rhyolite (yellow), dacite to andesite (orange) and basaltic andesite to basalt (green). The coloured box in the AAAI vs. AI box plot represents a range of least altered rock compositions.*

The Grand Duc and Mooshla A gold occurrences are both hosted by the porphyritic tonalite and trondhjemite phases of the MIC plus the phase E Doyon quartz diorite roof pendant from early stage MIC (Fig. 39). The two dominant trends are towards chlorite-pyrite for samples with proximal Au(-Cu) vein alteration and towards the albite-paragonite end point representing both the alteration preceding the Au mineralized event and distal Au(-Cu) vein alteration (Fig. 48C). The samples denoted as unit 4.3 in the Na metasomatic trend could well be misidentified due to intense alteration and are instead trondhjemite.

The alteration box plots (Fig. 49) characterize a series of north-south cross sections progressively westward of the Doyon mineral system alteration envelope that are dominated by Bousquet Formation lower and upper members volcanic strata intruded by a number of MIC-related porphyritic tonalite and trondhjemite dykes and Bousquet Formation upper member mafic feeder dykes and sills. The alteration trends for the volcanic strata support the presence of weak to moderate VMS-style alteration with mixed sericite-chlorite zones associated with disseminated to stockwork-type vein occurrences on the Authier property. In Figure 48A, the unit 4.3 felsic sill-dyke complex is still present, and although contains no known significant Au mineralization is still affected by weak to moderate Fe-Mg and K-Mg metasomatism. Drill hole logs record continued areas of strong sericite-quartz-pyrite alteration in this intrusive unit. Unit 5.2 rhyodacite shows some indication of Na metasomatism, a phenomenon noted by Yergeau et al. (2022b) eastward along strike in the hanging-wall strata to the Westwood deposit. Most of the Na and Na-Ca metasomatism shown in Figure 48A affects the MIC-related felsic dykes.

Several observations can be made from analysing the results shown on this series of box plots devised from north-south cross sections moving progressively westwards from the zones 1 and 2 alteration envelope. Firstly, there is an extensive zone of volcanic-hosted weak to moderate Fe-Mg and K-Mg metasomatism in the southwest quadrant of the study area representing footwall alteration to a VMS style that could represent the along strike continuation of the VMS event that occurred across the DBL camp during the beginning of emplacement of the Bousquet Formation upper member volcanism. Secondly, there is nothing distinctive with regards to the metasomatic trends defined from the ratios of the three alteration indices used here that differentiates Doyon-style Au(-Cu) vein-style mineralization from spatially associated VMS-style hydrothermal

alteration. The presence of Na metasomatic trends within the felsic phases of the MIC are not in themselves indicative of the presence of Doyon-style Au(-Cu) mineralization. It is only with the aid of alteration contour maps (see below) that that successive overprinting of Na and K metasomatic events can be observed to define the presence of the Doyon mineral system specifically.

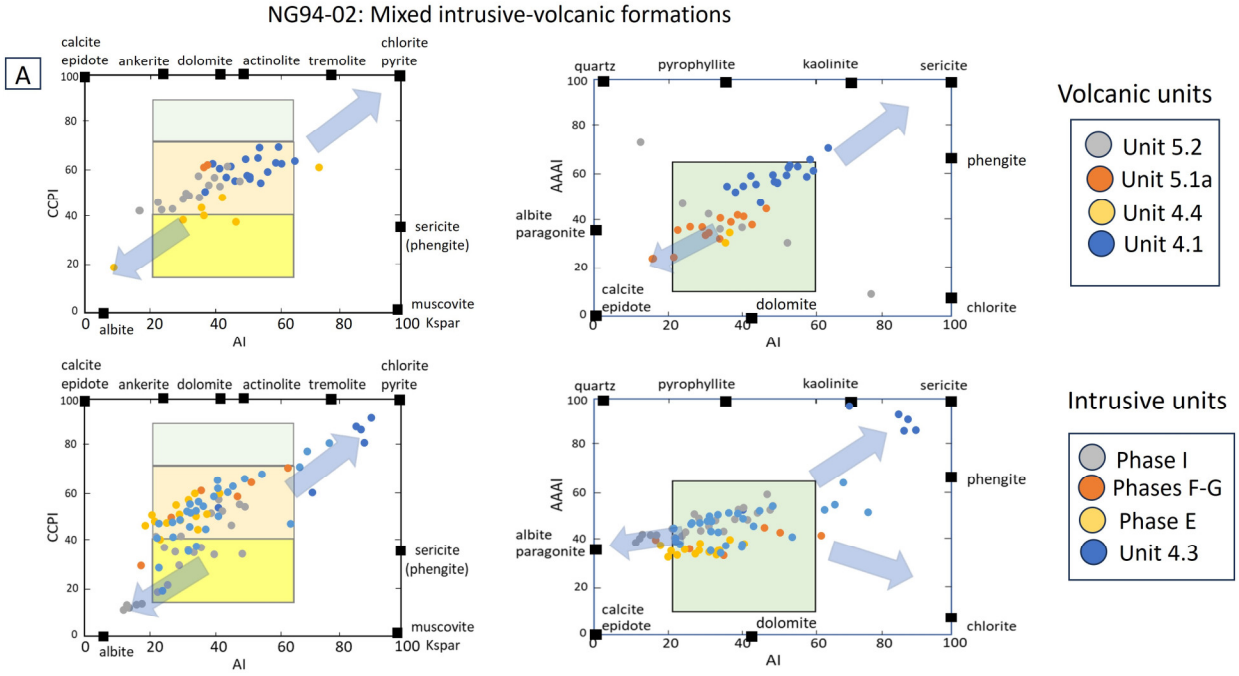

***Figure 49**. **A.** Alteration box plots for volcanic and intrusive units intersected by ddh NG95-02.*

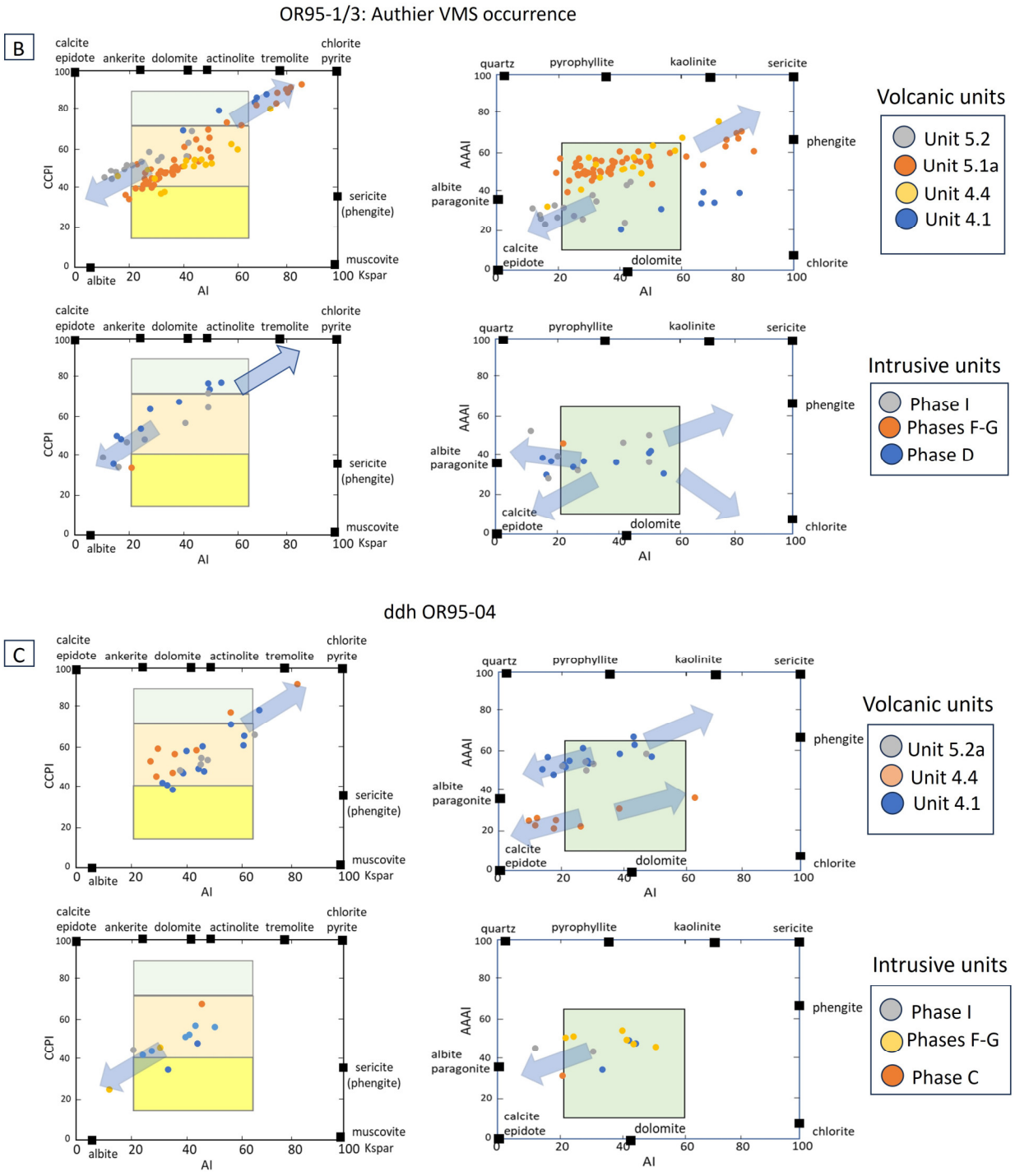

Figure 49. ***B.*** *Alteration box plots for volcanic and intrusive units interested by ddh OR95-01/03 that includes Authier occurrence VMS vein stockwork mineralization.* ***C.*** *Alteration box plots for volcanic and intrusive units intersected through ddh OR95-04 at the western end of the study area. See Galley and Lafrance (2007, 2014) for drill hole locations.*

Element net mass gains and losses

The method developed by Grant (1986) has been used to better understand some of fluid rock interactions that took place during the various alteration stages. The average compositions of the least-altered trondhjemite samples are compared to the average trondhjemite compositions derived for each of the defined alteration facies (Fig. 50). This is calculated by using the slope (altered/unaltered) defined by the elements considered to be the least mobile (for this study: Al_2O_3, Hf, Zr, Ti) in comparison to the calculated change in element concentration between the least altered and altered samples. The result is graphically represented to illustrate the percent change in element concentration during the various stages of alteration as defined by their characteristic mineral assemblages.

What must be kept in mind is that percentage changes are most significant for the major elements. For the minor elements commonly measured in ppm or ppb a change of hundreds to thousands of percent may be significant with respect to determining changes in fluid compositions but may represent rather small real additional concentrations. For instance, the average background Au value of 3.4 ppb for unaltered trondhjemite can be multiplied 1000% and still only represent a concentration of 340 ppb Au.

Increases in K_2O, BaO and F and decreases in the concentrations of Na_2O and CaO, as illustrated earlier by the bivariate plots in relation to the sericitization of both primary and secondary plagioclase. The greatest additions of K_2O and BaO are related to the concentration of sericite, except perhaps within the zone of vuggy quartz, where there may be minor concentrations of barite and potassium feldspar. Also present in the sericite-epidote and sericite alteration facies is fluorite in veinlets and interleaved within biotite flakes. The addition of $Fe_2O_3^T$ is related to the presence of sulphides (with increased S) and in a small part biotite, whereas the gains and losses in MgO are related to the presence and then replacement of Mg-rich biotite and chlorite. The variations in Al_2O_3 and TiO_2 as least mobile elements is reflected in their relative increase within the Al-silicate and quartz flooded alteration facies. The variation in TiO_2 concentrations is reflected in disappearance of primary Ti-bearing minerals (primary amphibole, titano-magnetite and titanite) for rutile, which though sparsely disseminated in the sericite-epidote, sericite, aluminosilicate and quartz flooded zones is also present in veinlets within the sericite-rich alteration facies.

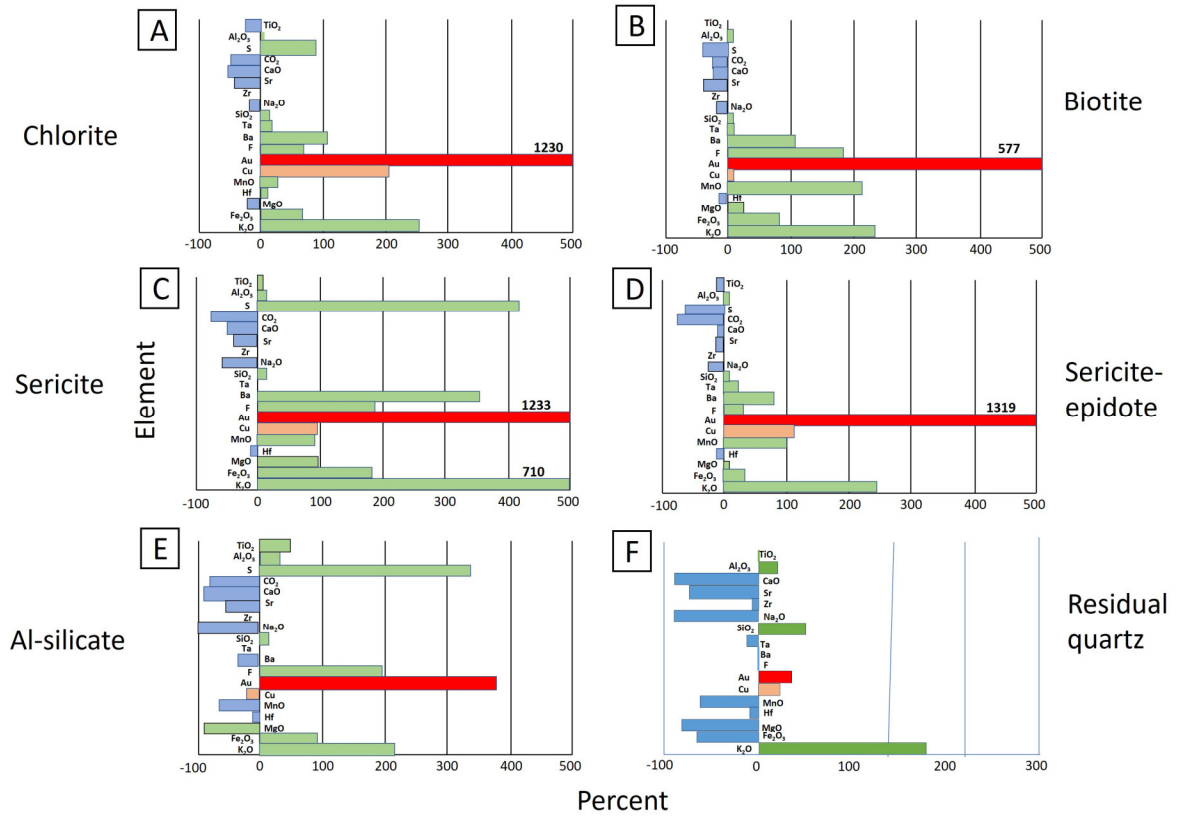

Figure 50. *Net mass gain histograms of various described alteration types. The least-altered baseline was defined as an average of least altered late-stage MIC trondhjemite samples. Zr was used as the baseline element using the net mass balance of method of Grant (1986) for the first five histograms, and TiO_2 used as the baseline for the sixth plot. Alteration types are defined as:* ***A.*** *chlorite facies,* ***B.*** *biotite facies,* ***C.*** *sericite facies,* ***D.*** *sericite-epidote sub-facies,* ***E.*** *aluminosilicate facies, and* ***F.*** *residual quartz facies.*

There is an addition of Au throughout all the alteration facies except for the vuggy quartz facies, which also has a coincident paucity of sulphides as denoted by the net mass gains in $Fe_2O_3^T$ and S. The +1000% gains in the other alteration facies up to a little over 300 ppb Au is significant as described in the next section, as this increase in concentration is only present in proximity to vein systems containing Au measurable in multiple grams per tonne.

Correlation coefficients with Au

There is an overall correlation of anomalous Au values with broad zones of sericite enrichment that extends 3000 m from the western margin of the late-stage MIC to west of the Bousquet fault, encapsulating both the Doyon and Westwood deposits footprint at surface (Fig

14). Correlation coefficients calculated from the Doyon study samples (Fig. 51) indicate that the strongest Au associations at the hand sample scale are with Mo and Cu, with moderate associations with Mn and $Fe_2O_3^T$, and only weak correlations with K_2O and BaO. Anomalous concentrations of the latter two elements are commonly associated with increased sericite content. Element correlations with K_2O indicate high values for Rb and Ba, as expected with sericite formation, and weaker correlations with Mo and Au.

	Mo	Cu	Mn	Fe+3	K2O	Ba
Au	0.76	0.53	0.49	0.40	0.30	0.30

	Rb	Ba	Cs	Mo	Au
K2O	0.86	0.85	0.57	0.34	0.30

Figure 51. *Pertinent correlation coefficients for Au and K_2O*

Alteration contour maps

Three alteration index maps (Figs. 52−54) were generated to better understand the nature and distribution of altered rock units hosting both VMS and Au(-Cu) vein-style mineralization within the study area. Geochemical data was collected from 47 exploration surface drill holes and 31 holes drilled underground around the West zone. Although most of the data is derived from samples spaced approximately 20 m apart from company data, there was a minor amount of fill-in geochemistry generated by the authors. This data was used to generate contour maps for the Alkali Index, Alteration Index and AAAI Index over areas underlain by the Upper Hébécourt and Bousquet formations surrounding the late-stage intrusive phases of the MIC, and the late-stage MIC intrusive phases themselves.

To better understand the results of this contouring exercise, a number of factors must be taken into account that add a level of uncertainty to the interpretation. These include:

a) The contours were generated by hand by the principal author taking into account an ESE bias controlled by the dominant regional S_2 foliation, original bedding orientation within the volcanic units, and the sill-dominated architecture of most of the late-stage MIC intrusive phase.
b) The contours were generated by extrapolating the variations in alteration indices from drill holes drilled with an average 70° dip striking perpendicular to the stratigraphic and structural trends. This extrapolation method thereby has offset contours to the south depending on sample depth, possibly up to 10's of metres at the northern termination of the longer drill holes.
c) The major element geochemical data was generated by various companies over several decades. The accuracy and precision of the whole rock data may therefore vary depending on the analytical methods used over this period, especially for Na_2O. The oldest data covers the areas containing the No.2 and West zones. The contours generated over these zones may well contain the greatest amount of uncertainty.

Alkali Index contour plot

The Alkali Index (Fig. 52) defines the degree of feldspar destruction undergone during alteration associated with the generation of various phyllosilicates, or in contrast, the production of secondary albite-rich alteration. In the northeast contour map quadrant feldspar destruction and attendant Na depletion is centered on both the silicified basalts of units 1.0 and 3.0, and further north on unit 2.0 felsic sills. The linear area of Na addition (between 5 and 7 wt.% Na_2O) coincides with an apophyse of trondhjemite from the late-stage MIC.

The western part of the contour map is underlain by Bousquet Formation upper and lower members of the volcanic units. Along the southern contact of the MIC the zone of Na depletion coincides with unit 3.0 silicification and bleaching. Farther up section (to the south) the dominantly felsic volcanic

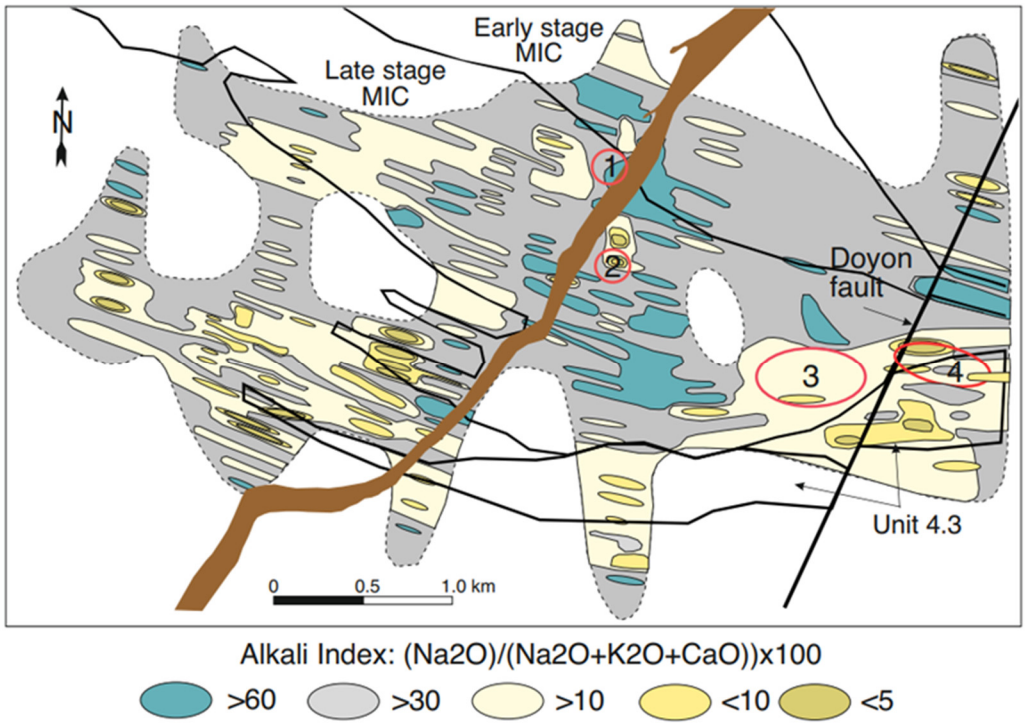

Figure 52. *The contour plot of the MIC intrusive complex and associated host rocks indicating areas of Na depletion (yellows) and enrichment (green). Red circles denote the approximate extent of Mooshla A (1), Grand Duc (2), West Zone (3), and Zone 2 (4) of the Doyon Au(-Cu) system.*

units are overprinted by discontinuous zones of Na depletion coinciding with the previously described sulphide vein stockwork-related sericite-chlorite alteration. Even farther up section these alteration zones form a series of semi-conformable, or concordant alteration zones with increased degrees of Na depletion. These appear to terminate along the lower contact of unit 5.2, which is host to VMS mineralization in the Westwood deposit.

Within the MIC there is a discontinuous, discordant zone of Na enrichment that extends from the Phase D tonalite southerly to terminate near the upper contact of the trondhjemite phases. MIC-hosted zones of Na depletion are both concordant to the strike length of the late-stage MIC intrusive phases but also form a more discontinuous discordant zone that includes the Grand Duc mineralization. It has been previously noted in the description of the various MIC-hosted alteration types that sericite-dominant alteration overprints an earlier-formed halo of albite enrichment.

This continuous zone of Na depletion (and sericite enrichment) trends southerly towards a larger, semi-conformable zone of Na depletion that hosts both the Zone 2 and West Zone ore lenses within the SE corner of the MIC and within the unit 4.2 felsic sill complex. The weak to moderate Na depletion follows the trend of unit 4.3 further to the west.

Alteration Index contour plot

Although the Hashimoto alteration index (AI: Ishikawa et al., 1976) is most used to define proximal VMS-related alteration, it is also applied here to the MIC intrusive complex and spatially associated intrusive units (Fig. 53). The MgO component of this index defines the amount of chlorite and phengite formed at the expense of primary feldspar in the volcanic-hosted alteration zones. Within the MIC intrusive complex, besides Mg-enriched chlorite, there is also an abundance of phengite and Mg-rich biotite to phlogopite.

Within the volcanic pile in the western half of the contour map, this alteration index clearly defines a zone of intense alteration within unit 3.0 mafic rocks that corresponds to a zone of moderate to intense sulphide stringer zone with associated chlorite-biotite alteration.

The Hashimoto alteration index contour map outlines the basal part of an extensive zone of sericite-chlorite alteration and associated sulphide vein stockworks that transect unit 4.1 volcaniclastic strata before changing to a semi-conformable morphology close to the lower contact with unit 4.4 mafic flows and associated volcaniclastic rocks. This alteration morphology continues further up section near the lower contact of unit 5.2 rhyodacite, which again is the host to the Westwood VMS-style mineralization. On the eastern margin of the MIC there is some weak semi-conformable alteration associated with sulphidized unit 1.0 pillowed flows.

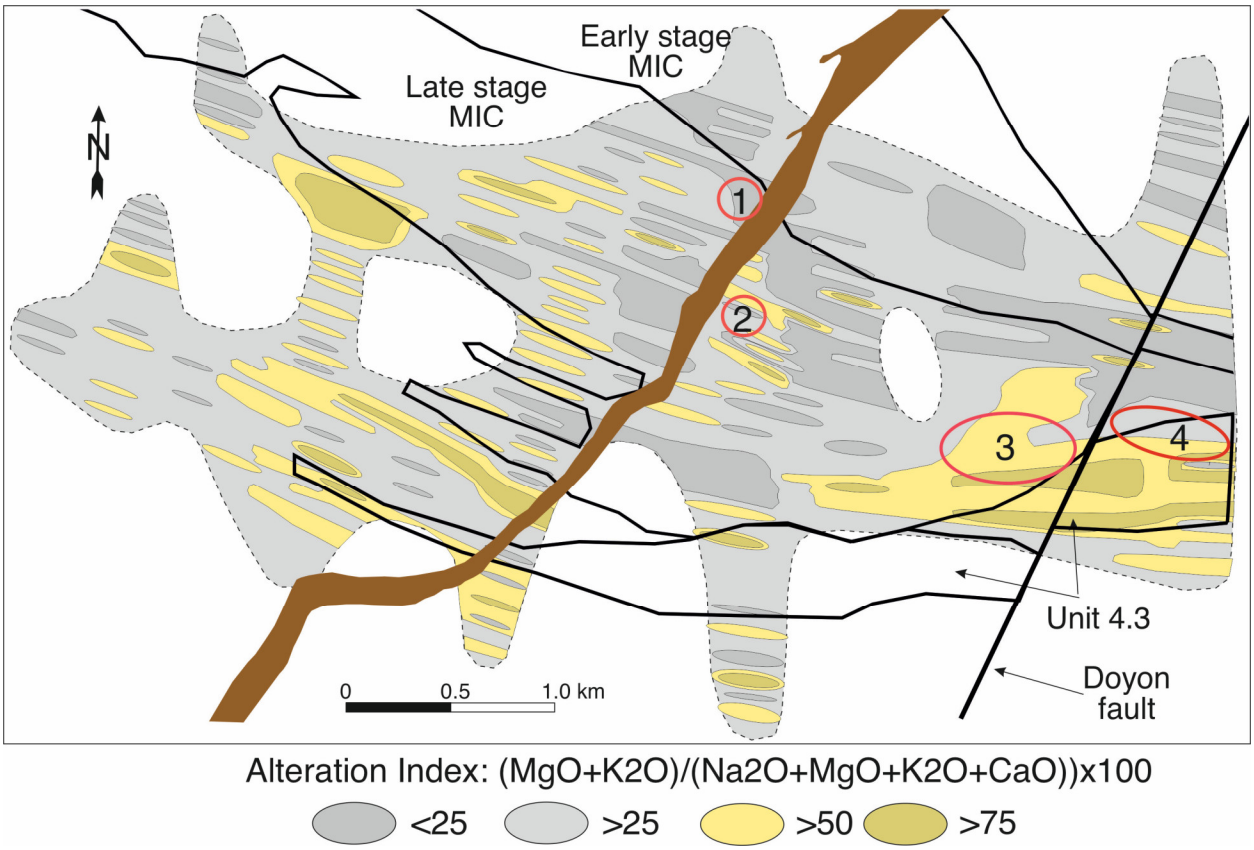

Figure 53. *The contour plot is defined by the Hashimoto alteration index (AI: Ishikawa et al., 1976) commonly used to define zones of VMS-related alteration. Red circles denote the approximate extent of Mooshla A (1), Grand Duc (2), West Zone (3), and Zone 2 (4) of the Doyon Au(-Cu) system. The purple bracket indicates the presence of an intense and extensive alteration zone rooted in unit 3.0 as mentioned in the text.*

In the central part of the late-stage MIC there are discontinuous zones of weak to moderate alteration that coincide with known zones of sericite-pyrite-Ti oxide alteration associated with auriferous quartz-pyrite-chalcopyrite-Ti oxide vein stockworks. To the west of the crossing Proterozoic dyke, the alteration zones are semi-conformable with the strikes of sills comprising the trondhjemite intrusive phases. Along the east margin of the Proterozoic dyke is a discontinuous zone of moderate to intense alteration that corresponds with the CT and Grand Duc auriferous quartz-pyrite-chalcopyrite-Ti oxide zones.

In the SE quadrant both the late-stage MIC and unit 4.3 felsic sill complex and immediate host rocks are strongly affected by weak to intense alteration. This zone is host to the West Zone and partial host to zones 1 and 2. This alteration zone only affects the footwall contact to unit 4.3 west of the Doyon Fault, which corresponds to a semi-conformable zone of intense vuggy quartz alteration. The alteration zone extends NE of the West Zone towards the east margin of the MIC where it hosts the Moulin veins and J zone (Fig. 21), which also coincides with the presence of the Mg-biotite enriched vein stockworks and micro-breccia. With the MgO component only included in this alteration index and not the other two it may explain why this is the only index showing this alteration apophyses.

AAAI contour plot

The AAAI contour plot overlaps with both the Alkali and Alteration indices but forms much more continuous and extensive alteration zones. This type of index was created to define zones of intense leaching by acidic fluids present in some VMS systems and more commonly associated with subaerial, epithermal-type sulphide vein stockworks where rock is leached of most elements except for Si, Al, and to some extent Ti and other resistant elements. Such alteration is usually the result of very low pH and high fO_2 reactions between boiling magmatic-hydrothermal fluid and host rock that results in varying degrees of leaching around vein-filled fracture systems known in porphyry-epithermal terms as argillic and advanced argillic alterations (Heald et al., 1987; Simmons et al., 2005). These zones are characterized by aluminosilicate, pyrite and quartz. In porphyry-epithermal systems, these argillic and advanced argillic alteration zones are commonly rooted within intrusion-hosted or -associated zones of phyllic alteration. In epithermal systems, this leaching is associated with sericite and sericite precursors such as illite and Mg smectites. Under upper greenschist regional metamorphic conditions that affects much of the surface geology in and around the MIC, the illite-smectite phyllic and kaolinite-diaspore-pyrophyllite-dickite±alunite mineral assemblages are converted to sericite-phengite and andalusite-kyanite-quartz, respectively. Topaz can be part of that assemblage in areas with high F. The zones of argillic alteration can be capped by silica-rich zones of intense leaching that correspond, in subaerial systems, to the most intense advanced argillic alteration zones.

Several previous researchers of the Doyon and Westwood systems have suggested that the quartz-pyrite-chalcopyrite-Ti oxide nature of the systems vein arrays, plus the presence of abundant sericite and aluminosilicates indicates an epithermal (or epithermal-like) origin for the Doyon mineral system. It is for this reason that an AAAI contour map may prove useful in further understanding the acidic alteration zones and possible origin of at least part of this system.

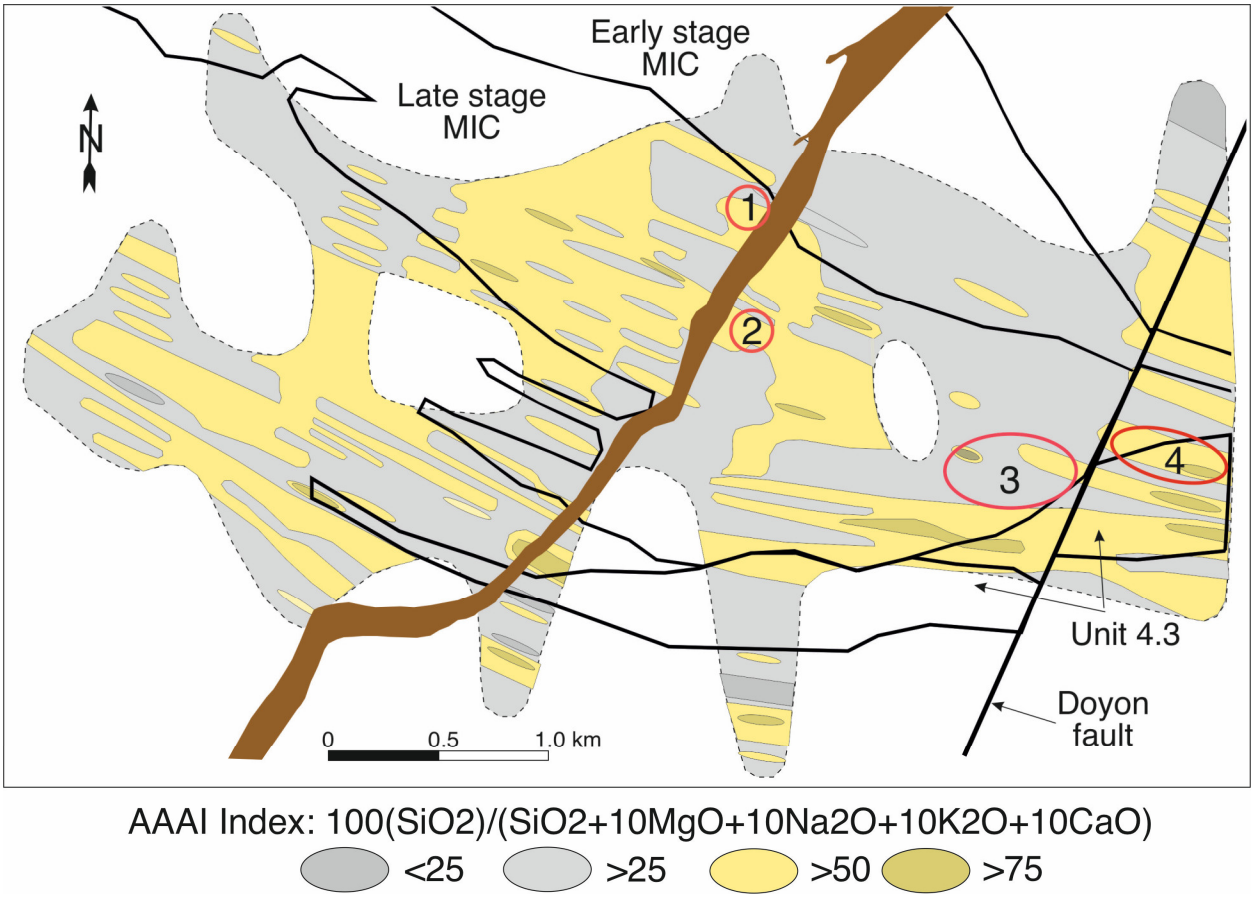

Figure 54. *The AAAI index (Williams and Davidson, 2004) is mostly used to define the presence of leached alteration zones often associated with strongly acidic alteration, which is a common characteristic of epithermal, or VMS-epithermal systems, and is therefore interesting to use to characterize intrusion-related Au systems. Red circles denote the approximate extent of Mooshla A (1), Grand Duc (2), West Zone (3), and Zone 2 (4) of the Doyon Au(-Cu) system.*

The AAAI contour plot (Fig. 54) defines areas of alteration that overlap in most cases with those of the Alkali and Alteration indices, but the defined zones are more continuous. Those hosted by the volcanic pile in the western map quadrant indicate a zone of continuous discordant alteration

linking to overlying zones of semi-conformable alteration below units 4.4 and 5.2. On the east margin of the MIC the zones of extensive alteration are most likely related to zones of extensive bleaching and silicification within the upper unit 1.0 pillowed Hébécourt Formation basalts and in the unit 3.0 mafic volcaniclastic rocks. The thin SE-striking band of unaltered rock within this zone of alteration defines the MIC-related trondhjemite apophyse (Fig. 54).

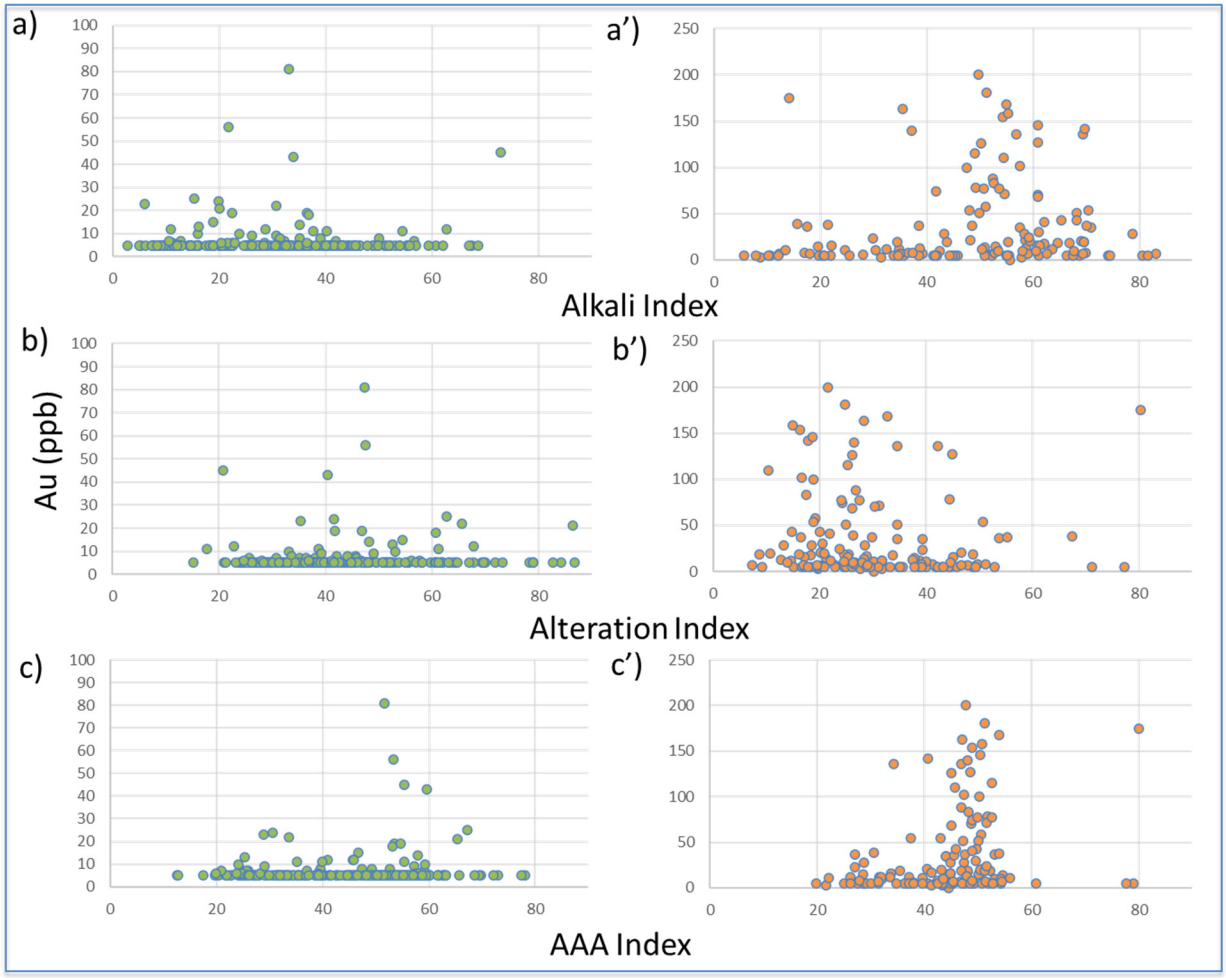

Figure 54. *Plots of drill hole data for dominantly volcanic (green) and MIC intrusive complex (orange) samples for the three different alteration indices described in the above section.*

A broad alteration zone affects the central part of the late-stage MIC intrusive phases and mimics the extent of sericite-enriched alteration identified from surface and drill core geology (Figs. 37 and 38). This zone encompasses the Mooshla A, Conduit (CT) and Grand Duc mineralized zones and continues south to link with the semi-conformable alteration zone that overprints the upper

contact of the MIC and the eastern part of the unit 4.3 felsic sill complex. West of the Doyon Fault this zone also affects the footwall contact to unit 4.3 where vuggy quartz alteration has been identified in drill core (Fig. 39). It should be noted that most of the West Zone is not included in this zone of alteration. This will be addressed in the discussion.

Alteration indices versus Au concentration

Although all three of the alteration contour maps suggest that zones of extensive alteration are indistinguishable between volcanic and intrusive units, even though the respective associated sulphide mineralization is clearly different, i.e. VMS in volcanics versus vein type Au(-Cu) in intrusions. With respect to the alteration zones identified on the AAAI contour map they can also be segregated into alteration in which there is no defined association with Au mineralization (VMS) and the intrusion-hosted alteration in both the late-stage MIC and unit 4.3 where there is a linear relationship between altered rocks and anomalous Au content (Fig. 54).

DISCUSSION

The following summary can be made from the data and observations gathered for this open file on the Doyon mineral system and its host rocks:

- The Doyon Au(-Cu) vein system is hosted within the Doyon late-stage intrusive phases of the MIC and within the adjacent and overlying rhyodacite sill-dyke complex.
- The MIC was emplaced along the contact between the tholeiitic Hébécourt Formation and the overlying low K transitional to calc-alkalic Bousquet Formation. The Hébécourt Formation consists of massive to pillowed basalt flows and associated autoclastic facies whereas the Bousquet Formation has a foundation of pillowed basaltic andesite flows, mafic to polymictic volcaniclastic units, and autoclastic facies overlain by rhyodacite to rhyolite flow dome complexes with associated volcaniclastics.
- The upper part of the Hébécourt Formation and overlying Bousquet Formation are affected to varying degrees by proximal to distal subsea floor hydrothermal alteration and associated sulphide mineralization, including the Zn-Ag-Au massive sulphide zones of the Westwood deposit.
- The early-stage MIC (Mouska stage) consists of a tholeiitic porphyritic diorite and layered gabbro, and transitional quartz diorite and tonalite whereas the late-stage MIC (Doyon stage) consists of low K calc-alkalic porphyritic tonalite, aphyric to quartz-feldspar phyric trondhjemite. Dyke swarms of Doyon stage porphyritic tonalite, trondhjemite and basalt cross the Mouska early-stage intrusive phases.
- Although precise timing between the two stages of the MIC cannot be obtained from published U-Pb ages, an age difference between the early and late MIC stages is calculated to be approximately 1.44 Ma using the newly developed high-precision chemical abrasion ID-TIMS geochronology (Neyedley et al., in press).
- The MIC is coeval with the Bousquet Formation (approximately 2698 Ma), with the mafic phases comparable in composition to the volcanic and intrusive rocks of the Bousquet Formation lower member, and the felsic late-stage intrusive phases geochemically like the rhyodacite and rhyolite flow-dome complexes of the Bousquet Formation upper member.

- Whereas the Mouska early-stage intrusive phases range in morphology from layered sill/laccolith to stocks, the Doyon late-stage intrusive phases consist of a series of sills and dykes emplaced within the upper margin of the earlier MIC stage. During this process much of the early stage upper xenolithic margin was disconnected as a roof pendant and now resides within the late-stage sill-dyke complex (Galley and Lafrance, 2014).
- Neyedley et al. (in press) proposes that the various phases of the MIC had a variety of lithospheric partial melt sources. The textures of early-stage quartz diorite and tonalite phases indicate that they were emplaced as crystal "mushes" indicating mid-crustal magma fractionation. The late-stage MIC phases are texturally consistent with high level emplacement (<2000 m), with corroded, resorbed phenocrysts, abundant miarolitic cavities, and granophyric groundmass. The MIC therefore represents a phase of resurgent magmatic activity that took place after emplacement of the Bousquet Formation.
- This magmatic event is postulated to represent early-stage back arc rifting of a previously formed primitive island arc-style succession present to the west as the Blake River Group (approximately 2700 Ma) (Galley and Lafrance, 2014; Mercier-Langevin et al., 2017; Yergeau et al., 2022a; Neyedley et al., in press).
- The Doyon Au(-Cu) vein system is a contiguous system of auriferous quartz-sulphide veins extending from the MIC-hosted Mooshla A Au occurrence through the Grand Duc and the West Zone deposits to the volcanic-intrusive-hosted Zones 1 and 2 (Fig. 13).
- The formation of the Doyon Au-bearing vein stockworks began with the emplacement of an NNE-WNW striking polygonal vein system of thin (<15 mm thick) quartz-pyrite-chalcopyrite-rutile-Au veins associated with quartz-sericite-pyrite alteration. Where the vein stockwork crosses xenolith-rich trondhjemite or the quartz diorite roof pendant it has a quartz-sericite-epidote-chlorite-pyrite altered margin. It is weakly auriferous (<1 g/t Au) and can be traced through the Doyon late phase trondhjemite, porphyritic tonalite and associated early-stage roof pendant into the overlying rhyodacite sill-dyke complex.

- This vein stockwork is overprinted by dominantly north to northeast striking, steeply dipping, thicker (up to 1 m in width) breccia vein stockwork that is more chalcopyrite, carbonate, and chlorite rich with sericite-chlorite-carbonate haloes. Higher Au values (up to tens of grams per tonne) are present as remobilized native Au and electrum accompanied by tellurides in the veins and vein margins and Au-Ag-Bi-Te-Sb-Pb-Ni-Cu-Zn-Cd enrichment in accompanying pyrite (Guha et al., 1982; Savoie et al., 1990; Neyedley et al., in press).
- Both stages of auriferous vein emplacement reside principally within an envelope of sericite-rich (and biotite-rich within the quartz diorite rood pendant) alteration that can be traced where it affects trondhjemite dykes within the Mouska stage extending northward and eastward to include the Zone 2 Extension of the Westwood deposit (Fig. 30). At the upper margin of the MIC and within the overlying unit 4.3 rhyodacite sills-dyke complex the sericite alteration halo includes a locally preserved sub-zone of aluminosilicate-rich alteration and patches of residual, or vuggy quartz alteration. These alteration facies overprint earlier-formed VMS-related alteration at the Westwood deposit (Yergeau et al., 2022b).
- This sericite-rich envelope coincides with a ≥20 ppb Au halo about the Doyon-Westwood Au systems (Fig. 14) and the AAAI alteration index contour pattern (Fig. 54) which is strongly influenced by Na and Ca depletion and K addition
- Within the MIC the sericite-rich alteration envelope overprints several earlier-formed alteration facies. The earliest is a set of vein dykes spatially associated with trondhjemite dykes cutting the early stage tonalite with open space cores infilled by quartz, plagioclase, and epidote. These are followed by a quartz-tourmaline fracture-controlled silicification, followed by a series of K metasomatic alteration facies that begins with Mg-biotite-phlogopite and Mg-biotite-potassium feldspar-sulphide enriched veins and vein breccias overprinted by quartz-anhydrite-sulphide veins. These alteration facies are overprinted by a more extensive fracture-controlled alteration event characterized by quartz-chlorite-albite-magnetite-pyrite that is associated with trondhjemite dykes crossing the early stage Mouska intrusions to become wider spread within the later Doyon stage. This Na metasomatic event extends eastwards out along a trondhjemite apophyse to affect Bousquet Formation lower member mafic units.

- Associated with these alteration events is an increase in whole rock concentrations with up to 2500 ppm F. The Mg-biotite and phlogopite contain up to several percent F, with lesser concentrations in muscovite and chlorite. Fluorite veins are locally associated with the Mg-biotite, chlorite, and sericite alteration facies, and can be traced into the hanging wall within the sericite and aluminosilicate alteration facies associated with Zone 2 mineralization. In the Westwood Zone 2 The fluorine anomaly is replaced by a Ba anomaly, along with gypsum instead of anhydrite.
- The Doyon mineral system and host rocks are all affected by varying degrees of deformation and regional metamorphism. There is secondary chlorite, sericite and carbonate within strata overprinted by upper greenschist mineral assemblages, with paragonite instead of muscovite present in pressure shadows around pyrite, and primary aluminosilicate minerals (e.g. dickite, pyrophyllite and kaolinite) replaced by andalusite, then retrograded to kaolinite and pyrophyllite. Approximately 1200-1500 m below the erosional surface there is biotite-spessartine-magnetite overprinting the MIC-hosted alteration, and kyanite replacing primary aluminosilicates.
- The Doyon mineral system and its host rocks are overprinted by a weak to moderate D_2 (D_3 in Dubé and Mercier-Langevin, 2020) easterly schistosity, with more intense northerly trending oblique-reverse shears focused on the zones of phyllosilicate alteration. This S_2 foliation crosses and is refracted by the northerly trending Doyon vein stockworks and shears in the easterly trending vein systems, especially those of Zones 1 and 2. Northerly striking vein sets at high angle to foliation are commonly folded. The steeply WSW plunging West Zone ore body parallels the calculated movement direction on associated S_2 related oblique-reverse shear zones and with a district-scale shape lineation. Syn-D_2 massive or laminated fault-fill- and extension-style quartz ±tourmaline-carbonate-euhedral pyrite and associated Fe-carbonate-dominant selvage alteration, which form by far the most important type of Au deposit in the southern Abitibi belt, are only locally present and are sparsely mineralized in the Doyon mine environment.

Evidence for a shallow-marine, intrusion- related Au(-Cu) vein system

The detailed studies of the host geology, geochemistry and mineralogy, and this compilation of the Doyon mineral system weigh heavily towards recognizing a magmatic-hydrothermal origin in a shallow marine setting that shares some analogies with porphyry-epithermal systems (e.g. Guha et al., 1982; Gosselin, 1998; Galley and LaFrance, 2014; Neyedley et al., 2021a, b; Yergeau et al., 2022a, b). A comparison of the Doyon mineral system characteristics with those of various types of documented Phanerozoic epithermal systems is tabulated in Table 3.

Tectonic setting

Although still debated, the tectonic setting for the Doyon mineral system (and the remainder of the DBL Au systems) is postulated to be associated with initial back arc rifting of an earlier formed primitive island arc defined by lithology and geochemistry of the lower Blake River Group. The subaqueous tholeiitic bimodal basalt-rhyolite flow architecture of the overlying upper Blake River Hébécourt Formation defines the initiation of back arc rifting whereas the succeeding Bousquet Formation more fractionated transitional to calc-alkalic basaltic andesite-andesite-dacite-rhyodacite-rhyolite suite is indicative deep (>40 km) partial melting of previously hydrated lithosphere, followed by mid crustal storage and fractionation and then volcanic eruption onto the seafloor (Neyedley et al., in press). The resultant seafloor terrane of calc-alkalic lava domes and flows and basins of volcaniclastic strata is characteristic of compressional-transpressional arc margins typical for subaerial high sulfidation epithermal deposits such as those defining the Yanacocha, Peru (Teal and Benavides, 2010; Longo et al., 2010) and subaerial to shallow marine systems such as Pueblo Viejo, Dominican Republic (Kesler et al., 2005; Sillitoe et al., 2007) districts. The Pueblo Viejo district has perhaps the greatest similarities due to the co-existence of Early Cretaceous epithermal-style and VMS-style deposits (Kesler et al., 2005; Sillitoe et al., 2006; Nelson et al., 2023).

The compressional-transpressional tectonic setting is also common for the generation of high-level porphyry systems (Seedorf, 1999, Sillitoe, 2012). This would allow for the high-level emplacement of the Mooshla Intrusive Complex with its porphyry-like characteristics described below.

***Table 3**. Comparison of summary characteristics of Phanerozoic epithermal systems with the Doyon Au(-Cu) system. Modified from John et al. (2010).*

	High-sulfidation	Low-sulfidation
Spatially and temporally associated volcanic rocks	Calc-alkaline, andesite-dacite	Calc-alkaline, andesite-dacite; tholeiitic, bimodal basalt-rhyolite
Volcanic landforms and deposits	Lanva domes and flows, diatremes, tuff rings, maars, and intrusive breccias assoc. with diatremes; uplands and basins of pyroclastic and volcaniclastic rocks	Lava domes and flows; uplands and basins of pyroclastic and volcaniclastic rocks; dikes
Tectonic setting	Compressional-transpressional continental margin arc or back arc; neutral stress to mildly extensional continental margin arc	Extensional continental margin and island arcs; extensional back arc; post-arc continental extension
Proximal alteration minerals	Alunite, kaolinite (dickite), pyrite, pyrophyllite, residual, vuggy quartz, aluminum-phosphate-sulphate (APS) minerals	Quartz-adularia±illite±pyrite
Silica and carbonate gangue and textural features	Structurally and stratigraphically controlled fine-grained silicification and residual, vuggy quartz; no carbonate minerals	Vein-filling crustiform and colloform chalcedony and quartz; minor late calcite and (or) calcite replacement texture
Other gangue	Minor barite common, typically late	Barite uncommon; fluorite present locally
Gold-silver and other ore minerals	Gold, electrum, Au-Ag tellurides, acanthite, Ag-bearing tennantite, enargite, luzonite, chalcopyrite	Electrum, Ag sulfides, selenides and sulfosalts; low Ag/Au; generally no other metals recovered
Sulfide abundance	5 to 90 vol.%	Typically <1 to 2 vol.% except where hosted by basalts (as much as 20 vol.%)
Sulfide minerals	Pyrite, enargite, luzonite, covellite-digenite, famatinite, chalcopyrite, tetrahedrite/tennantite, Fe-poor sphalerite	Pyrite/marcasite, Au-Ag sulfides/sulfosalts, arsenopyrite
Other enriched metals	As, Sb, Bi, Sn, Te, Se	As, Sb, Se, Hg
Te and Se minerals	Au-Ag tellurdies common; selenides present locally	Au-Ag selenides, Se sulfosalts common
Deposit style, veins and mineralerized structures	Breccias, diatremes; residual vuggy quartz; stratabound disseminated; massive sulfide; veins and stockworks; veins generally late	Multiple stage veins of fine concordant and discordant layered mineral assemblages and breccias, comb and crustiform textures; sheeted veins; vein stockworks and breccias; fault intersections; disseminated
Paleosurface indicators	Steam-heated blankets over some deposits	Sinter and explosion breccias; chalcedony blankets over some deposits; thin quartz veins and stockworks over some deposits
Depth to top of ore zones (metres below watertable)	Tens of metres to 700 m	Metres to several hundred metres
Vertical extent of ore	100 to 800 m	Mostly 100 to 400 m
Representative deposits	Yanacocha, Pueble Viejo, Pierina, Pascua-Lama, Goldfiled, Summitville	Hishikari, Midas, Sleeper, McLaughlin, National, Mule Canyon

*Metamorphosed and deformed with various degrees of remobilization of Au, Au-Ag tellurides, and base metal sulphides

***Table 3**. Continued.*

	Intermediate-sulfidation	Doyon*
Spatially and temporally associated volcanic rocks	Calc-alkaline, andesite-rhyolite	Transitional to low K calc-alkaline andesite-rhyodacite-rhyolite; tholeiitic to transitional basalt-basltic andesite base
Volcanic landforms and deposits	Lava domes and flows, diatremes, tuff rings, maars, and intrusive breccias assoc. with diatremes; uplands and basins of pyroclastic and volcaniclastic rocks	Lava domes and flows; uplands and basins of pyroclastic and volcaniclastic rocks; sills and dikes
Tectonic setting	Extensional continental margin arc; compressional island arc; continental rift	Compressional-transpressional island arc margin with early-stage oceanic back arc extension
Proximal alteration minerals	Quartz-adularia±illite±pyrite	**Zones 1 & 2**: Metamorphic Al-silicates replaced with dickite, pyrophyllite and kaolinite, residual, vuggy quartz (external to MIC)
Silica and carbonate gangue and textural features	Fault zone replacement and vein-filling by fine- to coarse-grained equigranualr quartz, and crustiform and comb quartz; calcite late or distal to thermal centres	Patchy residual, vuggy quartz and silicification above MIC contact
Other gangue	Barite and manganiferous silicates present locally	Barite uncommon in MIC-hosted vein system; anhydrite common in peripheral alteration; fluorite in MIC-hosted biotite enriched zones
Gold-silver and other ore minerals	Electrum, Ag sulfides and sulfosalts; high Ag/Au; chalcopyrite, galena, sphalerite	**Zone 2**: Electrum, petzite (Ag3AuTe2), calaverite (AuTe2), and hessite (Ag2Te); **Grand Duc**: Electrum, tellurobismuthite (Bi2Te3), volynskite (AgBiTe2), native Te, tsumoite (BiTe) or tetradymite (Bi2Te2S), altaite (PbTe), petzite, calaverite, and hessite
Sulfide abundance	5 to 20 vol.%	5 to 90 vol. %
Sulfide minerals	Pyrite, Au-Ag sulfides/sulfosalts, Fe-poor sphalerite, galena, chalcopyrite, tetrahedrite/tennantite	Pyrite, chalcopyrite, galena, sphalerite
Other enriched metals	Mn, Se	**Zone 2:** As-Bi-Te-Sb-Pb-Ni-Cu-Zn-Sn-Cd-In in pyrite; **Grand Duc:** Sb enrichment in pyrite
Te and Se minerals	Tellurides common locally; selenides uncommon	Au-Ag tellerides common, selenides uncommon
Deposit style, veins and mineralerized structures	Multistage veins and associated breccias with coarse layers and comb and crustoform textures; disseminated; diatremes	Vein stockworks and sheeted veins; stratabound disseminated; internal vein textures obliterated by metamorphic recrystallization
Paleosurface indicators	Rarely documented; thin quartz veins and stockworks over some deposits	None presently recognized
Depth to top of ore zones (metres below watertable)	Several hundred metres	Several hundred metres
Vertical extent of ore	Up to 1000 metres	Up to 1000 m
Representative deposits	Comstock Lode, Tonopah, Frsnillo, El Penon, Waihi, Penasquito, Rosia Montana	

*Metamorphosed and deformed with various degrees of remobilization of Au, Au-Ag tellurides, and base metal sulphides

Deposit environment

There are similar depositional environments described for Phanerozoic porphyry-epithermal systems (Fig. 55) but they usually include a high level subvolcanic intrusive system composed of multiple stocks and associated apophyses and dyke swarms as feeders to the overlying volcanic package (Seedorf, 1999; John et al., 2010; Sillitoe, 2010). The late Doyon stage

of the MIC (and the associated unit 4.3) which hosts the Doyon mineral system consists principally of a sill-dyke complex intruded <2000 m below the coeval upper Bousquet volcanic package. Whereas porphyry-epithermal models have the Au-Cu vein system rooted within the intrusive complex, much of the vein stockwork mineralization resides in the overlying volcanic package (Fig. 55). The Doyon mineral system remains encapsulated within the multi-phase MIC-unit 4.3 sill-dyke complex, suggesting a large component of lateral hydrothermal fluid movement like that modeled for the Lepanto porphyry-epithermal system (Hedenquist et al., 1998) if the current geometry of the units at Doyon is still representative of the original (pre-deformation) architecture. The unit 4.3 felsic sill-dyke complex may have acted as a layered aquiclude and thereby controlling hydrothermal fluid flow as suggested in Yergeau et al. (2022b).

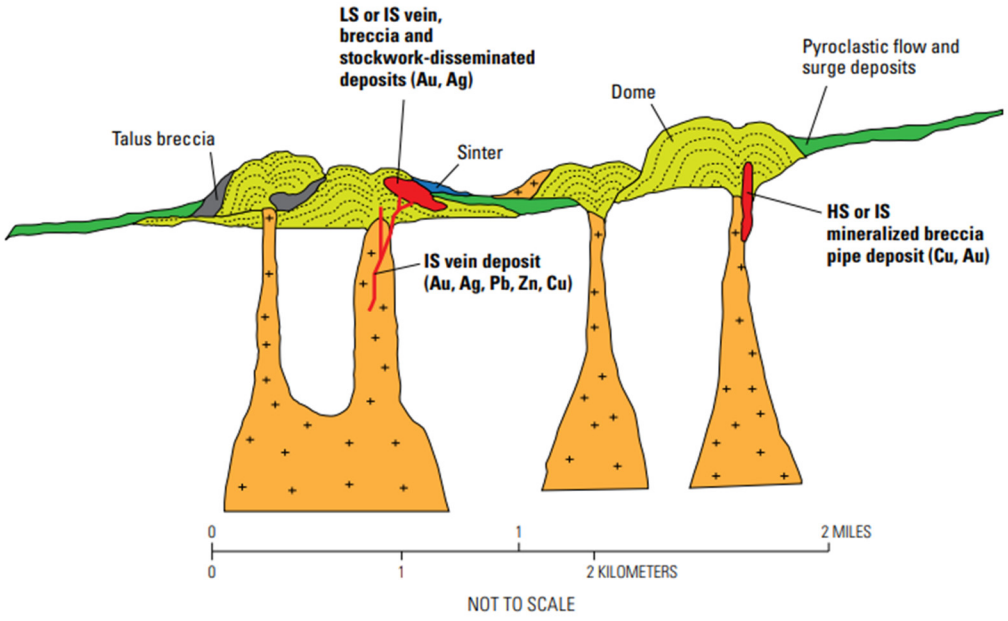

Figure 55. *Schematic model for epithermal deposits hosted within both hypabyssal stocks and coeval felsic flow dome complexes (John et al., 2010). Orange units represent high level felsic stocks, the light green felsic cryptodomes and dark green mafic flows. Ore bodies and associated vein systems in red. HS= high sulphidation; IS= intermediate sulphidation; LS= low sulphidation.*

Associated hydrothermal alteration

The Doyon Au(-Cu) mineral system resides in the core of a multi-phase alteration envelope that is comparable to a significant extent in evolution, composition, and morphology to models for Phanerozoic porphyry-epithermal systems (Fig. 56). Early formed vein dykes related to the late

stage trondhjemite sill complex are observed within the felsic-mafic dyke swarm that transects the MIC early stage tonalite phases. This is followed by fracture controlled silicification, biotite-potassium feldspar veins and breccias, Na metasomatic fracture-controlled chlorite-albite-pyrite-magnetite-carbonate. alteration, all overprinted by quartz-sericite-pyrite-Ti oxide alteration. The sericite-rich alteration stage itself transitions into aluminosilicate-rich alteration with locally preserved patches of residual, or vuggy quartz alteration. This alteration sequence closely resembles the potassic, sodic, phyllic to argillic and advanced-argillic alteration facies typical for high sulfidation porphyry-epithermal systems (Tables 3 and 4). Alteration of the early Mouska stage quartz diorite and tonalite MIC phases are described in detail by Galley and Lafrance (2014). Their tholeiitic to transitional compositions are typical of many Archean Na-enriched TTG suites (Meng et al., 2023). They have a complex syn- and post-crystallization alteration history in which primary magnesio-hornblende and possibly pyroxene (depending on the intrusive phase) are first altered to actinolite, epidote and titanite and then chlorite sericite and quartz, and finally biotite in sections of the quartz diorite and tonalite. The progression from primary to retrograde mineralogy is in part a product of metasomatic changes during late crystallization (Galley and Lafrance, 2014) and regional metamorphism. Crystallization and auto-metasomatism of the early phase MIC took place at least 1.5 million years before emplacement of the late-stage MIC phases (Neyedley et al. in press) and is unrelated to the alteration event that post-dated the latter.

Au(-Cu) vein system morphologies, mineralogy, and geochemical signatures

The Doyon Au(-Cu) vein systems were generated late in hydrothermal history of the mineral system and are hosted almost exclusively within the sericite- to sericite-aluminosilicate dominant alteration phases, although anomalous gold concentrations are present with all the described alteration facies. The rectilinear easterly and northerly trending pattern for both the preliminary quartz-pyrite-rutile-Au vein stockwork and the overprinting quartz-carbonate-chlorite-pyrite-chalcopyrite indicate that they formed under the same stress regime. If formed prior to deformation, the vein sets would have to be tilted 70^{o} northward to compensate for tilting during D_2 deformation. The result would be the easterly vein sets becoming sub-horizontal and the northerly set originally subvertical. Moreover, the vein system would have to be restored into its original configuration subtracting the effect of significant north-south shortening (rotation of veins and possible transposition), plus taking into account the possible effects of D_1, which is not very

well constrained in the study area. Nonetheless, simplistically put, the easterly horizontal vein sets would have formed parallel to trondhjemite and porphyritic tonalite sill margins whereas the steeper dipping vein set would parallel the orientation of many of the trondhjemite, porphyritic tonalite feeder dykes plus the felsic to mafic dykes feeding late stage Bousquet Formation upper member units.

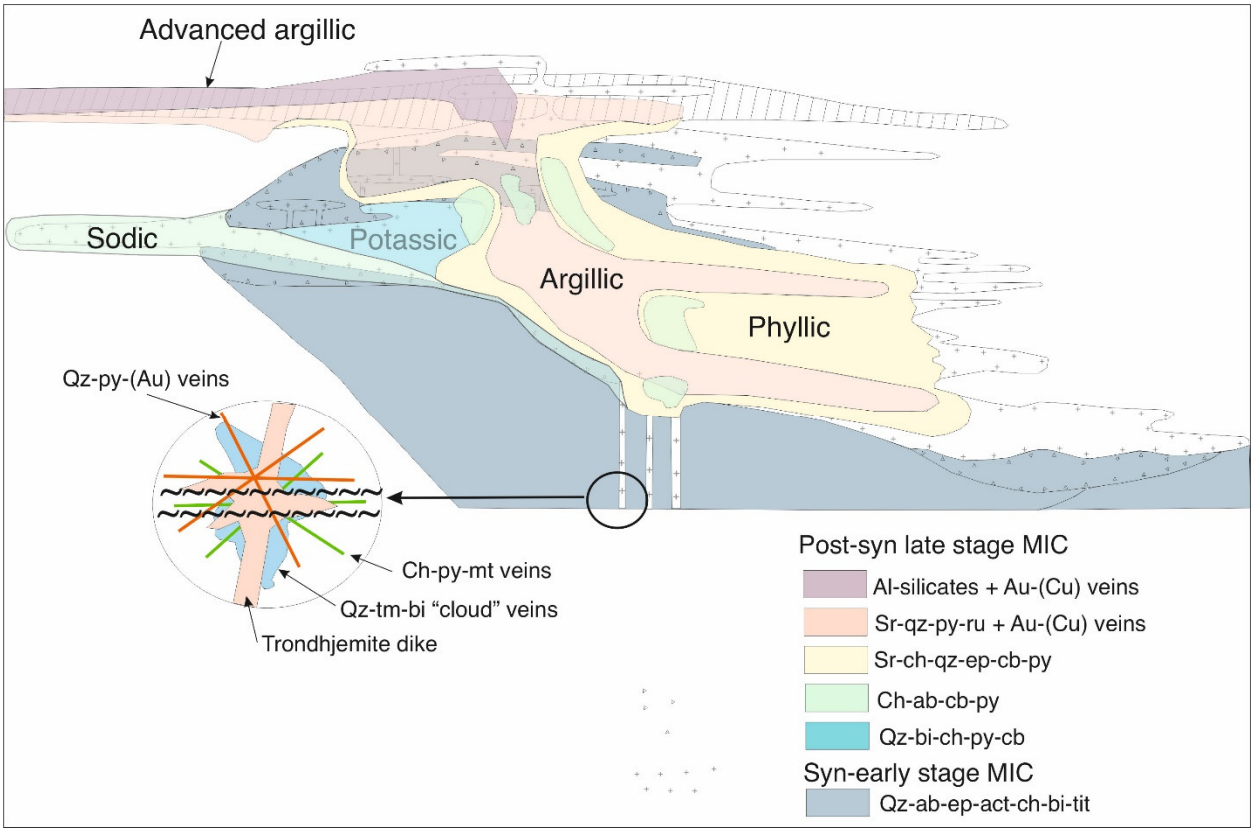

***Figure 56**. A schematic representation of the MIC and unit 4.3 sill-dyke complex restored to its inferred original configuration along with the distribution of overprinting alteration facies and hosted Au(-Cu) Doyon vein stockwork systems. The zoomed area illustrates the relative timing of the different vein systems as defined in Table 4. Squiggly lines represent overprinting shears. Ab=albite, act=actinolite, bi=biotite, cb=carbonate, ch/chl=chlorite, ep=epidote, py=pyrite, qz=quartz, ru=rutile, sr=sericite, tit=titanite.*

The vein stockworks are not associated with breccia pipes, submarine maars or diatremes, which are mostly absent within the late-stage MIC intrusive phases except for scattered sericite and quartz-biotite-filled micro-breccias. Although overprinting deformation may have modified the geometry of the vein systems, the quartz-pyrite-rutile-Au vein stockwork could be described as a

crackle breccia but was more likely formed as an anastomosing vein system (Figs. 29, 32 and 39). The main auriferous quartz-carbonate-chlorite-pyrite-chalcopyrite veins also form sets of anastomosing and crosscutting veins (Figs. 17 and 24) but also have internal zones of brecciation that are described earlier as a product of deformation-related vein brecciation but could as well be evidence for primary rock fragmentation during fracturing and vein infilling.

Table 4. *Distribution of the various vein systems associated with the Doyon mineral system and their association with the defined stages of alteration. Modified from Table 2.*

Vein progression	Host lithology						Alteration event
	Qtz diorite	Tonalite	Doyon QD	Trondhjemite	Porphyritic tonalite	Unit 4.3 sills	
Aplite vein dykes (qtz-fsp-ep-py-cp)							Early-stage magmatic-hydrothermal
Qtz-tm-py (cloud)							Silicification
Muscovite bx							Silicification
Qtz-bi-py-cp-(cb-fl) bx							Potassic
Qtz-anyd-py-cp							Potassic
Chl-qtz-mgt-(ab-tit-fl)							Na-Ca
Qtz-py-mu-rut-(fl)							Phyllic-argillic
Qtz-py-mu-ep-rut							Phyllic-argillic
Qtz-cb-chl-mu-py-cp (Au)							Intermediate argillic
Qtz-kspar*			?		?		Late potassic?
Qtz-Fe-cb							Orogenic
Qtz-tm-py (cloud)							Orogenic

*unknown extent due to limited staining

Anomalous Au

Lode veins

ab=albite, anyd=anhydrite, bi=biorite, bx=breccia, cb=carbonate, chl=chlorite, cp=chalcopyrite, ep=epidote, Fe-cb=iron carbonate, fl=fluorite, fsp=feldspar, kspar=potassium feldspar, mgt=magnetite, mu=muscovite, py=pyrite, qtz=quartz, rut=rutile, tit=titanite, tm=tourmaline.

There is very little evidence for high oxidation state sulphides or sulphosalts (e.g. bornite, tetrahedrite, enargite, tennantite) in the Doyon Au vein systems. The principal sulphides being pyrite and chalcopyrite, plus minor pyrrhotite and sphalerite. Minor bornite was observed by Savoie et al. (1990) in Zone 2. Regardless, pyrite and chalcopyrite can account for anywhere from 5-90% of the vein volume like documented high sulphidation Au-Ag vein systems (Table 3). The pyrite has trace concentrations of Te, Sb, Bi, As, and Sn, again typical of high sulphidation Au-Ag systems. Variations in pyrite textures suggest boiling may have occurred in the Grand Duc vein stockworks, but no such evidence is apparent in the West Zone (Neyedley et al. (2021a, b). The change in the host vein alteration from quartz-sericite-pyrite-rutile to the alteration suite at the West Zone to one that includes aluminosilicates in the unit 4.3-hosted Au mineralization may well indicate a lowering in pH and increase in fO_2 due to boiling in the most southerly part of the Doyon Au(-Cu) system. The presence of secondary kaolinite, pyrophyllite and dickite may also indicate the original presence of hydrothermal alunite. The patchy presence of vuggy quartz zones accompanying aluminosilicate-rich alteration would further support boiling as a viable magmatic-hydrothermal process for the Doyon system (Simmons et al., 2005; John et al., 2010).

At the same time, the presence of anhydrite interstitial to framework quartz and plagioclase in parts of the trondhjemite sill complex (Neyedley, pers comm.), and the presence of anhydrite and sulphide pairs in observed veins indicates during early phases of Doyon-related alteration a relatively elevated fO_2 was present. Sulphate-sulphide pairs also suggest that sulphur dissociation took place under these conditions, which would further decrease the magmatic-hydrothermal pH thereby allowing phyllic to advanced argillic alteration to take place (Einaudi et al., 2003; John et al., 2018).

The principal set of Au(-Cu) stockwork veins appear to have formed under slightly less oxidized and acidic conditions than the preliminary set of quartz-pyrite-rutile-Au veins. This would suggest that the redox conditions of the magmatic-hydrothermal fluids evolved during the evolution of the Doyon vein systems from advanced to intermediate argillic (Einaudi et al., 2003; Simmons et al., 2005; John et al., 2018). This could have been a function of host rock buffering, but there is no specific change in the affected lithologies between the overprinting auriferous vein stockworks.

Neyedley et al. (in press) have defined mildly to moderately oxidized ΔFMQ values (0-2.25) during emplacement of the MIC, which correlates well with the presence of magnetite and titanite.

Most Phanerozoic Au-Cu and Cu-Au porphyry systems are hosted within high-K calc-alkalic to alkalic intrusive complexes rather than tholeiitic to low-K calc-alkalic TTG and TTD intrusive suites (du Bray, 2017). High alkali magmas tend to originate through low degrees of partial melting from sources in which Au and Cu are concentrated due to the high oxidation state (FMQ + 1) of the source melts. The high oxidation state suppresses formation of sulphides whose precipitation would also capture Au and Cu (Mungall, 2002; Blevin, 2004). Alkali magmas generated from low degrees of partial melting have elevated concentrations of alkalis (such as K and Na) and volatiles such as F and Cl. Under oxidizing conditions Au can be complexed and transported as $NaAu(F,Cl)_2$, $KAu(F,Cl)_2$, and/or $NaAu(HS)_2$ and $KAu(HS)_2$ (Zajacz et al., 2010). This suggests that both high-K calc-alkalic and high Na transitional magmatic suites may supply ligands for Au transport under the right conditions.

The rare presence of Au-Cu and Cu-Au mineralization hosted within low-Al, high Na TTD magmatic suites may be explained by magma formation under an unusually high oxidation state and in the presence of high concentrations of F (and to a lesser extent Cl) as characterized by the late-stage intrusive phases of the MIC magmatic suite. The higher Au solubility in melt occurs for moderately oxidized (FMQ+1) magma, when sulphur is present as both sulphide and sulphate, and at a low degree of partial melting (Botcharnikov et al., 2011; Sun et al., 2015). The presence of anhydrite and sulphides in the late-stage MIC intrusive phases are indicative that these conditions were present. The presence of magnesio- hornblende and biotite in both early and late-stage MIC intrusive phases indicates H_2O contents $\geq$ 4%, and therefore a hydrous magma source (Seedorf, 2005). This, and the presence of magnetite and titanite all support Neyedley et al. (in press) analytical results with regards to an oxidation state within the FMQ stability field. The anomalously high F concentrations throughout parts of the Doyon Au(-Cu) system hydrothermal plume would result in increased H_2O solubility in the source melts, which may in part well explain part of the anomalous conditions within this TTD suite that allowed for the late crystallization generation of F-enriched hydrothermal fluids capable of carrying concentrated amounts of Au and Cu. The presence of anomalous F concentrations in all the intrusion-hosted Doyon alteration

phases suggests that this process was continuous over the hydrothermal history of the deposit which may account for the presence of anomalous Au in parts of all the alteration facies. Furthermore, variation in oxidation state during rock-fluid interaction (and boiling?) could be in part responsible for the generation of lower pH conditions to form argillic and advanced argillic alteration mineral assemblages through the reaction CaF + H_20 -> CaO + 2HF.

Neoarchean intrusion-hosted Au(-Cu) mineral systems

There are well documented examples of intrusion-associated to intrusion-hosted Neoarchean Au, Cu-Au, and Au-Cu vein and replacement systems associated emplaced during the various stages of the magmatic evolution of the host granite-greenstone belts (e.g., Kirkham et al., 1997; Davis et al., 2000; Kontak et al., 2008; Fayol and Jebrak, 2017; Mathieu and Racitot, 2019; Dubé and Mercier-Langevin, 2020; Katz et al., 2021; Meng et al., 2022) (Table 5). Such deposits commonly show unusual or complex characteristics that have been considered, depending on authors, as evidence of early (porphyry-epithermal like alteration), syn-deformation mineralization, or both. The Au-Cu deposits associated with calc-alkalic to alkalic intrusive hosts are characterized by both medium to high oxidation states (anhydrite, magnetite, and hematite) and elevated F concentrations (where known). These characteristics are well documented for Phanerozoic high K intrusive-hosted porphyry and IOCG Au-Cu deposits (Sillitoe, 2012).

The closest Neoarchean comparison for Doyon is the Coté Gold deposit hosted within the 2741 to 2739 Ma low-Al, tholeiite-calc-alkalic Chester Intrusive Complex (Katz et al., 2021) (Table 6). The contained Au(-Cu) mineralization at Côté Gold occurs as veins and disseminations associated with biotite-rich hydrothermal breccias. The potassic alteration overprints an earlier amphibole-rich calcic halo, with both overprinted by a sericite-dominant mineral assemblage. U-Pb dating of hydrothermal titanite and Re-Os dating of molybdenite confirms that the age of the Au(-Cu) mineralization overlaps with the age of emplacement of the Chester Intrusive Complex. Katz et al. (2017, 2021) suggest that unusually high Au(-Cu) concentration within this relatively primitive back-arc-style magmatic suite is due to its relatively high oxidation state (magnetite-titanite), water content (calcic amphibole alteration) and the presence of anomalous F in the auriferous biotite-rich breccias. The high oxidation state (>FMQ+1) of the magmas resulted in the retention and concentration of Au and Cu in the source magma chamber, and the high F content accelerated the

release of magmatic-hydrothermal fluid that collected and carried the metals to the crystallization site of the intrusive complex.

***Table 5**. Selected Neoarchean intrusion-associated/hosted Au(±Cu) vein systems.*

Deposit	Age of Mineral.	Related intrusion type and age	Type	Trace metals	Volatiles	Selected references
Coté Gold	2740 Ma	Tholeiitic to calc-alkalic (2740 Ma)	Au-Cu	Mo, Ag, Te	F	Katz et al. (2017, 2021)
Troîlus	≤2791 Ma - >2782 ± 6 Ma	Calk-alkalic (2791 Ma)	Au(-Cu)		?	Fraser (1993); Goodman et al. (2005)
La-Grande-Sud	≤2734 - ≥2721 Ma	Calc-alkalic (2734 Ma)	Au(-Cu)	Bi	?	Mercier-Langevin et al. (2012)
Beidelman Bay	~2720 Ma	Calc-alkalic (2720 Ma)	Cu-Mo-Au		F	Davis and Trowell (1982); Galley et al. (2000)
Lac Clark,	2715 Ma	Calc-alkalic (2715 Ma)	Cu-Au	Ag, Bi, Pb, Te	?	Pilote et al. (1993); Mathieu and Racitot (2019)
Don Rouyn*	2689 ± 11 Ma	Tholeiitic (2701 Ma)	Cu-Mo		?	Goldie et al. (1979); McNicoll et al. (2014); Mercier-Langevin et al. (2024c)
St. Jude	2697 Ma	Calc-alkalic (2697 Ma)	Cu- Au	Mo	?	Galley and van Breemen, (2002)
Doyon	2698 Ma	Tholeiitic to calc-alkalic(2698 Ma)	Au-Cu	As, Bi, Te, Sb, Pb, Ni, Sn, Zn, Cd	F-Cl	Galley and Lafrance (2014); McNicoll et al. (2014); Neyedley et al. (2021)
Windfall Lake	2697 Ma	Calc-alkalic (2697 Ma) pre- and post-ore dyke swarms	Au	Ag, As, Sb, S, Se, Bi, Te, ± Zn, Cu, Pb, Mo, W	?	Choquette and Kontak (2023)
Clifford Lake	2682 Ma	Calc-alkalic (2686 Ma)	Cu-Au		?	Chaloux (2005); Piercey et al. (2008)
Malartic	~2665-2660 Ma	High K Calc-alkalic (2678-2676 Ma)	Au	Te, W, Bi, Pb, Cu	F	Helt et al. (2014); De Souza et al. (2017, 2019, 2020); Perrouty et al. (2017)
Camflo	2621 Ma?	Alkaline (2685 Ma)	Au		F	Zweng et al. (1993)
Bachelor Lake	<2692 Ma	Shoshonitic porphyritic Qz-monzonite (O'Brien intrusion 2692 Ma)	Au	Ag, Te	F	Fayol and Jebrak (2017); Dubé and Mercier-Langevin (2020); Dubé et al. (2024)
Douay	≤2676 Ma	Syenite (2676 Ma)	Au	Te	F	Robert et al. (2007); Davis et al. (2000)
Upper Beaver	≤2685-≥2678 Ma Ma	Calc-alkaline to alkaline (≥ 2678 Ma)	Au-Cu	Bi, Mo, Te		Kontak et al. (2008, 2013); Mercier-Langevin et al. (2021); Dube et al. (2024)

*The Don Rouyn Cu-Mo vein system is probably related to an intrusive event younger than the host Powell intrusion (2698-2695 Ma: Mercier-Langevin et al., 2024c; Schofield et al., 2024).

The unique halogen geochemistry and elevated oxidation state and H_2O content of the MIC and Chester Intrusive Complex indicates that somewhat unique conditions were present during the generation of their source magmas in comparison to more typical Neoarchean TTD suites.

***Table 6**. Comparison of Neoarchean Doyon and Coté Gold mineral systems with common Phanerozoic Cu-MoAu-Ag porphyry-epithermal and Neoarchean to Phanerozoic alkalic Cu-Au systems.*

	Doyon Au(-Cu)	**Coté Gold Au-Cu[1]**	**Porphyry-epithermal Cu-Mo-Au-Ag[2]**	**Syenite-associated Au-Cu[3]**
Tectonic setting	Extensional to transtensional early back-arc	Extensional to transtensional early back-arc	Extensional to transtensional arc or back-arc	Compressional setting along a major fault zone
Host magmatic suite	Trondhjemite-tonalite-quartz diorite (TTD)	Trondhjemite-tonalite-quartz diorite (TTD)	Trondhjemite-tonalite-granodiorite (TTG)	Quartz monzonite-monzonite-syenite (Alkaline)
Host rocks	Trondhjemite and tonalite; tholeiitic to calc-alkalic	Tonalite and diorite; calc-alkalic to tholeiitic	Granodiorite to granite; calc-alkaline	Syenite to monzonite; alkaline
Depth	Shallow	Shallow	~1-5 km	Shallow
Oxidation state	Moderately oxidized	Oxidized	Oxidized	Oxidized
Alteration types	Silicic (quartz, tourmaline), potassic (Mg-biotite-Kspar), sodic (albite), phyllic (muscovite), argillic (Al-silicates)	Calcic (amphibole) potassic (biotite), phyllic (muscovite), sodic (albite)	Potassic, phyllic, calcic-sodic, propylitic, argillic	Carbonate, potassic, sodic,
Alteration zoning	Potassic, sodic, phyllic, argillic	Potassic, calcic, phyllic	Potassic, calcic-sodic, phyllic, argillic, propylitic	
Metal associations	Au ± (Cu, Ag, Te, Bi, Pb, Zn)	Au ± Cu ± Mo ± Ag ± Te	Cu ± Mo ± Au ± Ag ± (Zn, Pb, Te)	Au-Cu-As-Te-(Pb, W, Mo, Zn)
Halogens	F-(Cl)	F	Cl	F

[1]Katz et al. (2017, 2021)
[2]Seedorf (2005), Sillitoe (2010), Simmons et al. (2005)
[3]Robert et al. (2007); Lang et al., (1994); Bissig and Cooke (2014)

Structural controls on the Doyon Au(-Cu) system

The generation, transport and deposition of ore-forming hydrothermal fluids are essentially all structurally controlled and developed during cycles of hydrostatic and/or lithostatic stress (Sibson, 2000; Cox, 2016). Dyke patterns formed during intrusion of a porphyry-related intrusive system are related to the presence or absence of a directional stress field (Titley and Heidrick, 1978; Tosdal and Richards, 2001) and formation of porphyry and epithermal vein stockworks in turn develop along the margins of pre-existing dyke swarms and sill margins with propagation controlled by cycles in which enhanced fluid pressure assists in rock failure.

Porphyry-epithermal systems develop within tectonically active plate margins or continental rifts (Seedorf, 2005) in domains where accretionary tectonism develops along compressional and transpressional plate margins. Upper plate margin stratigraphy is rotated and faulted and pre-existing syn-arc and back-arc geological contacts, faults and fractures have their original geometry gradually modified. Pre-existing zones of hydrothermal alteration and accompanying mineralization are zones in which brittle-ductile strain will focus and result in mechanical deformation and remobilization of the more volatile or ductile elements.

The Doyon Au(-Cu) vein stockwork system displays abundant evidence of having undergone differential strain through broadly north-south shortening during at least two phases of regional deformation (Tourigny et al., 1988; Tourigny and Chartrand, 1994). The kinematic indicators developed in shear zones within the Doyon sericite-dominant alteration indicate steep subvertical NNE motion during the D_2 (and possible D_1) deformation events (Fig. 11) (Gosselin, 1998). This is mimicked by the plunge direction of the Doyon ore bodies (Fig. 19), which indicates either a very fortuitous and unlikely continuity in stress regime orientation between transpressional back-arc development and syn- to post-accretion tectonics, radical Au remobilization, and/or syn-deformation Au vein development.

All Neoarchean intrusion related Au-Cu vein systems contain at least two generations of vein development, with the second generation related to mechanical (and geochemical?) remobilization of the earlier-formed mineralized zones, usually within discrete shear zones. Examples include Coté Gold, Windfall, La-Grande-Sud, Malartic, Camflo and several Chibougamau Au-Cu systems (e.g.: Pilote et al. 1993; Zweng et al., 1993; Mercier-Langevin et al., 2012; Mathieu and Racicot, 2019; Katz et al., 2021; Choquette and Kontak, 2023).

The Doyon mineral system also contains two phases of auriferous Au vein stockworks. The first phase of quartz-pyrite-rutile(-chalcopyrite) veins and veinlets are generally low grade (<1 g/t Au) and are strongly deformed. The second generation of veining defines higher grade ore at Mooshla A, Grand Duc, West Zone, and Zones 1 and 2. This quartz-pyrite-chalcopyrite-carbonate-chlorite vein generation are thicker but are also deformed and crossed by the strong S_2 shear foliation

(Savoie et al., 1986; Gosselin, 1998; Mercier-Langevin et al., 2007d). We cannot entirely exclude the possibility that this second generation of veins formed or was significantly modified (i.e., remobilization, upgrading) during the development of either D_1 or D_2 shear zones (Fig. 12) and had scavenged and concentrated Au (and Cu) from the earlier formed low grade, porphyry-epithermal related vein system.

Typical quartz ±tourmaline-carbonate-pyrite laminated shear veins and extensional syn-D_2 veins are however present in the MIC and in the Doyon mine environment. Such veins, which are comparable to other orogenic vein systems typical of the main phase of Au mineralizing event in the southern Abitibi greenstone belt, are only sparsely mineralized at Doyon, and at other deposits of the DBL camp. Mineralized veins at Doyon were clearly strongly affected and most probably significantly modified during the regional deformation events, but it therefore seems unlikely that there was a strong input of new gold in the system during D_2. The principal objection to having the second-generation Doyon veins formed during a D_1 or D_2 shear event is the lack of evidence for multi-phase vein injection so typical of epigenetic vein systems that result in a very characteristic "crack and seal" vein structure (Groves et al., 2003; Goldfarb et al., 2005). The second is the large percentage of pyrite and chalcopyrite present, in some cases constituting over 90% of the Doyon deposit vein volume. It seems unlikely that this could be accomplished by the mechanical remobilization and concentration of pyrite and chalcopyrite (plus trace metals such as Bi and Te) without a large component of geochemical dissolution and precipitation that can only occur under high metamorphic pressure-temperature conditions (Tomkins and Mavrogenes, 2002). The veins and associated alteration mineralogy and geochemistry for epigenetic Au vein systems indicates high CO_2, near neutral pH fluid transport at temperatures between 350-400ºC with the Au ligands consisting mainly of bi-sulphide complexes that react with generally mafic vein wall rock to strip metals to precipitate disseminated pyrite and arsenopyrite (Groves et al., 2003). Generation of semi-massive to massive sulphides in porphyry-epithermal systems is a function of high fluid/rock ratios under moderate to high oxidation states with SO_2 rich magmatic gases. Upon cooling the gas disproportionates to produce H_2S, which in turn precipitates as metal sulphide (Einaudi et al., 2003).

Porphyry-epithermal-VMS relationships: Mineral system evolution and arc development

Sillitoe (1980) stated that porphyry and VMS systems were incompatible or mutually exclusive, as the former forms below stratovolcanoes and undergoes late stage devolatilization, whereas the felsic bimodal variety of the latter forms in caldera environments through early magma degassing explosive eruption, accompanied by the broad distribution of magmatic metals. Since this article was published, it is now known that VMS deposits form in several different depositional settings in which explosive volcanism is generally not a significant component (e.g. Large, 1992., Barrie and Hannington, 1999; Franklin et al., 2005). It is also well documented that auriferous metal rich VMS deposits can include epithermal characteristics due to hydrothermal fluid boiling, magmatic fluid contribution, or both (e.g. Sillitoe et al., 1996; Hannington et al.; Mercier-Langevin et al., 2007d, 2015; Yergeau et al., 2022a, b; Rabayrol et al., 2023). Considering the well-established genetic linkage between certain epithermal and porphyry systems (Hedquist et al., 1989; Simmons et al., 2005; John et al., 2018) the possible submarine porphyry-epithermal-VMS temporal and genetic linkage should therefore be reconsidered.

Spatial linkages between porphyry and VMS types of mineralization are present in both the Precambrian and Phanerozoic, but at times is misleading with respect to any temporal and genetic relationships. In the case of the 2735 Ma Archean Sturgeon Lake VMS district the F Group massive sulphide deposit has aluminosilicate-rich alteration closely resembling epithermal-type high sulphidation-style alteration (Morton et al., 1996; Galley et al., 2000; Franklin et al., 2005). Where the coeval Biedleman Bay subvolcanic intrusive complex directly underlies the F Group VMS-epithermal deposit, it contains extensive zones of vein-hosted, weak Cu-Mo porphyry-style sulphide mineralization associated with igneous and hydrothermal breccia zones, and a plagioclase-quartz and quartz-plagioclase porphyry dyke swarm approximately 14 million years younger than the host biotite trondhjemite phase of the Beidelman Bay intrusion. The dyke swarms are similar in composition to a 2717.9 +2.9/-1.5 Ma post-Sturgeon Lake cauldron rhyolite tuff unit.

In the Artvin Au-Cu district of the Eastern Pontides, Turkey, there are several examples of spatial relationships between Late Caroniferous porphyry, epithermal and VMS mineralization (Rabayrol et al., 2023 and references therein). It appears that VMS deposits (such as at Murgul, Tunca, and Dereici) formed between 91-85 Ma are overprinted to varying degrees by porphyry-epithermal

systems dated between 85.6 and 82 Ma. Rabayrol et al. (2023) suggest that this relationship was established during the evolution from submarine back-arc to arc settings.

The 2702 Ma subvolcanic Flavian-Powell intrusive complex is coeval with, and underlies the Noranda VMS camp (Galley, 2003; Gibson and Galley, 2007). There are several intrusion-hosted Cu-Mo±Au vein systems associated with the subvolcanic intrusive complex that includes the Don Rouyn deposit (Goldie et al., 1979; Schofield et al., 2024) and St. Jude magmatic-hydrothermal breccia pipe. Other examples include the Joliet and Anglo-Powell Cu-Zn-Ag-enriched breccia pipes. A quartz porphyritic aplite dyke associated with the Cu-Mo-Au-mineralized St. Jude intrusive breccia pipe returned an age of 2697 +/- 2 Ma, similar to the age of the post-Noranda cauldron Cléricy rhyolite (Galley and van Breemen, 2002), whereas dating of a trondhjemite dyke at the Joliet breccia pipe suggests a maximum age for magmatic Cu-Zn-Ag mineralization between 2697.6 ± 0.7 Ma and the minimum age to 2695.3 ± 1.0 Ma (Schofield et al., 2024), also postdating the age of the VMS-bearing host volcanic strata (2702-2699 Ma). The overprinting of the VMS-hosting primitive oceanic arc caldera by a succeeding magmatic event that included porphyry-style mineralization associated with magmatic-hydrothermal breccia pipes coincided with a magma evolution from tholeiitic to transitional calc-alkalic and an oceanic arc to rifted back-arc tectonic setting (Mercier-Langevin et al., 2007c, 2011; Monecke et al., 2017).

The upper end of this Noranda district arc-related magmatism (~2698 Ma) coincides with that for the MIC and host Bousquet Formation strata that host the Doyon-Westwood Au-(Cu) mineral system, as does the change in the upper Blake River tectonic evolution towards a rifted arc setting (Mercier-Langevin et al., 2015). The overprinting of the VMS-forming period with the porphyry-epithermal-like mineralization associated with the emplacement of the MIC represents a closer time association than that recorded for the Sturgeon Lake and Noranda camps, but in all the cases cited here the magmatism and associated submarine hydrothermal and magmatic hydrothermal activity were focused over an extended period of time within focused thermal corridors most likely controlled by the reactivation of deeply rooted synvolcanic faut systems.

CONCLUSION

The Doyon Au(-Cu) system is a component of a larger, semi-continuous mineral system that is over 3000 m in strike length and includes the Westwood polymetallic ore lenses as its eastern component. The deformed and metamorphosed Doyon and Westwood systems likely formed as part of a porphyry-epithermal-style vein system that intruded into the base of a pre-existing, but coeval (within geochronological resolution for Archean rocks) VMS seafloor hydrothermal system. The roots of the Doyon Au(-Cu) deposit can be traced down section for over 1000 m to a series of trondhjemite and porphyritic tonalite dykes that cross the early-stage tholeiitic to transitional phases of the MIC to feed the calc-alkalic late-stage MIC sill complex. The complex and overlapping vein stockworks overprinting the feeder dykes is focused up section into a corridor of auriferous vein stockworks with the Mooshla A deposit as its base, followed by the Grand Duc, West Zone and zones 1 and 2 ore bodies.

This was a two-stage process that began with the creation of a polygonal network of low-grade quartz-pyrite-rutile-chalcopyrite-Au veins and veinlets that are then overprinted by a polygonal network of higher grade larger quartz-pyrite-chalcopyrite-carbonate-chlorite-Au veins that comprised the economic part of the Doyon mineral system. The two vein systems are hosted within a multi-layered halo of alteration that began with a quartz-tourmaline dominated silicic stage, followed by a biotite-potassium feldspar dominant second stage. These two alteration phases are overprinted first by sodic albite-chlorite-epidote, sericite-quartz-pyrite phyllic and finally an argillic to advanced argillic alteration characterized by aluminosilicate minerals and quartz-rich residual zones.

The character of the zoned alteration halo and enclosed auriferous vein stockworks is similar to that for Phanerozoic Cu-Au porphyry-high sulphidation epithermal mineral systems. The unusual high Na composition of the host low-Al-K calc-alkalic trondhjemite-tonalite-quartz diorite for a Cu-Au porphyry-epithermal system can be explained by its moderately high oxidation and anomalously high F content. The oxidation state of the late-stage MIC intrusive phases resulted in the concentration of Au and Cu within a low sulphide environment and the higher F content

allowed for the early generation of magmatic-hydrothermal fluids to carry the concentrated Au and Cu to a shallow (< 1 kbar) depositional environment.

The consistent steeply dipping NNE-WNW dominant polygonal pattern of the low- and high-grade Doyon vein stockworks can be explained as having been controlled by the original orientation of layering in the MIC late stage trondhjemite-porphyritic tonalite sill complex and cross-stratal fracturing during feeder dyke injection. The re-orientation of and deformation of the vein sets within high strain zones affecting the MIC southern contact and overlying volcanic strata, plus the consistent steeply WSW plunging attitude of the principal Doyon ore zones indicate a realignment of much of the ore system during regional northward directed D_2 oblique reverse faulting during Neoarchean terrane agglomeration and consolidation.

ACKNOWLEDGMENTS

This report is a contribution to the "*OS-3 – Orogenic gold deposits: A closer look at the diversity of types, styles and ages of gold deposits in greenstone belts*" project of phase 6 of the Targeted Geoscience Initiative (TGI) program of the Geological Survey of Canada. This work however incorporates material that was collected through phases 1 (2000–2002), 3 (2005–2010), 4 (2010–2015) and 5 (2015–2020) of the TGI program, which were conducted in collaboration with the Ministère des Ressources naturelles et des Forêts du Québec (MRNF), the industry (Agnico Eagle Mines Limited, Iamgold Corporation, Cambior incorporated, Barrick Gold Corporation, and Ressources Yorbeau), and academia (the Institut national de la Recherche Scientifique – Centre Eau Terre et Environnement, and the Université du Québec à Chicoutimi). The authors are most grateful to the numerous colleagues and students who made major contributions to the advancement of knowledge and the development of the Doyon-Bousquet-LaRonde camp over the years. In particular, we would like to thank Guy Gosselin for supplying photographs from his Doyon thesis work, and Arnand Savoie for his patience in detailing his observations on the Doyon mineral system. M. Boutin helped prepare some of the figures. Thanks to Howard Poulsen, Dave Sinclair and Ian Honsberger for their constructive review of earlier versions of the manuscript.

REFERENCES

Asselin, R., 1999, Géologie de la Mine Mouska: Cambior Inc., Division Doyon, Unpublished Field Guide, 16 p.

Bailes, A. H., Galley, A.G., Paradis, S., and Taylor, B.E., 2016, Variations in large synvolcanic alteration zones at Snow Lake, Manitoba, Canada, with proximity to associated volcanogenic massive sulphide deposits: Economic Geology, v. 111, p. 933–962.

Bailey, J.C., 1977, Fluorite in granitic rocks and melts: A review: Chemical Geology, v. 19, p. 1–42.

Barrett, T.J., and MacLean, W.H., 1994, Chemostratigraphy and hydrothermal alteration in exploration for VHMS in greenstones and younger volcanic rocks: Geological Association of Canada, Mineral Deposits Division Short Course Notes, v. 11, p. 433−467.

Belkabir, A., 1995, Structure et métallogénie du secteur ouest du district aurifère archéen de Bousquet, Abitibi, Canada: Unpublished Ph.D. thesis, Université de Montréal, Montréal, Canada, 220 p.

Belkabir, A., and Hubert, C., 1995, Geology and structure of a sulphide-rich gold deposit: An example from the Mouska gold mine, Bousquet district, Canada: Economic Geology, v. 90, p. 1064−1079.

Belkabir, A., Hubert, C., and Hoy, L., 1998, Fluid-rock reactions and resulting change in rheological behaviour of a composite granitoid: The Archean Mooshla stock, Canada: Canadian Journal of Earth Sciences, v. 35, p. 131–146.

Bissig, T., and Cooke, D.R., 2014, Introduction to the special issue devoted to alkalic porphyry Cu-Au and epithermal Au deposits: Economic Geology, v. 109, p. 819−825.

Blevin, P.L., 2004, Redox and compositional parameters for interpreting the granitoid metallogeny of eastern Australia: Implications for gold-rich ore systems: Resource Geology, v. 54, pp. 241–252.

Botcharnikov, R. E., Linnen, R. L., Wilke, M., Holtz, F., Jugo, P. J. & Berndt, J., 2011, High gold concentrations in sulphide-bearing magma under oxidizing conditions: Nature Geoscience, v. 4, p. 112–115.

Choquette, B., and Kontak, D.J., 2023, Geologic and geochemical features of the world-class Archean Windfall intrusion-related Au deposit, Abitibi Subprovince, Canada: Economic Geology, v. 118, p. 999–1029.

Clayton, R.N., and Mayeda, T.K., 1963, The use of bromine pentafluoride in the extraction of oxygen from oxides and silicates for isotopic analysis: Geochimica et Cosmochimica Acta, v. 27, p. 43–52.

Cox, S.F., 2016, Injection-driven swarm seismicity and permeability enhancement: Implications for the dynamics of hydrothermal ore systems in high fluid-flux, over pressured faulting regimes—An invited paper: Economic Geology, v. 111, p. 559–587.

Chénard, L., 1990, La Mine Doyon, excursion sous-terre: *in* Sullivan, J.R., Côté, R., Bertrand, P., Chartrand, F., Chénard, L., Gaulin, R., Lacroix, S., and Racicot, D. (eds.), The Northwestern Quebec Polymetallic belt: A summary of 60 years of mining exploration - Excursion Guidebook, The Canadian Institute of mining and Metallurgy, p. 69–72.

Davis, D.W., 2002, U-Pb geochronology of Archean metasedimentary rocks in the Pontiac and Abitibi subprovinces, Quebec, constraints on timing, provenance and regional tectonics: Precambrian Research, v. 115, p. 97–117.

Davis, D.W and Trowell, N.F., 1982, U-Pb zircon ages from the eastern Savant Lake-Crow Lake metavolcanic-metasedimentary belt, northwest Ontario: Canadian Journal of Earth Sciences, v. 19, p. 868–877.

Davis, W.J., Lacroix, S., Gariépy, C., and Machado, N., 2000, Geochronology and radiogenic isotope geochemistry of plutonic rocks from the central Abitibi subprovince: Significance to the internal subdivision and plutono-tectonic evolution of the Abitibi belt: Canadian Journal of Earth Sciences, v. 37, p. 117–133.

De Souza, S., Dubé, B., McNicoll, V.J., Dupuis, C., Mercier-Langevin, P., Creaser, R.A., Kjarsgaard, I.M., 2017, Geology and hydrothermal alteration of the world-class Canadian Malartic gold deposit: Genesis of an Archean stockwork-disseminated gold deposit in the Abitibi greenstone belt, Quebec: Reviews in Economic Geology volume 19, p. 263−291.

De Souza, S., Dubé, B., Mercier-Langevin, P., McNicoll, V., Dupuis, C., Kjarsgaard, I., 2019, Hydrothermal alteration mineralogy and geochemistry of the Archean world-class Canadian Malartic disseminated-stockwork gold deposit, southern Abitibi greenstone belt, Quebec, Canada: Economic Geology, v. 114, p. 1057–1094.

De Souza, S., Perrouty, S., Dubé, B., Mercier-Langevin, P., Linnen, R.L., Olivo, G.R., 2020, Metallogeny of the Neoarchean Malartic gold mining camp, Quebec, Canada: Geology of the World's Major Gold Deposits and Provinces, Society of Economic Geologists Special Publication 23, p. 29−52.

Dubé, B., and Mercier-Langevin, P., 2020, Gold deposits of the Archean Abitibi greenstone belt, Canada: Society of Economic Geologists Special Publication 23, p. 669–708.

Dubé, B., Mercier-Langevin, P., Hannington, M., Davis, D., and Lafrance, B., 2004, Le gisement de sulfures massifs aurifères volcanogènes LaRonde, Abitibi, Québec: altérations, minéralisations et implications pour l'exploration: Ministère des Ressources naturelles, de la Faune et des Parcs du Québec, MB 2004-03, 112 p.

Dubé, B., Mercier-Langevin, P., Hannington, M.D., Lafrance, B., Gosselin, G., and Gosselin, P., 2007, The LaRonde Penna world-class Au-rich volcanogenic massive sulphide deposit, Abitibi, Quebec: Mineralogy and geochemistry of alteration and implications for genesis and exploration: Economic Geology, v. 102, p. 633−666.

Dubé, B., Mercier-Langevin, P., Kjarsgaard, I., Hannington, M., Bécu, V., Côté, J., Moorhead, J., Legault, M., and Bédard, N., 2014, The Bousquet 2-Dumagami world-class Archean Au-rich volcanogenic massive sulphide deposit, Abitibi, Quebec: metamorphosed submarine advanced argillic alteration footprint and genesis: Economic Geology, v. 109, p. 121–166.

du Bray, E.A., 2017, Geochemical characteristics of igneous rocks associated with epithermal mineral deposits—A review: Ore Geology Reviews, v. 80, p. 767–783.

Dupéré, M., and Gagnon, G., 2010, NI 43-101 Preliminary economic assessment of the Douay West mineral deposit: Société d'exploration minière Vior inc., 106 p.

Einaudi, M.T., Hedenquist, J.W., and Inan, E., 2003, Sulfidation state of hydrothermal fluids—The porphyry-epithermal transition and beyond: Society of Economic Geologists Special Publication 10, p. 285–313.

Fayol, N., and Jebrak, M., 2017, Archean sanukitoid gold porphyry deposits: A new understanding and genetic model from the Lac Bachelor gold deposit, Abitibi, Canada: Economic Geology, v. 112, p. 1913–1936.

Filion, M., Vallée, M., and Lavoie, C., 1977, Les gisements d'or de la SOQUEM Silverstack, Canton Bousquet, Québec: Canadian Institute of Mining and Metallurgy, Bulletin, v. 70, p. 159−172.

Franklin, J.M., Lydon, J.M., and Sangster, D.F., 1981, Volcanic-associated massive sulphide deposits: Economic Geology 75th Anniversary Volume, p. 485–627.

Franklin, J.M., Gibson, H.L., Jonasson, I.R., and Galley, A.G., 2005, Volcanogenic massive sulphide deposits: Economic Geology 100th Anniversary Volume, p. 523–560.

Fraser, R.J., 1993, The lac Troilus gold-copper deposit, northwestern Quebec: A possible Archean porphyry system: Economic Geology, v. 88, p. 1685−1699.

Gaillard, N., Williams-Jones, A.E., Clark, J.R., Lypaczewski, P., Salvi, S. Perrouty, S., Piette-Lauzière, N., Guilmette, C., and Linnen, R., 2018, Mica composition as a vector to gold mineralization: Deciphering hydrothermal and metamorphic effects in the Malartic district, Quebec: Ore Geology Reviews, v. 95, p. 789–820.

Galley, A.G., 1993, Characteristics of semi-conformable alteration zones associated with volcanogenic massive sulphide districts: Journal of Geochemical Exploration, v. 48, p. 175–200.

Galley, A.G., 2003, Composite synvolcanic intrusions associated with Precambrian VMS-related hydrothermal systems: Mineralium Deposita, v. 38, p. 443–473.

Galley, G., and van Breemen, O., 2002, Timing of synvolcanic magmatism in relation to base-metal mineralization, Rouyn-Noranda, Abitibi volcanic belt, Quebec: Geological Survey of Canada, Current Research 2002-F8, 9 p.

Galley, A.G., and Lafrance, B., 2007, Évolution et metallogénie du pluton de Mooshla: Ministère des Ressources naturelles et de la Faune, report ET 2007-02, 31 p.

Galley, A., van Breemen, O., and Franklin, J., 2000, The relationship between intrusion-hosted Cu-Mo mineralization and the VMS deposits of the Archean Sturgeon Lake mining camp, northwestern Ontario: Economic Geology, v. 95, p. 1543–1550.

Galley, A.G., Hannington, M., and Jonasson, I., 2007, Volcanogenic massive sulphide deposits: Geological Association of Canada, Mineral Deposits Division, Special Publication no. 5, p. 141–161.

Galley, A.G., and Dubé, B., 2014, Lithogeochemical data from the Mooshla Intrusive Complex and associated gold mineralization, Doyon-Bousquet-LaRonde gold district, Abitibi Subprovince, Quebec, Canada: Geological Survey of Canada, Open File 7630, 12 p.

Gibson, H.L., and Galley, A.G., 2007, Volcanogenic massive sulphide deposits of the Archean, Noranda district, Quebec: Geological Association of Canada, Mineral Deposits Division, Special Publication No. 5, p. 533–552.

Gibson, H.L., Watkinson, D.H., and Comba, C.D.A., 1983, Silicification: hydrothermal alteration in an Archean geothermal system within the Amulet rhyolite formation: Economic Geology, v. 78, p. 954–971.

Goldfarb, R.J., Baker, T., Dube, B., Groves, D.I., Hart, C.J.R., and Gosselin, P., 2005, Distribution, character, and genesis of gold deposits in metamorphic terranes: Economic Geology 100th Anniversary Volume, p. 407–450.

Goldie, R., Kotila, B., and Seward, D., 1979, The Don Rouyn mine: an Archean porphyry copper deposit near Noranda, Quebec: Economic Geology, v. 74, p. 1680–1684.

Goodman, S., Williams-Jones, A.E., and Carles, P., 2005, Structural controls on the Archean Troilus gold-copper deposit, Quebec, Canada: Economic Geology, v. 100, p. 577−582.

Gosselin, G., 1998, Veines de quartz aurifères précoces à la zone ouest de la mine Doyon, Canton de Bousquet, Preissac, Abitibi: Unpublished M.Sc. thesis, Université du Québec à Chicoutimi, Chicoutimi, Canada, 128 p.

Grant, J.A., 1986, The isocon diagram – A simple solution to the Gresens equations for metasomatic alteration: Economic geology, v. 81, p. 1976–1982.

Groves, D.I., Goldfarb, R.J., Robert, F., and Hart, C.J., 2003, Gold deposits in metamorphic belts; Overview of current understanding, outstanding problems, future research, and exploration significance: Economic Geology, v. 98, p. 1–29.

Guha, J., Gauthier, A., Vallée, M., Descarreaux, J., and Lange-Berard, F., 1982, Gold mineralization at the Doyon mine (Silverstack), Bousquet, Quebec: CIM Special Volume 24, p. 50–57.

Gunning, H.C., 1941, Region de Bousquet-Joannès, Québec: Geological Survey of Canada, Memoir 206, 80 p.

Heald, P., Hayba, D.O., and Foley, N.K., 1987, Comparative anatomy of volcanic-hosted epithermal deposits: Acid-sulfate and adularia-sericite types: Economic Geology, v. 82, p. 1–26.

Hedenquist, J.W., Arribas, A., and Reynolds, T.J., 1998, Evolution of an intrusion-centered hydrothermal system— Far Southeast-Lepanto porphyry and epithermal Cu-Au deposits, Philippines: Economic Geology, v. 93, p. 373–404.

Helt, K.M., Williams-Jones, A.E., Clark, J.R., Wing, B.A. and Wares, R.P., 2014, Constraints on the genesis of the Archean oxidized, intrusion related Canadian Malartic gold deposit, Quebec, Canada: Economic Geology, v. 109, p. 713−753.

Holk, G.J., Taylor, B.E., Galley, A., Hannington, M., and Timbal, A., 1998, Geochemical and alteration studies of the Surgeon Lake caldera complex: Camiro project 94E07, Third Annual Report, p. 333–369.

Holk, G.J., Taylor, B.E., and Galley, A.G., 2008, Oxygen isotope mapping of the Archean Sturgeon Lake caldera complex and VMS-related hydrothermal system, Northwestern Ontario, Canada: Mineralium Deposita, v. 43, p. 623–640.

Hoy, L.D., Trudel, P., Tourigny, G., Kheang, L., Savoie, A., and Crépeau, R., 1990, Isotopic and fluid inclusion constraints on the origin of vein Au mineralization at Bousquet township, Quebec: CIM Special Volume 43, p. 413–423.

Ishikawa, Y., Sawaguchi, T., Iwaya, S., and Horiuchi, M., 1976, Delineation of prospecting targets for Kuroko deposits based on modes of volcanism of underlying dacite and alteration halos: Mining Geology, v. 26, p. 105–117 (in Japanese with English abs.).

John, D.A., Vikre, P.G., du Bray, E.A., Blakely, R.J., Fey, D.L., Rockwell, B.W., Mauk, J.L., Anderson, E.D., and Graybeal, F.T., 2018, Descriptive models for epithermal gold-silver deposits: U.S. Geological Survey Scientific Investigations Report 2010–5070–Q, 247 p.

Kalogeropoulos, S.I., and Scott, S.D., 1989, Mineralogy and geochemistry of an Archean tuffaceous exhalite—The main contact tuff, Millenbach mine area, Noranda, Quebec: Canadian Journal of Earth Sciences, v. 26, p. 88–105.

Katz, L.R., Kontak, D.J., Dubé, B., and McNicoll, V., 2017, The geology, petrology, and geochronology of the Archean Côté Gold large-tonnage, low-grade intrusion-related Au(-Cu) deposit, Swayze greenstone belt, Ontario, Canada: Canadian Journal of Earth Sciences, v. 54, p. 173–202.

Katz, L.R, Kontak, D.J., Dubé, B., McNicoll, V., Creaser, R.A., and Petrus J.A., 2021, An Archean porphyry-type gold deposit: The Côté Gold Au(-Cu) deposit, Swayze greenstone belt, Superior Province, Ontario, Canada: Economic Geology, v. 116, p. 47−89.

Kesler, S.E., Campbell, I.H., Smith, C.N., Hall, C.M., Allen, C.M., 2005, Age of the Pueblo Viejo gold-silver deposit and its significance to models for high-sulfidation epithermal mineralization: Economic Geology, v. 100, p. 253−272.

Kirkham, R.V., Robert, F., Sinclair, W.D., Pilote, P., and Daigneault, T.R., 1997, Chibougamau mining district, Quebec, Canada: vein Cu-Au and porphyry Cu(-Mo) deposits related to a composite Archean tonalitic batholith: in Papunen, H., ed. Mineral deposits research and exploration, where they meet?: A.A. Balkema, Rotterdam, p. 647−649.

Kontak, D., Dubé, B., and Benham, W., 2008, The Upper Beaver project, Kirkland Lake area: Investigation of a syenite-associated copper-gold deposit with magnetite-epidote-feldspar alteration: Ontario Geological Survey, Open File Report 6226, p. 12-1 to 12-12.

Kontak, D., Dubé, B., McNicoll, V., Creaser, R., and Kyser, K., 2013, The Upper Beaver Au-Cu deposit, Kirkland Lake, Ontario, Canada: An Archean IOCG analogue or just an intrusion-related iron oxide copper-gold deposit? [abs.]: Geological Association of Canada-Mineralogical Association of Canada (GAC-MAC) Annual Joint Meeting, Winnipeg, May 22–24, 2013, Abstract Volume 36, p. 122.

Lafrance, B., Moorhead, J., Davis, D.W., 2003, Cadre géologique du camp minier de Doyon-Bousquet-LaRonde: Ministère des Ressources naturelles, de la Faune et des Parcs, Québec, report ET 2002-07, 45 p.

Lafrance, B., Davis, D.W., Goutier, J., Moorhead, J., Pilote, P., Mercier-Langevin, P., Dubé, B., and Galley, A., 2005, Nouvelles datations isotopiques dans la portion québécoise du Groupe de Blake River et des unités adjacentes: Ministère des Ressources naturelles et de la Faune, Québec, report RP 2005-01, 26 p.

Lang, J.R., Stanley, C. R. and Thompson, J.F.H., 1994, Porphyry copper deposits related to alkalic igneous rocks in the Triassic-Jurassic arc terranes of British Columbia: Ariz. Geol. Soc., Digest 20.

Langshur, A., 1990, The geology, geochemistry, and structure of the Mooshla intrusion, Bousquet mining centre, Québec: Unpublished M.Sc. thesis, University of Ottawa, Ottawa, Canada, 172 p.

Large, R.R., 1992, Australian volcanic-hosted massive sulphide deposits: Features, styles and genetic models: Economic Geology, v. 87, p. 471-510.

Large, R.R., Gemmell, J.B., Paulick, H., and Huston, D.L., 2001, The alteration box plot: A single approach to understanding the relationship between alteration, mineralogy and lithogeochemistry associated with volcanogenic-hosted massive sulphide deposits: Economic Geology, v. 96, p. 957–971.

Longo, A.A., Dilles, J.H., Grunder, A.L., Duncan, R., 2010, Evolution of calc-alkaline volcanism and associated hydrothermal gold deposits at Yanacocha, Peru: Economic Geology, v. 107, p. 1191−1241.

Lulin, J.-M., 1990, Une analyse du développement minier du nord-ouest québécois: CIM Special Volume 43, p. 17–34.

Marquis, P., Hubert, Brown, A.C., and Rigg, D.M., 1990, An evaluation of genetic models for gold deposits of the Bousquet district, Quebec, based on their mineralogical, geochemical and structural characteristics: CIM Special volume 24, p. 383–399.

Mason, R.A, 1992, Models of order and iron-fluorine avoidance in biotite: The Canadian Mineralogist, v. 30, p. 343–354.

Mathieu, L., and Racicot, D., 2019, Petrogenetic study of the multiphase Chibougamau Pluton: Archaean magmas associated with Cu–Au magmato-hydrothermal systems: Minerals, v. 9, 35 p.

McDonough, W.F., and Sun, S.S., 1995, The composition of the Earth: Chemical Geology, v. 120, p. 223−253.

McLeod, P., and Sparks, R., 1998, The dynamics of xenolith assimilation: Contributions to Mineralogy and Petrology, v.132, p. 21–33.

McNicoll, V., Goutier, J., Dubé, B., Mercier-Langevin, P., Ross, P.-S., Dion, C., Monecke, T., Legault, M., Percival, J., and Gibson, H., 2014, New U-Pb geochronology from the Blake River Group, Abitibi Subprovince, Québec: implications for geological interpretations and base metal exploration: Economic Geology, v. 109, p. 27–59.

Meng, X., Richards, J., Kontak, D., Simon, A.C., Kleinsasser, J. M., Marsh, J. H., Stern, R.A., Jugo, P.J., 2021, Variable modes of formation for tonalite –trondhjemite –granodiorite –diorite (TTG)-related porphyry-type Cu ± Au deposits in the Neoarchean southern Abitibi Subprovince (Canada): Evidence from petrochronology and oxybarometry: Journal of Petrology, v. 62, p. 1–29.

Mercier-Langevin, P., 2005, Géologie du gisement de sulfures massifs volcanogènes aurifères LaRonde, Abitibi, Québec: Unpublished Ph.D. thesis, Institut national de la recherche scientifique – Centre Eau Terre Environnement, Québec, Canada, 698 p.

Mercier-Langevin, P., Dubé, B., Hannington, M.D., Lafrance, B., Galley, A.G., and Moorhead, J., 2007a, A group of papers devoted to the LaRonde Penna Au-rich volcanogenic massive sulfide deposit, eastern Blake River Group, Abitibi greenstone belt, Quebec – Preface: Economic Geology, v. 102, p. 577–583.

Mercier-Langevin, P., Dubé, B., Hannington, M.D., Davis, D.W., Lafrance, B., and Gosselin, G., 2007b, The LaRonde Penna Au-rich volcanogenic massive sulfide deposit, Abitibi greenstone belt. Quebec: Part I. Geology and geochronology: Economic Geology, v. 102, p. 585–609.

Mercier-Langevin, P., Dubé, B., Hannington, M.D., Richer-Laflèche, M., and Gosselin, G., 2007c, The LaRonde Penna Au-rich volcanogenic massive sulfide deposit, Abitibi greenstone belt, Quebec: Part II. Lithogeochemistry and paleotectonic setting: Economic Geology, v. 102, p. 611–631.

Mercier-Langevin, P., Dubé, B., Lafrance, B., Hannington, M., Galley, A., Moorhead, J., and Gosselin, P., 2007d, Metallogeny of the Doyon-Bousquet-LaRonde mining camp, Abitibi greenstone belt, Quebec: Geological Association of Canada, Mineral Deposits Division, Special Publication no. 5, p. 673–701.

Mercier-Langevin, P., Ross, P.-S., Lafrance, B., and Dubé, B., 2008, Volcaniclastic rocks of the Bousquet scoriaceous tuff units north of the LaRonde Penna mine, Doyon-Bousquet-LaRonde mining camp, Abitibi greenstone belt, Quebec: Geological Survey of Canada, Current Research Paper 2008-11, 19 p.

Mercier-Langevin, P., Wright-Holfeld, A., Dubé, B., Bernier, C., Houle, N., Savoie, A., and Simard, P., 2009, Stratigraphic setting of the Westwood-Warrenmac ore zones, Westwood Project, Doyon-Bousquet-LaRonde mining camp, Abitibi, Quebec: Geological Survey of Canada, Current Research Paper 2009-03, 20 p.

Mercier-Langevin, P., Hannington, M., Dubé, B., McNicoll, V., Goutier, J., and Monecke, T., 2011, Geodynamic influences on the genesis of Archean world-class gold-rich VMS deposits: examples from the Blake River Group, Abitibi greenstone belt, Canada. 11th Biennal SGA2011 meeting, Antofagasta, Chile, September 2011, Let's talk Ore Deposits – Proceedings of the Eleventh Biennal SGA Meeting, p. 85–87.

Mercier-Langevin, P., Daignault, R., Goutier, J., Dion, C., and Archer, P., 2012, Geology of the Archean intrusion-hosted La-Grande-Sud Au-Cu prospect, la Grande subprovince, James Bay region, Quebec: Economic Geology, v. 107, p. 935-962.

Mercier-Langevin, P., Hannington, M.D., Dubé, B., Piercey, S.J., Peter, J.M., and Pehrsson, S.J., 2015, Precious metal enrichment processes in volcanogenic massive sulphide deposits – a summary of key features, with an emphasis on TGI-4 research contributions: Geological Survey of Canada Open File 7853, p. 117–130.

Mercier-Langevin, P., Dubé, B., Blanchet, F., Pitre, D., and Laberge, A., 2017, The LaRonde Penna Au-rich volcanic-hosted massive sulfide deposit: Reviews in Economic Geology, v. 19, p. 225–245.

Mercier-Langevin, P., Lawley, C.J.M., Castonguay, S., Dubé, B., Bleeker, W., Pinet, N., Bécu, V., Pilote, J.-L., Jackson, S.E., Wodicka, N., Honsberger, I.W., Davis, W.J., Petts, D.C., Yang, Z., Jautzy, J., and Lauzière, K., 2020, Targeted Geoscience Initiative 5, Gold Project: A summary of contributions to the understanding of Canadian gold systems: Geological Survey of Canada, Open File 8712, p. 1–30.

Mercier-Langevin, P., Creaser, R.A., Dubé, B., Dubé, J., Kontak, D.J., Sutton, J., and Côté-Mantha, O., 2021, Molybdenite Re-Os ages of a gold-rich vein, Porphyry zone, Upper Beaver deposit, Abitibi greenstone belt, Ontario: Geological Survey of Canada, Open File 8789, 13 p.

Mercier-Langevin P., Dubé, B., and Fortin, D., 2021, The Doyon-Bousquet-LaRonde mining camp – Historical and geological overview of an exceptional camp: Resources & Industry – Mines, v. 2, p. 44–61.

Mercier-Langevin, P., Dubé, B., Houlé, M.G., Bécu, V., Sappin, A.-A., Pilote, J.-L., and Castonguay, S., 2024a, Metallogeny of the Abitibi greenstone belt, Canada: In S. Decrée (ed.), Metallic Resources 2 Geodynamic Framework and Remarkable Examples in the World, Sciences – Geosciences – Natural Resources Series: Applied Basic Research, ISTE Editions, London, p. 63–142.

Mercier-Langevin, P., Bécu, V., Lauzière, K., Galley, A.G., and Savoie, A., 2024b, Whole-rock lithogeochemistry of zones 1 and 2 of the Doyon Au(-Cu) deposit, Doyon-Bousquet-LaRonde mining camp, Québec, Canada; Geological Survey of Canada, Open File 9192, 1 .zip file.

Mercier-Langevin, P., Creaser, R.A., Goutier, J., and Kjarsgaard, I., 2024c, Rhenium-rich molybdenite and Re-Os age of the Archean porphyry-style Don Rouyn deposit, Abitibi greenstone belt, Rouyn-Noranda, Quebec: Geological Survey of Canada, Open File 9161, 31 p.

Monecke, T., Mercier-Langevin, P., Dubé, B., and Frieman, B., 2017, Geology of the Abitibi greenstone belt: Reviews in Economic Geology volume 19, p. 7–49.

Morton R., Hudak G, 1and Koopman, E., 1996, Physical volcanology, hydrothermal alteration and mineral deposits of the Sturgeon Lake caldera: Geological Association of Canada, Guidebook B3, 37 p.

Mueller, W.U., Friedman, R., Daigneault, R., Moore, L., and Mortensen, J., 2012, Timing and characteristics of the Archean subaqueous Blake River megacaldera complex, Abitibi greenstone belt, Canada: Precambrian Research, v. 214-215, p. 1−27.

Mungall, J.E., 2002, Roasting the mantle: Slab melting and the genesis of major Au and Au-rich Cu deposits: Geology, v. 30, p. 915–918.

Nelson, C.E., Dominquez, H., Leonardo A.R., Polanco, J., and Carrasco, C.C., 2023, Geologic setting of the Pueblo Viejo Au–Ag–Cu-(Zn) mining district, Dominican Republic - Links to volcanic domes and volcanogenic massive sulfide mineralization: Journal of South American Earth Sciences, v. 123, Article 104158.

Neyedley, K., Hanley, J.J., Mercier-Langevin, P., and Fayek, M., 2021a, Ore mineralogy, pyrite chemistry, and S isotope systematics of magmatic-hydrothermal Au mineralization associated with the Mooshla Intrusive Complex (MIC), Doyon-Bousquet-LaRonde mining camp, Abitibi greenstone belt, Québec: Geological Survey of Canada, Open File 8755, p. 129–148.

Neyedley, K., Hanley, J.J., Zajacz, Z., and Fayek, M., 2021b, Accessory mineral thermobarometry, trace element chemistry, and stable O isotope systematics, Mooshla Intrusive Complex (MIC), Doyon-Bousquet-LaRonde mining camp, Abitibi greenstone belt, Québec: Geological Survey of Canada, Open File 8755, p. 149–168.

Perrouty, S., Gaillard, N., Piette-Lauzière, N., Mir, R., Bardoux, M., Olivo, G.R., Linnen, R.L., Bérubé, C.L., Lypaczewski, P., Guilmette, C., 2017, Structural setting for Canadian Malartic style of gold mineralization in the Pontiac Subprovince, south of the Cadillac Larder Lake deformation zone, Quebec, Canada: Ore Geology Reviews, v. 84, p. 185–201.

Piercey, S.J., Chaloux, E.C., Péloquin, A.S., Hamilton, M.A., and Creaser, R.A., 2008, Synvolcanic and younger plutonic rocks from the Blake River Group: Implications for regional metallogenesis: Economic Geology, v. 103, p. 1243–1268.

Pilote, P., Cimon, J., Dion, C., Kirkham, R., Robert, F., Sinclair, W.D., and Daigneault, R., 1993, Les gisements de type Cu-Au porphyrique de la région de Chibougamau: Ministère des Ressources Naturelles, report DP 93-02.

Rabayrol, F., Wainwright, A.G., Lee, R.G. Hart, C.J.R., Creaser, R.A., and Camacho, A., 2023, District-scale VMS to porphyry-epithermal transitions in subduction to postcollisional tectonic environments: The Artvin Au-Cu district and the Hod Gold corridor, Eastern Pontides belt, Turkey: Economic Geology, v. 118, p. 801–822.

Rogers, R., Ross, P.-S., Goutier, J., and Mercier-Langevin, P., 2014, Using physical volcanology, chemical stratigraphy, and pyrite geochemistry for volcanogenic massive sulphide exploration: An example from the Blake River Group, Abitibi greenstone belt: Economic Geology, v. 109, p. 61–88.

Russell, J.K., Edwards, B.R., and Snyder, L.D., 1995, Volatile production possibilities during magmatic assimilation: Heat and mass balance constraints: Mineralogical Association of Canada Short Course notes, v. 23, p. 1-24.

Sangster, D.F., 1978, Exhalites associated with Archaean volcanogenic massive sulphide deposits: Perth, Australia, University of Western Australia, Geology Department and Extension Service Publication 2, p. 70–81.

Santaguida, F., 1999, The paragenetic relationships of epidote-quartz hydrothermal alteration within the Noranda volcanic complex, Quebec: Unpublished Ph.D. thesis, Carleton University, Ottawa, Canada, 302 p.

Savoie, A., Perrault, G., and Filion, G., 1986, Geological setting of the Doyon gold deposit, Bousquet Township, Abitibi, Québec, Canada: Proceedings on Gold'86, An international symposium on the geology of gold, Toronto, Ontario, p. 97–107.

Savoie, A., Trudel, P., Sauvé, P., and Perrault, G., 1990, Géologie de la mine Doyon, Cadillac, Québec: CIM Special Volume 43, p. 401–411.

Savoie, A., Trudel, P., Sauvé, P., Hoy, L., and Lao, K., 1991, Géologie de la mine Doyon (région de Cadillac) : Ministère de l'Énergie et des Ressources, Québec, report ET 90-05, 80 p.

Seedorf, E., Dilles, J.H., Profett, Jr. J.M., Einaudi, M.T., Zurcher, L., Stavast, W.J.A., Johnson, D.A., and Barton, M.D., 2005, Porphyry deposits: Character and origins of hypogene features: Economic Geology 100th Anniversary Volume, p. 251−298.

Schofield, M.D., Lafrance B., Gibson H.L., Poulsen K.H, Scheffer C., Quesnel, B., Beaudoin, G., and Hamilton, M.A., 2024, Discriminating superimposed alteration associated with epigenetic base and precious metal vein systems in the Rouyn-Noranda mining district, Quebec; Implications for exploration in ancient volcanic districts: Economic Geology, v. 119, p. 617–641.

Sharma, T., and Clayton, R.N., 1965, Measurement of O^{18}/O^{16} ratios of total oxygen of carbonates: Geochimica et Cosmochimica Acta, v. 29, p. 1347–1354.

Sillitoe, R.H., 1980, Are porphyry copper and Kuroko-type massive sulfide deposits incompatible?: Geology, v. 8, p. 11–14.

Sillitoe, R.H., Hannington, M.D., and Thompson, J.F.H., 1996, High Sulfidation Deposits in a Massive Sulphide Environment: Economic Geology, v. 91, p. 204–212.

Sillitoe, R.H., 2010, Porphyry copper systems: Economic Geology, v. 105, p. 3–41.

Sillitoe, R.H., 2012, Copper Provinces: Economic Geology, Spec. v. 16, p. 1–18.

Sillitoe, R.H., Hall, D.J., Redwood, S.D., and Waddell, A., 2007, Pueblo Viejo high-sulfidation epithermal gold-silver deposit, Dominican Republic: A new model of formation beneath barren limestone cover: Economic Geology, v. 102, p. 1427–1435.

Simmons, S.F., White, N.C., and John, D.A., 2005, Geological characteristics of epithermal precious and base metal deposits: Economic Geology 100th Anniversary Volume, p. 485–522.

Skirrow, R.G., and Franklin, J.M., 1994, Silicification and metal leaching in semi-conformable alteration beneath the Chisel Lake massive sulfide deposit, Snow Lake, Manitoba: Economic Geology, v. 89, p. 31–50.

Stecher, O., 1998, Fluorine geochemistry in volcanic rock series: examples from Iceland and Jan Mayen: Geochimica et Cosmochimica Acta, v. 62, p. 3117–3130.

Stone, W.E., 1988, The nature and significance of metamorphism in gold concentration, Bousquet township, Abitibi greenstone belt, northwest Quebec: Unpublished Ph.D. thesis, University of Western Ontario, London, Canada, 441 p.

Sun, W., Huang, R.-f., Li, H., Hu, Y.-b., Zhang, C.-c., Sun, S.-j., Zhang, L.-p., Ding, X., Li, C.-y., Zartman, R.E., and Ling, M.-x., 2015, Porphyry deposits and oxidized magmas: Ore Geology Reviews, v. 65, p. 97–131.

Teal, L., and Benavides, A., 2010, History and geologic overview of the Yanacocha mining district, Cajamarca, Peru: Economic Geology, v. 105, p. 1173–1190.

Titley, S.R., Heidrick, T.L., 1978, Intrusion and fracture styles of some mineralized porphyry systems of the southwestern Pacific and their relationship to plate interactions: Economic Geology, v. 73, p. 891−903.

Tompkins, A.G., and Mavrogenes, J.A., 2002, Mobilization of gold as a polymetallic melt during pelite anatexis at the Challenger deposit, South Australia: A metamorphosed Archean gold deposit: Economic Geology, v. 97, p. 1249-1271.

Tosdal, R., and Richards, J.P., 2001, Magmatic and structural controls on the development of porphyry Cu + Mo + Au deposits: Reviews in Economic Geology volume14, p. 157–181.

Tourigny, G., and Chartrand, F., 1994, Kinematic evolution of metre-scale shear zones in foliated low-grade tectonites: an example from the Bousquet gold district, Quebec: Canadian Journal of Earth Sciences, v. 31, p. 1301–1308.

Tourigny, G., Hubert, C., Brown, A.C., and Crépeau, R., 1988, Structural geology of the Blake River at the Bousquet mine, Abitibi, Quebec: Canadian Journal of Earth Sciences, v. 25, p. 581–592.

Tourigny, G., Brown, A.C., Hubert, C., and Crépeau, R., 1989, Synvolcanic and syntectonic gold mineralization at the Bousquet mine, Abitibi greenstone belt, Quebec: Economic Geology, v. 84, p. 1875–1890.

Tourigny, G., Doucet, D., and Bourget, A., 1993, Geology of the Bousquet 2 mine: An example of a deformed, gold-bearing polymetallic sulfide deposit: Economic Geology, v. 88, p. 1578–1597.

Tremblay, A., Tourigny, G., and Machado, N., 1995, Zircon U/Pb age constraints on deformation and gold mineralization of the Mooshla pluton, southern Abitibi belt, Canada: Geological Society of America annual meeting, New Orleans, abstracts with programs, page A-163.

Trudel, P., Sauvé, P., Tourigny, G., Hubert, C., and Hoy, L., 1992, Synthèse des caractéristiques géologiques des gisements d'or de la région de Cadillac (Abitibi): Ministère de l'Énergie et des Ressources du Québec, report MM 91-01, 106 p.

Valliant, R.I., and Barnett, R.L., 1982, Manganiferous garnet underlying the Bousquet gold orebody, Quebec: metamorphosed manganese sediment as a guide to gold ore: Canadian Journal of Earth Sciences. v. 19, p. 993–1010.

Valliant, R.I., and Hutchinson, R.W., 1982, Stratigraphic distribution and genesis of gold deposits, Bousquet région, Northwestern Quebec: CIM Special Volume 24, p. 27-40.

Williams, N.C., and Davidson, G.J., 2004, Possible submarine advanced argillic alteration at the Basin Lake prospect, western Tasmania, Australia: Economic Geology, v. 99, p. 987–1002.

Winchester, J.A., and Floyd, P.A., 1977, Geochemical discrimination of different magma series and their differentiation products using immobile elements: Chemical Geology, v. 20, p. 325−343.

Wright-Holfeld, A., Mercier-Langevin, P., and Dubé, B., 2010, Contrasting alteration mineral assemblages associated with the Westwood deposit ore zones, Doyon-Bousquet-LaRonde mining camp, Abitibi, Quebec: Geological Survey of Canada, Current Research Paper 2010-9, 24 p.

Wright-Holfeld, A., Mercier-Langevin, P., and Dubé, B., 2011, Mass changes and element mobility associated with the Westwood deposit ore zones, Doyon-Bousquet-LaRonde mining camp, Abitibi, Quebec: Geological Survey of Canada, Current Research Paper 2011-8, 15 p.

Yergeau, D., 2015, Géologie du gisement synvolcanique aurifère atypique Westwood, Abitibi, Québec: Unpublished PhD thesis, Institut national de la Recherche scientifique, Centre Eau, Terre et Environnement, Quebec, Canada, 643 p.

Yergeau, D., Mercier-Langevin, P., Dubé, B., Malo, M., McNicoll, V.J., Jackson, S.E., Savoie, A., and La Rochelle, F., 2015, The Archean Westwood Au deposit, southern Abitibi: Telescoped Au-rich VMS and intrusion-related Au systems: Geological Survey of Canada, Open File 7852, p. 177–191.

Yergeau, D., Mercier-Langevin, P., Dubé, B., Malo, M., and Savoie, A., 2022a, The Westwood deposit, southern Abitibi greenstone belt, Canada: An Archean Au-rich polymetallic magmatic-hydrothermal system - Part 1. Volcanic architecture, deformation, and metamorphism: Economic Geology, v. 117, p. 545–575.

Yergeau, D., Mercier-Langevin, P., Dubé, B., McNicoll, V., Jackson, S., Malo, M., and Savoie, A., 2022b, The Westwood deposit, southern Abitibi greenstone belt, Canada: An Archean Au-rich polymetallic magmatic-hydrothermal system – Part 2. Hydrothermal alteration, mineralization, and geological model: Economic Geology, v. 117, p. 577–608.

Zaleski, E., 1989, Relationship between deformation and metamorphism at the Linda volcanogenic massive sulphide deposit, Snow Lake, Manitoba: Geological Survey of Canada, Open File 2133, 7 p.

Zajacz, Z., Candela, P. A., Piccoli, P. M., Wälle, M., and Sanchez-Valle, C., 2012, Gold and copper in volatile saturated mafic to intermediate magmas: Solubilities, partitioning, and implications for ore deposit formation: Geochimica et Cosmochimica Acta, v. 91, p. 140–159.

Zweng, P.L., Mortensen, J.K., Dalrymple, B.G., 1993, Thermochronology of the Camflo gold deposit, Malartic, Quebec: Implications for magmatic underplating and the formation of gold-bearing quartz veins: Economic Geology, v. 88, p. 1700−1721.

APPENDIX 1

Geochemical characterization and classification of whole-rock samples taken along section 3180E, Doyon mine Zone 2 (see Fig. 15).

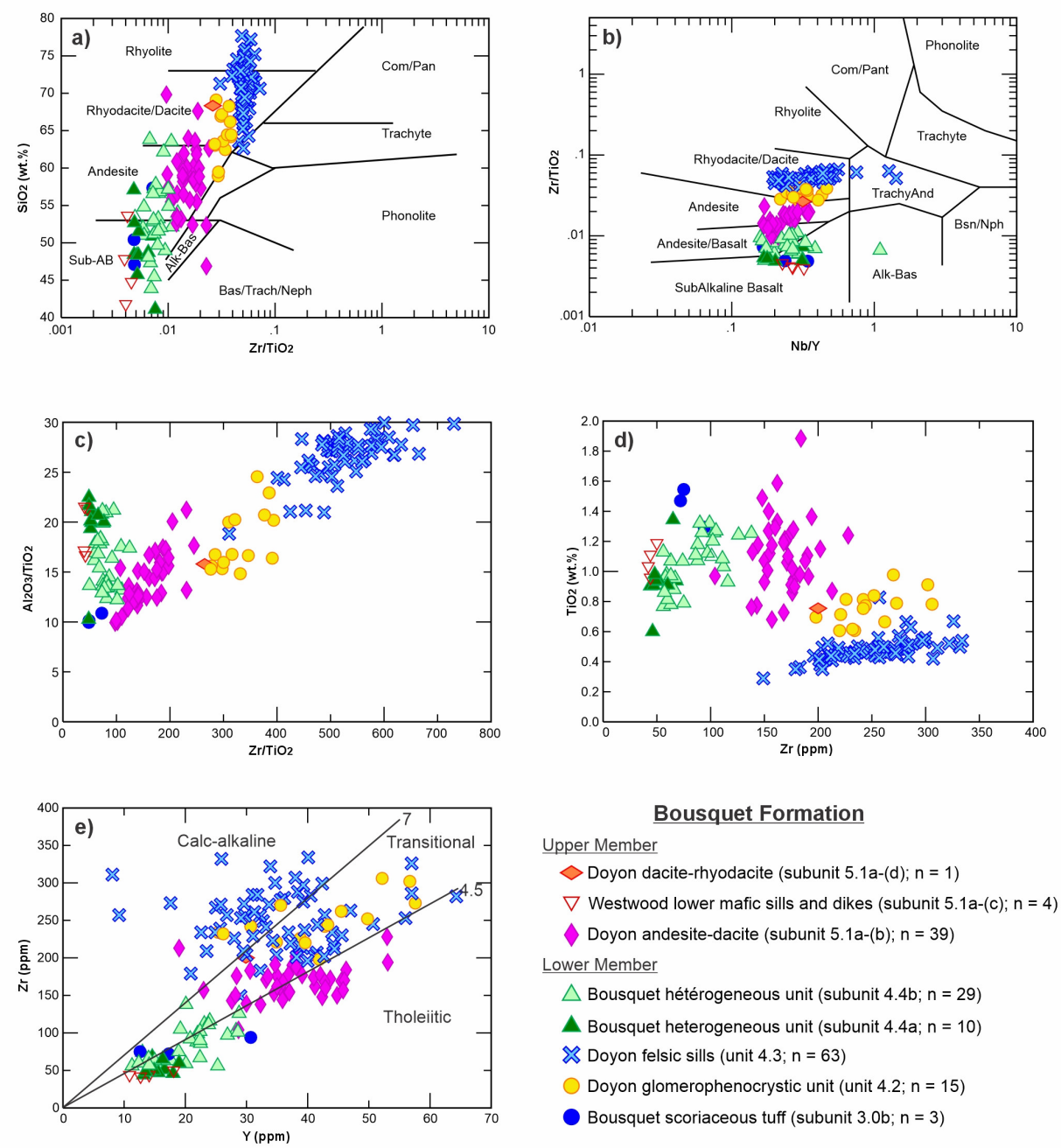

Figure A1.1. *Major and trace element plots of the host units of the Doyon deposit Zone 2.* ***A.*** *SiO_2 vs. Zr/TiO_2 classification diagram from Winchester and Floyd (1977).* ***B.*** *Zr/TiO_2 vs. Nb/Y classification diagram from Winchester and Floyd (1977).* ***C.*** *Al_2O_3/TiO_2 versus Zr/TiO_2 discrimination diagram.* ***D.*** *TiO_2 vs. Zr discrimination diagram.* ***E.*** *Zr vs. Y plot of tholeiitic vs. calc-alkalic magmatic affinity for volcanic rocks. Fields from Barrett and MacLean (1994).*

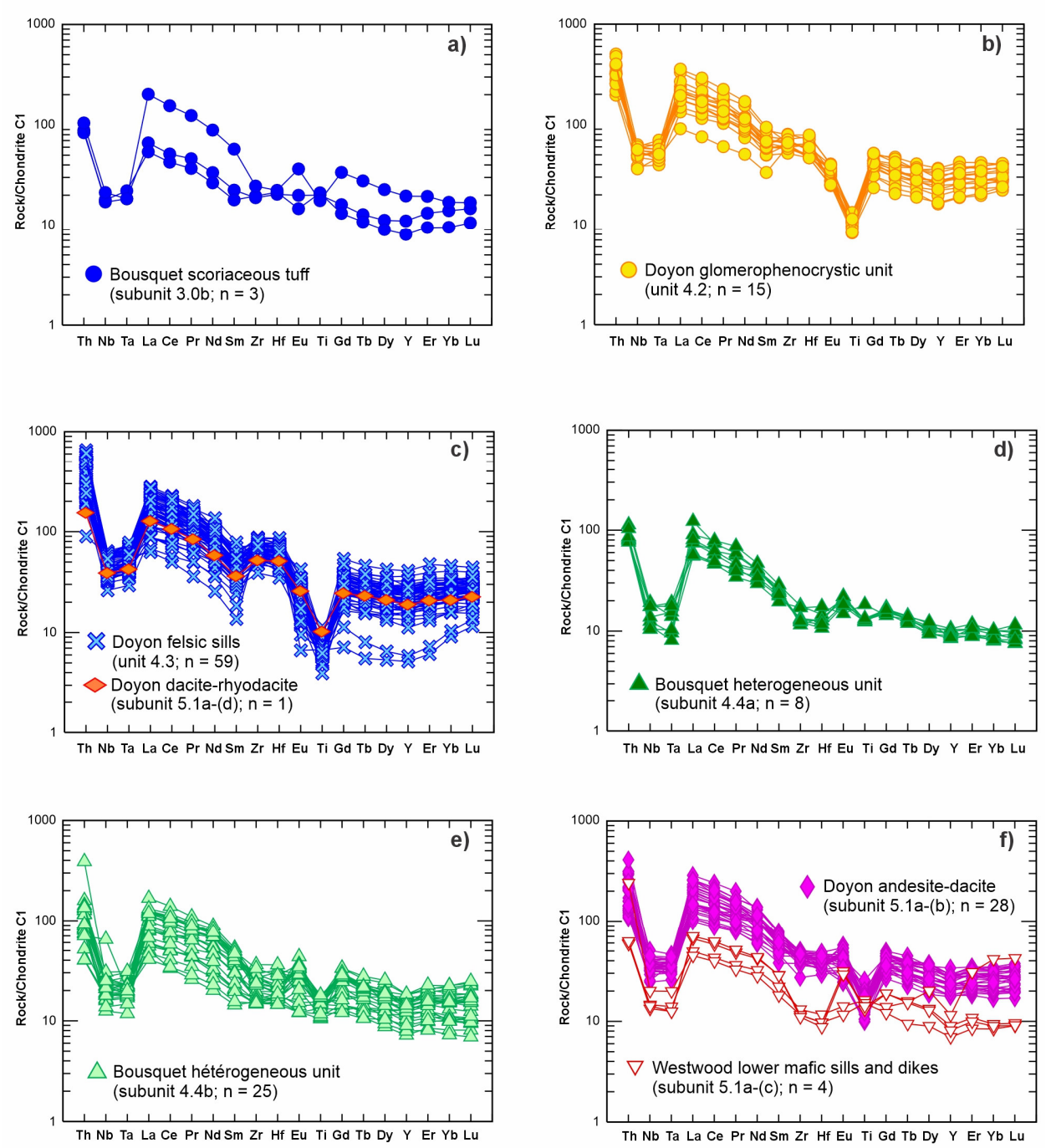

Figure A1.2. *Chondrite-normalized trace and rare-earth element plots for the host units of the Doyon deposit Zone 2. C1 chondrite normalization values from McDonough and Sun (1995).*

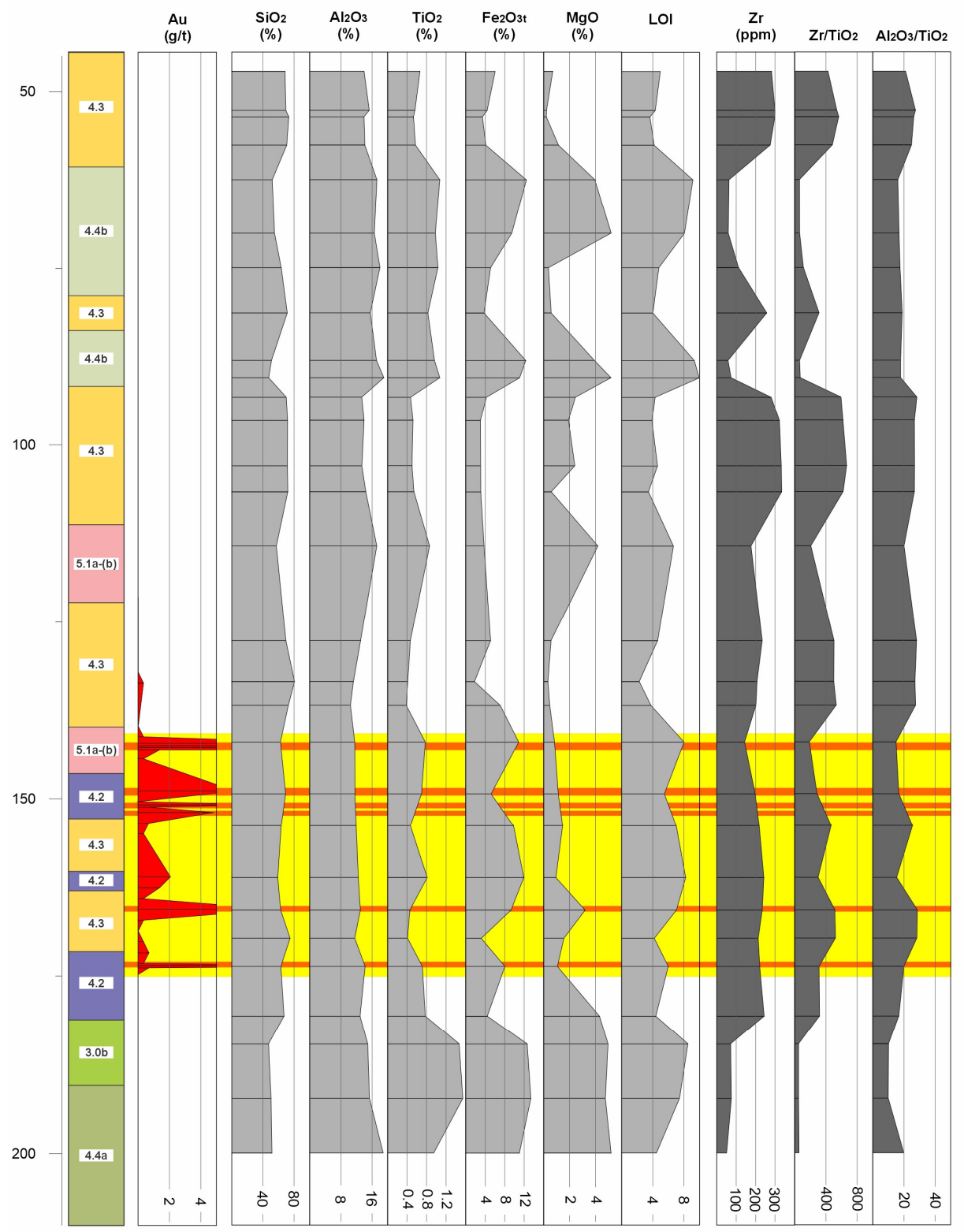

Figure A1.3. *Geology and geochemical profiles of drill hole 11-832-58 (location shown on Fig. 15). The location and distribution of the analyzed samples and results are indicated by horizontal lines. Unit names and legend are given in Fig. 15).*

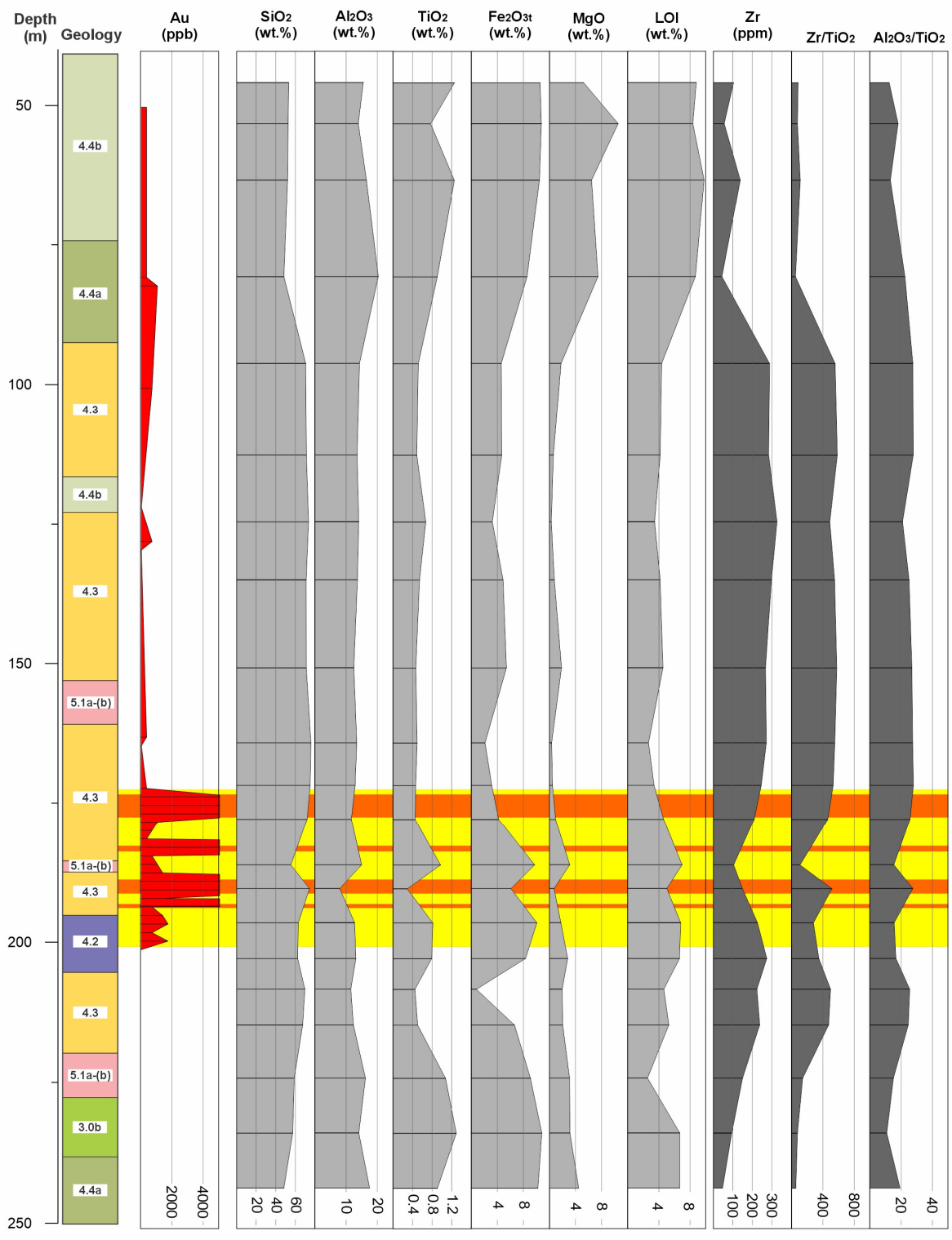

Figure A1.4. *Geology and geochemical profiles of drill hole 11-832-37 (location shown on Fig. 15). The location and distribution of the analyzed samples and results are indicated by horizontal lines. Unit names and legend are given in Fig. 15).*

APPENDIX 2

Whole-rock oxygen isotopes, Doyon mine Zone 2.

Analytical methods whole-rock O isotope analysis

Whole-rock oxygen isotope compositions were determined at the Laboratory for Stable Isotope Science at the University of Western Ontario, London, Canada. Results are reported in the usual δ notation in parts per thousand (‰), relative to Vienna standard mean ocean water (VSMOW). Oxygen was extracted from silicates and oxides using the BrF_5 method of Clayton and Mayeda (1963) and converted quantitatively to CO_2 over red-hot graphite. The oxygen isotope composition of the evolved CO_2 was calculated using a phosphoric acid-CO_2 fractionation factor of 1.01025 (Sharma and Clayton, 1965). The $^{18}O/^{16}O$ ratio was measured using an Optima, triple-collecting, dual inlet, stable isotope ratio mass spectrometer. Precision was better than ±0.67‰ for oxygen isotopes (avg ±0.24‰). Laboratory reference materials calibrated to VSMOW were accurate to ±0.11‰.

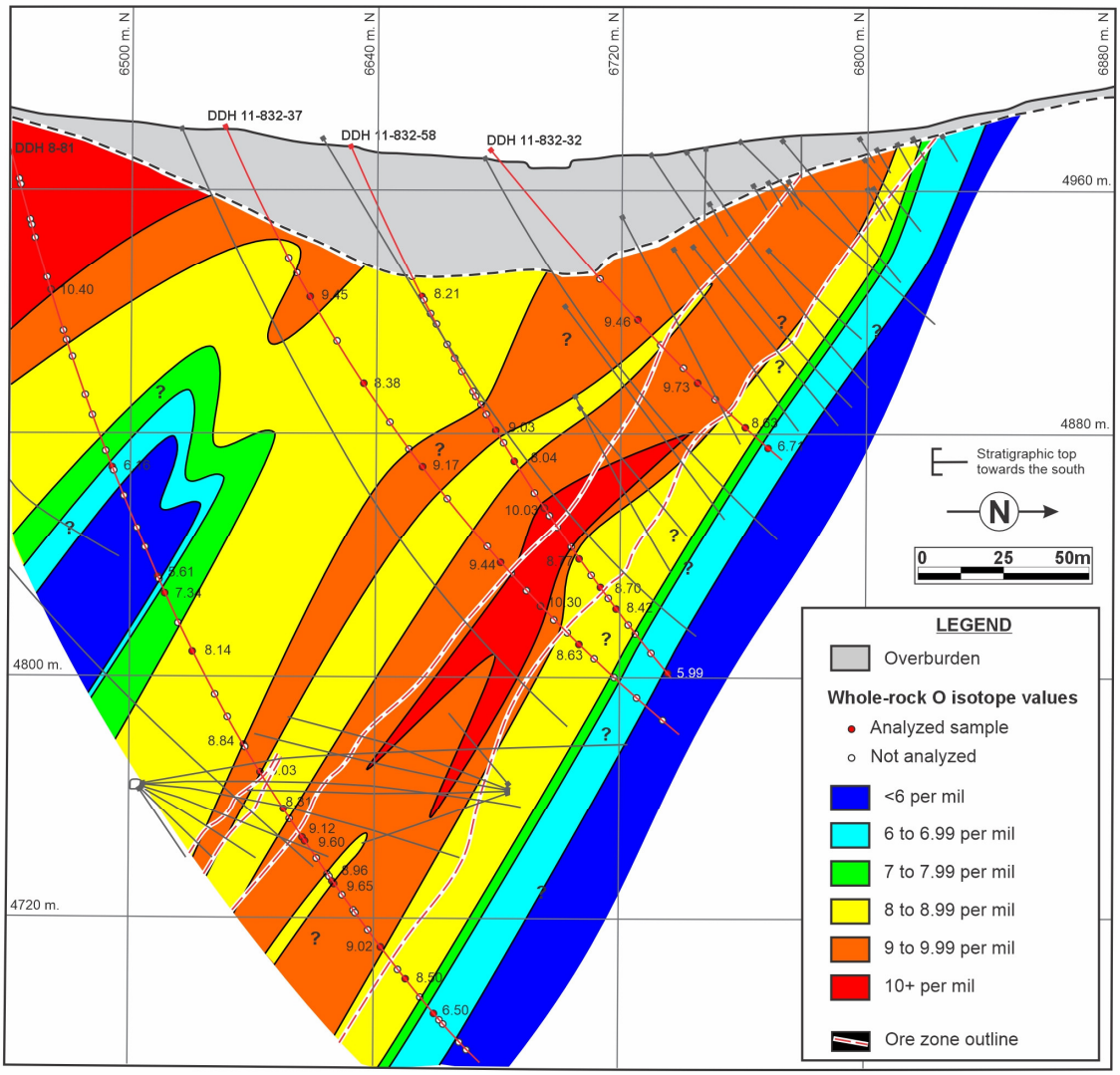

Figure A2.1. *North-south section through Zone 2 (see Fig. 15) showing whole-rock oxygen isotope values and interpolation.*

Table A2.1. *Whole-rock oxygen isotope analyses – lab results. See Mercier-Langevin et al. (2024b) for details about the samples.*

Sample	δ^{18}O VSMOW	Yield	Standards	δ^{18}O VSMOW	Yield	Accepted Values
		µmol/mg			µmol/mg	
561230	**8.2119184**	13.55	Laboratory standard quartz	**11.8224276**	16.27	11.5
561241	**9.0286016**	15.19	Laboratory standard quartz	**11.5765228**	16.2	11.5
561243	**8.039876**	12.88	Laboratory standard quartz	**11.4906128** ?		11.5
561245	**10.029764**	14.26	Laboratory standard quartz	**11.384986**	15.17	11.5
561249	**8.7695016**	11.84	Laboratory standard quartz	**11.7101628**	15.12	11.5
561251	**8.6969536**	12.51	Laboratory standard quartz	**11.461088**	15.07	11.5
561253	**8.4171256**	11.61	Laboratory standard quartz	**11.581452**	15.92	11.5
561257	**5.6478648**	12.73	Laboratory standard quartz	**11.3872812**	15.56	11.5
561257-dup	**6.332536**	12.42	Laboratory standard quartz	**11.502974**	16.34	11.5
561260	**9.4544812**	11.77	Laboratory standard quartz	**11.4796876**	15.93	11.5
561262	**8.3776616**	13.58	Laboratory standard quartz	**11.5946472**	15.53	11.5
561265	**9.1684348**	13.51	Laboratory standard quartz	**11.619718**	15.78	11.5
561268	**9.4378988**	13.86	Laboratory standard quartz	**11.5356028**	15.48	11.5
561271	**10.130214**	12.87	Laboratory standard quartz	**11.5184844**	15.28	11.5
561271 dup	**10.4620592**	13.29	Laboratory standard quartz	**11.459182**	15.6	11.5
561274	**8.6305432**	13.5	Laboratory standard quartz	**11.4477816**	16.62	11.5
561280	**9.461736**	13.19				
561283	**9.7280908**	10.57	Laboratory standard carbon dioxide II	**10.24427246**		10.2
561286	**8.6336524**	13.24	Laboratory standard carbon dioxide II	**10.24427246**		10.2
561287	**6.6665652**	13.25	Laboratory standard carbon dioxide II	**10.22714328**		10.2
561287-dup	**6.7499524**	13.46	Laboratory standard carbon dioxide II	**10.14267676**		10.2
561292	**10.4009116**	11.25	Laboratory standard carbon dioxide II	**10.20659292**		10.2
561295	**6.1599628**	13.11	Laboratory standard carbon dioxide II	**10.17354995**		10.2
561298	**5.6096344**	12.78	Laboratory standard carbon dioxide II	**10.17049327**		10.2
549301	**7.3392192**	11.92	Laboratory standard carbon dioxide II	**10.20061681**		10.2
549302	**8.1403564**	12.01	Laboratory standard carbon dioxide II	**10.13550776**		10.2
549304	**8.8430356**	11.09	Laboratory standard carbon dioxide II	**10.17568823**		10.2
549305	**9.025442**	11.93	Laboratory standard carbon dioxide II	**10.16267137**		10.2
549305-dup	**8.9929748**	11.52	Laboratory standard carbon dioxide II	**10.24021189**		10.2
549306	**8.3123988**	10.21	Laboratory standard carbon dioxide II	**10.24026814**		10.2
549307	**9.118718**	12.85	Laboratory standard carbon dioxide (II)	**10.33396583**		10.2
549308	**9.5975348**	15.06	Laboratory standard carbon dioxide II	**10.24024114**		10.2
549311	**8.9647948**	12.01	Laboratory standard carbon dioxide (II) Optima	**10.21339252**		10.2
549312	**9.6477824**	12.85	Laboratory standard carbon dioxide II (Prism)	**10.26766614**		10.2
549314	**9.0186876**	13.09	Laboratory standard carbon dioxide II	**10.21339252**		10.2
549315	**8.496342**	13.82				
549316	**6.5033448**	13.56	Laboratory standard basalt	**7.4997752**	12.56	7.5
			Laboratory standard basalt	**7.496494**	13	7.5
			Laboratory standard basalt	**7.4980612**	13.07	7.5
			Laboratory standard basalt	**7.5045324**	13.07	7.5